MINISTERE DE L'ENSEIGNEMENT SUPERIEUR ET DE LA RECHERCHE SCIENTIFIQUE

UNIVERSITE MOHAMED KHIDER BISKRA

FACULTE DES SCIENCES EXACTES ET DES SCIENCES DE LA NATURE ET DE LA VIE

Département des Sciences de la matière

THESE

Présentée par

KHELFAOUI Hadjer

En vue de l'obtention du diplôme de:

Doctorat LMD en chimie

Option:

Chimie computationnelle et pharmaceutique

Intitulé

Une approche computationnelle pour le développement d'agents thérapeutiques

Soutenue le:08/06/2022

Devant la commission d'examen:

Mr. Salah BELAIDI	Pr.	Université de Biskra	Président
Mme. Dalal HARKATI	Pr.	Université de Biskra	Directrice de thèse
Mr. Abdelkader HELLAL	MCA	Université de Sétif 1	Examinateur
Mr. Yacine NOUAR	MCA	Université de Sétif 1	Examinateur

2021/2022

MINISTRY OF HIGHER EDUCATION AND SCIENTIFIC RESEARCH

MOHAMED KHIDER BISKRA UNIVERSITY

FACULTY OF EXACT SCIENCES AND SCIENCES OF NATURE AND LIFE

Matter Sciences Department

THESIS

Presented by

KHELFAOUI Hadjer

In order to obtain the diploma of:

LMD Doctorate in Chemistry

Option:

Computational and pharmaceutical chemistry

Entitled

A computational approach for the development of therapeutic agents

Defended on: 08/06/2022

In front of the thesis committee members:

Mr. Salah BELAIDI	Pr.	Biskra University	President
Mrs. Dalal HARKATI	Pr.	Biskra University	Supervisor
Mr. Abdelkader HELLAL	MCA	Setif 1University	Examiner
Mr. Yacine NOUAR	MCA	Setif 1University	Examiner

2021/2022

To my dear parents

To my sisters

To my brother

To all those who are dear to me

Acknowledgements

ABSTRACT

Over the last few decades, computer-aided drug design (CADD) has established as a strong tool for developing novel therapeutic compounds. In computer-aided drug design, two methodologies are typically used: structure-based drug design and ligand-based drug design. Molecular docking combined with molecular dynamics is one of the most important tools of drug discovery and drug design, which it used to examine the type of binding between the ligand and its protein enzyme. Global reactivity has important properties, which enable chemists to understand the chemical reactivity and kinetic stability of compounds.

The recent new contagion coronavirus 2019 (COVID-19) disease is a new generation of severe acute respiratory syndrome coronavirus-2 SARS-CoV-2 which infected millions confirmed cases and hundreds of thousands death cases around the world so far. In this study, molecular docking and reactivity were applied for eighteen drugs, which are similar in structure to chloroquine and hydroxychloroquine, the potential inhibitors to angiotensin-converting enzyme (ACE2). Those drugs were selected from DrugBank. The reactivity, molecular docking and molecular dynamics were performed for two receptors ACE2 and Crystal structure SARS-CoV-2 spike receptor-binding with ACE2 complex receptor in two active sites to find a ligand, which may inhibit COVID-19. The results obtained from this study showed that Ramipril, Delapril and Lisinopril could bind with ACE2 receptor and Crystal structure SARS-CoV-2 spike receptor-binding with ACE2 complex better than chloroquine and hydroxychloroquine.

The tyrosine kinase inhibitors gefitinib and erlotinib activated mutations of the epidermal growth factor receptor (EGFR) in non-small cell lung cancer. Quinazolines and pyridopyrimidines are antibacterial, antifungal, and cancer-fighting compounds. The goal of this study is to look into the absorption, distribution, metabolism, excretion, and toxicity (ADMET) of a series of quinazolines and pyrido[3,4-d]pyrimidines as irreversible inhibitors of wild-type (WT) and L858R and T790M EGFR kinase domain mutants, as well as their reactivity, molecular docking, and molecular dynamics simulation. The 27 heterocycles under examination show a wide range of affinities for WT, L858R, and T790M, as well as strong chemical reactivity and kinetic stability. The compounds were found to have high ADMET characteristics, and pyrido[3,4-d]pyrimidines had good reactivity and affinity towards WT, L858R, and T790M mutations. New, powerful, irreversible tyrosine kinase inhibitors have been discovered.

Keywords: Covid-19, EGFR, Molecular Docking, Molecular Dyamics, Reactivity, ADMET

الملخص

أصبح تصميم الدواء بمساعدة الكمبيوتر (CADD) بمثابة أداة قوية لتطوير المركبات العلاجية جديدة. في تصميم الأدوية بمساعدة الكمبيوتر، يتم استخدام طريقتين: تصميم الأدوية القائم على البنية وتصميم الأدوية القائم على الترابط. يعد الارساء الجزيئي و الديناميك الجزيئي أحد أهم أدوات اكتشاف الأدوية وتصميمها ، والتي تستخدم لفحص نوع الارتباط بين المركب الفعال والبروتين. الفعالية الكيميائية الشاملة لها خصائص مهمة ، تمكن الكيميائيين من فهم التفاعل الكيميائي ومدى استقرارية المركبات.

يعد مرض كورونا الجديد 2019 (كوفيد-19) جيلًا جديدًا من متلازمة الالتهاب التنفسي الحاد SARS-CoV-2 الناتجة من الفايروس التاجي والذي أصاب ملايين من الناس وتسبب بملايين الوفيات حول العالم حتى الآن. في هذه الدراسة، تم تطبيق الارساء الجزيئي والفعالية الكيميائية لثمانية عشر دواءً، والتي تشبه في تركيبها كلوروكين وهيدروكسي كلوروكين، وهي مثبطات محتملة للإنزيم المحول للأنجيوتنسين (ACE2). تم اختيار هذه الأدوية من DrugBank. بعدها تم إجراء التفاعل والارساء الجزيئي والديناميك الجزيئي لمستقبلين هما مستقبل ACE2 والمعقد [SARS-CoV-2 / ACE2] في موقعين نشطين لغرض اختيار المركب الاكثر فعالية ، والذي قد يثبط COVID-19. أظهرت النتائج التي تم الحصول عليها من هذه الدراسة أن راميبريل وديلابريل وليزينوبريل يمكن أن يرتبط بمستقبلات ACE2 والمعقد [SARS-CoV-2 / ACE2] بشكل أفضل من الكلوروكين والهيدروكسي كلوروكين.

مثبطات التيروزين كيناز gefitinib و erlotinib تنشط الطفرات لمستقبل (EGFR) في سرطان الرئة. الكينازولين والبيريدوبيريميدين مركبات متنوعة الفعالية ، مضادة للبكتيريا والفطريات ومقاومة للسرطان. الهدف من هذه الدراسة هو النظر في الامتصاص والتوزيع والتمثيل الغذائي والإفراز والسمية (ADMET) لسلسلة من الكينازولين والبيريدو [3،4-د] بيريميدين كمثبطات من النوع WT و L858R و T790M ، بالإضافة إلى تفاعلها ، الإرساء الجزيئي ، ومحاكاة الديناميات الجزيئية. أظهر المركبات المدروسة البالغ عددها 27 علاقة جيدة مع البروتينات WT و L858R و T790M في الإرساء الجزيئي ، بالإضافة إلى فعالية كيميائية قوية واستقرار حركي. تم العثور على المركبات ذات خصائص ADMET عالية ، وكان البيريدو [4،3-د] بيريميدين تفاعل جيد وانجذاب نحو طفرات WT و L858R و T790M.

الكلمات المفتاحية: Covid-19، EGFR، الإرساء الجزيئي، الديناميكيات الجزيئية، التفاعلية، ADMET

Contents

Chapter I: General concepts

Chapter II: Literature review

Chapter III: Materials and methods

Chapter IV: Results and discussion

Contributions of author

Publications:

[1] **Khelfaoui, H.,** Harkati, D., & Saleh, B. A. (2021). Molecular docking, molecular dynamics simulations and reactivity, studies on approved drugs library targeting ACE2 and SARS-CoV-2 binding with ACE2. *Journal of Biomolecular Structure and Dynamics*, *39*(18), 7246–7262. https://doi.org/10.1080/07391102.2020.1803967

[2] Abdulhassan, H. A., Saleh BA, Harkati, D., **Khelfaoui, H.**, Hewitt, N. L., & El-hiti, G. A. (2022). In Silico Pesticide Discovery for New Anti-Tobacco Mosaic Virus Agents : Reactivity, Molecular Docking , and Molecular Dynamics Simulations. *Applied Sciences, 12*(6), 2818. https://doi.org/10.3390/app12062818

[3] **Khelfaoui, H**., Harkati, D., Saleh B. A., Hewitt, N. L., & El-hiti, G. A..In Silico Evaluation, Molecular Docking, Molecular Dynamics Simulations, and Reactivity of Various Quinazolines and Pyridopyrimidines as Inhibitors of the Epidermal Growth Factor Receptor (In progress).

International conferences:

[1] **Khelfaoui, H** and Harkati, D. Quantitative structure- activity relationships for a series of the thieno [3,4-d] pyrimidine derivatives; International Conference Applied and Theory of Nanostructures ICATN'2019. 18-19 June 2019, Kenitra, Morocco. Poster

[2] **Khelfaoui, H** and Harkati, D. Chalcone as a Privileged Scaffold in Drug Discovery: Molecular Structure, Spectroscopic, Chemical Reactivity and Molecular Docking; 13th International Days of Theoretical and Computational Chemistry, 02-03 February 2020, Biskra, Algeria. Oral.

[3] **Khelfaoui, H** et Harkati, D. Une étude computationnelle sur un ensemble de composés dérivés de Thienopyrimidine. Journées Scientifiques Internationales « Modélisation Moléculaire : enjeux d'application à la lutte contre les maladies émergentes », 25-26 Décembre 2020, Casablanca, Maroc. E-poster.

National conferences:

[1] **Khelfaoui, H.** and Harkati, D. Virtual screening in drug-likeness and quantitative structure-activity relationship of Thieno[2,3-d]pyrimidines derivatives as anticancer drugs. 1st Study Day on Chemistry and its Applications JECA-1-2019. 27 November 2019, Batna, Algeria. Poster.

[2] **Khelfaoui, H.,** Harkati, D. & Saleh, B. A.computational study of SARS-CoV-2 receptors antagonists from already approved drugs. 2ème Séminaire National des Sciences d'Interfaces Chimie-Biologie, 20 Février 2021, Souk Ahras, Algerie

[3] **Khelfaoui, H** and Harkati, D. Molecular docking and dynamics study on approved drug against COVID-19 receptors. 1st Spring School on In Silico Drug Design: From Computational Methods to Experimental Filters. 23- 27th May 2021, Constantine- Algeria

List of Abbreviations

A

ACE2: Angiotensin-Converting Enzyme 2

ADMET: Absorption, Distribution, Metabolism, Elimination, and Toxicity

AIBV: Avian Infectious Bronchitis Virus

AKT: protein kinase B

Ala: Alanine

Arg: Arginine

Asn: Asparagine

Asp: Aspartic acid

ATP: Adenosine Triphosphate

B

B3LYP: Becke, three-parameter, Lee-Yang-Parr

BBB: Blood-Brain Barrier

BCL2-like 11/BIM: B-cell CL **L**/lymphoma-2 like 11

BER: Berendsen velocity/position

BRAF: B-Raf proto-oncogène

C

CADD: Computer Aided Drug Design

caco-2: human colorectal adenocarcinoma cells

CDK: cyclin-dependent kinase

CHARMM: Chemistry at Harvard Macromolecular Mechanics

CHEMBL: Chemical European Molecular Biology Laboratory

CL: clearance

CLpro: Chymotrypsin-Like Protease

COVID-19: Corona Virus Diseases 2019

Cys: cystine

D

DFT: Density Functional Theory

DNA: Deoxyribonucleic Acid

dsDNA: double-stranded DNA

dsRNA: double-stranded RNA

E

EGFR: Epidermal Growth Factor Receptor

ErbB: receptor tyrosine kinase

ELREA: removal of amino acids Glucine-Leucine-Arginine-Glucine-Alanine

ERK: Extracellular signal-regulated kinases

Europort-D,: parallel computing for European industry

F

FDA: Food and Drug Administration

G

Gln: Glutamin

Glu: Glutamic acid

Gly: Glycine

GRB-2: Growth factor receptor-bound protein 2

H

HA: Hemagglutinin

hCoV: human CoV

HER: Human Epidermal Receptor

hERG: human Ether-à-go-go-Related Gene

HIA: Human intestinal absorption

HIV: Human Immunodeficiency Virus

H-HT: human hepatotoxicity

HOMO: Highest Occupied Molecular Orbital

HPC: High-performance computing

HR: helical region

HTS: High-throughput screening

His: Histidine

I

Ile: Isoleucine

IND: Investigational New Drug

InChIKey: International Chemical Identifier key

IUPAC: International Union of Pure and Applied Chemistry

J

JAK: Janus Kinase

K

KRAS: Kirsten Rat Sarcoma

L

LBDD: Ligand-based drug design

Leu: Leucine

LUMO: Lowest Unoccupied Molecular Orbital

Lys: Lysine

L858R: leucine-to-arginine mutation at codon 858

M

MAPK: Mitogen-Activated Protein Kinase

MCF7: human mammary cancer cell line

MD: Molecular Dynamics

MDA-MB231: triple negative breast cancer cell line

Met: Methionine

MHV: murine hepatitis virus

MM-GBSA: Molecular mechanics generalized Born surface area

MM-PBSA: Molecular mechanics Poisson-Boltzmann surface area

N

N: Nucleophilicity

NAMD: Nanoscale Molecular Dynamics

NHA: The Nosé-Hoover-Andersen

NMR: Nuclear Magnetic Resonance

NPA: The Nosé-Poincaré-Andersen

nspl: non-structural polyproteins

O

ORFs: open reading frames

P

PDB: Protein Data Bank

PDGFR β: Platelet-derived growth factor receptor beta

PI3K: Phosphatidylinositol-3-Kinase

PL-pro: Papain-like protease

Phe: Phenylalanine

pp: Polypeptides

PPB: Plasma protein binding

Pro: Proline

Ps: Pico second

Q

QSAR: Quantitative structure-activity relationship

R

RAF: Rapidly Accelerated Fibrosarcoma

RAS: Rat Sarcoma

RNA: Ribonucleic Acid

RMS: Root-Mean Squared

RMSD: Root-Mean Squared Deviation

RTK: Receptor Tyrosine Kinase

S

S: Softness

SAR: Structure-activity relationship

SARS-CoV-2: Severe Acute Respiratory Syndrome Coronavirus-2

SASA: Solvent accessible surface area

SBDD: Structure-Based Drug Design

Ser: Serine

SHC: Src Homologous and Collagen

SMILES: Simplified Molecular Input Line System

ssDNA: single-stranded DNA

ssRNA: single-stranded RNA

STAT: Signal Transducers and Activators of Transcription

T

TGF-α: Transforming Growth Factor-alpha

Thr: Threonine

TK: Tyrosine Kinase

Trp: Tryptophan

Tyr: Tyrosin

T790M: Substitution of Threonine with Methionine at 790 Mutation

T1/2: half-life

V

Val: valine

VD: Volume distribution

VS: Virtual screening

W

WHO: World Health Organization

Z

Zn: Zinc

ΔE: energy gap

ω: electrophilicity

η: chemical hardness

μ: chemical potential

List of Figures

Chapter I

Chapter II

Chapter III

Chapter IV

Appendix

List of Tables

Preface

Drug development was complicated process, costly and time consuming. Classical methods of drug design take long duration from 10-15 years or more longer. Drug development can be divided into several stages; including target identification and validation by finding the molecular structure of protein related to disease, lead discovery, drug candidate selection, preclinical and clinical studies. Nowadays, computational approach era has become useful and successful tool in drug discovery and development filed. Structure-based and ligand-based methods were used to get information about ligand and to apply homology modelling and determination of the binding and interaction between the compound and the receptor.

This thesis consists of four chapters:

❖ Chapter I: **General concepts**

The first chapter discusses computer-aided drug design. Computer-aided drug design can be used to develop drugs based on knowledge about the receptors on which they act. Computers help not only in drug design but also in biologic screening of molecules. By means of computers, screening of tens of thousands of compounds can be carried out in a week. At the same time, the incentive to develop drugs by playing around with their structures is spurred by the need to develop molecules that are safer, more effective, and cheaper, and have better kinetics. Also, we discussed the generality about virus and viral diseases life cycle and the generality about epidermal growth factor receptor tyrosine kinase EGFR-TK.

❖ Chapter II: Literature Review

This chapter provides a review of the literature on SARS-CoV-2 and the various molecular modeling methods used in this pandemic (molecular docking, DFT, genetic algorithm and molecular dynamics) and a review of the literature on quinazoline and pyrido[3,4-d]pyrimidine and their activity

❖ Chapter III: Materials and Methods

The third chapter presents definition, theoretical details of each method (global reactivity descriptors, molecular docking and molecular dynamics) and softwares (i.e. Hyperchem, Gaussian 09, Gaussview 16, MarvanSketch and MOE) used in this study.

❖ **Chapter IV: Results and discussions**

The fourth Chapter consists in discussing all the important results based on different approaches.

At first, we aimed to study the global reactivity descriptors on 18 approved drugs. Those drugs were chosen due to their similarities in structure with chloroquine and hydroxychloroquine using DFT method by employing the B3LYP/6-31G+d basis set to identify the most reactive drug.

Then, we studied the affinity of 18 drugs with two receptors in two active sites, the first receptor was ACE2 and the second one was SARS-CoV-2 complexed with ACE2 receptor, using molecular docking method by Molecular Operation Environment MOE software.

Finally, we applied molecular dynamics simulation on the best result of molecular docking in two receptors and studied the stabilization of three drugs Delapril, Ramipril and Lisinopril.

Second, we aimed to study the global reactivity descriptors on 27 derivatives of quinazoline and pyrido[3,4-d]pyrimidine with seven approved drugs. Those compounds were chosen due to their range biological activities using DFT method by employing the B3LYP/6-31G+d basis set to identify the most reactive ligand against EGFR mutation.

Then, we studied the affinity of 27 derivatives of quinazoline and pyrido[3,4-d]pyrimidine with 7 drugs with three receptors, the first receptor was wild-type receptor, the second one was L858R mutation receptor, and the third was T790M mutation receptor, using molecular docking method by Molecular Operation Environment MOE software.

Also, molecular dynamics simulation was applied on the best result of molecular docking in three receptors and studied their stabilization.

Finally, pharmacokinetics properties; absorption, distribution, metabolism, excretion and toxicity was analysed to 27 compounds.

Chapter I:

GNERAL CONCEPTS

Chapter I: General concept

I.   Foundation of Computer-Aided Drug Design (CADD)

I.1.   Overview of CADD

People have used drugs derived from plants or animals to prevent and treat disease since the dawn of civilization. The search for drugs to treat illness and alter mood and consciousness is almost as important as finding food and shelter. Although many medications derived from natural sources are prized, the majority of drugs used in modern medicine are the result of developments in synthetic organic chemistry and biotechnology. As a result, a drug is defined as a natural or synthetic chemical used in the diagnosis, cure, alleviation, treatment, or prevention of disease, or designed to change the structure or function of the body. As a result, a drug is a substance that has an effect on the body's activities [1,2].

A brief history of Computer-Aided Drug Design [3]

- In the 1930s, the X-ray diffraction technique was introduced to reveal the chemical composition and three-dimensional (3D) geometry of tiny molecules.
- A look back at drug-target interactions in the 1960s.
- In the 1980s, automation included high-throughput target/drug selection, information technology, and a Docking research.
- In the 1990s, a computer was used to assemble a genome and conduct a genomic-based target selection study.
- Identifying a large amount of data: Pharmacogenomics in the 2000s.

I.1.1.   Drug Design development steps

The usual drug discovery method is lengthy, complicated, extensive, and costly [4]. Usually takes 13-15 years to develop a drug from concept to commercialization, and it costs 2-3$ billion in the United States in nine years [5]. Several new approaches have been developed and applied in drug research and development (R&D) to exceed the limitations of the traditional research and to reduce the costs. Computational methodologies have been instrumental at various stages of drug discovery [6–8]. Computer-Aided Drug Design (CADD) methods have emerged as a powerful tool in the development of therapeutically important small molecules for over three decades, enabling higher hit rates than experimental High-Throughput Screening (HTS) approaches alone [9,10].

It arose from the following consideration:

- Determine the causes of the sickness.

- Search for the target.

- Carried out bioassay tests for lead compound.

- Finding a lead compound of the target.

- Clinical trials: phase I, phase II and phase III.

- Approval process, drug available.

When a lead substance has some therapeutically undesirable symptoms, drug discovery is focused on structural alteration of the lead compound. Hansch (1964) defined correlations between biological activity and physiochemical aspects of structure using an equation. Using Hammett's substituent constants, the Quantitative Structure Activity Relationship (QSAR) has aided in drug design [1,2].

Only one medicine is released after 5,000 to 10,000 compounds have been studied. Each medicine costs around 156$ million during the discovery phase. Clinical trials process I, II, and III of the Food and Drug Administration (FDA) cost another 75$ million. Then, in order to obtain FDA approval, a lengthy and costly procedure must be followed [2].

I.1.2. Drug Discovery Contributing factors

Other factors, in addition to the costly and lengthy drug discovery cycle, contribute to the constantly changing landscape of the drug discovery environment [2,11,12]:

❖ High-throughput screening and molecular biology advancements.
❖ Basics of demand:
  ➢ Baby boomer population aging.
  ➢ Consumer demand for high-quality health care.
  ➢ Expanded access as well as universal health care.
  ➢ New ground-breaking technologies.
  ➢ Consumer awareness of the quality of nutrition and supplements.
 ❖ Supply fundamentals:
  ➢ Healthcare downsizing.
  ➢ Reluctance of insurers to pay high reimbursements rate.
  ➢ Transition from inpatient to outpatient procedures.

➢ Disease management as well as global management are two conditions that come to mind when thinking about disease management.

I.1.3.   Computer-Aided Drug Design position in the Drug Discovery Pipeline

Because CADD uses a much more targeted search than traditional HTS and combinatorial chemistry, it can enhance the hit rate of novel drug compounds it. Its goal is to understand the molecular basis of therapeutic effect and predict possible derivatives that could help with improve training. The position of CADD in the drug discovery pipeline is represented in Figure 1.
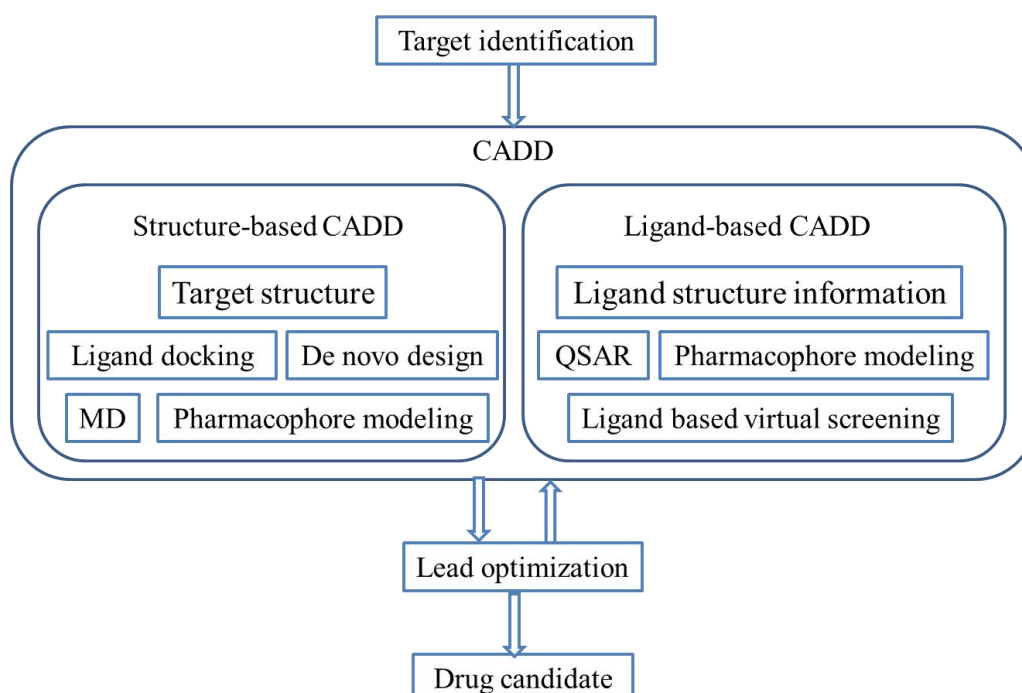
Figure 1 The position of CADD in the drug discovery pipeline.

Note: CADD is used in the drug discovery and development process. A therapeutic target is discovered, and a medication must be designed to combat it. A structure-based or ligand-based strategy is applied depending on the availability of structure information. A successful CADD campaign will allow many lead compounds to be identified. Lead identification is frequently followed by many rounds of lead optimization and then CADD-based lead identification. To identify therapeutic candidates, lead compounds are evaluated in vivo.

I.1.4. The Process of Drug Discovery

Following the identification of the biologic target, the following are the primary steps in the drug discovery process[2,11,12]:

A. Hit identification. This involves screening a vast number of compounds to identify those that interact with the biological target. A hit is a chemical that interacts with a specific target protein.

B. Hit evaluation. This describes the process of hits identified during first screening using varied methods, including biophysical methods and chemical modification of hits by repeated cycles of synthesizing and testing of analogues to generate leads, which are compounds with improved chemical characteristics, thereby increasing their applicability as potential drugs.

C. Lead optimization. Essentially involves further optimizing leads through continuous modification to provide drug development candidates with optimized characteristics for preclinical and clinical testing. The goal of target validation is to find a correlation between the target protein and the specific clinical disease. Changes in the amount of the target protein in cells or animals are frequently correlated with changes in cell biology or animal physiology that are indicative of the illness state.

I.1.5. Computer's roles in Drug Design

1. Information storage and retrieval.
2. Develop information about toxicity and structural activity relationship (SAR).
3. Visualize the similarities between molecules (drugs) that work in the same way.
4. Research the interactions between drugs and receptors.
5. Preform interaction strength and motion dynamics calculations.

I.1.6. Computer Simulation for Drug Design

The first step in developing a new drug is to construct a good candidate molecule, known as a ligand, and then to recognize the target protein and determine how to bind it. Proteins, on the other hand, are extremely adaptable, and their forms frequently alter as they perform their various functions.

As a result, many methodologies are used to investigate protein dynamics. However, in every scenario, the cost and time element are issues to be concerned about. This is why computer simulation of molecular dynamics (MD) is becoming increasingly important.

To get to the point where MD simulation becomes a useful tool for industry, high-performance computing (HPC) is required. However, HPC is a relatively new concept in most pharmaceutical businesses, and supercomputers are not commonly available to industrial researchers. With the introduction of affordable high-performance multi-processors and related development of parallel software industry researchers may now do more realistic computations that were before impossible. Scientists at NOVO Nordisk, a large Danish pharmaceutical company, are convinced that this new capability will change the acceptance of MD simulation dramatically as a tool in the design of novel ligands. They could examine the kinetics of complicated molecular interactions required for ligand recognition by their target proteins for the first time during "Europort-D." [11,12].

I.1.7.   Drug Design Theory

Understanding how the active site of a receptor selectively inhibits the binding of unsuitable structures is the fundamental notion behind drug design. A ligand is any potential chemical that can bind to a receptor. A precise combination of atoms with the correct size, shape, and charge composition is required for a ligand to bind and interact with a receptor. The size and shape of a putative ligand-receptor interaction are complementary, a phenomenon known as steric complementarity (Figure 2).
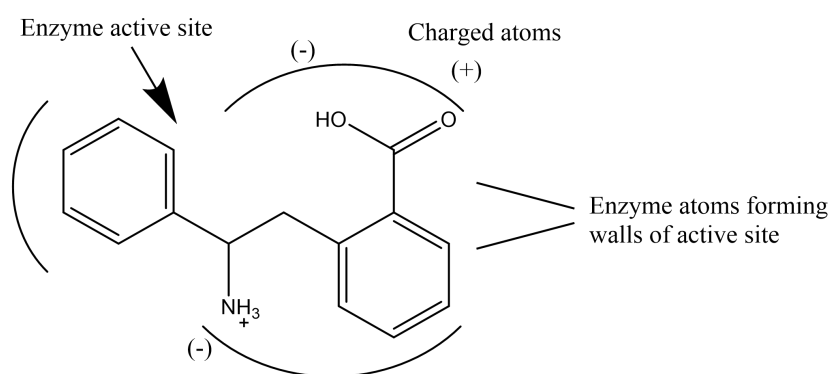
Figure 2 Enzyme active site-Ligand complimentary interactions.

Electrostatic interactions, in addition to steric complementarity, influence ligand binding by preventing inappropriate molecules from interacting since the ligand must have precisely arranged complementary charged atoms for contact to occur. Hydrophobic

contact, on the other hand, is the fundamental driving force behind receptor binding. Water makes up two-thirds of our bodies, and the hydrophobic property of the ligand provides the driving force for it to leave the water and bind to a receptor. There are several potential interactions between ligands and receptors, and the pharmacophore refers to the precise interactions that are required for ligand recognition and binding by a receptor [13].

We may imagine a lock with several tumblers using the lock-and-key analogy. There may now be a variety of keys that are sterically compatible with the lock and fit into the keyhole. However, all keys except the proper one will displace the incorrect tumblers, resulting in a poor interaction with the lock. Only the correct key contacts the relevant tumblers and interacts appropriately with the lock to unlock it, presenting the pharmacophore to the receptor. This is critical in pharmaceutical development since any successful drug must include the necessary chemical structures and deliver the pharmacophore to the receptor (Figure 3) [14].
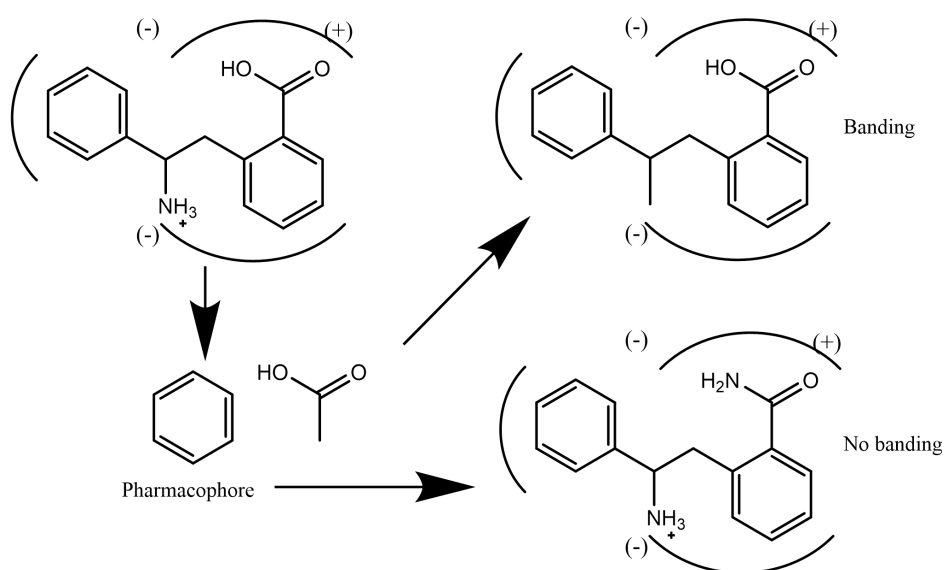
Figure 3 Pharmacophore and receptor binding.

The following are the primary concerns that must be addressed when creating a drug that targets a certain target receptor:

1. Identify receptor targets and define the disease state.

2. Steric, electrostatic, and hydrophobic complementarity of active sites.

3. To assume about receptor biochemical mechanisms.

4. Respect chemistry's laws.

5. To make synthesizing possible.

6. To take into account biological factors.

7. To Consideration of patents

I.1.8. Computers in Drug Design: Success and challenges

There are several papers which describe the successful applications of CADD in the development of novel and potent drug candidates in drug discovery. During the 1990s there were successful applications of CADD in the development of drugs for HIV and flu (influenza). The two most successful outcomes of CADD are Relenza and HIV protease inhibitors [15–17]. Ritonavir was the first HIV protease inhibitor; it was synthesized with sufficient oral bioavailability in 1991[18]. This compound was approved by FDA in 1996, in record time (72 days). The development of this drug took eight years, about half of what a typical drug would need. This achievement was due to application of a structure-based approach and the FDA's rapid review. The same time was observed for saquinavir (Roche) and nelfinavir (developed by Agouron, now a subsidiary of Pfizer) other HIV proteases inhibitors [19,20] which helped transforming the treatment of HIV. Author large number of drugs was identified using CADD. Captopril, an antihypertensive medication licensed in 1981 [21], is an inhibitor of the Angiotensin-Converting Enzyme (ACE). Dorzolamide was approved as a carbonic anhydrase inhibitor in 1995 [22]. A recent study by Kokkonen et al recently revealed that CADD was successful in identifying inhibitors of Sirtuins, a NAD-dependent deacetylase that is a well-known therapeutic target in neurological disorders and cancer [23]. A successful application of CADD against tuberculosis was recently reported [24]. The CADD has had great success in developing and identifying inhibitors for a variety of diseases, including neurological disorders [25], cancer [26,27] and diabetes [28].

In CADD, there are several limits. As a result, copying and simulating the entire biological system on a computer system is not feasible. Target flexibility in drug discovery is one of the most difficult issues to overcome. The ligand is given a lot of flexibility in most molecular docking tools, but the protein is kept fixed or given only limited flexibility to the residues within or near the active site. It is extremely difficult to supply full molecular flexibility to a protein because this increases the computation's space and temporal complexity [29].

However, efforts are being made to add as many parameters as possible. Receptor and target molecules are highly flexible in solution because of conformational changes and shows their impact on the accuracy of docking and scoring [30].

As a result, creating an inhibitor based solely on the search for a single, rigid structure may result in the wrong outcome. The ligand has enough flexibility with docking tools, but the residues near the protein's binding sites have little flexibility. Because of their conformational changes, proteins and ligand molecules have a lot of flexibility in solution [31]. In cellular processes, water molecules perform a crucial role. As a result, docking algorithms must incorporate the effects of water molecules and other solvents [32].

One of the most limitations of pharmacophore-based LBDD is the reliance on pre-computed databases with a finite number of low-energy conformations per molecule. This limits the probability of identifying an active molecule because many conformations are missing; especially those for rotatable bonds of small functional groups such as methyl group in methoxy groups. This limits the approach's capacity to discern between distinct rotations during conformer generation, which has an impact on sampling [33].

However, generation of chemical derivatives is highly amenable to computerized automation. Computers can rapidly generate and predict the binding of all potential derivatives, creating a list of the best potential candidates. Thus, using CADD software helps in the refinement of weakly binding lead compounds in the most effective manner [34,35].

I.1.9.   Chemical structure, representation and analysis

I.1.9.1.   Library

A virtual library must be available for screening in order to perform a virtual screen. Virtual libraries come in a range of sizes and designs, including broad libraries that can be used to screen against any target, focused libraries for a group of related targets, and targeted libraries for a single target [10,36]. A variety of computational technologies can be used to create library databases:

1. Ligand libraries are often constructed by enriching ligands for drug likeness or physiochemical properties suitable for interested target. Drug likeness is commonly checked using Lipinski's rule of five [37].

2. Representation of Small Molecules as "SMILES" (Simplified Molecular Input Line System). Development and efficient use of ligand databases require universally applicable methods for the virtual representation of small molecules SMILES [38].

3. Small Molecule Representations for Modern Search Engines: InChIKey. InChI (International Chemical Identifier)

I.1.9.2. Virtual Screening

Virtual screening is a method of determining if known compounds are likely to be lead compounds for a specific target using computer systems. Although there is no guarantee that 'positive hits' from a virtual screening will be active, and the compounds must still be tested experimentally, the results from a virtual screening can be utilized to improve the efficiency of experimental screening procedures. In other words, if a large number of compounds are available for testing, virtual screening can be used to identify which compounds are most likely to be active, and hence which structures should be prioritized for actual screening. Virtual screening can include looking for pharmacophores that also are known to be effective or docking molecules into target binding sites [39].

- Pharmaceutical investigators are more emphasizes on generating medications that have better properties than already available drugs.
- A molecular target is chosen that is thought to influence a certain disease when it is influenced by a drug. The higher the selectivity, the less the negative effects.
- A useful bioassay must be developed to show whether or not a drug has activity against a specific target.
- Compounds can be tested for their affinity to a macromolecular target by NMR spectroscopy. The relaxation times of ligands bound to a macromolecule are shorter than when they are unbound.
- Virtual screening can used to identify compounds most activated in experimental screening.

I.1.10. Biological structures

Knowledge of the 3D structures of proteins has long been recognized as having the potential to speed up drug discovery, but recent advances in genome sequencing, robotics, and bioinformatics have dramatically expanded the possibilities. Many new protein targets have been developed by starting with a gene sequence, producing a functional protein, and

then determining the three-dimensional structure of the protein. Structural biology has played a key role in not just lead optimization and target identification, where it has a long history, but also lead discovery, now that high-throughput structure determination technologies may provide powerful screening approaches [12,40,41].

I.1.11. Molecular modelling and energy minimization

The current growth in gene databases and "structural genomics" will eventually give vital sequence information, but inferring structure from sequence is typically impossible due to a lack of understanding of the principles of protein folding. More promising are targeted investigations that strive to understand the basic chemistry and physiology of a disease. For instance, the invention of HIV proteinase inhibitors [42,43] has to be one of the most remarkable accomplishments in the brief history of structure-based drug design. A new approach uses molecular biology technologies to scan a diseased vector; out of the many important proteins produced, just a few can be isolated, crystallized, and structurally characterized. *Pyrobaculum aerophilum*, for example, has been identified as a cofactor for HIV-1 and T-cell leukemia virus I transactivator proteins Rev and Rex. It was investigated at 1.75 resolution [44] and recognized as a chemical interdiction target. Compounds can be created to specifically block pathogenic enzymes or receptors by comparing the structures of normal and sick molecules.

So, if you know the structure of a target protein and the function of its receptor or active site, you can use computer tools to design and dock a ligand or inhibitor ("new leads") before spending time and money on synthesis and testing. Large-scale screening, on the other hand, may uncover "new leads" that must be modelled before further research into synthetic analogues. In either situation, molecular modeling is required to comprehend and investigate the structure-function link. The sum of attractive and repulsive forces can be calculated, and the fit can be measured. To ensure that novel compounds can be tested before being manufactured, a correlated listing of experimental and computational values is ideal [45].

The equilibrium configuration of molecules and solids is computed using energy minimization, also known as energy optimization or geometry optimization. We can only get a final state of the system that corresponds to a minimum of potential energy using this strategy. GAMESS, Ghemical, PS13, and TINKER are energy minimization tools. Quantum mechanical computations can be done with Ghemical or PS13 [46].

I.2.   Structure-Based Drug Design (SBDD)

SBDD, or direct drug design, is based on understanding the 3D structure of the biological target (protein), which can be determined using techniques like X-ray crystallography or NMR spectroscopy. To begin the SBDD structure paradigm, a 3D-protein structure of the receptor at atomic resolution is required. The crystal structure should be well defined, with a resolution of at least 2.5 usually being required [47]. When the target's 3D structure is not available, a virtual model can be created by homology modeling the protein closest to the target that has a known and available 3D structure [48]. However, unless receptor site residues are highly conserved, utilizing homology models for virtual screening is significantly riskier than using solved structures.

I.2.1.   Molecular Docking

I.2.1.1.   Concept of Molecular Docking

Molecular docking is a rapid approach to anticipate the orientation of a ligand-receptor complex while accounting for receptor structure [49]. Docking is the process of computing the binding affinity of a protein structure to a ligand. This method entails meticulous sampling of all possible ligand poses in the target protein's binding pocket in order to facilitate optimal binding geometry, as determined by established scoring functions [50,51]. Small molecule docking can be done in one of three ways: rigid docking, where both the target and the ligand are treated as rigid; flexible ligand docking, where the target is held stiff; or flexible docking, where both the target and the ligand are treated as flexible [52]. Molecular Docking can be used to investigate several elements of ligand-receptor binding characteristics such as complementarity and affinity, among other things. Genetic algorithms, molecular dynamics, simulated hardening, Monte Carlo methods, and other approaches are commonly employed in Molecular Docking. The docking technique has two key steps: the first is a search algorithm, and the second is a scoring function [53]. A good docking method should explore all possible binding modes between the ligand and the receptor target; however, due to the huge size of the search space, this is impossible.

As a result, constraints, restraints, and approximations are used to reduce the problem's dimensionality in order to discover the global minima as quickly as possible. Partial flexibility (side chain) has recently been added into certain docking algorithms, such as GLIDE [54], GOLD [55], FlexX[56], and others, because protein structures have a lot of

conformational space. A lot of people employ genetic algorithms: AUTODOCK, GOLD, MOE and Monte Carlo simulated annealing techniques GLIDE.

The genetic algorithm is an iterative procedure that maintains a population of individuals who are contenders for the problem's solution. Simulated annealing, on the other hand, is an iterative technique in which one candidate solution is repeatedly updated until it reaches a termination condition [12].

I.2.1.2.   Virtual Screening

Virtual screening, as previously said, is a multi-step procedure. Although the entire process can be totally automated in theory, it is strongly recommended to allow for manual interventions, as visual inspection and selection still play a significant role. Typically, the procedure begins with a thorough examination of the available 3D protein structures. Highly similar structures will be examined if possible, either to create new ideas for ligand structural motifs or to get insight into how to achieve selectivity against other proteins in the same class. A superposition of various protein-ligand complexes yields some insights into critical interactions seen in tight-binding protein-ligand complexes. An overlay like this will also draw attention to flexible portions of the protein or recurrent water molecules in the binding location that could be used in the docking process [57].

I.2.2.   Molecular Dynamics Simulations

Studying macromolecules like proteins, DNA or RNA on an atomic level using experimental techniques is very complex, time consuming and expensive [58].

Molecular Dynamics (MD) simulations are a computational approach that provides access to a receptor protein's conformational ensemble [59]. A numerical solution of Newton's law of motion over time is used to mimic the evolution of an atomic system. A molecular mechanics force field evaluates the potential energy at each time step [60]. A surrounding water shell is added to the system's beginning configuration, which is produced from an X-ray or NMR structure of the macromolecule. The quickest movements in the system (hydrogen locations) are chosen as the time interval, which is typically in the sub-femto-second scale, allowing for numerical integration over the differential equation for particle movements. As a result, for each atom in the system, new locations, forces, and velocities are calculated after each time step. A so-called system trajectory is successfully created

after a large number of iterations, providing an in silico image of biomolecular motions in solution [61].

I.2.2.1. *Principals of Molecular Dynamics Simulations*

MD simulations provide a complete atomistic view of (bio-) molecular motions on the femtosecond to microsecond scale. The free energy landscape determines which states will contribute to an ensemble of structures at a given temperature. Also kinetic aspects, e.g., transition frequencies between different states are determined by the energy barriers within the free energy landscape of the system [59]. Molecular dynamics simulations explore the landscape given an energy distribution determined by the system's temperature. First computer simulations of a protein system were described in 1977 [62] with a trajectory length of 9 ps in vacuo. Within this time scale side chain movements could be observed, whereas the backbone geometry remained virtually unaffected. Since then continuous increase in computing power allowed extension of sampling time. Time scale of most publications we will refer to is in the nanosecond range. Loop movements including fast domain motions can be observed within this time scale [59].

I.2.2.2. *Free energy calculation: MM-GBSA*

To evaluate the theoretical free energies of binding of ligands to the receptor, generally, two methods are commonly used first, the molecular mechanics generalized Born surface area (MM-GBSA) and second molecular mechanics Poisson-Boltzmann surface area (MM-PBSA). These two methods are equally efficient in predicting the correct binding affinities [63,64].The MM-GBSA method was used to calculate the relative binding free energies of anti-HIV drugs and B. papyrifera polyphenols to Mpro.

The free energy of binding can be calculated as:

$$\Delta G_{bind} = \Delta H - T\Delta S \tag{1}$$

$$\Delta H = \Delta E_{elec} + \Delta E_{vdW} + \Delta G_{polar} + \Delta G_{non\text{-}polar} \tag{2}$$

where E_{elec} and E_{vdW} are the electrostatic and Van Der Waal's contributions, and G polar and G non-polar are the polar and non-polar solvation terms, respectively. The polar contribution of the free energy is estimated by a generalized Born model with an external dielectric constant of 80 and an internal dielectric constant of 1, while the non-polar energy contribution is calculated from the solvent accessible surface area (SASA). As similar

types of ligands bind to the receptor, the entropic contribution is neglected here. Therefore, our calculated values referred to as relative binding free energies (ΔG bind). MM-GBSA is a popular method to calculate binding energy, which uses energy properties of free ligand, free receptor and receptor-ligand complex for binding affinity calculation.

I.3.   Ligand-Based Drug Design

I.3.1.   Conceptual Density Functional Theory (DFT)

The use of Computational Chemistry methodologies has a very important role in the practice of modern medicinal chemistry, offering a great potential for the improvement of the different phases of drug research, with special emphasis on time and cost savings [65]. The recent impact of density functional theory (DFT) in the development of quantum chemistry is considerable, and can be linked to achievement of so-called ''chemical accuracy'' at the end of the 1980s when gradient-corrected and hybrid functional methods were introduced [66,67]. Based on the the famous Hohenberg and Kohn theorems in 1964 [68], DFT focuses on the electron, density, $p(\mathbf{r})$, itself as the carrier of properties of molecules (or atoms) at much lower costs than traditional ab initio wave function techniques [69].

Introducing orbitals into conceptual DFT was done in the Kohn-Sham formalism [70]. Kohn-Sham methodology includes the estimation of the molecular energy and density of a given system, as well as the orbital energies, explicitly connected with the frontier orbitals including the Highest Occupied Molecular Orbital (HOMO) and Lowest Unoccupied Molecular Orbital (LUMO)

I.3.1.1.   Fundamental and Computational Aspects of DFT

a.   The Basics of DFT: The Hohenberg−Kohn Theorems

In chemical reactions, bonds form and break due to accumulation and depletion of electron density in between the nuclei. Understanding of how the electron density in molecules is redistributed in course of a chemical reaction is thus the crux of chemistry. For system containing N electrons bound by an external potential v(r), the Hamiltonian H is completely specified by N and v(r). Knowing Hˆ one can solve the Schrödinger equation to obtain the many-electron wavefunction ψ (r$_1$, r$_2$, ... , r$_N$), which contains all the physical information about the system. Integrating over the coordinates of (N-1) electrons one obtains the single-particle density or the electron density p(r) as:

$$p(r) = N\int\ldots\int\psi^*(r_1, r_2, \ldots r_N)\,\psi(r_1, r_2, \ldots, r_N)\,dr_2\ldots dr_N \tag{3}$$

which integrates to the total number of electrons,

$$\int p(r)dr = N \tag{4}$$

Therefore N and v(r) determine $p(r)$. That is, there is a mapping from v(r) to $p(r)$[70].

b. DFT as a Tool for Calculating Atomic and Molecular Properties: The Kohn−Sham Equations

When considering quantitative aspects associated with Conceptual DFT descriptors, the Kohn-Sham approach comes in handy. The employment of a range-separated exchange-correlation density functional in Kohn–Sham DFT is causing a lot of controversy right now. [71]. The partitioning of the exchange and the operator into long- and short-ranged components, along with a range-separation parameter that governs the rate at which long-range behavior is obtained, is critical to the construction of these density functional. Using a molecule-by-molecule approach and following to some tuning criteria, the estimation of can be fixed or "tuned." The optimum tuning process relies on the KS HOMO energy being related to the vertical ionization potential (IP), which is a calculation of the energy differential, E(N-1)-E(N-1) (N). In the case of an N-electron molecular system, the Generalized KS theory should be applied.

$$-IP(N) = e_H(N) \tag{5}$$

It might be thought of as the DFT equivalent of the well-known Koopmans' theorem. In reality, only the exact density functional is valid. In the case where we must examine an approximated density functional for practical reasons, there may be a significant difference between -IP(N) and eH. (N), As a result, perfect tuning entails establishing a system-specific range-separation parameter.

I.3.2. Pharmacokinetics Properties

During the early stages of drug development, candidate drugs' activities and specificities are typically assessed first, followed by pharmacokinetics and toxicities evaluations [72]. However, many candidate drugs failed in the final stage due to poor efficacy and safety, which was mostly, caused by absorption, distribution, metabolism, excretion, and toxicity (ADMET) characteristics [73]. They discovered that the most important causes for the

failure of more than half of all project closures were poor safety and toxicity. The importance of filtering and optimizing the ADMET features for pharmaceuticals at an early stage has been recognized and widely employed to lower the attrition rate in drug research and development, similar to the development of drug discovery [74]. In vitro and in vivo ADMET prediction approaches have been popular in recent years, however doing sophisticated and expensive ADMET tests on a large number of drugs is unfeasible. As a cost-effective and high-throughput alternative to experimental testing methods, an in silico way to predict ADMET characteristics has become particularly appealing [75].

I.3.2.1.   Computational tools employed in ADMET

There are two components to consider: data modelling and molecular modelling, each with its own toolbox. Quantitative Structure Activity Relationship (QSAR) techniques are commonly used in data modelling. The QSAR method looks for connections between a particular property and a series of chemical and structural descriptors for the molecules in consideration. Over the previous 60 years, a wide range of descriptors for use in QSAR research have been generated (e.g, those available in the program Dragon) [76]. A subset of these descriptors may be useful in forecasting ADME features in the future.

Molecular modelling uses quantum mechanical methods to analyse the possibility for interaction between small compounds and proteins known to be involved in ADME processes, such as cytochrome P450s. If the human protein structure is not known, homology modelling of related structures can be used to construct three-dimensional structural information on the protein [77].

II.   Virus and Viral Diseases

II.1.   Overview

Viruses are non-cellular, infectious agents which take over a host cell in order to survive and multiply. There are many different viruses able to infecting bacterial, plant, or animal cells, with greater than 400 known to contaminate people. Those capable of being transmitted to humans from animals or insects can be particularly dangerous and belong to a class of diseases defined as zoonoses. Consequently, each human and veterinary medicine play important roles in the control of such diseases. Viruses may be transmitted in a variety of ways. Those responsible for diseases such as influenza (flu), chicken pox,

measles, mumps, viral pneumonia, rubella, and small-pox may be transmitted through the air by an infected host sneezing or coughing. Other viruses may be transmitted by means of arthropods or ticks, leading to diseases such as Colorado tick fever and yellow fever. Some viruses are unable to live for long outside the host and are transmitted through physical contact [39].

Various flu epidemics and pandemics have proved devastating. The number of deaths worldwide due to the flu pandemic of 1918-1919 is estimated to be over 20 million-far larger than the number killed by military action during World War I. Since the 1980s to 2007, 30 million people have died as a result of HIV infection [78,79].

Nowadays, with reasonably-priced and with ease to be had air travel, travellers are able to visit remote areas, thus increasing the possibilities of rare or new viral diseases spreading around the world. Therefore, it is important that world health authority's monitor potential risks and take speedy, appropriate action when required. The outbreak of severe acute respiratory syndrome (SARS) in May 2003 could have had a devastating effect worldwide if it had been ignored. Fortunately, the world community acted rapidly and the disease was brought under control relatively quickly. Nevertheless, the SARS outbreak serves as a timely warning of how dangerous viral infections can be [80].

II.2. Structure of Viruses

At their simplest, viruses can be regarded as protein packages transmitting foreign nucleic acid between host cells. The type of nucleic acid present depends on the virus concerned. All viruses contain one or more molecules of either RNA or DNA, but not both. They can, therefore, be defined as RNA or DNA viruses. Most RNA (animal/plant) viruses contain single-stranded RNA (ssRNA), however some viruses contain double-stranded RNA (dsRNA). If the base sequence of the RNA strand is identical to viral mRNA, it is called the positive (+) strand. If it is complementary, it is called the negative (-) strand. Most DNA viruses contain double-stranded DNA (dsDNA), but a small number contain single-stranded DNA (ssDNA). The size of the nucleic acid varies widely, with the smallest viral genomes coding for 3-4 proteins and the largest coding for over 100 proteins [81]. The viral nucleic acid is contained and protected within a protein coat called the capsid. Capsids are usually made up of protein subunits called protomers which are generated in the host cell and can interact spontaneously to form the capsid in a process called self-

assembly. Once the capsid contains the viral nucleic acid, the whole assembly is known as the nucleocapsid. In some viruses, the nucleocapsid may contain viral enzymes which are crucial to its replication in the host cell. For example, the flu virus contains an enzyme called RNA-dependent RNA polymerase within its nucleocapsid (Figure 4).
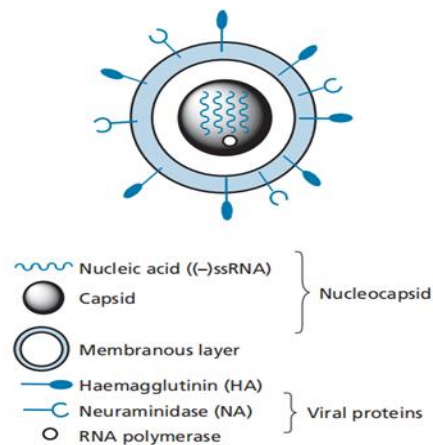
Figure 4 Diagrammatic representation of the flu virus.

II.3. Life cycle of viruses

The various stages involved in the life cycle of a virus are as follows [82]:

a. **Adsorption**: A virion must initially bind to the host cell's outer surface. This occurs when a specific molecule on the virion's outer surface binds to a protein or carbohydrate in the host cell membrane. As a result, the appropriate molecule on the host cell can be thought of as a virion's'receptor.' Of course, this molecule was not generated by the host cell in order to serve as a viral receptor. The molecules in question are usually glycoproteins, which perform important biological tasks such as hormone binding. The virion, on the other hand, takes advantage of these, and once bound, the next stage may begin: viral nucleic acid introduction into the host cell.

b.   **Penetration and uncoating**: Different viruses employ different mechanisms to get their nucleic acid into the host cell. Some nucleic acids are injected through the cell membrane, while others enter the cell uncoated. This can happen in a number of different ways. Some virions' viral envelopes merge with the plasma membrane, allowing the nucleocapsid to enter the cell (Figure 5). Other virions enter the cell through endocytosis, in which the cell membrane wraps around the virion and is

subsequently pinched off, forming an endosome. These vesicles subsequently fuse with lysosomes, allowing the virus to uncoat itself with the help of host cell enzymes. Uncoating is also triggered by a low endosomal pH. The nucleocapsid is released into the cell when the viral envelope unites with the lysosome membrane. Whatever technique is used, the end outcome is viral nucleic acid being released into the cell.

c. **Replication and transcription**: There are two types of viral genes: early and late. The host cell is taken over by early genes, which cause viral DNA and/or RNA to be generated. From virus to virus, the process involved is different.

d. **Synthesis and assembly of nucleocapsids**: Late genes control the production of capsid proteins, which self-assemble to form the capsid. The nucleocapsid is formed by incorporating viral nucleic acid into the capsid.

e. **Release**: Cell lysis, in which the cell is destroyed, releases naked virions. Viruses with envelopes, on the other hand, are frequently disseminated through a process known as budding (Figure 5). Viral proteins are initially integrated into the plasma membrane of the host cell. The nucleocapsid then attaches to the cell membrane's inner surface, causing viral proteins to accumulate at the location while host cell proteins are excluded. The viral proteins-containing plasma membrane wraps around the nucleocapsid and is squeezed away from the cell, releasing the mature virion.
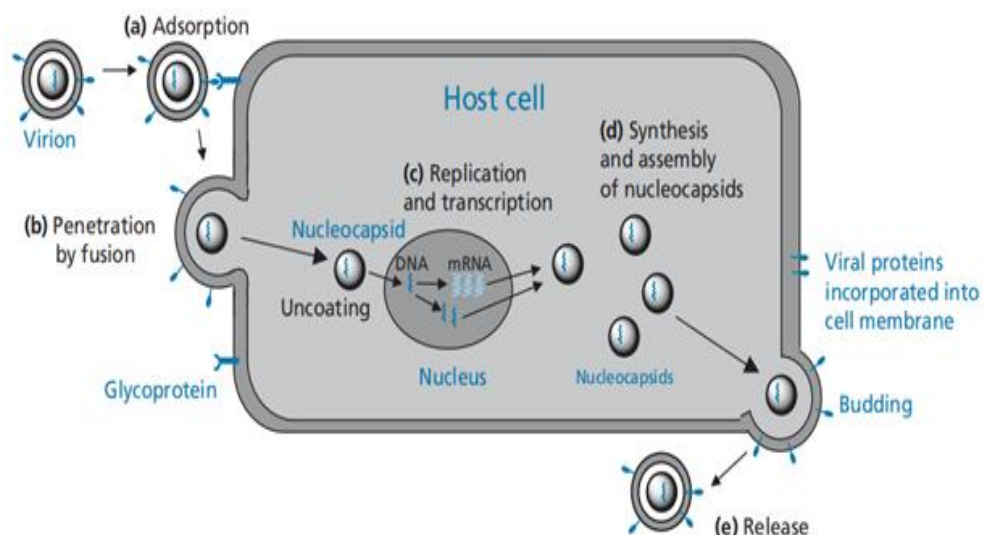
Figure 5 Life cycle of a DNA virus such as herpes simplex.

II.4. The Spike Protein: Key to the Host Cell

The SARS-S protein is a type I transmembrane protein that has 1,255 amino acids and 23 N-linked glycosylation consensus signals [83]. The secretory pathway of infected cells produces S protein. It has a signal sequence at the N-terminus that allows the nascent protein to be imported into the endoplasmic reticulum, where it is folded and modified with mannose-rich carbohydrates. Most, if not all, of a high-mannose carbohydrates are converted into complex glycans when the protein is transported into the Golgi apparatus [84]. There has been no evidence of SARS-S being O-glycosylated. The cytoplasmic tail of SARS-S has an unique dibasic ER retrieval motif that enhances S protein accumulation at the ER–Golgi intermediate compartment and the Golgi region [85], the locations where progeny particles are put together [86,87]. The membrane protein (M), the envelope protein (E), and the nucleocapsid protein (N) are all involved in the formation and budding of new particles [87]; Interactions with the M protein may make it easier for the S protein to get inside nanoparticles. The S protein trimers protrude from the viral envelope and give virions a crown-like appearance, hence the term "coronaviruses".

SARS-S has a domain arrangement that is similar to that of some well-studied viral membrane proteins, such as influenza virus hemagglutinin (HA) and HIV envelope protein [83]. These proteins, known as class I fusion proteins, use similar mechanisms to assist the fusion of viral and host cell membranes. Class II fusion proteins, such as those present on flavi- and alphaviruses, are differentiated by their distinct spatial structure and the specific configuration of functional components required for fusion with target cells: Class I fusion proteins have an N-terminal surface unit (SU) and a C-terminal transmembrane unit and are inserted perpendicular to the viral membrane (TM). The globular SU interacts with cellular receptors, whereas the TM facilitates viral-host cell membrane fusion [88]. The existence of a fusion peptide and two helical regions (HR), which are conserved elements that are intricately involved in the membrane fusion process, is required for the latter step Figure 6 [89].
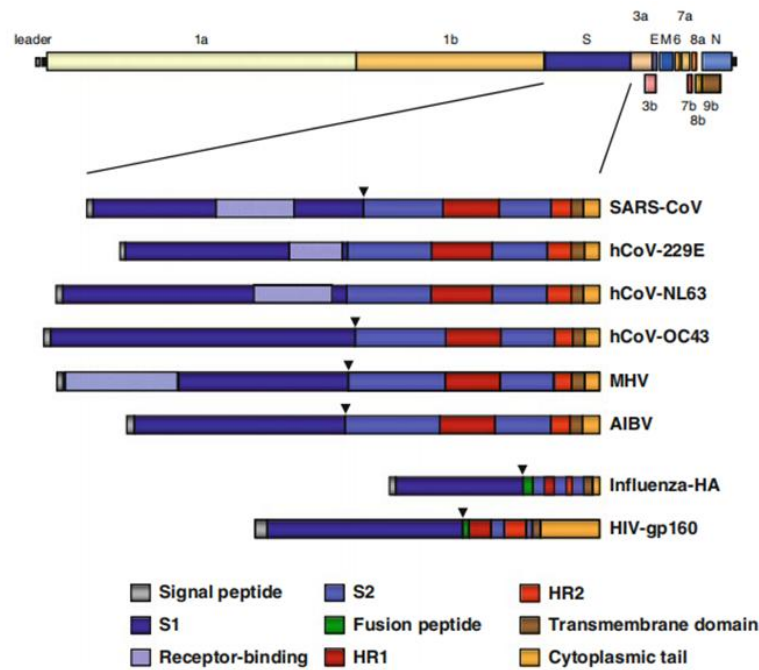
Figure 6 Domain organization of coronavirus S proteins.

Note: AIBV: avian infectious bronchitis virus; hCoV: human CoV; HR: helical region; MHV: murine hepatitis virus; SARS: severe acute respiratory syndrome. The position of the S protein open reading frame in the SARS-CoV genome is indicated in the upper panel. Coronavirus S proteins exhibit a domain organization characteristic for class I fusion proteins. The domain organization of prototype class I fusion proteins, the HIV envelope protein, and the influenza virus HA is shown below. A signal peptide is located at the N terminus and mediates import of the nascent protein into the secretory pathway of infected cells. The surface unit S1 contains a receptor binding domain (RBD), which allows engagement of cellular receptors for infectious entry. The transmembrane unit (S2) harbors functional elements pivotal to membrane fusion: a fusion peptide, two helical regions, and a transmembrane domain. Proteolytic cleavage into the S1 and S2 subunits by host-cell proteases is indicated by a triangular arrow [83].

II.5.   The Two Faces of ACE2: SARS-CoV Receptor and Protector against Lung Damage

SARS-S-dependent cell–cell and virus–cell fusion [90], suggesting that ACE2 might play In contrast to attachment factors, cellular receptors are indispensable for infectious viral entry. In order to discover such factors, several laboratories used the soluble SARS-S1 subunit for co-immunoprecipitation of cellular binding partners. A milestone study by Li

and colleagues identified the carboxypeptidase ACE2, an integral part of the renin-angiotensin system, as a high-affinity SARS-S interactor [90]. Ectopic expression of ACE2 on barely permissive 293T cells facilitated efficient an important role in SARS-CoV entry. Similar results were obtained by an independent study [91], which used a comparable approach to identify cellular binding partners of SARS-S. Subsequently, it was shown that endogenous expression of ACE2 correlates with susceptibility to SARS-CoV infection of cell lines [92] and that ectopic expression of ACE2 facilitates SARS-S-driven infection of otherwise nonsusceptible cells [93]. Moreover, it was demonstrated that SARS-CoV infects ACE2-positive type II pneumocytes and ACE2-positive cells in the intestinal epithelium. Finally, knock-out of ACE2 in mice was found to largely abrogate susceptibility to SARS-CoV infection [94], indicating that ACE2 functions as a bona fide SARS-CoV receptor, which is necessary and sufficient for infectious entry into target cells.

II.6.   Severe Acute Respiratory Syndrome CoronaVirus-2

Coronavirus severe acute respiratory syndrome coronavirus-2 (SARS-CoV-2) belongs to enveloped positive-sense, single-stranded RNA virus Similar to SARS and MERS. It belongs to the family Coronaviridae and the order Nidovirales, are classified as α-, β-, γ- and δ-coronavirus. α- and β-coronavirus can infect humans, while γ- and δ-coronavirus can infect humans indirectly by animals [95]. The coronavirus (severe acute respiratory syndrome coronavirus-2) causing COVID-19 is a β-coronavirus and shares about 80% RNA sequence consistency with SARS-CoV. The SARS-CoV-2 genome encodes four main non-structural proteins: helicase, M pro, RNA-dependent papain-like protease and RNA polymerase [96].

II.6.1. SARS-CoV-2 life cycle

The virus particles are spherical or pleomorphic in shape. The genome organization of SARS-CoV-2 is similar to other coronaviruses, which is composed of mainly the open reading frames (ORFs). Roughly 67% of the genome encodes by the ORF1a/b and it encodes for 16 non-structural polyproteins (nsp1-16), while the remaining 33% encodes for accessory proteins and structural proteins. ORF1a and ORF1b contain a frameshift which produces two polypeptides, pp1a and pp1ab. Papain-like protease (PL-pro) or chymotrypsin-like protease (3CLpro), process these two polypeptides into 16 nsps [97]. Cell entry of coronaviruses depends on binding of the viral spike (S) proteins to cellular receptors and on S protein priming by host cell proteases. Unravelling which cellular

factors are used by SARS-CoV-2 for entry might provide insights into viral transmission and reveal therapeutic targets [98].In the following the replication cycle of SARS-CoV-2 is explained together with possible inhibitors and their respective targets. The life cycle of SARS-CoV-2 was presented in Figure 7[99].
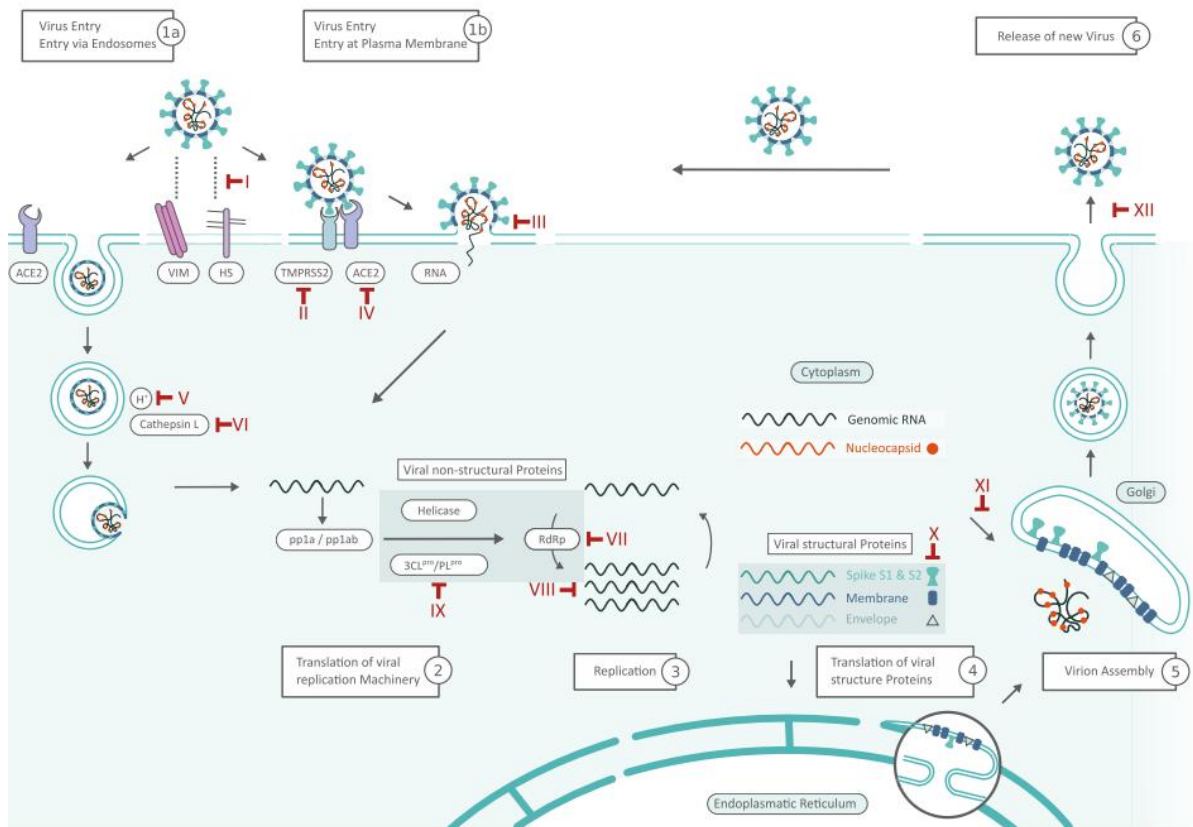
Figure 7 SARS-CoV-2 Replication Cycle.

III.   Epidermal growth factor receptor tyrosine kinase

III.1. EGFR signal pathway and cancers

EGFR is a transmembrane tyrosine kinase receptor that goes by the names ERBB1 and HER1. The human epidermal receptor (HER) family includes EGFR, which is an important component of cell signaling pathways. Binding of ligands (EGF and TGF-α) causes conformational changes in EGFR, as well as homodimerization or heterodimerization with other members of the HER family. With the help of adaptor

proteins (e.g., SHC and GRB-2), the cytoplasmic tyrosine kinase (TK) domain is autophosphorylated, triggering downstream signaling. There are three major downstream pathways: (1) the rat sarcoma (RAS)/rapidly accelerated fibrosarcoma (RAF)/mitogen-activated protein kinase (MAPK) pathway; (2) the phosphatidylinositol-3-kinase (PI3K)/protein kinase B (AKT) pathway; and (3) the janus kinase (JAK)/signal transducers. EGFR is also a stimulator of cancer growth. Cancers, particularly lung cancer, are linked to EGFR gene mutations and protein overexpression, both of which activate downstream pathways. The significance of EGFR in lung tumors lends credence to the concept of 'oncogene addiction.' Tyrosine kinase inhibitors (TKIs) are used to treat cancers with EGFR mutations or abnormal EGFR activity. Through competitive interaction with ATP, TKIs can reversibly block the EGFR TK domain. These pathways are essential for cell development in the normal state (Figure 8 [100]). TKIs also cause tumor cell death by apoptosis mediated by BCL2-like 11 (BIM). Patients with EGFR-activating mutations, on the other hand, benefit from treatment with EGFR-TKIs (e.g., gefitinib and erlotinib) for less than a year before developing drug resistance. EGFR-TKI resistance has a complicated origin. The etiology of EGFR-TKI resistance can be categorized into the following categories based on the cell signal transduction pathway.
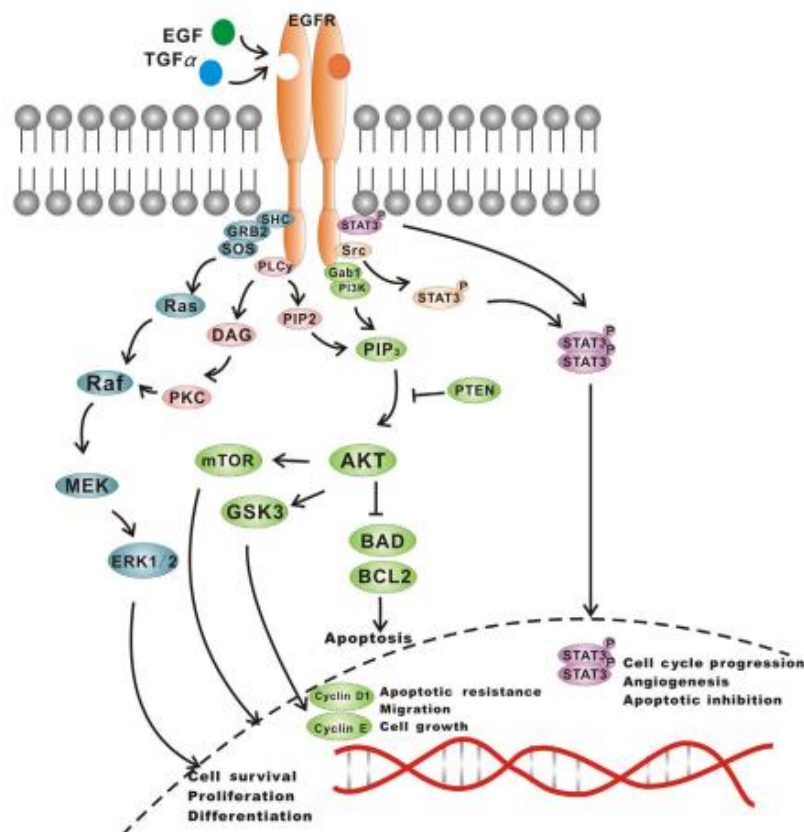
Figure 8 EGFR and its signal pathway.

Note: There is subsequent autophosphorylation of the cytoplasmic tyrosine kinase domain, which, with the aid of adapter proteins (e.g., SHC and GRB-2), triggers downstream signaling. The principal pathways included: (1) RAS/RAF/MEK, (2) PI3K/AKT and (3) JAK/STAT pathways.

III.2. Mutation status of related genes

EGFR (HER1 or ERBB1), HER2 (EGFR2 or ERBB2/NEU), HER3 (EGFR3 or ERBB3), and HER4 (EGFR4 or ERBB4) are the four molecules that make up the EGFR family. HER2 has significant kinase activity but no known ligand, whereas HER3 has no kinase activity. Lung adenocarcinomas have recently been found to have somatic HER2 TK domain mutations. HER2 mutations were similar to EGFR in-frame duplications/insertions in that they targeted the same location (3′ of the C-helix) in exon 20 (Figure 9 [101]). East Asian ethnicity, female gender, and never-smoker status were also linked to HER2 mutations. The striking resemblance between these two genes' mutations is unparalleled. KRAS, which encodes a tiny GTP-binding protein, is a well-known oncogene that is frequently triggered in human malignancies by missense mutations. KRAS mutations were

found in about 20% of NSCLC cases, particularly in adenocarcinoma and smokers. [102]. Because KRAS binds to BRAF, both genes are members of the EGFR family signaling pathway. BRAF mutations, on the other hand, are far less common (0–3%) in lung cancer [103] than KRAS mutations.. Although BRAF is a nonreceptor serine/threonine kinase, its kinase domain is comparable to that of other protein kinases, such as the EGFR family [101].
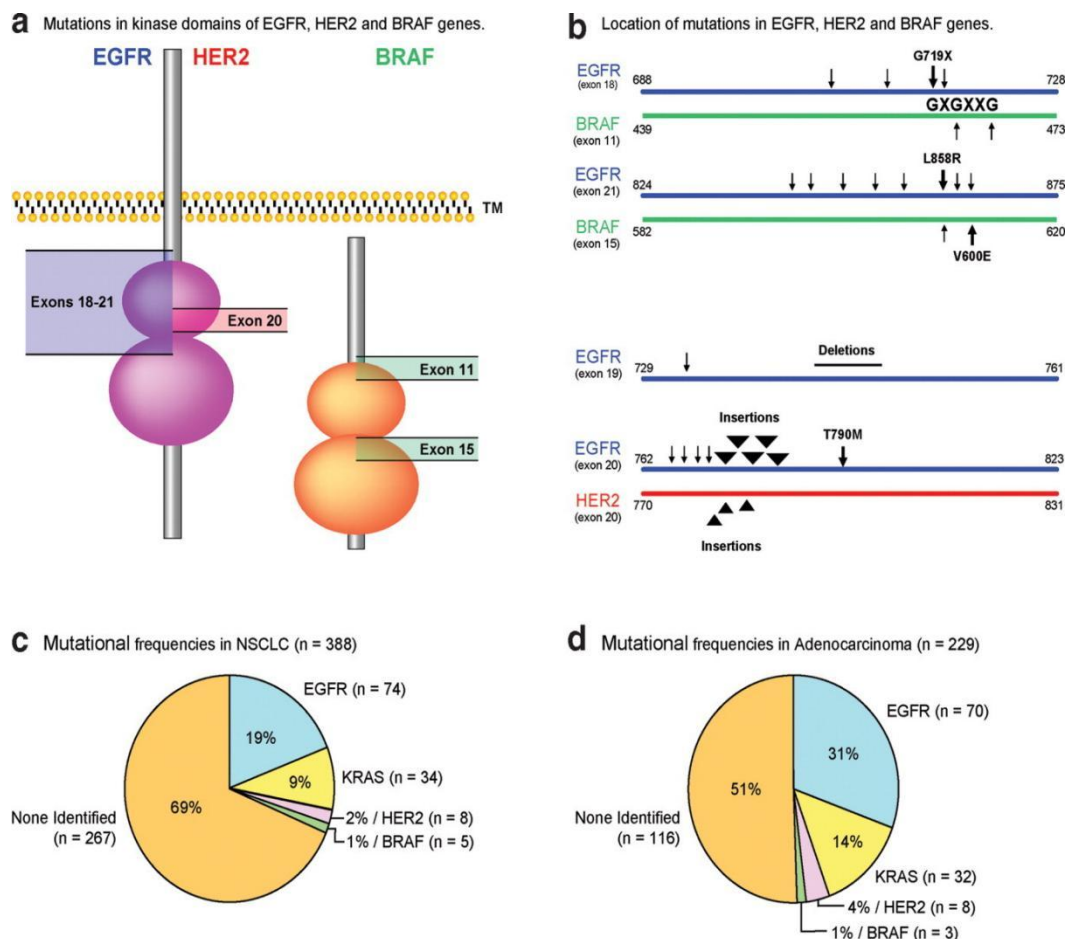
Figure 9 Mutations of related genes in lung cancers.

Note: (a) Mutations in kinase domains of EGFR, HER2 and BRAF genes. Exons 11 and 15 of BRAF are homologous to exons 18 and 21 of the EGFR gene. TM, transmembrane region. (b) Location of mutations in EGFR, HER2 and BRAF genes. Thin arrows indicate rare missense mutations. Numbers are codons for each gene. (c) Mutational frequencies in NSCLC (n = 388). (d) Mutational frequencies in adenocarcinomas (n = 229).

III.3. Biological and clinical implications of EGFR mutations in lung cancer

The tyrosine kinase domain of EGFR has mutations. Point mutations at codon 719 (G719X), deletions in exon 19, insertion mutations in exon 20, and a point mutation at codon 858 in exon 21 are the four main types of mutations. At codon 719 (3.2 %), mutations are common, and the patterns of amino acid substitutions are not homogeneous, resulting in alterations from glycine to cysteine, serine, or alanine (Figure10 [104]). Exon 19 mutations resulting in the deletion of five amino acids Glucine-Leucine-Arginine-Glucine-Alanine (ELREA) and a leucine-to-arginine mutation at codon 858 (L858R) are the two most common types of mutations, accounting for 90% of all mutations. These two forms of EGFR mutations result in enhanced and persistent phosphorylation of EGFR, as well as activation of downstream antiapoptotic enzymes (PI3K/AKT and STAT). EGFR mutations, on the other hand, have a smaller impact on proliferation via the RAS/RAF/ERK/MAPK pathway [104].
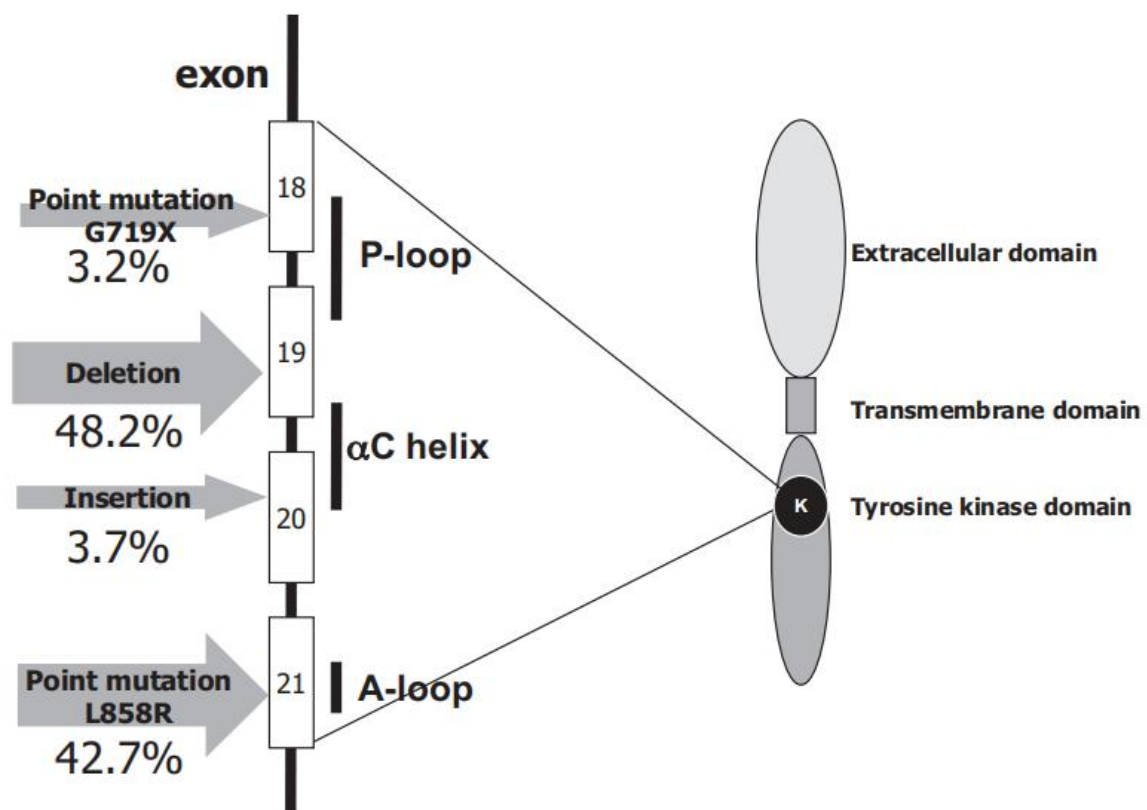
Figure 10 Distribution of EGFR mutations (n = 569).

IV.   References

1.   Fujita T, Iwasa J, Hansch C. A New Substituent Constant, ir, Derived from Partition Coefficients. J Am Chem Soc. 1964;86(23):5175–80.

2.   Lemke TL, Williams DA, Roche VF, Zito S. W. FOYE'S Principales of Medicinal Chemistry. 7th ed. Philadelphia, PA 19103; 2012.

3.   Prada-Gracia D, Huerta-Yépez S, Moreno-Vargas LM. Application of computational methods for anticancer drug discovery, design, and optimization. Boletín Médico Del Hosp Infant México (English Ed [Internet]. 2016;73(6):411–23. Available from: http://dx.doi.org/10.1016/j.bmhime.2017.11.040

4.   DiMasi JA, Hansen RW, Grabowski HG. The price of innovation: New estimates of drug development costs. J Health Econ. 2003;22(2):151–85.

5.   NOSENGO N. New tricks for old drugs. Nature. 2016;534:314–6.

6.   Nantasenamat C, Prachayasittikul V. Maximizing computational tools for successful drug discovery. Expert Opin Drug Discov. 2015;10(4):321–9.

7.   Gasteiger J. Chemoinformatics: Achievements and challenges, a personal view. Molecules. 2016;21(2).

8.   Nag A, Dey B. Computer-Aided Drug Design and Delivery Systems. McGraw-Hill Education; 2011.

9.   Mueller R, Dawson ES, Meiler J, Rodriguez AL, Chauder BA, Bates BS, et al. Discovery of 2-(2-Benzoxazoyl amino)-4-Aryl-5-Cyanopyrimidine as Negative Allosteric Modulators (NAMs) of Metabotropic Glutamate Receptor5 (mGlu 5): From an Artificial Neural Network Virtual Screen to an In Vivo Tool Compound. ChemMedChem. 2012;7(3):406–14.

10. Sliwoski GR, Meiler J, Lowe EW. Computational Methods in Drug Discovery Prediction of protein structure and ensembles from limited experimental data View project Antibody modeling, Antibody design and Antigen-Antibody interactions View project. Comput Methods Drug Discov. 2014;66(1):334–95.

11. Ellis G, West G. Progress in medicinal chemistry. LONDON BUTTERWORTHS; 1967.

12. Abraham DJ. BURGER's Medicinal Chemistry and Drug Discovery Vol 1. 6th ed. Wiley Online Library; 1998.

13. van Drie JH. Pharmacophore Discovery - Lessons Learned. Front Med Chem - (Volume 2). 2012;511–32.

14. A T, VA B. Molecular Docking: From Lock and Key to Combination Lock. J Mol Med Clin Appl. 2018;2(1):1–19.

15. Armour D, de Groot MJ, Edwards M, Perros M, Price DA, Stammen BL, et al. The discovery of CCR5 receptor antagonists for the treatment of HIV infection: hit-to-lead studies. ChemMedChem Chem Enabling Drug Discov. 2006;1(7):706–9.

16. Filikov A V, James TL. Structure-based design of ligands for protein basic domains: Application to the HIV-1 Tat protein. J Comput Aided Mol Des. 1998;12(3):229–40.

17. Wang S, Milne GWA, Yan X, Posey IJ, Nicklaus MC, Graham L, et al. Discovery of novel, non-peptide HIV-1 protease inhibitors by pharmacophore searching. J Med Chem. 1996;39(10):2047–54.

18. Krohn A, Redshaw S, Ritchie JC, Graves BJ, Hatada MH. Novel binding mode of highly potent HIV-proteinase inhibitors incorporating the (R)-hydroxyethylamine isostere. J Med Chem. 1991;34(11):3340–2.

19. Pai VB, Nahata MC. Nelfinavir mesylate: a protease inhibitor. Ann Pharmacother. 1999;33(3):325–39.

20. Pajonk F, Himmelsbach J, Riess K, Sommer A, McBride WH. The human

immunodeficiency virus (HIV)-1 protease inhibitor saquinavir inhibits proteasome function and causes apoptosis and radiosensitization in non-HIV-associated human cancer cells. Cancer Res. 2002;62(18):5230–5.

21. Cushman DW, Cheung HS, Sabo EF, Ondetti MA. Design of potent competitive inhibitors of angiotensin-converting enzyme. Carboxyalkanoyl and mercaptoalkanoyl amino acids. Biochemistry. 1977;16(25):5484–91.

22. Pfeiffer N. Dorzolamide: development and clinical application of a topical carbonic anhydrase inhibitor. Surv Ophthalmol. 1997;42(2):137–51.

23. Kokkonen P, Kokkola T, Suuronen T, Poso A, Jarho E, Lahtela-Kakkonen M. Virtual screening approach of sirtuin inhibitors results in two new scaffolds. Eur J Pharm Sci. 2015;76:27–32.

24. Singh N, Tiwari S, Srivastava KK, Siddiqi MI. Identification of novel inhibitors of Mycobacterium tuberculosis PknG using pharmacophore based virtual screening, docking, molecular dynamics simulation, and their biological evaluation. J Chem Inf Model. 2015;55(6):1120–9.

25. Nogara PA, Saraiva R de A, Caeran Bueno D, Lissner LJ, Lenz Dalla Corte C, Braga MM, et al. Virtual screening of acetylcholinesterase inhibitors using the Lipinski's rule of five and ZINC databank. Biomed Res Int. 2015;2015.

26. Xie Y, Zhou R, Lian F, Liu Y, Chen L, Shi Z, et al. Virtual screening and biological evaluation of novel small molecular inhibitors against protein arginine methyltransferase 1 (PRMT1). Org Biomol Chem. 2014;12(47):9665–73.

27. Neidle S. Discovery of new anticancer drugs by computer-aided drug design. Ann Oncol. 1994;5:S51–4.

28. Semighini EP, Resende JA, de Andrade P, Morais PAB, Carvalho I, Taft CA, et al. Using computer-aided drug design and medicinal chemistry strategies in the fight against diabetes. J Biomol Struct Dyn. 2011;28(5):787–96.

29. Teague SJ. Implications of protein flexibility for drug discovery. Nat Rev Drug Discov. 2003;2(7):527–41.

30. Kokh DB, Wade RC, Wenzel W. Receptor flexibility in small-molecule docking calculations. Wiley Interdiscip Rev Comput Mol Sci. 2011;1(2):298–314.

31. Liu J, He X, Zhang JZH. Improving the scoring of protein–ligand binding affinity by including the effects of structural water and electronic polarization. J Chem Inf Model. 2013;53(6):1306–14.

32. Baig MH, Balaramnavar VM, Wadhwa G, Khan AU. Homology modeling and virtual screening of inhibitors against TEM-and SHV-type-resistant mutants: A multilayer filtering approach. Biotechnol Appl Biochem. 2015;62(5):669–80.

33. De Luca L, Barreca ML, Ferro S, Christ F, Iraci N, Gitto R, et al. Pharmacophore-based discovery of small-molecule inhibitors of protein-protein interactions between HIV-1 integrase and cellular cofactor LEDGF/p75. ChemMedChem. 2009;4(8):1311–6.

34. Hansch C. Quantitative structure-activity relationships in drug design. Drug Des. 1971;271–342.

35. Smith RN, Hansch C, Ames MM. Selection of a reference partitioning system for drug design work. J Pharm Sci. 1975;64(4):599–606.

36. Takahashi T, Zhou S-Y, Nakamura K, Tanino R, Furuichi A, Kido M, et al. A follow-up MRI study of the fusiform gyrus and middle and inferior temporal gyri in schizophrenia spectrum. Prog Neuro-Psychopharmacology Biol Psychiatry. 2011;35(8):1957–64.

37. Lipinski CA. Lead- and drug-like compounds: The rule-of-five revolution. Drug Discov Today Technol. 2004;1(4):337–41.

38. Wiswesser WJ. Historic development of chemical notations. J Chem Inf Comput Sci. 1985;25(3):258–63.
39. Patrick GL. An Introduction to Medicinal Chemistry. 5th ed. oxford; 2013.
40. Congreve M, Murray CW, Blundell TL. Keynote review : Structural biology and drug discovery. 2005;10(13).
41. Renaud JP. Structural Biology in Drug Discovery. Structural Biology in Drug Discovery. 2020.
42. Kaldor SW, Kalish VJ, Davies JF, Shetty B V, Fritz JE, Appelt K, et al. Viracept (nelfinavir mesylate, AG1343): a potent, orally bioavailable inhibitor of HIV-1 protease. J Med Chem. 1997;40(24):3979–85.
43. Appelt K. Crystal structures of HIV-1 protease-inhibitor complexes. Perspect Drug Discov Des. 1993;1(1):23–48.
44. Redhu S, Jindal A. Molecular modelling: A new scaffold for drug design. Int J Pharm Pharm Sci. 2013;5(SUPPL.1):5–8.
45. Meyer EF, Swanson SM, Williams JA. Molecular modelling and drug design. Pharmacol Ther. 2000;85(3):113–21.
46. Geldenhuys WJ, Gaasch KE, Watson M, Allen DD, Van Der Schyf CJ. Optimizing the use of open-source software applications in drug discovery. Drug Discov Today. 2006;11(3–4):127–32.
47. Jones S, Thornton JM. Analysis of protein-protein interaction sites using surface patches. J Mol Biol. 1997;272(1):121–32.
48. Holliday JD, Willett P. Using a genetic algorithm to identify common structural features in sets of ligands. J Mol Graph Model. 1997;15(4):221–32.
49. Taylor RD, Jewsbury PJ, Essex JW. A review of protein-small molecule docking methods. J ofComputer-Aided Mol Des. 2002;16:151–66.
50. Looger LL, Dwyer MA, Smith JJ, Hellinga HW. Computational design of receptor and sensor proteins with novel functions. Nature. 2003;423(6936):185–90.
51. Gilson MK, Zhou H-X. Calculation of protein-ligand binding affinities. Annu Rev Biophys Biomol Struct. 2007;36:21–42.
52. Mohan V, Gibbs AC, Cummings MD, Jaeger EP, DesJarlais RL. Docking: successes and challenges. Curr Pharm Des. 2005;11(3):323–33.
53. Islam B, Sharma C, Adem A, Aburawi E, Ojha S. Insight into the mechanism of polyphenols on the activity of HMGR by molecular docking. Drug Des Devel Ther. 2015;9:4943.
54. Friesner RA, Banks JL, Murphy RB, Halgren TA, Klicic JJ, Mainz DT, et al. Glide: a new approach for rapid, accurate docking and scoring. 1. Method and assessment of docking accuracy. J Med Chem. 2004;47(7):1739–49.
55. Jones G, Willett P, Glen RC. Molecular recognition of receptor sites using a genetic algorithm with a description of desolvation. J Mol Biol. 1995;245(1):43–53.
56. Kramer B, Rarey M, Lengauer T. Evaluation of the FLEXX incremental construction algorithm for protein–ligand docking. Proteins Struct Funct Bioinforma. 1999;37(2):228–41.
57. Sandor M, Kiss R, Keserű GM. Virtual fragment docking by Glide: a validation study on 190 protein− fragment complexes. J Chem Inf Model. 2010;50(6):1165–72.
58. Schmidtke P. Protein-ligand binding sites Identification , characterization and interrelations. 2011.
59. Henzler-Wildman KA, Lei M, Thai V, Kerns SJ, Karplus M, Kern D. A hierarchy of timescales in protein dynamics is linked to enzyme catalysis. Nature. 2007;450(7171):913–6.
60. Lindorff-Larsen K, Piana S, Palmo K, Maragakis P, Klepeis JL, Dror RO, et al.

Improved side-chain torsion potentials for theAmber ff99SB protein force field. Proteins: Structure, Function, and Bioinformatics, 78, 8, 1950-1958. 2010;

61. Grafenstein S von, Fuchs JE, R.Liedl K. (How to) Profit from Molecular Dynamics-based Ensemble Docking. Vol. 17, Application of Computational Techniques in Pharmacy and Medicine. Springer Science & Business Media; 2014. 501–538 p.

62. J. Andrew M, Bruce R. G, Martin K. Dynamics of folded proteins. Nature. 1977;

63. Chen J. Drug resistance mechanisms of three mutations V32I, I47V and V82I in HIV-1 protease toward inhibitors probed by molecular dynamics simulations and binding free energy predictions. RSC Adv. 2016;6(63):58573–85.

64. Venugopal PP, Das BK, Soorya E, Chakraborty D. Effect of hydrophobic and hydrogen bonding interactions on the potency of ß-alanine analogs of G-protein coupled glucagon receptor inhibitors. Proteins Struct Funct Bioinforma. 2020;88(2):327–44.

65. Flores-Holguín N, Frau J, Glossman-Mitnik D. Conceptual DFT-based computational peptidology of marine natural compounds: Discodermins A–H. Molecules. 2020;25(18):1–20.

66. Ziegler T. Approximate density functional theory as a practical tool in molecular energetics and dynamics. Chem Rev. 1991;91(5):651–67.

67. Becke AD. Density-functional thermochemistry. V. Systematic optimization of exchange-correlation functionals. J Chem Phys. 1997;107(20):8554–60.

68. Hohenberg P, Kohn W. Inhomogeneous electron gas. Phys Rev. 1964;136(3B):B864.

69. Geerlings P, De Proft F, Langenaeker W. Conceptual density functional theory. Chem Rev. 2003;103(5):1793–873.

70. Kohn W, Sham LJ. Self-consistent equations including exchange and correlation effects. Phys Rev. 1965;140(4A):A1133.

71. Heyd J, Scuseria GE. Efficient hybrid density functional calculations in solids: Assessment of the Heyd-Scuseria-Ernzerhof screened Coulomb hybrid functional. J Chem Phys. 2004;121(3):1187–92.

72. Selick HE, Beresford AP, Tarbit MH. The emerging importance of predictive ADME simulation in drug discovery. Drug Discov Today. 2002;7(2):109–16.

73. Caldwell G, Yan Z, Tang W, Dasgupta M, Hasting B. ADME Optimization and Toxicity Assessment in Early- and Late-Phase Drug Discovery. Curr Top Med Chem. 2009;9(11):965–80.

74. Yu H, Adedoyin A. ADME-Tox in drug discovery: Integration of experimental and computational technologies. Drug Discov Today. 2003;8(18):852–61.

75. Moroy G, Martiny VY, Vayer P, Villoutreix BO, Miteva MA. Toward in silico structure-based ADMET prediction in drug discovery. Drug Discov Today [Internet]. 2012;17(1–2):44–55. Available from: http://dx.doi.org/10.1016/j.drudis.2011.10.023

76. Todeschini R, Consonni V. Handbook of molecular descriptors. John Wiley & Sons; 2008.

77. Güner OF. Pharmacophore perception, development, and use in drug design. Vol. 2. Internat'l University Line; 2000.

78. Merson MH, Malley JO, Serwadda D, Apisuk C. Series HIV Prevention 1 The history and challenge of HIV prevention. 2008;475–88.

79. Kaur H, Garg S, Joshi H, Ayaz S, Sharma S, Bhandari M. A Review: Epidemics and Pandemics in Human History. Int J Pharma Res Heal Sci. 2020;8(2):3139–42.

80. Heymann DL. The international response to the outbreak of SARS in 2003. Philos Trans R Soc B Biol Sci. 2004;359(1447):1127–9.

81. Rossmann MG. Structure of viruses: A short history. Q Rev Biophys.

2013;46(2):133–80.

82. Mtsweni ES, Hörne T, Poll JA van der, Rosli M, Tempero E, Luxton-reilly A, et al. Virus Life Cycle Chapter. Eng Constr Archit Manag. 2020;25(1):1–9.

83. Hofmann H, Pöhlmann S. Cellular entry of the SARS coronavirus. Trends Microbiol. 2004;12(10):466–72.

84. Nal B, Chan C, Kien F, Siu L, Tse J, Chu K, et al. Differential maturation and subcellular localization of severe acute respiratory syndrome coronavirus surface proteins S, M and E. J Gen Virol. 2005;86(5):1423–34.

85. McBride CE, Li J, Machamer CE. The cytoplasmic tail of the severe acute respiratory syndrome coronavirus spike protein contains a novel endoplasmic reticulum retrieval signal that binds COPI and promotes interaction with membrane protein. J Virol. 2007;81(5):2418–28.

86. Stertz S, Reichelt M, Spiegel M, Kuri T, Martínez-Sobrido L, García-Sastre A, et al. The intracellular sites of early replication and budding of SARS-coronavirus. Virology. 2007;361(2):304–15.

87. Siu YL, Teoh KT, Lo J, Chan CM, Kien F, Escriou N, et al. The M, E, and N structural proteins of the severe acute respiratory syndrome coronavirus are required for efficient assembly, trafficking, and release of virus-like particles. J Virol. 2008;82(22):11318–30.

88. Kielian M, Rey FA. Virus membrane-fusion proteins: more than one way to make a hairpin. Nat Rev Microbiol. 2006;4(1):67–76.

89. Lal S k. MOlecular Biology of the SARS-Coronavirus. Vol. 91, PLACEHOLD - Mol Bio of SARS-Coronavirus. Springer Berlin Heidelberg; 2010.

90. Li W, Moore MJ, Vasilieva N, Sui J, Wong SK, Berne MA, et al. Angiotensin-converting enzyme 2 is a functional receptor for the SARS coronavirus. Nature. 2003;426(6965):450–4.

91. Wang P, Chen J, Zheng A, Nie Y, Shi X, Wang W, et al. Expression cloning of functional receptor used by SARS coronavirus. Biochem Biophys Res Commun. 2004;315(2):439–44.

92. Nie Y, Wang P, Shi X, Wang G, Chen J, Zheng A, et al. Highly infectious SARS-CoV pseudotyped virus reveals the cell tropism and its correlation with receptor expression. Biochem Biophys Res Commun. 2004;321(4):994–1000.

93. Mossel EC, Huang C, Narayanan K, Makino S, Tesh RB, Peters CJ. Exogenous ACE2 expression allows refractory cell lines to support severe acute respiratory syndrome coronavirus replication. J Virol. 2005;79(6):3846–50.

94. Kuba K, Imai Y, Rao S, Gao H, Guo F, Guan B, et al. A crucial role of angiotensin converting enzyme 2 (ACE2) in SARS coronavirus–induced lung injury. Nat Med. 2005;11(8):875–9.

95. Cui J, Li F, Shi Z-L. Origin and evolution of pathogenic coronaviruses. Nat Rev Microbiol. 2019;17(3):181–92.

96. Li G, De Clercq E. Therapeutic options for the 2019 novel coronavirus (2019-nCoV). Nat Rev Drug Discov [Internet]. 2020;19(3):149–50. Available from: http://dx.doi.org/10.1038/d41573-020-00016-0

97. Liu Y, Liang C, Xin L, Ren X, Tian L, Ju X, et al. The development of Coronavirus 3C-Like protease (3CLpro) inhibitors from 2010 to 2020. Eur J Med Chem. 2020;206:112711.

98. Hoffmann M, Kleine-Weber H, Schroeder S, Krüger N, Herrler T, Erichsen S, et al. SARS-CoV-2 Cell Entry Depends on ACE2 and TMPRSS2 and Is Blocked by a Clinically Proven Protease Inhibitor. Cell. 2020;181(2):271-280.e8.

99. SARS-CoV-2 Replication Cycle. :5410. Available from: https://www.antikoerper-

online.de/resources/18/5410/sars-cov-2-life-cycle-stages-and-inhibition-targets/

100. Huang L, Fu L. Mechanisms of resistance to EGFR tyrosine kinase inhibitors. Acta Pharm Sin B. 2015;5(5):390–401.

101. Shigematsu H, Gazdar AF. Somatic mutations of epidermal growth factor receptor signaling pathway in lung cancers. Int J Cancer. 2006;118(2):257–62.

102. Shigematsu H, Gazdar AF. Somatic mutations of epidermal growth factor receptor signaling pathway in lung cancers. Int J Cancer. 2006;118(2):257–62.

103. Brose MS, Volpe P, Feldman M, Kumar M, Rishi I, Gerrero R, et al. BRAF and RAS mutations in human lung cancer and melanoma. Cancer Res. 2002;62(23):6997–7000.

104. Mitsudomi T, Kosaka T, Yatabe Y. Biological and clinical implications of EGFR mutations in lung cancer. Int J Clin Oncol. 2006;11(3):190–8.

Chapter II:

LETERATURE

REVIEW

Chapter II: Literature review

I.   Literature review on covid-19 inhibitors

I.1. History

In late 2019, a new generation of coronavirus appeared in Wuhan City in the Hubei Province in central China [1,2]. This virus causes severe acute respiratory syndrome. The first case was reported on the 8th of December 2019 for many patients lived around the local Huanan Seafood Wholesale Market [3]. The novel coronavirus was identified from the throat swab sample of a patient [4]. World Health Organization has abbreviated this novel coronavirus as 2019-nCoV then the pathogen was renamed to SARS-CoV-2 [5]. After that, World Health Organization declared the pandemic when the virus hit many other countries.

Human infections by the SARS coronavirus are known to be closely associated with interactions between the viral spike protein (S-protein) which has favorable binding affinity for the human Angiotensin-Converting Enzyme 2 (ACE2) [6–9]. Several studies have also provided evidence of the COVID-19 S-protein binding to the ACE2 receptor [10–12].

Angiotensin-converting enzyme (ACE)-related carboxypeptidase is a zinc metallopeptidase ectoenzyme, which is predominantly found in the lungs [13]. ACE2, is a type I integral membrane protein, which it consists of 805 amino acid residues with one Zn^{2+} essential for enzyme activity. ACE2 was implicated in the regulation of heart function and as a functional receptor for the coronavirus, which is linked to the severe acute respiratory syndrome (SARS). ACE2 is the cellular receptor for the new coronavirus (SARS-CoV-2) which is causing the serious pandemic COVID-19 [14–17].

 In a recent study, it was suggested that the 2019-nCoV binds to the human ACE2 receptor via densely glycosylated spike (S) protein as the initiation step of the entry mechanism to human cells [10,18,19]. The entry of the virus depends on its binding with the cell surface units at site 1 and site 2 S1/S2 that contains Zn^{2+}, an important cofactor for numerous viral proteins as well [20]. Existence of this metallic ion facilitates the viral attachment to the surface of target cells. It is well known that zinc ions serve as intracellular second messenger and may trigger apoptosis or efficiently impair replication of a number of viruses and this effect may be based on direct inhibition [20–23].

ACE2 exists in every human body but in different quantities [24]. Patients, who suffer from hypertension, diabetes or cardiovascular diseases, have high concentration of ACE2 enzyme in their bodies [24–26]. These categories of people can be easily infected by

coronavirus compared with children who have low concentration of ACE2 enzyme, their infection percentage is only 2% [27].

Blocking the active site of ACE2 by suitable pharmaceutical compound will prevent the virus entering to the human cells. Therefore, synthesis of such pharmaceutical compound is in great demand. Many scientists worldwide are trying to synthesise new drugs to stop spreading the new infectious disease. We think that this route takes a long time, at least 18 months, until the new vaccine will be available in the markets. Thus, using medicaments already exist is the shortcut to tackle such issue. In 2005, chloroquine was found as a potent inhibitor of SARS coronavirus infection and it was suggested to treat the new novel coronavirus SARS-CoV-2 with hydroxychloroquine [7,28–31].

I.2. Evaluation of drug testing

Following the outbreak of the COVID-19 pandemic, several drug candidates from the repository of existing drugs have been tested for activity against SARS-CoV-2. A review of the currently available literature shows that several existing antiviral drugs that target the viral replicating mechanism are under investigation for the treatment of COVID-19. The list of antiviral drugs being tested for COVID-19 includes remdesivir, hydroxychloroquine, chloroquine, lopinavir, darunavir, baloxavir, imatinib, and favipiravir [32].

Cava et al [33] examined the mechanism of the angiotensin-converting enzyme 2 (ACE2) in lung tissue. Gene expression profiles were used to investigate the main function of co-expressed gene to ACE2 to identify the interaction that caused the viral infection. After that several interesting potential effective drugs candidates for COVID-19 with antiviral properties (Nimesulide, Fluticasone Propionate, Thiabendazole, Photofrin, Didanosine and Flutamide Figure 1) were suggested.
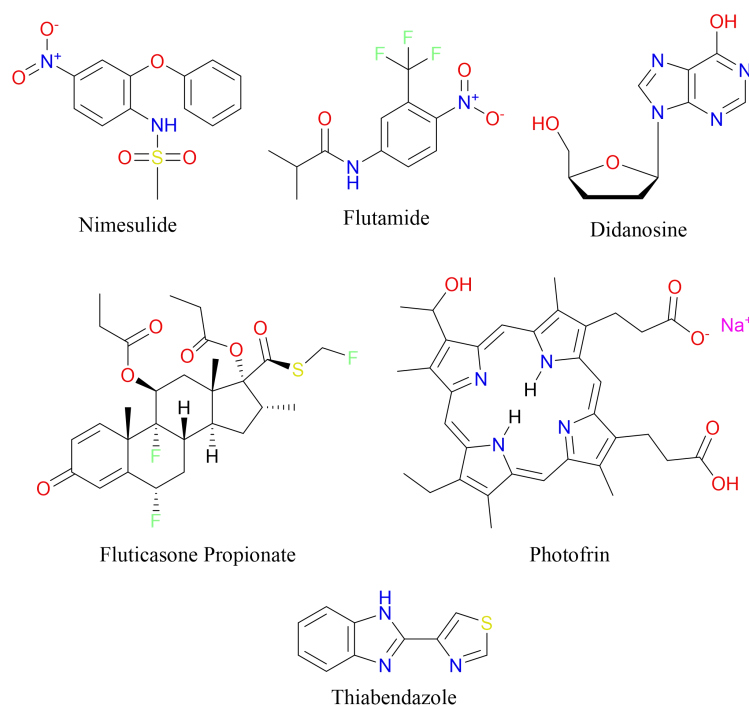
Figure 1 Chemical structures of promising drugs for Nimesulide, Fluticasone Propionate, Thiabendazole, Photofrin, Didanosine and Flutamide.

Wang et al [34] preformed virtual docking screening of the approved drugs. Then the authors applied molecular dynamics simulations followed by MM-PBSA-weighted solvent-accessible surface area (WSAS) free binding energy and MM-GBSA to the top docking hits to identify inhibitors for SARS-CoV-2 main protease. Several existing drugs (carfilzomib, eravacycline, valrubicin, lopinavir, and elbasvir Figure 2) showed high binding affinity against 3CL pro.
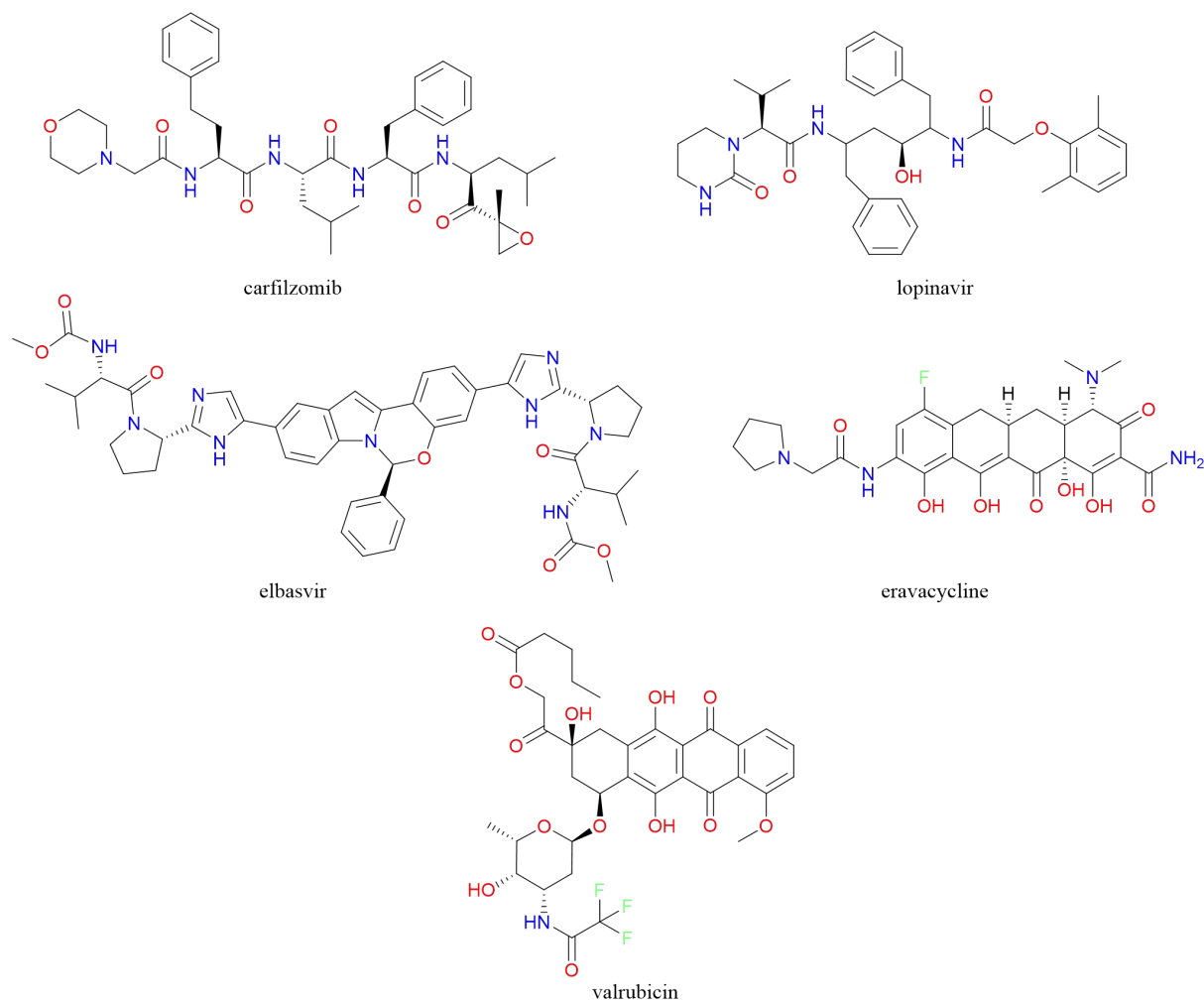
Figure 2 Chemical structures of promising drugs for carfilzomib, eravacycline, valrubicin, lopinavir, and elbasvir.

Lima de Oliveira and Teixeira de Oliveira [35] preformed docking molecular simulations on already approved drug tested against covid-19 followed by a structure-based virtual screening and study physico-chemical and pharmacokinetic properties. The results, in comparative terms, remdesivir, simeprevir, paritaprevir and baricitinib Figure 3 are currently among the most promising in remission of symptoms from the disease.
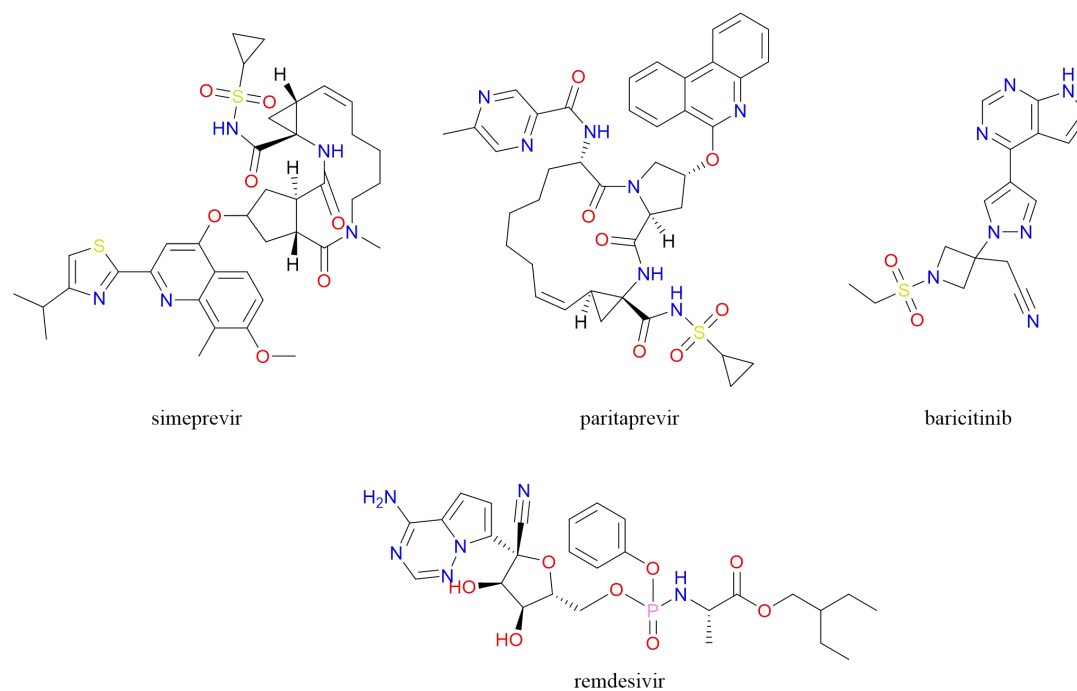
Figure 3 Chemical structures of promising drugs for simeprevir, paritaprevir, remdesivir and baricitinib.

Farag et al [36] adopted a repositioning approach using in silico molecular modeling screening using FDA approved drugs with established safety profiles for potential inhibitory effects on Covid-19 virus. They started with structure-based drug design by screening more than 2000 FDA approved drugs against Covid-19 virus main protease enzyme (M pro) substrate-binding pocket to identify potential hits based on their binding energies, binding modes, interacting amino acids, and therapeutic indications. In addition, they elucidated preliminary pharmacophore features for candidates bound to Covid-19 virus M pro substrate-binding pocket. The top hits include antiviral drugs such as Darunavir, Nelfinavir and Saquinavir, some of which are already being tested in Covid-19 patients. Interestingly, Figure 4 represent one of the most promising hits in our screen is the hypercholesterolemia drug Rosuvastatin. These results certainly do not confirm or indicate antiviral activity, but can rather be used as a starting point for further in vitro and in vivo testing, either individually or in combination.
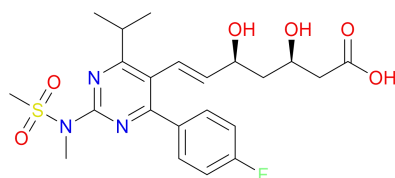
Figure 4 Chemical structure of rosuvastatin.

Barros et al [37] applied molecular docking to study in silico the interaction of twenty-four ligands with four important SARS-CoV-2 receptors. The results showed that an antimalarial substance Metaquine and anti-HIV antiretroviral Saquinavir in Figure 5, interacted with all the studied receptors. The results indicated that they are potential candidates for multi-target drugs for COVID-19.
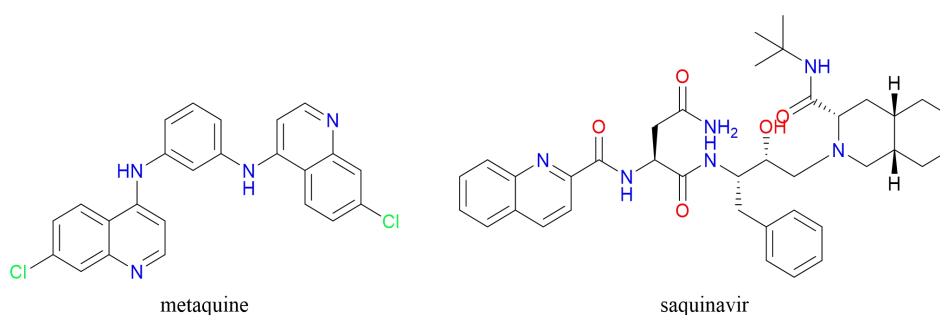
Figure 5 Chemical structures of metaquine and saquinavir.

Sourav et al [38] applied a blind molecular docking approach to identify the possible inhibitors of the SARS-CoV-2 main protease, by screening a total of 33 molecules which includes natural products. All the studied molecules could bind to the active site of the SARS-CoV-2 protease, a natural compound rutin has the highest inhibitor efficiency among the 33 molecules studied, followed by ritonavir, emetine, hesperidin, lopinavir and indinavir. The compounds were presented in Figure 6.
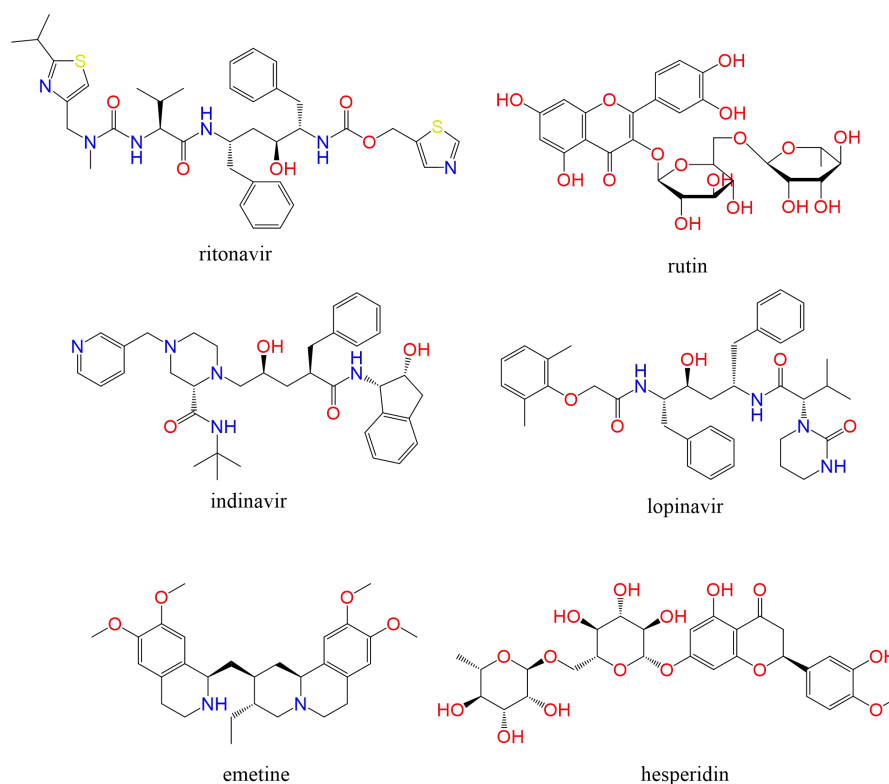
Figure 6 Chemical structures of rutin, ritonavir, emetine, hesperidin, lopinavir and indinavir.

I.3. Evaluation of natural compounds

Zhang et al [39] search for natural compounds that had been biologically confirmed as against sever acute respiratory syndrome coronavirus or Middle East respiratory syndrome coronavirus and tested their absorption, distribution, metabolism and excretion (ADME) followed by molecular docking study. After ADME analysis, 13 compounds were selected. The Chinese herbal that contains two or more of the compounds was selected. Several traditional Chinese medicines plants were identified. *Forsythiae fructus* Figure 7, contain the majority of compounds. *Forsythiae fructus* related to regulating viral infection and identified as potential SARS-CoV-2 inhibitors.
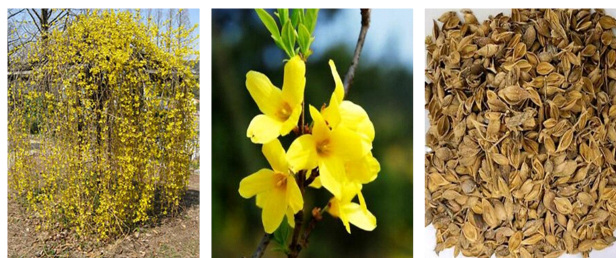
Figure 7 Image of traditional Chinese medicines plant *Forsythiae fructus.*

Bouchentouf et Missoun [40] applied molecular docking on North African medicinal herb; Nigella sativa L compounds. Two compounds, Nigellidine and α-hederin, were identified as potential SARS-CoV-2 inhibitors. Figure 8 shows Nigella sativa L compounds, Nigellidine and α-hederin and the herbal Nigella sativa L.
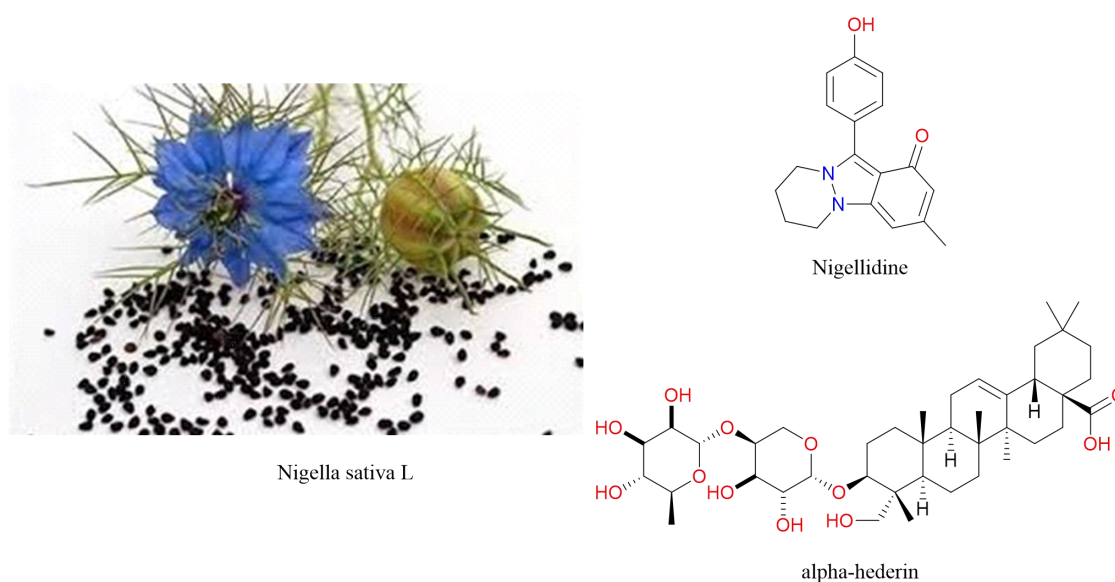
Figure 8 Image of Nigella sativa L compounds and structures of Nigellidine and α-hederin.

Cheng et al [41] studied active compounds in Citrus plants in silico. Citrus is rich in bioactive compounds and some varieties are used as Chinese folk medicine. They have been clinically documented for roles in the relief of cough and the promotion of digestive health. Citrus fruits are rich of flavonoid compounds (naringenin, naringin, hesperetin, hesperidin, neohesperidin and nobiletin), they are expected to be developed as anti-viral drugs. From Figure 9, Hesperetin and naringin were found as the highest potent inhibitors of SARS-CoV 3CLpro among others. Meanwhile, nutrient supplements could reduce the host immune responses.
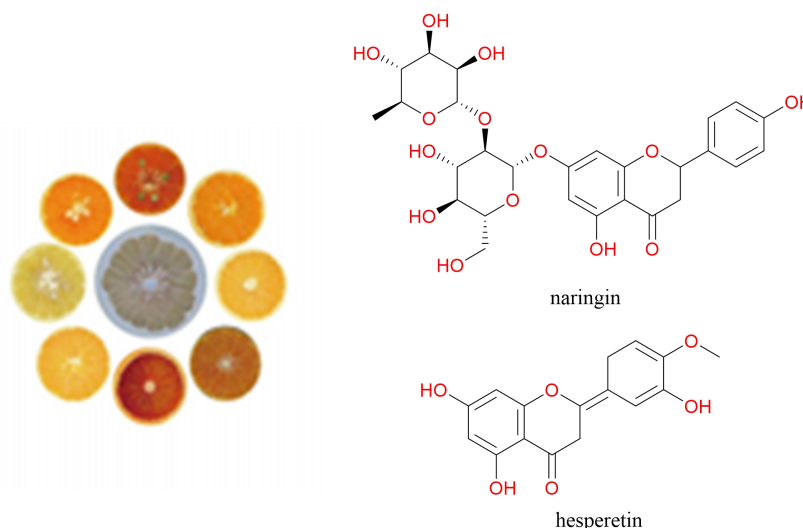
Figure 9 citrus fruits and chemical structures of naringin and hesperetin.

Khaerunnisa et al [42] assessed the bioactive compounds in medicinal plants as potential COVID-19 M pro inhibitors, using a molecular docking study. Nelfinavir and lopinavir were used as standards for comparison. The binding energies obtained from the docking of 6LU7 with native ligand, nelfinavir, lopinavir, kaempferol, quercetin, luteolin-7-glucoside, demethoxycurcumin, naringenin, apigenin-7-glucoside, oleuropein, curcumin, catechin, epicatechin-gallate, zingerol, gingerol, and allicin. Therefore, nelfinavir and lopinavir may represent potential treatment options, and luteolin-7-glucoside, demethoxycurcumin, apigenin-7-glucoside, oleuropein, curcumin, catechin, and epicatechin-gallate appeared to have the best potential to act as COVID-19 M pro inhibitors.

Bhowmik et al [43] aimed to study the receptor-binding domain of S protein (RBD of nCoV-SP) and ACE-2 receptor as a promising target for the development of drugs against SARS-CoV-2. Different flavonoids with antioxidant, anti-inflammatory and antiviral properties from different literatures were taken as a ligand or inhibitor for molecular docking against target protein RBD of nCoV-SP and ACE-2. Top flavonoids ligand based on docking score were selected for pharmacokinetic study. Selected flavonoid (hesperidin, naringin, ECGC and quercetin Figure 10) showed extremely good pharmacokinetics properties with good absorption, solubility, permeability, distribution, metabolism, minimal toxicity and good bioavailability. These identified lead flavonoids may act as potential compounds for the development of effective drugs and may help in controlling the rapid spread of SARS-CoV-2 by potentially inhibiting the virus entry into the host cell.
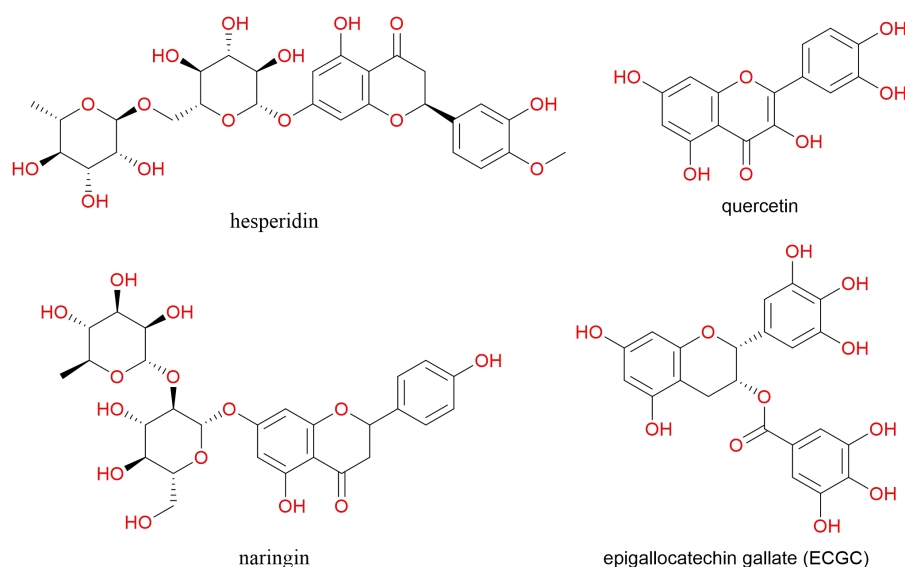
Figure 10 chemical structures of hesperidin, naringin, ECGC and quercetin.

I.4. Syntheses compounds

Liang et al [44] performed molecular docking combined with molecular dynamics simulation to demonstrate the binding stability of an α-ketoamide 13b inhibitor inside the SARS-CoV-2 main protease. Their aim was to further investigate the interaction of the α-ketoamide 13b with the SARS-CoV-2 Mpro in silico. Throughout molecular dynamics simulations, they compared the properties of α-ketoamide 13b, with one of the most widely prescribed antibiotics, amoxicillin. Amoxicillin was chosen for comparison for two reasons: first, although it does not possess antiviral properties and second it binds to the active site of the SARS-CoV-2 Mpro akin to α-ketoamide 13b Figure 11, albeit with lower affinity.
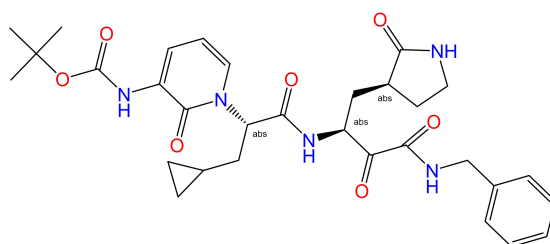
Figure 11 Chemical structure of α-ketoamide 13b.

Kumar et al [45] examined natural coumarin analogues psoralen, bergapten, imper-atorin, heraclenin, heraclenol, saxalin, oxapeucedanin, angelicin, toddacoumaquinone, aesculetin as potential inhibitor candidates for protease of SARS Coronavirus in intricate with α-ketoamide and compared them with hydroxychloroquine and coumarin analogue. α-

ketoamide and toddacoumaquinone showed respectable pharmacokinetic properties. The outcomes of this study will offer other investigators with prospects to find the precise medication to fight COVID-19.

However, due to its cardiotoxicity hydroxychloroquine has been red flagged by USFDA for use as a prophylactic measure. In this rapidly evolving pandemic, repurposing existing drugs and evaluating commercially available inhibitors against the druggable targets of SARS-CoV-2 should be an effective strategy to accelerate the drug discovery process. Consequently, taking advantage of the availability of the X-ray crystal structure of two receptors ACE2 and SARS-CoV-2 binding with ACE2 complex) (PDB code 1R42 and 6M0J). In this study, 18 drugs were selected to evaluate their binding with two receptors ACE2 and SARS-CoV-2 binding with ACE2 complex. These drugs were chosen due to their similarities in structure with chloroquine and hydroxychloroquine in order to find an alternative drug for COVID-19 [46].

Various researchers have been studied on coronavirus SARS-CoV-2. Zia et al [47] applied bioinformatics analysis on the spike protein of Corona Virus and human angiotensin receptor 2 (ACE-2) with already anti-HCV approved drug. Velpatasvir has been reported as one of anti-HCV. Molecular docking was applied to determine the mode of interaction of velpatasvir and RNA dependent RNA polymerase enzyme as well as inhibition of attachment of S-protein with human host receptor ACE-2. The result noted that, velpatasvir binds tightly with S-protein-ACE2 interface and with Covid-19 RdRp.

Dasgupta et al [48] preformed mixed-solvent molecular dynamics (MixMD) simulations to find binding hotspots through mapping the surface of unbound proteins with 5% cosolvents in water. They have performed virtual screening against the active site and allosteric sites with 361 hits from Mpro screenings available through the National Centre for Advancing Translational Sciences. The results identified that National Centre for Advancing Translational Sciences inhibitors bind to the allosteric sites better than the active site of Mpro. The identified sites are accurate and druggable.

Narayanan et al [49] applied an antiviral screening strategy involving a novel in-cell protease assay as well as structural determinations for rapid identification of protease inhibitors with low cytotoxicity. They identified eight compounds with anti-SARS-CoV-2 activity using molecular docking. They demonstrated that Sitagliptin and Daclatasvir inhibit PLpro and MG-101, Lycorine HCl and Nelfinavir mesylate inhibit Mpro of SARS-

CoV-2. The X-ray crystal structure of Mpro in complex with MG-101 shows a covalent bond formation between the inhibitor and the active site Cys145 residue indicating its mechanism of inhibition is by blocking the substrate binding at the active site.

II. Literature review on quinazoline and pyridopyrimidine

II.1. Overview

Epidermal growth factor receptor (EGFR) is family of tyrosine kinase. It divides to four transmembrane, ERBB1/HER1, ERBB2/HER2, ERBB3/HER3 and ERBB4/HER [50–52]. The uncontrolled activity for this receptor is responsible for resulting proliferation, differentiation, migration and angiogenesis which associated to variety of human cancer. The transforming deregulation of EGFR in several cancer family: breast cancer, non-small cell cancer (NSCLC) and glioblastomas are presented [53]. This deregulation may be caused by activating mutations [54,55]. EGFR tyrosine kinase domain encoded by six exons. Most commonly, EGFR kinase activated mutations occur from 18-21 exons. The mutations classified to three categories; first, the deletion of exon-19, second, substitution of single nucleotide that cause a alterations of amino acid and third, in-frame duplications and/or insertions of exon 20 [55]. The first category, the deletions of exon 19, includes changing Leucine-747 to Glutamic acid-749, while the second category, mutation on exon 21, includes changing an Arginine to Leucine at 858 codon (L858R) mutation. Often EGFR-TK mutations respond to Anilinoquinazoline based on structure of gefitinib, erlotinib and lapatinib inhibitors Figure 1[56]. Recently EGFR wild-type inhibitors canartinib [57], afattinib [58], pelitinib and neratinib [59] showed a significant clinical response for NSCLC patient and increase in the sensitivity of NSCLC cells. The third category, mutation T790M of exon 20, substitution of threonine 790 to methionine, which is also named as gatekeeper. This mutation is a hydrophobic pocket in the back of ATP binding which enhances the resistance of the first and second generations of EGFR tyrosine kinase inhibitors [60,61]. The sensitivity of first and second generations against EGFR mutations, Wild-type, L858R and T790M orientate to develop new inhibitors to block mutations in cancer cells of patients [62].

Nowadays, computational approach methods are being used in many different fields [63–65]. Also, they are important and accelerating the development of new tyrosine kinase inhibitors. Quinazoline and pyrido[3,4-d]pyrimidine are important and privileged

structures in many drugs and have different biological activities such as anticancer, anti-inflammatory, anti-HIV, antibacterial and antifungal activity [66–69].

II.2.Biological importance of quinazolines

II.2.1. Quinazolines as anticancer activity

Amine et al [70] synthesized some new quinazoline derivatives. The synthesized compounds were evaluated in vitro against the human mammary cancer cell line (MCF7), which has a high level of epidermal growth factor receptor (EGFR) tyrosine kinase expression. Also, molecular docking study was applied to the proposed compounds into the ATP binding site of the EGFR tyrosine kinase to compare their binding mechanism to that of the known EGFR inhibitor, lapatinib, N,N'-Bis-quinazolin-4-ylbenzene-1,4-diamine Figure 12 was remarked as the most active compound with (IC_{50} = 0.06 µg/ml; 1.64 nmol/ml).
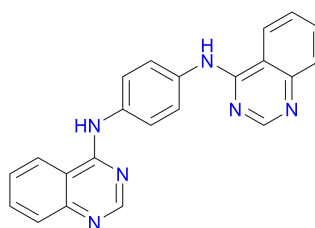
Figure 12 chemical structure of *N,N'*-Bis-quinazolin-4-ylbenzene-1,4-diamine.

Asadollahi-Baboli [71] prefomed molecular docking and QSAR analysis on a series of fifty three quinazoline derivatives to elucidate significant structural and physiochemical properties that affect inhibiting activity. According to the high predictive QSAR model, eight novel compounds were designed as potent EGFR T790M inhibitors.

Abdullahi et al [72] applied a computational study to quinazoline derivatives for their antiproliferative activity against triple negative breast cancer (MDA-MB231) cell line. According to QSAR analysis and molecular docking, 2-(3-((3-benzyl-6-methyl-4-oxo-3,4-dihydroquinazolin-2-yl)thio)propyl)isoindoline-1,3-dione was identified as the best compound with pIC50 predictive = 5.67, least residual value = -0.04 and docking score -123.238, the compound was showed in Figure 13. Ten novel compounds were designed and have good predicted activity and better docking score.
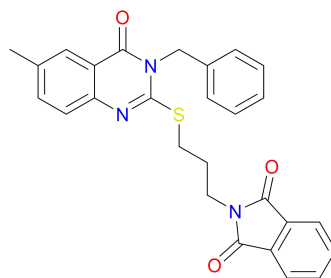
Figure 13 chemical structure of 2-(3-((3-benzyl-6-methyl-4-oxo-3,4-dihydroquinazolin-2-yl)thio)propyl)isoindoline-1,3-dione.

II.2.2. Quinazoline as antioxidant activity

Al-Salahi et al [73] were investigated the antioxidant properties of fifteen 2-thioxobenzo [g] quinazoline derivatives using three different assays. The molecular docking study was applied to coumpounds and results three best ligands.

Santos-Ballardo et al [74] synthesized, evaluated the activity and applied molecular docking of 3-substituted quinazoline-2,4(1H, 3H)-diones. the synthesized compound have α-amylase, α-glucosidase, and Antioxidant activity confirmed by molecular docking study.

II.2.3. Quinazoline as antibacterial activity

Ghorab et al [68] synthesized quinazoline compounds and tested them in vitro for antibacterial activity, finding that some of them showed promise when compared to ampicillin as a positive control. The proposed pharmacophore shape is effectively satisfied by compounds that have shown considerable activity.

Vijayakumar et al [69] synthesized 11 compounds of quinazoline-1 derivatives and to test their antimicrobial and anti-HIV1 activities. The antimicrobial and anti-HIV1 activities of the compounds were tested in-vitro. They found that five compounds possessed a wide range of anti-microbial and anti-HIV1 activity.

II.3. Biological importance of Pyridopyrimidine

II.3.1. Pyridopyrimidine as anticancer activity

Wei et Malhotra [75] synthesized a series of 4-substituted 2-amino pyrido[3,4-d]pyrimidine compounds as potential anticancer agents. Breast cancer and renal cancer cell lines have shown extremely selective activity towards synthesized compounds. They

results two promising lead compounds: N4-(4-Chlorophenyl)-8-methoxypyrido[3,4-d]pyrimidine-2,4-diamine and 8-Methoxy-4-phenoxypyrido[3,4-d]pyrimidin-2-amine, Figure 14, for cancer treatment.

N4-(4-Chlorophenyl)-8-methoxypyrido[3,4-d]pyrimidine-2,4-diamine

8-Methoxy-4-phenoxypyrido[3,4-d]pyrimidin-2-amine
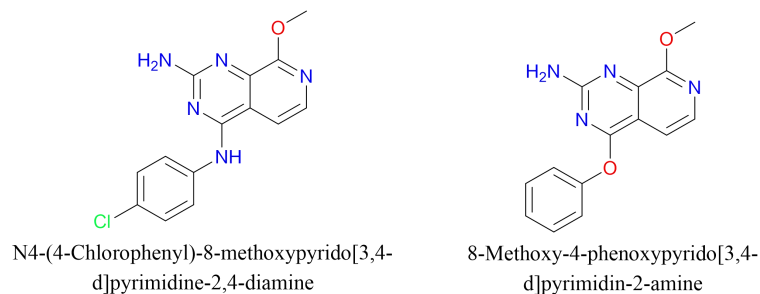
Figure 14 chemical structure of N4-(4-Chlorophenyl)-8-methoxypyrido[3,4-d]pyrimidine-2,4-diamine and 8-Methoxy-4-phenoxypyrido[3,4-d]pyrimidin-2-amine.

Zhang et al [76] designed a new derivative of pyrido[3,4-d]pyrimidine as novel generation of epidermal growth factor receptor tyrosine kinase inhibitors EGFR-TKIs. The compound (1-(6-((5-(4-(Dimethylamino)piperidin-1-yl)pyridin-2-yl)amino)-2-((4-fluorophenyl)amino) pyrido[3,4-d]pyrimidin-4-yl)piperidin-4-yl)methanol was found as the most promising inhibitor for HCC827 and H1975 cells growth with the IC 50 values of 0.044 μM and 0.40 μM, respectively. The compound was presented in Figure 15. Also this compound inhibited $EGFR^{L858R}$ (IC_{50} = 1.1 nM) and $EGFR^{L858R/T790M/C797S}$ (IC_{50} = 7.2 nM) with significant inhibitory activity.
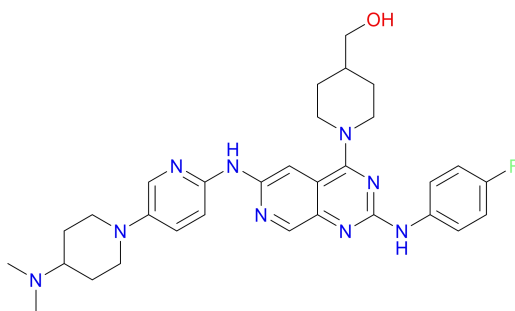
Figure 15 chemical structure of (1-(6-((5-(4-(Dimethylamino)piperidin-1-yl)pyridin-2-yl)amino)-2-((4-fluorophenyl)amino)pyrido[3,4-d]pyrimidin-4-yl)piperidin-4-yl)methanol.

Deng et al [77] synthesized a new derivative of pyrido[2,3-d]pyrimidine with six step process. Antitumor, antibacterial, anti-inflammatory, and antimicrobial properties have been demonstrated. A Density Functional heory study was applied to the lead compound

N-{4-[(6-bromopyrido[2,3-d]pyrimidin-4-yl)oxy]phenyl}morpholine-4-   carboxamide,
Figure 16. Molecular docking resulted strong binding interaction. The lead compound
exhibited antiproliferative activity against human malignant melanoma cells (A375 cells).
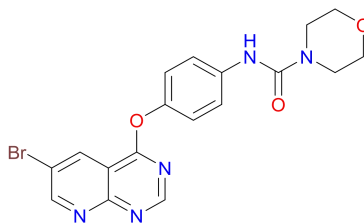
Figure 16 chemical structure of N-{4-[(6-bromopyrido[2,3-d]pyrimidin-4-yl)oxy]phenyl}morpholine-4- carboxamide.

II.3.2. Pyridopyrimidine as antifungal activity

Aryan et al [78] synthesized a new derivatives of pyrido[2,3-d]pyrimidine. The
antibacterial and antifungal activity were investigated to compounds using twenty-two
bacterial and three fungal pathogens. Quantum chemical computational analyses were
performed on the derivatives with bioactivity effects to elucidate the likely structural and
electronic effects governing the identified bioactivities.

Appana et al [79] synthesized a series of novel 2-substituted 4-hydrazone functionalized
pyrido[2,3-d]pyrimidine and 1,2,4-triazole fused pyrido[2,3-d]pyrimidine derivatives. The
antifungal activity was investigated to compounds. Docking studies on active compounds
revealed that they fit nicely into the active site cavity of the target protein. All of Lipinski's
parameters are within the allowed range for human use, implying that they have the
potential to be used as drug-like molecules.

II.3.3. Pyridopyrimidine as anti-inflammatory activity

El-Gazzar et Hafez [80] synthesized a new 4-substituted-pyrido[2,3-d]pyrimidin-4(1H)-
ones.an analgesic and anti-inflammatory activity was investigated to compounds. The
compound   7-amino-6-cyano-5-[4-(4-morpholinyl)phenyl]-2-thioxopyrido[2,3-
d]pyrimidin4 (1H)-one, Figure 17, showed 50% and 65% anti-inflammatory activity at the
dose 10 and 20 mg/kg respectively.
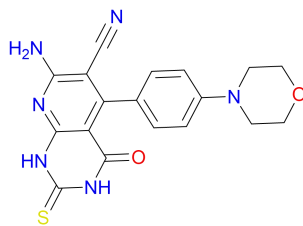
Figure 17 chemical structure of 7-Amino-6-cyano-5-[4-(4-morpholinyl)phenyl]-2-thioxopyrido[2,3-d]pyrimidin4(1H)-one.

II.3.4. Pyridopyrimidine as anti-diabetes activity

Adib et al [81] created a new series of 6-amino-pyrido[2,3-d]pyrimidine-2, 4-diones derivatives and tested their anti-diabetic effectiveness. Furthermore, when compared to acarbose as a reference, the active derivative 6-Amino-7-(4-chlorophenyl)-5-(4-methoxyphenyl)-1,3-dimethylpyrido[2,3-d]pyrimidine2,4(1H,3H)-dione was found to be 10-fold more active (IC_{50} = 750.0 ±1.5 µM). The compound was presented in Figure 18. To establish its binding to a specific location, molecular modeling was used.
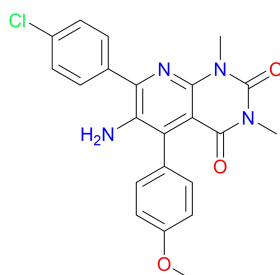
Figure 18 chemical structure of 6-Amino-7-(4-chlorophenyl)-5-(4-methoxyphenyl)-1,3-dimethylpyrido[2,3-d]pyrimidine2,4(1H,3H)-dione.

Toobaei et al [82] synthesized a new derivatives of chromeno[3',4':5,6]pyrido[2,3-d]pyrimi-dine and tested their anti-diabetic activity. (S)-12-(4-(4-aminophenoxy)phenyl)-7-((1S,2R,3R,   4R)-1,2,3,4,5-pentahydroxypentyl)-7,12-dihydro-6H-chromeno[3',4':5,6]pyrido[2,3-d]   pyrimidine-6,8,10(9H,11H)-trione   was   the   most promising inhibitor of both yeast and rat α-Gls enzymes among the synthesized substances. The compound was presented in Figure19.
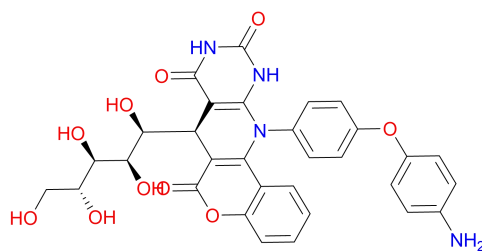
Figure 19 chemical structure of (S)-12-(4-(4-aminophenoxy)phenyl)-7-((1S,2R,3R,4R)-1,2,3,4,5-pentahydroxypentyl)-7,12-dihydro-6H-chromeno[3',4':5,6]pyrido[2,3-d]pyrimidine-6,8,10(9H,11H)-trione.

III.   References

1.   Zhu N, Zhang D, Wang W, Li X, Yang B, Song J, et al. A novel coronavirus from patients with pneumonia in China, 2019. N Engl J Med. 2020;382(8):727–33.

2.   Wang C, Horby PW, Hayden FG, Gao GF. A novel coronavirus outbreak of global health concern. Lancet. 2020;395(10223):470–3.

3.   Chan JF-W, Yuan S, Kok K-H, To KK-W, Chu H, Yang J, et al. A familial cluster of pneumonia associated with the 2019 novel coronavirus indicating person-to-person transmission: a study of a family cluster. Lancet. 2020;395(10223):514–23.

4.   Wang D, Hu B, Hu C, Zhu F, Liu X, Zhang J, et al. Clinical Characteristics of 138 Hospitalized Patients with 2019 Novel Coronavirus-Infected Pneumonia in Wuhan, China. JAMA - J Am Med Assoc. 2020;323(11):1061–9.

5.   WHO. World Health Organization [Internet]. 2020. Available from: https://www.who.int/emergencies/diseases/novel-coronavirus-2019.

6.   Prabakaran P, Xiao X, Dimitrov DS. A model of the ACE2 structure and function as a SARS-CoV receptor. Biochem Biophys Res Commun. 2004;314(1):235–41.

7.   Böhm HJ, Schneider G. Protein-Ligand Interactions: From Molecular Recognition to Drug Design. Protein-Ligand Interactions: From Molecular Recognition to Drug Design. 2003. 1–242 p.

8.   Li W, Zhang C, Sui J, Kuhn JH, Moore MJ, Luo S, et al. Receptor and viral determinants of SARS-coronavirus adaptation to human ACE2. EMBO J. 2005;24(8):1634–43.

9.   Veeramachaneni GK, Thunuguntla VBSC, Bobbillapati J, Bondili JS. Structural and simulation analysis of hotspot residues interactions of SARS-CoV 2 with human ACE2 receptor. J Biomol Struct Dyn. 2020;(just-accepted):1–11.

10. Hoffmann M, Kleine-Weber H, Schroeder S, Krüger N, Herrler T, Erichsen S, et al. SARS-CoV-2 Cell Entry Depends on ACE2 and TMPRSS2 and Is Blocked by a Clinically Proven Protease Inhibitor. Cell. 2020;181(2):271-280.e8.

11. Wan Y, Shang J, Graham R, Baric RS, Li F. Receptor Recognition by the Novel Coronavirus from Wuhan: an Analysis Based on Decade-Long Structural Studies of SARS Coronavirus. J Virol. 2020;94(7).

12. Lu R, Zhao X, Li J, Niu P, Yang B, Wu H, et al. Genomic characterisation and epidemiology of 2019 novel coronavirus: implications for virus origins and receptor binding. Lancet. 2020;395(10224):565–74.

13. Skeggs LT, Kahn JR, Shumway NP. The preparation and function of the hypertensin-converting enzyme. J Exp Med. 1956;103(3):295–9.

14. Li W, Moore MJ, Vasilieva N, Sui J, Wong SK, Berne MA, et al. Angiotensin-converting enzyme 2 is a functional receptor for the SARS coronavirus. Nature. 2003;426(6965):450–4.

15. Towler P, Staker B, Prasad SG, Menon S, Tang J, Parsons T, et al. ACE2 X-Ray Structures Reveal a Large Hinge-bending Motion Important for Inhibitor Binding and Catalysis. J Biol Chem. 2004;279(17):17996–8007.

16. Hasan A, Paray BA, Hussain A, Qadir FA, Attar F, Aziz FM, et al. A review on the

cleavage priming of the spike protein on coronavirus by angiotensin-converting enzyme-2 and furin. J Biomol Struct Dyn. 2020;1–9.

17.   Yan R, Zhang Y, Li Y, Xia L, Guo Y, Zhou Q. Structural basis for the recognition of SARS-CoV-2 by full-length human ACE2. Science (80-). 2020;367(6485):1444–8.

18.   Basit A, Ali T, Rehman SU. Truncated human angiotensin converting enzyme 2; a potential inhibitor of SARS-CoV-2 spike glycoprotein and potent COVID-19 therapeutic agent. J Biomol Struct Dyn. 2020;(just-accepted):1–17.

19.   Boopathi S, Poma AB, Kolandaivel P. Novel 2019 Coronavirus Structure, Mechanism of Action, Antiviral drug promises and rule out against its treatment. J Biomol Struct Dyn. 2020;1–14.

20.   te Velthuis AJW, van den Worml SHE, Sims AC, Baric RS, Snijder EJ, van Hemert MJ. Zn2+ inhibits coronavirus and arterivirus RNA polymerase activity in vitro and zinc ionophores block the replication of these viruses in cell culture. PLoS Pathog. 2010;6(11):e1001176.

21.   Alirezaei M, Nairn AC, Glowinski J, Prémont J, Marin P. Zinc inhibits protein synthesis in neurons. Potential role of phosphorylation of translation initiation factor-2α. J Biol Chem. 1999;274(45):32433–8.

22.   Frederickson CJ, Koh JY, Bush AI. The neurobiology of zinc in health and disease. Nat Rev Neurosci. 2005;6(6):449–62.

23.   Lazarczyk M, Favre M. Role of Zn2+ Ions in Host-Virus Interactions. J Virol. 2008;82(23):11486–94.

24.   Gurley SB, Coffman TM. Angiotensin-converting enzyme 2 gene targeting studies in mice: Mixed messages. Exp Physiol. 2008;93(5):538–42.

25.   Fang L, Karakiulakis G, Roth M. Are patients with hypertension and diabetes mellitus at increased risk for COVID-19 infection? Lancet Respir Med. 2020;8(4):e21.

26.   Zhou F, Yu T, Du R, Fan G, Liu Y, Liu Z, et al. Clinical course and risk factors for mortality of adult inpatients with COVID-19 in Wuhan, China: a retrospective cohort study. Lancet. 2020;395(10229):1054–62.

27.   Bunyavanich S, Do A, Vicencio A. Nasal Gene Expression of Angiotensin-Converting Enzyme 2 in Children and Adults. JAMA - J Am Med Assoc. 2020;

28.   Vincent MJ, Bergeron E, Benjannet S, Erickson BR, Rollin PE, Ksiazek TG, et al. Chloroquine is a potent inhibitor of SARS coronavirus infection and spread. Virol J. 2005;2(1):1–10.

29.   Adeoye AO, Oso BJ, Olaoye IF, Tijjani H, Adebayo AI. Repurposing of chloroquine and some clinically approved antiviral drugs as effective therapeutics to prevent cellular entry and replication of coronavirus. J Biomol Struct Dyn. 2020;(just-accepted):1–14.

30.   Amin M, Abbas G. Docking study of chloroquine and hydroxychloroquine interaction with RNA binding domain of nucleocapsid phospho-protein–an in silico insight into the comparative efficacy of repurposing antiviral drugs. J Biomol Struct Dyn. 2020;(just-accepted):1–11.

31.   Smith M, Smith JC. Repurposing Therapeutics for COVID-19: Supercomputer-

Based Docking to the SARS-CoV-2 Viral Spike Protein and Viral Spike Protein-Human ACE2 Interface. ChemRxiv. 2020;(2).

32. Javorac D, Grahovac L, Manić L, Stojilković N, Anđelković M, Bulat Z, et al. An overview of the safety assessment of medicines currently used in the COVID-19 disease treatment. Food Chem Toxicol. 2020;144(May).

33. Cava C, Bertoli G, Castiglioni I. In silico discovery of candidate drugs against covid-19. Viruses. 2020;12(4):1–14.

34. Wang J. Fast Identification of Possible Drug Treatment of Coronavirus Disease-19 (COVID-19) through Computational Drug Repurposing Study. J Chem Inf Model. 2020;60(6):3277–86.

35. Lima de Oliveira MD, Teixeira de Oliveira KM. Comparative Computational Study of SARS-CoV-2 Receptors Antagonists from Already Approved Drugs. ChemRxiv. 2020;269.

36. Farag A, Wang P, Ahmed M, Sadek H. Identification of FDA Approved Drugs Targeting COVID-19 Virus by Structure-Based Drug Repositioning. 2020;(1).

37. Barros RO, Junior FLCC, Pereira WS, Oliveira NMN, Ramos RM. Interaction of Drug Candidates with Various SARS-CoV-2 Receptors: An in Silico Study to Combat COVID-19. J Proteome Res. 2020;19(11):4567–75.

38. Das S, Sarmah S, Lyndem S, Singha Roy A. An investigation into the identification of potential inhibitors of SARS-CoV-2 main protease using molecular docking study. J Biomol Struct Dyn [Internet]. 2021;39(9):3347–57. Available from: https://doi.org/10.1080/07391102.2020.1763201

39. Zhang D hai, Wu K lun, Zhang X, Deng S qiong, Peng B. In silico screening of Chinese herbal medicines with the potential to directly inhibit 2019 novel coronavirus. J Integr Med [Internet]. 2020;18(2):152–8. Available from: https://doi.org/10.1016/j.joim.2020.02.005

40. Bouchentouf S, Missoum N. Identification of Compounds from Nigella Sativa as New Potential Inhibitors of 2019 Novel Coronasvirus (Covid-19): Molecular Docking Study. ChemRxiv. 2020;19:1–12.

41. Cheng L, Zheng W, Li M, Huang J, Bao S. Citrus fruits are rich in flavonoids for immunoregulation and potential targeting ACE2 These authors contributed equally to this study Corresponding : Dr . Zhaocheng Ma : mzhaocheng@mail.hzau.edu.cn. Preprints [Internet]. 2020;(February). Available from: https://www.preprints.org/manuscript/202002.0313/v1

42. Khaerunnisa S, Kurniawan H, Awaluddin R, Suhartati S. Potential Inhibitor of COVID-19 Main Protease (M pro) from Several Medicinal Plant Compounds by Molecular Docking Study. Preprints [Internet]. 2020;(March):1–14. Available from: https://www.preprints.org/manuscript/202003.0226/v1

43. Bhowmik D, Nandi R, Kumar D. Evaluation of flavonoids as 2019-nCoV cell entry inhibitor through molecular docking and pharmacological analysis. 2019;

44. Liang J, Pitsillou E, Karagiannis C, Darmawan KK, Ng K, Hung A, et al. Interaction of the prototypical α-ketoamide inhibitor with the SARS-CoV-2 main protease active site in silico: Molecular dynamic simulations highlight the stability of the ligand-protein complex. Comput Biol Chem [Internet]. 2020;87(May):107292.

Available from: https://doi.org/10.1016/j.compbiolchem.2020.107292

45.   Chidambaram SK, Ali D, Alarifi S, Radhakrishnan S, Akbar I. In silico molecular docking: Evaluation of coumarin based derivatives against SARS-CoV-2. J Infect Public Health [Internet]. 2020;13(11):1671–7. Available from: https://doi.org/10.1016/j.jiph.2020.09.002

46.   Khelfaoui H, Harkati D, Saleh BA. Molecular docking, molecular dynamics simulations and reactivity, studies on approved drugs library targeting ACE2 and SARS-CoV-2 binding with ACE2. J Biomol Struct Dyn [Internet]. 2020;0(0):1–17. Available from: https://doi.org/10.1080/07391102.2020.1803967

47.   Zia A. Docking of Velpatasvir to the SARS-CoV-2 Viral Spike Protein-Human ACE2 Complex : repurposing for COVID-19. 2021;1–16.

48.   DasGupta D, Chan WKB, Carlson HA. Computational Identification of Possible Allosteric Sites and Modulators of the SARS-CoV-2 Main Protease. J Chem Inf Model. 2022;62(3):618–26.

49.   Narayanan A, Narwal M, Majowicz SA, Varricchio C, Toner SA, Ballatore C, et al. Identification of SARS-CoV-2 inhibitors targeting Mpro and PLpro using in-cell-protease assay. Commun Biol. 2022;5(1):1–17.

50.   Schreiber AB, Libermann TA, Lax I, Yarden Y, Schlessinger J. Biological role of epidermal growth factor-receptor clustering. Investigation with monoclonal anti-receptor antibodies. J Biol Chem. 1983;258(2):846–53.

51.   Arteaga C. Targeting HER1/EGFR: A molecular approach to cancer therapy. Semin Oncol. 2003;30(3H):3–14.

52.   Mendelsohn J, Baselga J. Epidermal growth factor receptor targeting in cancer. In: Seminars in oncology. Elsevier; 2006. p. 369–85.

53.   Yarden Y, Sliwkowski MX. Untangling the ErbB signalling network. Nat Rev Mol cell Biol. 2001;2(2):127–37.

54.   Lynch TJ, Bell DW, Sordella R, Gurubhagavatula S, Okimoto RA, Brannigan BW, et al. Activating Mutations in the Epidermal Growth Factor Receptor Underlying Responsiveness of Non–Small-Cell Lung Cancer to Gefitinib. N Engl J Med. 2004;350(21):2129–39.

55.   Shigematsu H, Gazdar AF. Somatic mutations of epidermal growth factor receptor signaling pathway in lung cancers. Int J Cancer. 2006;118(2):257–62.

56.   Greulich H, Chen TH, Feng W, Jänne PA, Alvarez J V., Zappaterra M, et al. Oncogenic transformation by inhibitor-sensitive and -resistant EGFR mutants. PLoS Med. 2005;2(11):1167–76.

57.   Allen LF, Eiseman IA, Fry DW, Lenehan PF. CI-1033, an Irreversible pan-erbB Receptor Inhibitor and its Potential Application for the Treatment of Breast Cancer. Semin Oncol. 2003;30(5 SUPPL. 16):65–78.

58.   Miller VA, Hirsh V, Cadranel J, Chen YM, Park K, Kim SW, et al. Afatinib versus placebo for patients with advanced, metastatic non-small-cell lung cancer after failure of erlotinib, gefitinib, or both, and one or two lines of chemotherapy (LUX-Lung 1): A phase 2b/3 randomised trial. Lancet Oncol [Internet]. 2012;13(5):528–38. Available from: http://dx.doi.org/10.1016/S1470-2045(12)70087-6

59.   Wang S, Song Y, Liu D. EAI045: The fourth-generation EGFR inhibitor

overcoming T790M and C797S resistance. Cancer Lett [Internet]. 2016;385:51–4. Available from: http://dx.doi.org/10.1016/j.canlet.2016.11.008

60.   Yun CH, Mengwasser KE, Toms A V., Woo MS, Greulich H, Wong KK, et al. The T790M mutation in EGFR kinase causes drug resistance by increasing the affinity for ATP. Proc Natl Acad Sci U S A. 2008;105(6):2070–5.

61.   Jia Y, Yun CH, Park E, Ercan D, Manuia M, Juarez J, et al. Overcoming EGFR(T790M) and EGFR(C797S) resistance with mutant-selective allosteric inhibitors. Nature [Internet]. 2016;534(7605):129–32. Available from: http://dx.doi.org/10.1038/nature17960

62.   Choi YW, Jeon SY, Jeong GS, Lee HW, Jeong SH, Kang SY, et al. EGFR Exon 19 Deletion is Associated with Favorable Overall Survival after First-line Gefitinib Therapy in Advanced Non-Small Cell Lung Cancer Patients. Am J Clin Oncol Cancer Clin Trials. 2018;41(4):385–90.

63.   Saleh BA. Quantum chemical studies on para-substituted styrenyl fullerene. Study of substitution effects on structural and electronic properties. J Mol Struct THEOCHEM. 2009;915(1–3):47–50.

64.   Saleh BA, Essa AH, Al-Shawi SAO, Jalbout AF. Correlation analysis of the substituent electronic effects on the Mulliken charge. Resonance and field effects of substituents at para-substituted styrenyl fullerene. J Mol Struct THEOCHEM. 2009;909(1–3):107–10.

65.   Saleh BA, Abood HA, Miyamoto R, Bortoluzzi M. Theoretical Study of Substituent Effects on Electronic and Structural Properties of 2, 4-Diamino-5-para-substituted-phenyl-6-ethyl-pyrimidines. J Iran Chem Soc. 2011;8(3):653–61.

66.   Behalo MS. Synthesis and Antimicrobial Activities of Some Novel Pyrido[2,3-d]pyrimidine Derivatives. Phosphorus Sulfur Silicon Relat Elem [Internet]. 2008 Dec 23;184(1):206–19. Available from: https://doi.org/10.1080/10426500802095764

67.   Samira I, Patel S, Hasmin M, Patel S. Biological Profile of Quinazoline. Int J Pharm Chem Sci [Internet]. 2012;1(4):1519–28. Available from: www.ijpcsonline.com

68.   Ghorab MM, Ismail ZH, Radwan AA, Abdalla M. Synthesis and pharmacophore modeling of novel quinazolines bearing a biologically active sulfonamide moiety. Acta Pharm. 2013;63(1):1–18.

69.   Vijayakumar K, Ahamed AJ, Thiruneelakandan G. Synthesis, antimicrobial, and anti-HIV1 activity of quinazoline-4 (3H)-one derivatives. J Appl Chem. 2013;2013:5.

70.   Amin KM, Georgey HH, Awadallah FM. EGFR tyrosine kinase targeted compounds: Synthesis, docking study, and in vitro antitumor activity of some new quinazoline and benzo[d]isothiazole derivatives. Med Chem Res. 2011;20(7):1042–53.

71.   Asadollahi-Baboli M. In silico evaluation, molecular docking and QSAR analysis of quinazoline-based EGFR-T790M inhibitors. Mol Divers. 2016;20(3):729–39.

72.   Abdullahi SH, Uzairu A, Shallangwa GA, Uba S, Umar AB. In-silico activity prediction, structure-based drug design, molecular docking and pharmacokinetic studies of selected quinazoline derivatives for their antiproliferative activity against

triple negative breast cancer (MDA-MB231) cell line. Bull Natl Res Cent [Internet]. 2022;46(1). Available from: https://doi.org/10.1186/s42269-021-00690-z

73.   Al-Salahi R, Taie HAA, Bakheit AH, Marzouk M, Almehizia AA, Herqash R, et al. Antioxidant activities and molecular docking of 2-thioxobenzo[g]quinazoline derivatives. Pharmacol Reports. 2019;71(4):695–700.

74.   Santos-Ballardo L, García-Páez F, Picos-Corrales LA, Ochoa-Terán A, Bastidas P, Calderón-Zamora L, et al. Synthesis, biological evaluation and molecular docking of 3-substituted quinazoline-2,4(1H, 3H)-diones. J Chem Sci. 2020;132(1):1–10.

75.   Wei L, Malhotra S V. Synthesis and cytotoxicity evaluation of novel pyrido[3,4-d]pyrimidine derivatives as potential anticancer agents. Medchemcomm. 2012;3(10):1250–7.

76.   Zhang H, Wang J, Shen Y, Wang HY, Duan WM, Zhao HY, et al. Discovery of 2,4,6-trisubstitued pyrido[3,4-d]pyrimidine derivatives as new EGFR-TKIs. Eur J Med Chem [Internet]. 2018;148:221–37. Available from: https://doi.org/10.1016/j.ejmech.2018.02.051

77.   Deng L, Sun H, Hu W, Liao W, Zhou Z, Pan H. Synthesis, Crystal Structure, and DFT Study of a New Derivative of Pyrido[2,3-d]pyrimidine. Russ J Gen Chem. 2021;91(12):2489–96.

78.   Aryan R, Beyzaei H, Nojavan M, Pirani F, Samareh Delarami H, Sanchooli M. Expedient multicomponent synthesis of a small library of some novel highly substituted pyrido[2,3-d]pyrimidine derivatives mediated and promoted by deep eutectic solvent and in vitro and quantum mechanical study of their antibacterial and antifungal activ. Mol Divers [Internet]. 2019;23(1):93–105. Available from: https://doi.org/10.1007/s11030-018-9859-7

79.   Appna NR, Nagiri RK, Korupolu RB, Kanugala S, Chityal GK, Thipparapu G, et al. Design and synthesis of novel 4-hydrazone functionalized/1,2,4-triazole fused pyrido[2,3-d]pyrimidine derivatives, their evaluation for antifungal activity and docking studies. Med Chem Res [Internet]. 2019;28(9):1509–28. Available from: http://dx.doi.org/10.1007/s00044-019-02390-w

80.   El-Gazzar ARBA, Hafez HN. Synthesis of 4-substituted pyrido[2,3-d]pyrimidin-4(1H)-one as analgesic and anti-inflammatory agents. Bioorganic Med Chem Lett [Internet]. 2009;19(13):3392–7. Available from: http://dx.doi.org/10.1016/j.bmcl.2009.05.044

81.   Adib M, Peytam F, Rahmanian-Jazi M, Mahernia S, Bijanzadeh HR, Jahani M, et al. New 6-amino-pyrido[2,3-d]pyrimidine-2,4-diones as novel agents to treat type 2 diabetes: A simple and efficient synthesis, α-glucosidase inhibition, molecular modeling and kinetic study. Eur J Med Chem [Internet]. 2018;155:353–63. Available from: https://doi.org/10.1016/j.ejmech.2018.05.046

82.   Toobaei Z, Yousefi R, Panahi F, Shahidpour S, Nourisefat M, Doroodmand MM, et al. Synthesis of novel poly-hydroxyl functionalized acridine derivatives as inhibitors of α-Glucosidase and α-Amylase. Carbohydr Res [Internet]. 2015;411:22–32. Available from: http://dx.doi.org/10.1016/j.carres.2015.04.005

Chapter III:

MATERIALS AND METHODS

Chapter III: Materials and methods

I.   Overview

This work was divided to two studies, computational approaches were applied to know inhibitor for COVID-19 and for Epidermal Growth Factor Receptor Tyrosine Kinase mutations.

In the first study, molecular docking and molecular dynamics simulation was applied to the drugs selected from the DrugBank database [1] to study their affinity with coronavirus antibody ACE2 receptor (**PDB ID: 1R42**) [2] and also with the crystal structure of SARS-CoV-2 spike receptor-binding with ACE2 complex (**PDB ID: 6M0J**) [3] to select the most active drugs that inhibit COVID-19. Global reactivity descriptors of the selected drugs were calculated to understand their structures, stability and reactivity. The methodology of the first study was illustrated in Figure 1.
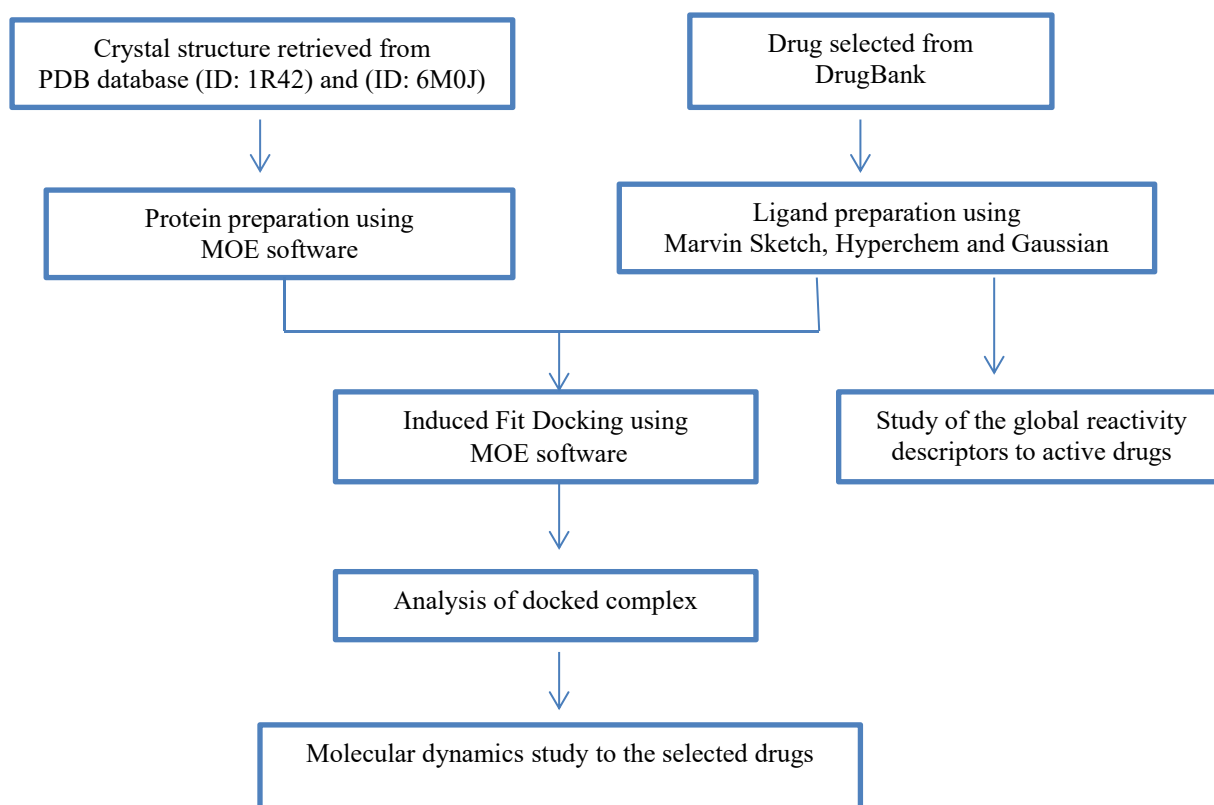

Figure 1 Schematic representation of the docking procedure, analysis of drugs and reactivity

Meanwhile, in second study computational approach for some selected quinazoline and pyrido[3,4-d]pyrimidine derivatives [4] were applied to characterize their chemical properties and interaction bonding domain to EGFR, WT, L858R and T790M mutations by chemical reactivity, Absorption, Distribution, Metabolism, Excretion and Toxicity analysis, molecular docking and molecular dynamics simulation. The methodology of the second study was illustrated in Figure 2.

Figure 2 Schematic representation of the computation approaches used to ligands.

II.   Molecule library preparation

The structures were optimized using Density Functional Theory DFT method by employing the B3LYP (Becke's three parameter hyprid functional with Lee-Yang-Parr correlation functional LYP) combined with the 6-31G basis set [5,6] to obtain the most stable conformation, which was also used to calculate the global reactivity descriptors through Gaussian 09 [6]. Maximum force, Root-Mean-Squared (RMS) force, maximum displacement, and RMS displacement are all set to convergent values by default, and 'YES' is attained. After calculating vibrational frequencies to drugs, all values are positive,

indicating that the compounds are stable. [7]. The optimized structures were combined in one database on MOE software [8] in order to study the affinity of ligands.

II.1. Molecular library preparation for COVID-19 inhibitors

The chemical structure of drugs inhibitors of ACE2 and similar structures were extracted from the DrugBank database Figure 3 [9] in MDL Mol format and converted to 3D format using Mervin Sketch [10]. The structures were pre-optimized with semi-empirical AM1 method [11] using Hyperchem 8.08 software [12]. The clinical indications for drugs are cited in Table 1.
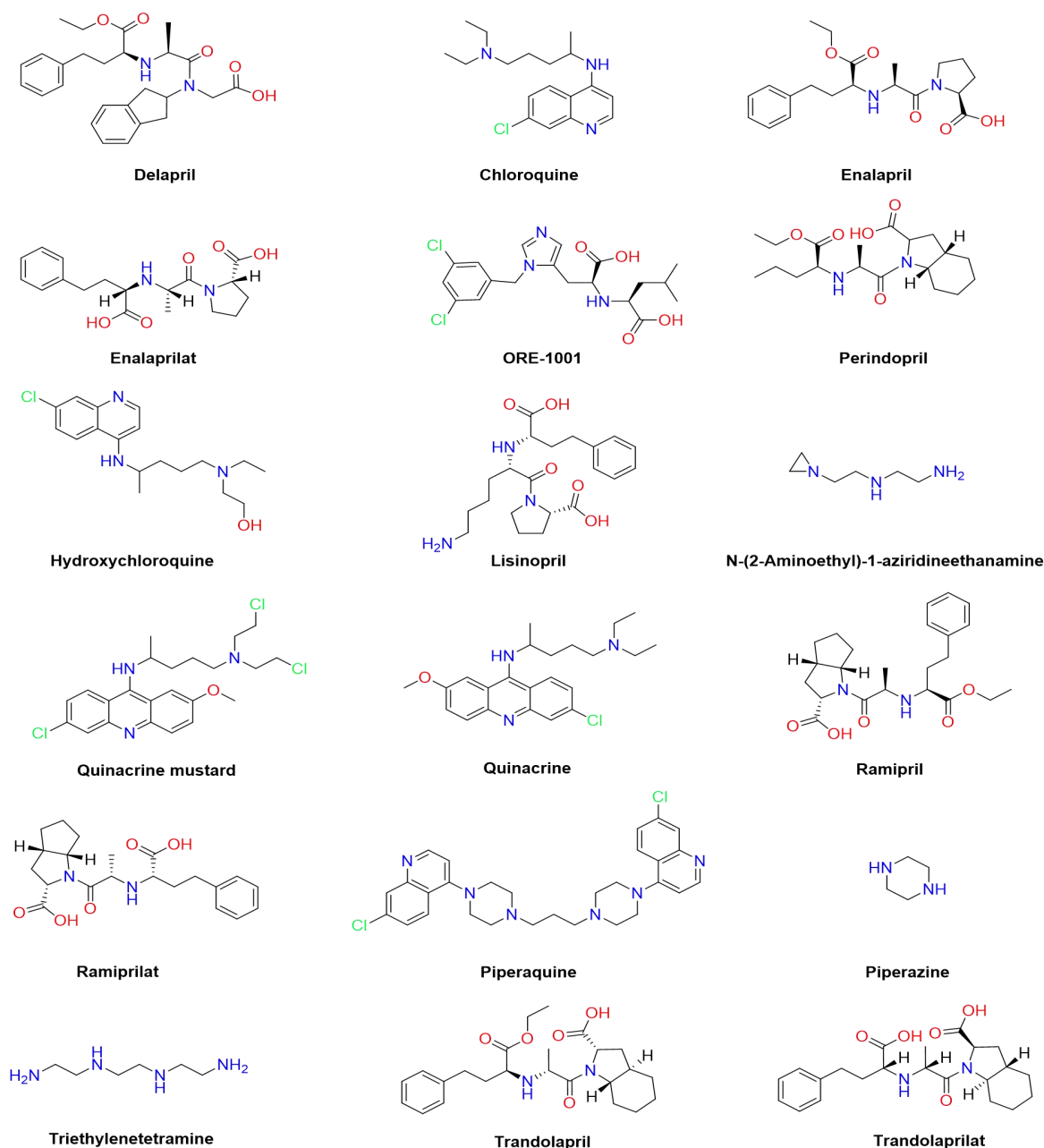
Delapril	**Chloroquine**	**Enalapril**
Enalaprilat	**ORE-1001**	**Perindopril**
Hydroxychloroquine	**Lisinopril**	**N-(2-Aminoethyl)-1-aziridineethanamine**
Quinacrine mustard	**Quinacrine**	**Ramipril**
Ramiprilat	**Piperaquine**	**Piperazine**
Triethylenetetramine	**Trandolapril**	**Trandolaprilat**

Figure 3 The structures of selected drugs.

Table 1 Names, accessions numbers and clinical indication of drugs.

Drugs names	Accessions Numbers	Clinical Indication
Chloroquine	DB00608 (APRD00468)	Anti-malarial Anti-inflammatory Anti-parasitic
Hydroxychloroquine	DB01611	Anti-malarial Anti-parasitic Anti-rheumatic Anti-infective

Quinacrine	DB01103 (APRD00317)	Anti-infective Anti-malarial Anti-parasitic
Quinacrine mustard	DB02240 (EXPT02733)	Anti-parasitic
Piperaquine	DB13941	Anti-infective Anti-malarial Anti-parasitic
Ramipril	DB00178 (APRD00009)	Angiotensin-Converting Enzyme inhibitors Anti-hypertensive Cardiovascular
Trandolapril	DB00519 (APRD01269)	Angiotensin-Converting Enzyme inhibitors Anti-hypertensive Cardiovascular
Ramiprilat	DB14208	Angiotensin-Converting Enzyme inhibitors Anti-hypertensive Cardiovascular
Enalapril	DB00584 (APRD00510)	Angiotensin-Converting Enzyme inhibitors Anti-hypertensive Cardiovascular
Trandolaprilat	DB14209	Angiotensin-Converting Enzyme inhibitors
Lisinopril	DB00722 (APRD00560)	Angiotensin-Converting Enzyme inhibitors Anti-hypertensive Cardiovascular
Perindopril	DB00790 (APRD01178)	Angiotensin-Converting Enzyme inhibitors Anti-hypertensive Cardiovascular
Enalaprilat	DB09477	Angiotensin-Converting Enzyme inhibitors Anti-hypertensive Cardiovascular Decreased blood pressure
Delapril	DB13312	Angiotensin-Converting Enzyme inhibitors Anti-hypertensive Cardiovascular
ORE-1001	DB12271 (DB06387)	Angiotensin-Converting Enzyme inhibitors
N-**(2-Aminoethyl)-1-aziridineethanamine**	DB15643	Angiotensin-Converting Enzyme inhibitors

Triethylenetetramine	DB06824		Copper chelator agent
Piperazine	DB00592 DB11514)	(APRD00225,	Anti-parasitic Anti-infective

II.2. Molecular library preparation for EGFR inhibitors

A dataset of substituted quinazoline and pyrido[3,4-d]pyrimidine derivatives as irreversible tyrosine kinase inhibitors of the epidermal growth factor receptor family were extracted from the literature[4]. In the present study, 27 active compounds, are shown in Table 2 with smiles and IC_{50} values ranging from 0.002 to 0.026 (µM), also their structures are presented in Figure 4. Also seven approved drugs were selected, Figure 5.

Table 2 The smiles compounds and respective experimental IC50

Compounds	SMILES	IC_{50} (µM)
L1	Clc1c(F)ccc(Nc2ncnc3c2cc(NC(=O)C(=C)C)c(OCCCN2CCOCC2)c3)c1	0.021
L2	Clc1c(F)ccc(Nc2ncnc3c2cc(NC(=O)/C=C/C)c(OCCCN2CCOCC2)c3)c1	0.022
L3	Clc1c(F)ccc(Nc2ncnc3c2cc(NC(=O)C2=CCCC2)c(OCCCN2CCOCC2)c3)c1	0.007
L4	Clc1c(F)ccc(Nc2ncnc3c2cc(NC(=O)CC)c(OCCCN2CCOCC2)c3)c1	0.009
L5	Clc1c(F)ccc(Nc2ncnc3c2cc(NC(=O)CC)c(OC)c3)c1	0.002
L6	O=C(Nc1c(OC)cc2ncnc(Nc3cc4c([nH]cc4)cc3)c2c1)CC	0.006
L7	O=C(Nc1c(OC)cc2ncnc(Nc3cc4c(n(Cc5ccccc5)cc4)cc3)c2c1)CC	0.021
L8	O=C(Nc1c(OC)cc2ncnc(Nc3cc4c(n(Cc5ccccc5)nc4)cc3)c2c1)CC	0.017
L9	O=C(Nc1c(OCC)cc2ncnc(Nc3cc4c(n(Cc5ccccc5)nc4)cc3)c2c1)/C=C/CN(C)C	0.006
L10	O=C(Nc1c(OCC)cc2ncnc(Nc3cc4c(n(Cc5ccccc5)nc4)cc3)c2c1)/C=C\CN(C(C)C)C(C)C	0.015
L11	O=C(Nc1c(OCC)cc2ncnc(Nc3cc4c(n(Cc5ccccc5)nc4)cc3)c2c1)/C=C\CN1CCCC1	0.007
L12	O=C(Nc1c(OCC)cc2ncnc(Nc3cc4c(n(Cc5ccccc5)nc4)cc3)c2c1)/C=C\CN1CCCCC1	0.008
L13	O=C(Nc1c(OCC)cc2ncnc(Nc3cc4c(n(Cc5ccccc5)nc4)cc3)c2c1)/C=C\CN1CCOCC1	0.026
L14	O=C(Nc1c(OCC)cc2ncnc(Nc3cc4c(n(Cc5ccccc5)nc4)cc3)c2c1)/C=C\CN1CCN(C)CC1	0.023
L15	O=C(Nc1c(OCC)cc2ncnc(Nc3cc4c(n(Cc5ccccc5)nc4)cc3)c2c1)/C=C\CN1CC(C)NC(C)C1	0.017
L16	Clc1c(F)ccc(Nc2ncnc3c2cc(NC(=O)/C=C\CN(C(C)C)C(C)C)c(OC)c3)c1	0.002
L17	Clc1c(F)ccc(Nc2ncnc3c2cc(NC(=O)/C=C\CN2CCCCC2)c(OC)c3)c1	0.006
L18	O=C(Nc1c(OCCOC)cc2ncnc(Nc3cc4c(n(Cc5ccccc5)nc4)cc3)c2c1)/C=C\CN(C)C	0.007
L19	O=C(Nc1c(OCCOC)cc2ncnc(Nc3cc4c(n(Cc5ccccc5)nc4)cc3)c2c1)/C=C\C	0.010

	N1CCCC1	
L20	O=C(Nc1c(OCCOC)cc2ncnc(Nc3cc4c(n(Cc5ccccc5)nc4)cc3)c2c1)/C=C\CN1CCN(C)CC1	0.016
L21	Clc1c(OCc2cc(F)ccc2)ccc(Nc2ncnc3c2cc(NC(=O)/C=C\CN2CCN(C)CC2)c(OCC)c3)c1	0.023
L22	S(=O)(=O)(Nc1ccc(Nc2ncnc3c2cc(NC(=O)/C=C\CN2CCCC2)c(OCC)c3)cc1)c1ccccc1	0.021
L23	Clc1c(F)ccc(Nc2ncnc3c2cc(NC(=O)/C=C\CN(C)C)nc3)c1	0.002
L24	Clc1c(F)ccc(Nc2ncnc3c2cc(NC(=O)/C=C\CN2CCCCC2)nc3)c1	0.014
L25	Clc1c(F)ccc(Nc2ncnc3c2cc(NC(=O)/C=C\CN2CCOCC2)nc3)c1	0.012
L26	Clc1c(F)ccc(Nc2ncnc3c2cc(NC(=O)/C=C\CN2CCN(C)CC2)nc3)c1	0.019
L27	Clc1c(OCc2cc(F)ccc2)ccc(Nc2ncnc3c2cc(NC(=O)/C=C\CN(C)C)nc3)c1	0.025

IC$_{50}$ (L1)=0.021 μM   IC$_{50}$ (L2)=0.022 μM   IC$_{50}$ (L3)=0.007 μM   IC$_{50}$ (L4)=0.009 μM

IC$_{50}$ (L4)=0.002 μM   IC$_{50}$ (L5)=0.006 μM   IC$_{50}$ (L7)=0.021 μM   IC$_{50}$ (L8)=0.017 μM

IC$_{50}$ (L9)=0.006 μM   IC$_{50}$ (L10)=0.015 μM   IC$_{50}$ (L11)=0.007 μM   IC$_{50}$ (L12)=0.008 μM

IC$_{50}$ (L13)=0.026 μM   IC$_{50}$ (L14)=0.023 μM   IC$_{50}$ (L15)=0.017 μM   IC$_{50}$ (L16)=0.002 μM

IC$_{50}$ (L17)=0.006 μM   IC$_{50}$ (L18)=0.007 μM   IC$_{50}$ (L19)=0.010 μM   IC$_{50}$ (L20)=0.016 μM

IC$_{50}$ (L21)=0.023 μM   IC$_{50}$ (L22)=0.021 μM   IC$_{50}$ (L23)=0.002 μM   IC$_{50}$ (L24)=0.014 μM

IC$_{50}$ (L25)=0.012 μM   IC$_{50}$ (L26)=0.019 μM   IC$_{50}$ (L27)=0.025 μM

Figure 4 The chemical structures of 27 quinazoline and pyrido[3,4-d]pyrimidine derivatives of tyrosine kinase inhibitors.
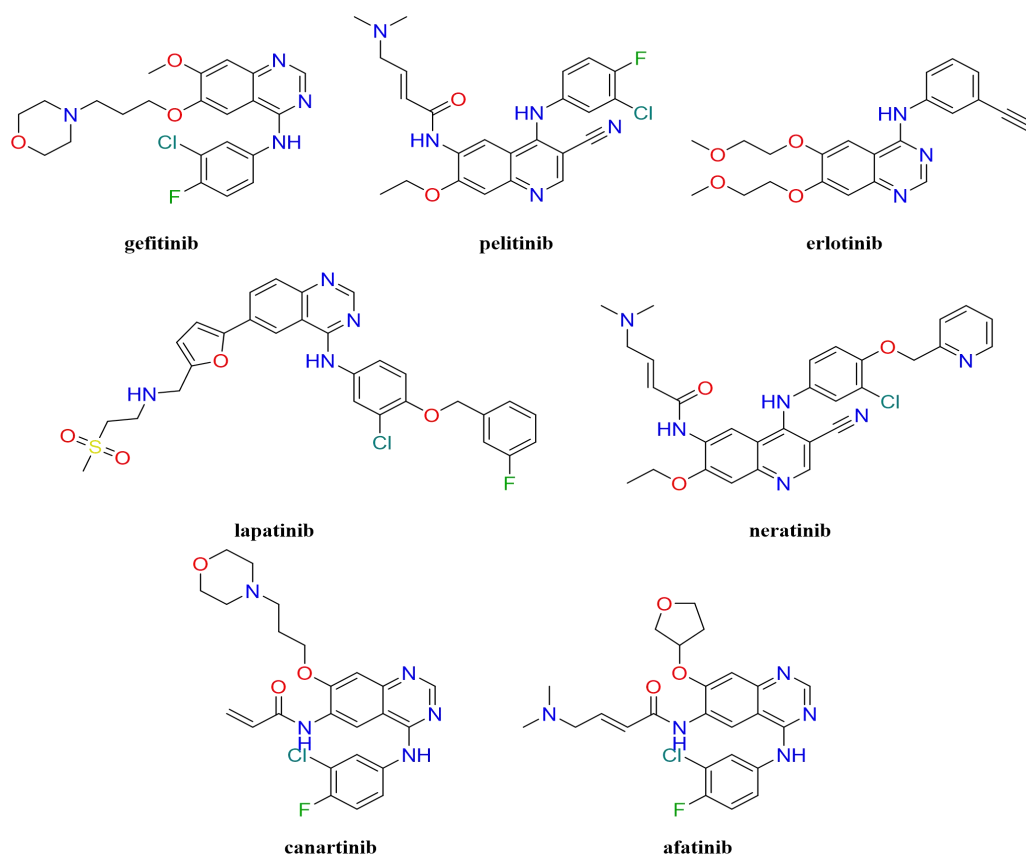
Figure 5 The chemical structures of first and second generation of tyrosine kinase inhibitors.

III.   Receptor preparation

Because the water molecule in the active site of the target enzyme plays an important role, it was inserted in the active sites to ensure making a hydrogen bond between the ligand and the target [17–19]. The protein structures were prepared by correcting the missing bonds, which were broken in X-ray diffraction, and then the hydrogen atoms were added. The protein structures were optimized with Amber 10: EHT force field. MOE software was used to all the steps of enzyme preparation[8] .The residues of the active sites to each enzyme were obtained using site finder.

III.1. Preparation of 1R42 and 6M0J receptors

The crystal structure of *t*he angiotensin-converting enzyme related carboxypeptidase ACE2 receptor **PDB ID: 1R42** [2] and Crystal structure SARS-CoV-2 spike receptor-binding with ACE2 complex **PDB ID: 6M0J** [3] were found in the Protein Data Bank.

Firstly, the enzymes were prepared by removing the *N*-acetyl-D-glucosamine in sequence editor.

Because Zn^{2+} is an important cofactor for many viral proteins, Zn^{2+} can inhibit the replication of ARN polymerase [13], two active sites containing zinc (Zn^{2+}) in 1R42 and 6M0J enzymes were chosen as shown in Figure 6, the residues of the sites are presented in Table 3.

Table 3 Binding sites residues used as input for receptor grid generation during Induced Fit Docking

Receptors	Sites	Residues
1R42	**Site 1**	**1**: (Arg73, Phe274, Pro346, Asp367, Leu370, Thr371, His374, Glu375, Glu402, Glu406, Ser409, Leu410, Ala413, Phe438, Gln442, Thr445, Ile446, Thr449, Thr453, Phe512, Tyr515, Arg518, Thr519, Gln522) **2** : **(Zn804)**
	Site 2	**1** : (Phe40, Pro346, Thr347, Ala348, Asp350, Gly352, His374, Glu375, His378, Asp382, Tyr385, Phe390, Arg393, Asn394, His401, Glu402) **2: (Zn804)**
6M0J	**Site 1**	**1**: (Tyr127, Asn149, Asp269, Trp271, Arg273, Phe274, Thr276, Tyr279, Lys288, Pro289, Asn290, Ile291, Asp292, Thr294, His345, Pro346, Thr365, Met366, Asp367, Leu370, Thr371, His374, Glu375, Glu402, Glu406, Ser409, Leu410, Ala413, Thr414, Pro415, Leu418 Phe428, Glu430, Asp431, Thr434, Glu435, Asn437, Phe438, Lys441, Gln442, Thr445, Ile446, Thr449, Leu503, Phe504, His505, Tyr515, Arg518, Thr519, Gln522, Phe523, His540) **3** :**(Zn901)**
	Site 2	**1:** (His345, Pro346, Thr347, Ala348, Glu375, His378, Asp382, His401, Glu402) **3 :(Zn901)**
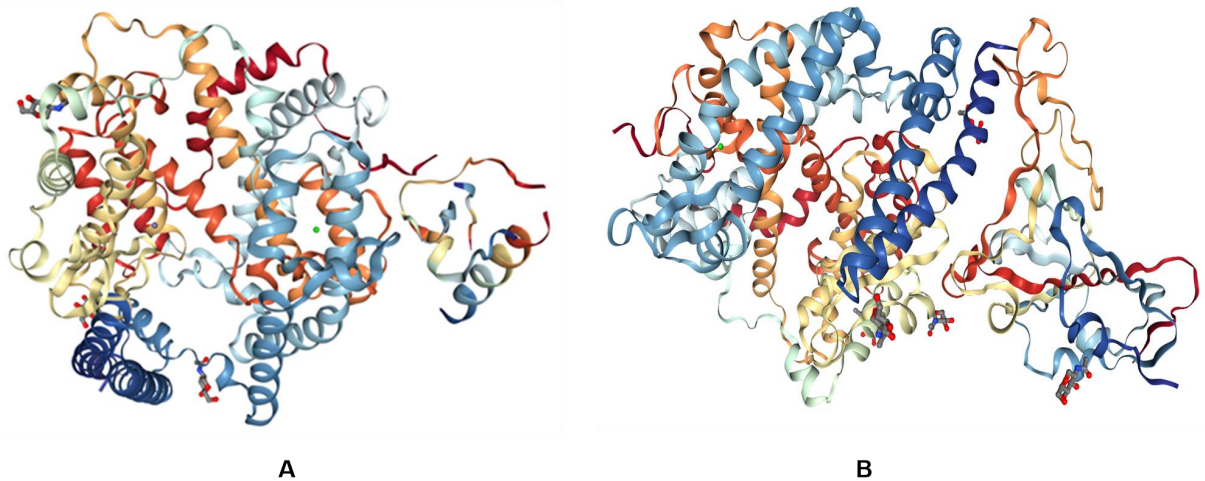
Figure 6 A: Crystal structure of native human Angiotensin Converting Enzyme-related carboxypeptidase ACE2 (PDB ID: 1R42), and B: Crystal structure of SARS-CoV-2 spike receptor-binding with ACE2 complex (PDB ID: 6M0J).

III.2. Preparation of 1XKK, 2ITV and 5HG5 receptors

The three-dimensional crystal structures of three mutated proteins were obtained from the RSCB PDB database [14], Wild-Type **PDB ID: 1XKK** [15], L858R mutation **PDB ID: 2ITV** [16], T790M mutation **PDB ID: 5HG5** [17], as shown in Figure 7. The enzymes were prepared by removing the cofactors, phosphate ion (PO_4^{3-}) for **1XKK** and sulfate ion (SO_4^{2+}) and glycerol (GOL) for **5HG5**. The residues of the active sites to each enzyme were obtained using site finder and they are presented in Table 4.
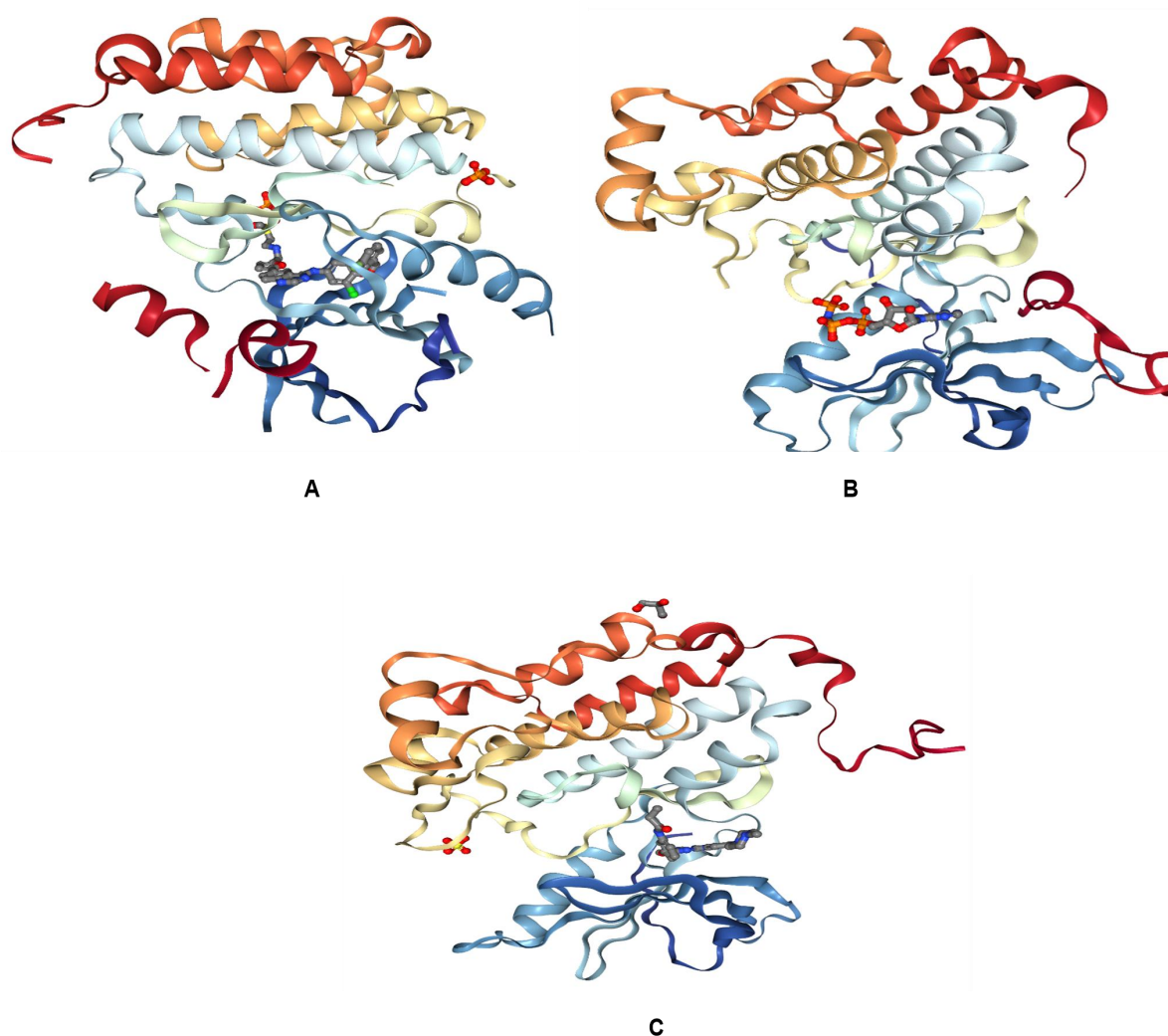
Figure 7 Crystals structure of EGFR kinase domain A: WT in complexed with a quinazoline inhibitor-GW572016 (lapatinib/FMM) (PDB ID: 1XKK), B: L858R mutation in complex with phosphoaminophosphonic acid-adenylate ester (AMP-PNP/ANP) (PDB ID: 2ITV) and C: T790M mutation in complex with N-{3-[(2-{[4-(4-methylpiperazin-1-yl)phenyl]amino}-7H-pyrrolo[2,3-d]pyrimidin-4-yl)oxy]phenyl}prop-2-enamide (633) (PDB ID: 5HG5).

Table 4 Binding sites residues used as input for receptor grid generation during Induced Fit Docking

Receptors	Residues
1XKK	Leu718, Gly719, Ser720, Gly721, Val726, Ala743, Ile744, Lys745, Met766, Cys775, Arg776, Leu777, Leu788, Thr790, Gln791, Leu792, Met793, Phe795, Gly796, Cys797, Asp800, Tyr801, Glu804, Arg841, Asn842, Leu844, Ile853, Thr854, Asp855, Phe856, Leu858, Phe997, Tyr998, Leu1001, Met1002.

2ITV	Gly696, Glu697, Ala698, Pro699, Asn700, Gln701, Ala702, Leu718, Gly719, Ser720, Ala722, Phe723, Gly724, Thr725, Val726, Ala743, Ile744, Lys745, Leu747, Ala755, Lys757, Glu758, Ile759, Asp761, Glu762, Tyr764, Val765, Met766, Ala767, Ser768, Val769, Asp770, Cys775, Leu788, Ile789, Thr790, Gln791, Leu792, Met793, Pro794, Gly796, Cys797, Asp800, Tyr827, Asp830, Arg831, Arg832, Leu833, Arg836, Asp837, Leu844, Thr854, Asp855, Phe856, Gly857, Arg858, Ala859, Lys860, Leu861, Ala864, Glu866, Ace875, Val876
5HG5	Leu718, Gly719, Ser720, Gly721, Ala722, Phe723, Val726, Lys728, Lys745, Leu747, Arg748, Glu749, Ala750, Ser752, Pro753, Lys754, Ile759, Glu762, Ala763, Val765, Met766, Leu777, Ile780, Ser784, Thr785, Val786, Leu788, Leu792, Met793, Pro794, Phe795, Gly796, Cys797, Leu833, Arg836, Asp837 Arg841, Asn842, Leu844, Asp855, Phe856, Gly857, Arg858, Ala859, Lys860, Leu861, Tyr869, Ala871, Glu872, Gly873, Gly874, Lys875, Val876, Tyr891

IV.   Global reactivity descriptors

Global reactivity indices are the most relevant traits, which can be derived from the conceptual Density Functional Theory (DFT). They have important properties which enable us to understand the chemical reactivity and kinetic stability of compounds [18]. The global reactivity descriptors can be described by energy of the highest occupied molecular orbital (E_{HOMO}) and energy of the lowest occupied molecular orbital (E_{LUMO}). (E_{HOMO}) and (E_{LUMO}) were obtained from occupied and virtual eigenvalues of Gaussian output file to calculate global reactivity descriptors such as energy gap (ΔE), global electrophilicity (ω), chemical potential (μ), chemical hardness (η), chemical softness (S) and nucleophilicity (N) [19–22]. Those descriptors were calculated at B3LYP/6-31G at Gaussian 09.

The following equation used to calculate energy gap index ΔE:

$$\Delta E = E_{LUMO} - E_{HOMO} \tag{1}$$

The global electrophilicity index ω as a measure of the reduction in energy due to the maximum electron transfer according to the following equation:

$$\omega = \mu^2/2\eta \tag{2}$$

Chemical potential μ is calculated according to the following equation:

$$\mu = (E_{LUMO} + E_{HOMO})/2 \qquad\qquad (3)$$

Hardness **η** and softness **S** can calculate according to the following equation:

$$\eta = (E_{LUMO} - E_{HOMO})/2 \qquad\qquad (4)$$

$$S = 1/(2\,\eta) \qquad\qquad (5)$$

High values of nucleophilicity **N** correspond to low values of ionization potential and vice versa. Domingo et al. have introduced a relative nucleophilicity index **N** based on the HOMO energies obtained within the Kohn-Sham scheme[23] and defined as:

$$N = E_{HOMO} \textbf{ (Nucleophile)} - E_{HOMO} \textbf{ (TCE)} \qquad\qquad (6)$$

In this study, the global reactivity descriptors were calculated to compounds that have best result in docking with ACE2 and SARS-CoV-2 spike receptor-binding with ACE2 complex. Meanwhile, the global reactivity descriptors were calculated to 27 quinazoline and pyrido[3,4-d]pyrimidine derivatives and 7drugs for EGFR inhibitors.

V.   Molecular Docking

All the molecular docking and scoring calculations were performed using the molecular operation environment software (MOE.2019)[8]. After 30 poses, the docking inhibitors will attacked the protein's internal grooves, resulting in the most stable docking ligand-receptor complexes. The scoring energies were increased by two unrelated adjustments by the triangular Matcher techniques, which were the mean values of trials utilizing the London dG scoring function. In addition to important interaction characteristics, the interacting complexes were retrieved. The level of inhibition was determined using extracted characteristics such ligand locations, receptor backbones (amino acids), interaction type, bond lengths, and internal and scoring energies. It is well known that the optimal RMSD score is near 2 with an energy score of less than or equal to -7 Kcal/mol [24,25]. These two numbers are frequently used as a criterion for evaluating the molecular docking results. Also the bond length must be not exceeding than 3.5 Å to be effective [26].

The molecular docking process inserted in software (MOE) [8] was implemented for the selected drugs from DrugBank database [9]. The tested inhibitors were chosen based on their structural similarities to chloroquine and hydroxycholroquine, also ACE2 inhibitors,

to provide a broad overview of their interactions with selected receptors. Regarding the selected receptors, human Angiotensin Converting Enzyme-related carboxypeptidase (ACE2) and SARS-CoV-2 spike receptor-binding domain bound with ACE2 were selected, which will simulate the intended screening in vitro study. 1R42 and 6M0J, were the co-crystalline structures obtained from RCSB PDB [14]. The crystal structure of human angiotensin converting enzyme (PDB entry: 1R42) [2] at a resolution of 2.20 Å and the crystal structure of SARS-CoV-2 spike receptor-binding with ACE2 complex (PDB entry: 6M0J) [3] at a resolution of 2.45 Å.

Also, The crystal structures of EGFR wild-type (PDB entry: 1XKK) [15] is at a resolution of 2.40 Å, while the crystal structure of EGFR L858R mutation (PDB entry: 2ITV) [16] is at a resolution of 2.47 Å and the crystal structure of EGFR T790M mutation (PDB entry: 5HG5) [17], Table 5 summarizes the protein information is at resolution of 1.52 Å. A resolution between 1.5 and 2.5 Å is considered as a good quality for docking studies [27,28].

Table 5 Crystallization, data collection and refinement statistics.

EGFR kinase domain	Wild-type	L858R	T790M
Complex with Crystallization conditions	FMM 100 mM CAPS, 200 mM LiSO4, 2M NaKPO4, pH 9, temperature 293K	ANP 40% PEG400, 0.15M NACL, 0.1M HEPES 7.5, pH 7.50	633 0.1 M Sodium acetate trihydrate, 20 % PEG 8000, 10 % iso-propanol, 0.2 M Ammonium sulfate, pH 7.50, temperature 286K
Data collection			
Space group	P $2_12_12_1$	I 2 3	P $2_12_12_1$
Cell dimensions			
a, b, c (Å)	45.653, 67.144, 102.88	145.081, 145.081, 145.081	40.321, 70.002, 111.114
α, β, γ (°)	90, 90, 90	90, 90, 90	90, 90, 90
Resolution (Å)	2.40	2.47	1.52
PDB ID	1XKK	2ITV	5HG5

VI. Molecular Dynamics Simulations

Molecular dynamics simulation was used to confirm the reliability of molecular docking and reveal the binding mode and conformational changes during the interaction between drugs and receptor protein. The molecular dynamics (MD) simulation study was carried out for the most promising drugs **Delapril**, **Lisinopril** and **Ramipril** to target SARS-CoV-2 spike receptor-binding with ACE2 complex (**6M0J**), and for the most promising ligands to EGFR receptors using standard default parameter setting in the MOE software to evaluate protein-ligand interactions [8].

There are four algorithms implemented in MOE software for MD simulations; the Nosé-Poincaré-Andesen (NPA), the Nosé-Hoover-Andersen (NHA), Berendsen velocity/position (BER) and Nanoscale Molecular Dynamics (NAMD). In this study, the NPA: the most precise and the most sensitive, was used to study the molecular dynamics of ligands [29]. The systems were solvated in droplet mode and sphere shape with 6 as margins margins and delete far existing solvent with distance greater than 4 Å. The minimization steps were applied for the systems using MMFF94x force field. The system was further equilibrated to carry out 600 ps MD simulations while temperature was set at 300 K and the heavy atom tether standard deviation at r =0.5 Å. MD simulation was run for 600 ps for the docked complex in 6M0J receptor, meanwhile in EGFR mutation were run for 1600 ps writing coordinates every 0.002 ps interval, constrain at light bonds. Finally, result trajectories of simulated systems were saved for detailed analysis.

VII. Computational Pharmacokinetics

Due to poor ADMET characteristics, the majority of therapeutic drugs failed in clinical trials [30]. QSAR models are now commonly utilized to predict ADMET analyses for medications in the CADD stage [31,32]. ADMETlab [31], SwissADME [33] and admetSAR [34] are currently relevant databases for predicting ADMET characteristics. The ADMET characteristics were predicted using ADMETlab, which provided a more precise prediction than the SwissADME and the admetSAR [32].

For newly developed quinazoline and pyrido[3,4-d]pyrimidine derivatives as tyrosine kinase inhibitors of the EGFR family, absorption, distribution, metabolism, excretion, and toxicity analyses were calculated. To achieve oral bioavailability, ADMET was a crucial step. ADMET was an important step to achieve oral bioavailability. Those parameters are

important for absorption (caco-2 permeability > -5.15, Pgp-inhibitor, Pgp-substrat and HIA human intestinal absorption), Distribution (PPB: plasma protein binding, VD: volume distribution and BBB: blood-brain barrier), metabolism CYP450 enzyme (1A2-inhibitor and substrate, 3A4-inhibitor and substrate, 2C9-inhibitor and substrate, 2C19-inhibitor and substrate and 2D6-inhibitor and substrate), Excretion (T1/2: half-life and CL: clearance) and for toxicity (hERG, H-HT: human hepatotoxicity, AMES and LD50). ADMET properties were predicted using ADMETlab online software [31]. The results of ADMET properties are classified by (1: inhibitor, substrate or blocker; 0: non inhibitor, no substrate or no blocker).

VIII.   References

1.   DrugBank [Internet]. 2020. Available from: https://www.drugbank.ca/

2.   Towler P, Staker B, Prasad SG, Menon S, Tang J, Parsons T, et al. ACE2 X-Ray Structures Reveal a Large Hinge-bending Motion Important for Inhibitor Binding and Catalysis. J Biol Chem. 2004;279(17):17996–8007.

3.   Lan J, Ge J, Yu J, Shan S, Zhou H, Fan S, et al. Structure of the SARS-CoV-2 spike receptor-binding domain bound to the ACE2 receptor. Nature. 2020;581(7807):215–20.

4.   Smaill JB, Gonzales AJ, Spicer JA, Lee H, Reed JE, Sexton K, et al. Tyrosine Kinase Inhibitors . 20 . Optimization of substituted quinazoline and pyrido [3 , 4-d] pyrimidine derivatives as orally active , irreversible inhibitors of the epidermal growth factor receptor family . J Med Chem. 2016;

5.   Becke AD. Density-functional thermochemistry. V. Systematic optimization of exchange-correlation functionals. J Chem Phys. 1997;107(20):8554–60.

6.   Frisch MJ, Trucks GW, Schlegel HB, Scuseria GE, Robb MA, Cheeseman JR, et al. gaussian. Wallingford, CT; 2009.

7.   Cavalli A, Carloni P, Recanatini M. Target-related applications of first principles quantum chemical methods in drug design. Chem Rev. 2006;106(9):3497–519.

8.   Molecular Operating Environment. (MOE). Montreal, QC, Canada, H3A 2R7,: Chemical Computing Group Inc., 1010 Sherbooke St. West, Suite #910; 2019.

9.   DS W, YD F, AC G, EJ L, A M, JR G, et al. DrugBank [Internet]. 2020. Available from: https://www.drugbank.ca/.

10.   MarvinSketch. Budapest, Hungary: Calculation Module Developed by ChemAxon; 2019.

11.   Stewart JJP. Optimization of parameters for semiempirical methods VI: More modifications to the NDDO approximations and re-optimization of parameters. J Mol Model. 2013;19(1):1–32.

12.   HyperChem. 1115 NW 4th, Street, Gainesville, FL 32601, USA,: molecular modelling system.Hypercube Inc; 2009.

13.   te Velthuis AJW, van den Worml SHE, Sims AC, Baric RS, Snijder EJ, van Hemert MJ. Zn2+ inhibits coronavirus and arterivirus RNA polymerase activity in vitro and zinc ionophores block the replication of these viruses in cell culture. PLoS Pathog. 2010;6(11):e1001176.

14.   Berman HM, Westbrook J, Feng Z, Gilliland G, Bhat TN, Weissig H, et al. The Protein Data Bank [Internet]. 2020. Available from: https://www.rcsb.org/pdb.

15.   Wood ER, Truesdale AT, McDonald OB, Yuan D, Hassell A, Dickerson SH, et al. A unique structure for epidermal growth factor receptor bound to GW572016 (Lapatinib): Relationships among protein conformation, inhibitor off-rate, and receptor activity in tumor cells. Cancer Res. 2004;64(18):6652–9.

16.   Yun CH, Boggon TJ, Li Y, Woo MS, Greulich H, Meyerson M, et al. Structures of Lung Cancer-Derived EGFR Mutants and Inhibitor Complexes: Mechanism of Activation and Insights into Differential Inhibitor Sensitivity. Cancer Cell.

2007;11(3):217–27.

17.   Cheng H, Nair SK, Murray BW, Almaden C, Bailey S, Baxi S, et al. Discovery of 1-{(3R,4R)-3-[({5-Chloro-2-[(1-methyl-1H-pyrazol-4-yl)amino]-7H-pyrrolo[2,3-d]pyrimidin-4-yl}oxy)methyl]-4-methoxypyrrolidin-1-yl}prop-2-en-1-one (PF-06459988), a Potent, WT Sparing, Irreversible Inhibitor of T790M-Containing EGFR Mutants. J Med Chem. 2016;59(5):2005–24.

18.   Shahab S, Hajikolaee FH, Filippovich L, Darroudi M, Loiko VA, Kumar R, et al. Molecular structure and UV–Vis spectral analysis of new synthesized azo dyes for application in polarizing films. Dye Pigment [Internet]. 2016;129(February):9–17. Available from: http://dx.doi.org/10.1016/j.dyepig.2016.02.003

19.   Defranceschi M, C. Le Bris. Mathematical Models and Methods for Ab Initio Quantum Chemistry. Vol. 136, Journal of Molecular Structure: THEOCHEM. Springer Science & Business Media; 2000. 202 p.

20.   Domingo LR, Ríos-Gutiérrez M, Pérez P. Applications of the conceptual density functional theory indices to organic chemistry reactivity. Molecules. 2016;21(6).

21.   Zekri A, Harkati D, Kenouche S, Saleh BA. QSAR modeling, docking, ADME and reactivity of indazole derivatives as antagonizes of estrogen receptor alpha (ER-α) positive in breast cancer. J Mol Struct. 2020;1217:128442.

22.   Harkati D, Belaidi S, Saleh BA. A Theoretical Investigation on the Structures,Global and Local Reactivity Descriptors of Oxazolidine-2,4-Dione, Imidazolidine-2,4-Dione and Thiazolidine-2,4-Dione. Quantum Matter. 2017;6.

23.   Domingo LR, Pérez P, Sáez JA. Understanding the local reactivity in polar organic reactions through electrophilic and nucleophilic Parr functions. RSC Adv. 2013;3(5):1486–94.

24.   Ramalho TC, Caetano MS, da Cunha EFF, Souza TCS, Rocha MVJ. Construction and assessment of reaction models of class i epsp synthase: Molecular docking and density functional theoretical calculations. J Biomol Struct Dyn. 2009;27(2):195–207.

25.   Kellenberger E, Rodrigo J, Muller P, Rognan D. Comparative evaluation of eight docking tools for docking and virtual screening accuracy. Proteins Struct Funct Genet. 2004;57(2):225–42.

26.   Althagafi I, El-Metwaly N, Farghaly TA. New series of thiazole derivatives: Synthesis, structural elucidation, antimicrobial activity, molecular modeling and MOE docking. Molecules. 2019;24(9).

27.   Venugopal C, Demos CM, Jagannatha Rao KS, Pappolla MA, Sambamurti K. Beta-secretase: structure, function, and evolution. CNS Neurol Disord Targets (Formerly Curr Drug Targets-CNS Neurol Disord. 2008;7(3):278–94.

28.   Didierjean C, Tête-Favier F. Introduction to Protein Science. Architecture, Function and Genomics. Third Edition. By Arthur M. Lesk. Oxford University Press, 2016. Pp. 466. Paperback. Price GBP 39.99. ISBN 9780198716846. Acta Crystallogr Sect D Struct Biol. 2016;72(12):1308–9.

29.   Sturgeon JB, Laird BB. Symplectic algorithm for constant-pressure molecular dynamics using a Nosé-Poincaré thermostat. J Chem Phys. 2000;112(8):3474–82.

30.   van de Waterbeemd H, Gifford E. ADMET in silico modelling: Towards prediction

paradise? Nat Rev Drug Discov. 2003;2(3):192–204.

31. Dong J, Wang N-N, Yao Z-J, Zhang L, Cheng Y, Ouyang D, et al. ADMETlab: a platform for systematic ADMET evaluation based on a comprehensively collected ADMET database. J Cheminform [Internet]. 2018; Available from: http://admet.scbdd.com/

32. Wu F, Zhou Y, Li L, Shen X, Chen G, Wang X, et al. Computational Approaches in Preclinical Studies on Drug Discovery and Development. Front Chem. 2020;8(September).

33. Daina A, Michielin O, Zoete V. SwissADME: A free web tool to evaluate pharmacokinetics, drug-likeness and medicinal chemistry friendliness of small molecules. Sci Rep [Internet]. 2017;7(March):1–13. Available from: http://dx.doi.org/10.1038/srep42717

34. Cheng F, Li W, Zhou Y, Shen J, Wu Z, Liu G, et al. AdmetSAR: A comprehensive source and free tool for assessment of chemical ADMET properties. Vol. 52, Journal of Chemical Information and Modeling. ACS Publications; 2012. p. 3099–105.

Chapter IV:

RESULTS AND

DISCUSSION

Chapter IV: Results and discussion

I. Results and discussion on approved drugs library targeting ACE2 and SARS-CoV-2 binding with ACE2.

I.1. Reactivity

I.1.1. Results

The chemical reactivity descriptors were calculated and presented in Table 1. The E_{HOMO} and E_{LUMO} were obtained from GaussView [1]. The results of the global hardness and softness, which they are related to the stability of chemical system, as shown in Table 1, indicate that **Ramipril** have the smaller energy gap (ΔE= 2.9508 eV), **Delapril** and **Lisinopril** have smaller energy gaps than **Hydroxychloroquine**.

In addition, **Ramipril**, **Chloroquine**, **ORE-1001** and **Delapril** are harder than the **Hydroxychloroquine** and other compounds. Moreover, **Ramipril**, **Chloroquine**, **ORE-1001** and **Delapril** have softness values higher than that of **Hydroxychloroquine**.

The electronic chemical potential (μ) for **Perindopril** (μ= -2.6386 eV) is higher than other compounds followed by **Hydroxychloroquine**, **Enalapril** and **Delapril**.

According to the results in Table 1, **Chloroquine** had the highest nucleophilicity value (N = 3.1698 eV) followed by **Perindopril** and **Hydroxychloroquine** (N= 2.9995 eV), (N=2.9124 eV) respectively, meanwhile **ORE-1001** had the nucleophilicity value (N= 1.7213eV).

Ramipril had the highest electrophilicity value (ω = 7.1873 eV), whereas as **Delapril** had an electrophilicity value (ω = 1.9888 eV) higher more than that of **Hydroxychloroquine** (ω = 1.4291 eV).

Table 1 HOMO and LUMO energy, energy gap ΔE and global reactivity indices μ, ω, η and N for drugs

Drugs	HOMO (eV)	LUMO (eV)	ΔE (eV)	η (eV)	S (eV)	μ (eV)	ω (eV)	N (eV)
Chloroquine	-5.4861	-1.2232	4.2629	2.1315	0.2346	-3.3546	2.6398	3.1698
Delapril	-5.9438	-0.5853	5.3585	2.6792	0.1866	-3.2646	1.9888	2.7121
Enalapril	-5.7435	-0.738	5.0055	2.5028	0.1998	-3.2407	2.0981	2.9124
Hydroxy-chloroquine	-6.5095	0.2797	6.7892	3.3946	0.1473	-3.1149	1.4291	2.1464
Lisinopril	-6.6328	-1.0583	5.5745	2.7873	0.1794	-3.8455	2.6527	2.0231
ORE-1001	-6.9346	-1.9323	5.0023	2.5011	0.1999	-4.4334	3.9292	1.7213
Perindopril	-5.6564	0.3793	6.0358	3.0179	0.1657	-2.6386	1.1534	2.9995
Pipraquine	-6.9269	0.0678	6.9947	3.4973	0.1430	-3.4296	1.6815	1.729
Ramipril	-6.0807	-3.1299	2.9508	1.4754	0.3389	-4.6053	7.1873	2.5752
Ramiprilat	-6.4178	-0.342	6.0758	3.0379	0.1646	-3.3799	1.8802	2.2381
Trandolapril	-6.1084	-0.7565	5.3519	2.676	0.1868	-3.4324	2.2013	2.5475

Notes: the HOMO energy -8.6559 eV. of the reference system (TCE) has been calculated at DFT/B3LYP 6-31G

I.1.2.   Discussion

From the results, E_{HOMO} and E_{LUMO} have negative values [2], that's refer to stability of investigated complexes, the result of the global hardness and softness, indicate that **Ramipril**, **Chloroquine**, **ORE-1001** and **Delapril** are harder and softer than the **Hydroxychloroquine** and other compounds.

ΔE is used to measure the chemical reactivity and the kinetic stability of a molecule. A large ΔE gap means high kinetic stability, low reactivity and a poorly polarizable molecule that therefore [3]. **Ramipril** have the higher reactivity, polarizability and more stable followed by **Delapril** and **Lisinopril,** in comparing to **Hydroxychloroquine.**

According to results of electronic chemical potential (μ), **Perindopril** followed by **Hydroxychloroquine**, **Enalapril** and **Delapril** can exchange electron density with the environment efficiently better than other compounds [4].

A further classification of organic molecules as strong (N > 3 eV), moderate (2.0 eV $\leq$ N $\leq$ 3.0 eV) and marginal nucleophilic (N < 2.0 eV) were obtained by analysis of a series of common nucleophilic species participating in polar organic reaction. Note that nucleophilicity value is referred to tetracyanoethylen (TCE) taken as a reference, because it presents the lowest E_{HOMO} in a large series of molecule already investigated [5]. According to the results in Table 1, **Chloroquine** can be classified as strong nucleophile and the others as moderate nucleophile except **ORE-1001**, which is considered as marginal nucleophile.

The electrophilicity ω had become a potent tool for the study of the reactivity of organic compounds that can participate in polar reaction [6,7]. **Ramipril** and **Delapril** are more electrophilic than **Hydroxychloroquine**.

I.2.   Molecular Docking

I.2.1.   Results

I.2.1.1.   *The binding affinities of the drugs into ACE2 active sites*

Molecular docking simulation of Chloroquine, Hydroxychloroquine, Quinacrine, Quinacrine mustard, Piperaquine, Ramipril, Trandolapril, Ramiprilat, Enalapril, Trandolaprilat, Lisinopril, Perindopril, Enalaprilat, Delapril, ORE-1001, N-(2-Aminoethyl)-1-aziridineethanamine, Triethylenetetramine, Piperazine into ACE2 active

sites (pockets S1 and S2 respectively) **PDB ID: 1R42** [8] was performed. The results, as shown in Table 2, indicate that only seven ligands have an interaction with the receptor in pocket S1.The selection of the best-docked drugs based on both the binding scores and RMSDs value. Table 2 show the binding score and RMSD value of drugs in S1. **Delapril** has the best docking score (-6.9809 kcal/mol) followed by **Lisinopril** (-6.6886 kcal/mol)) with RMSDs 2.2570 Å and 1.5417 Å respectively.

Table 2 The results obtained from docking of Drugs with 1R42 in site 1.

Drugs	S score (kcal/mol)	RMSD (Å)	Bonds between atoms of compounds and residues of active site 1 of 1R42					
			Atom of compound	Atom of receptor	Involved receptor residues	Type of interaction bond	Distance (Å)	E (kcal/mol)
Chloroquine	-6.1074	1.1063	N-1	O	H_2O 932	H-acceptor	2.79	-1
Delapril	-6.9809	2.2570	O-31	OG	Ser 409	H-donor	3.08	-0.7
			O-24	O	H_2O 932	H-acceptor	2.84	-1.3
			O-25	NE2	Gln 442		3.16	-1.7
			C-43	5-ring	His 374	H-pi	3.71	-1
			6-ring	O	H_2O 932	pi-H	4.08	-1.2
Lisinopril	-6.6886	1.5417	O-5	O	H_2O 932	H-donor	3.24	-0.6
Perindopril	-6.5856	1.1260	O-42	NE2	Gln 442	H-acceptor	3.3	-0.8
Piperaquine	-6.6531	3.2826	6-ring	CD	Pro 346	pi-H	4.35	-0.8
Ramiprilat	-6.6703	4.3112	O-46	O	H_2O 1075	H-donor	2.98	-1.6
			O-51	OE1	Glu 406		2.9	-2.3
				O	H_2O 1099		2.89	-1.1
			O-45	NE2	Gln 442	H-acceptor	3	-1
Trandolaprilat	-6.7507	1.4433	N-45	OE1	Gln 442	H-donor	3.09	-1.6

Interactions were further examined for bond lengths and hydrogen bonds in site 1 and were illustrated in Figure 1-5. The results from this Figure 1 showed that **Delapril** interacts with three amino acids Ser409, Gln442 and His374 residues in three different interactions; H-donor interaction with Ser409 (O-H….O-C) with a length 3.08 Å , H-acceptor with Gln442 (O-H…N-C) with a length 3.16 Å, H-pi with His374 (C-H…imidazole cycle) with a length 3.71 Å as well as two interaction H-acceptor interaction (O=C.. O-H) with a length 2.84 Å and pi-H interaction (benzene cycle…O-H) with a length 4.08 Å to two molecules water.
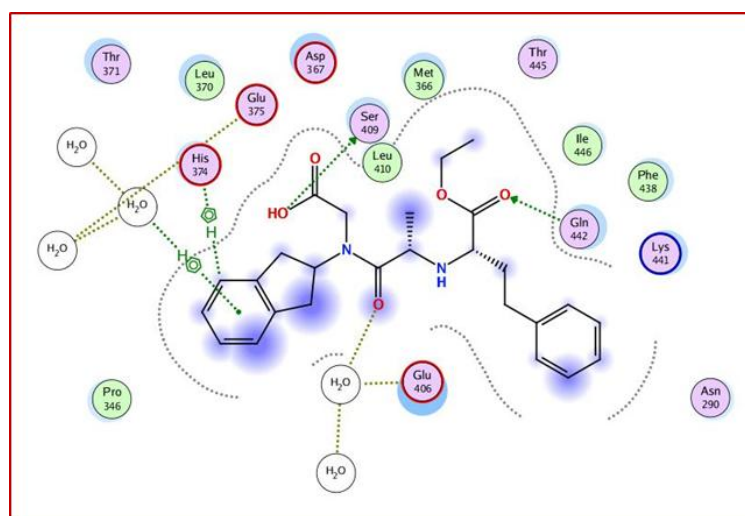
(a)
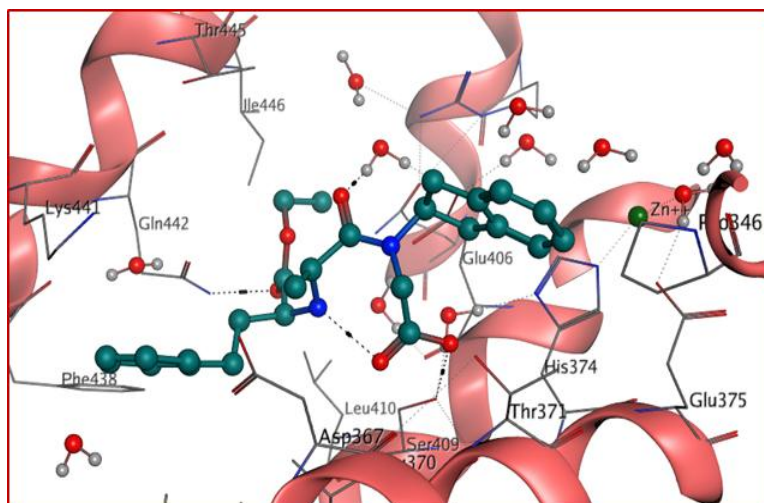
(b)

Figure 1 Interactions between Delapril and 1R42 receptor in site 1(2D (a); 3D (b)).

The results from this Figure 2 showed that **Lisinopril** had forming only one hydrogen bond, H-donor interaction with water (O-H.... O-H) with a length 3.24 Å.
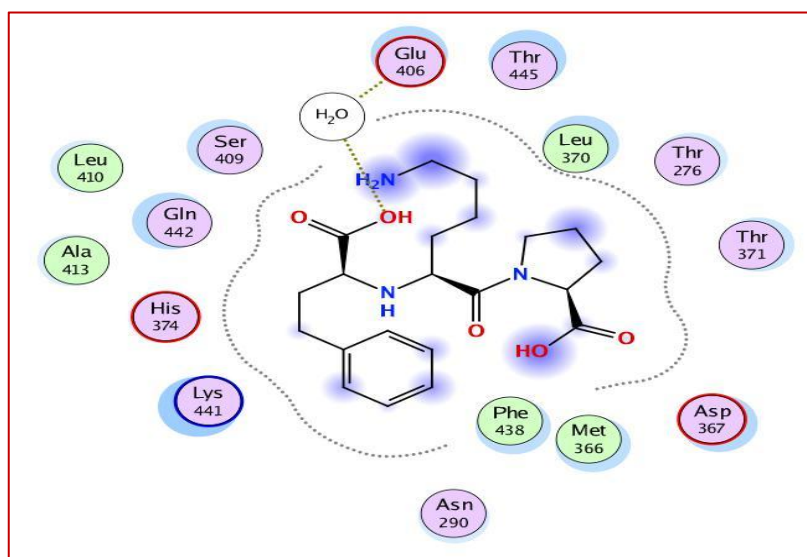
(a)
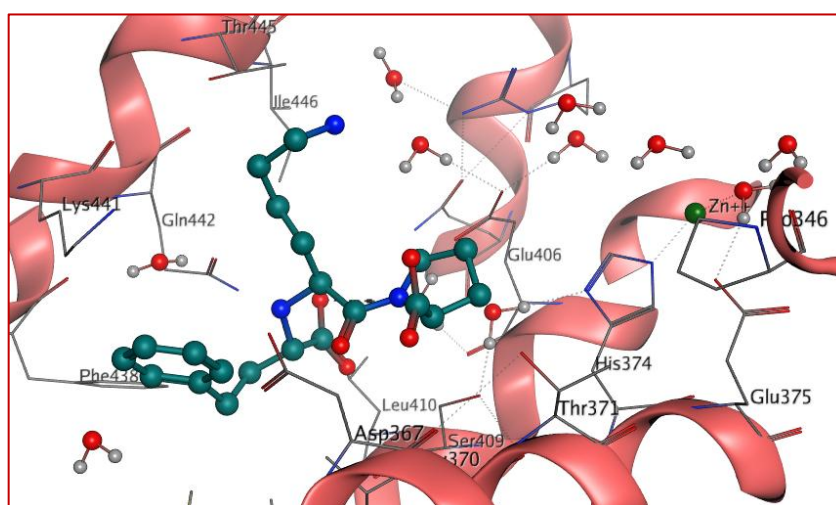
(b)

Figure 2 Interaction between Lisinopril and 1R42 receptor in site 1(2D (a); 3D (b)).

The results from this Figure 3 showed that **Trandolaprilat** had forming only one hydrogen bond with one amino acid Gln442. The interaction was H-donor with amino acid Gln442 (O-H...O=C) with a length 3.09 Å.
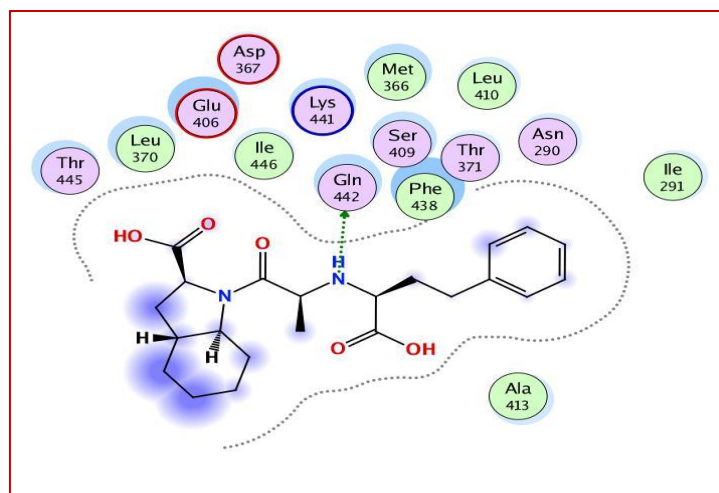
(a)
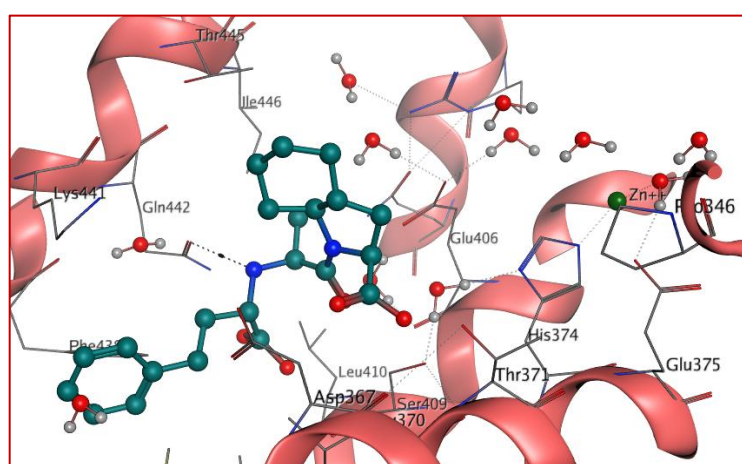
(b)

Figure 3 Interaction between Trandolaprilat and 1R42 receptor in site 1(2D (a); 3D (b)).

The results from this Figure 4 showed that **Ramiprilat** interacts with two amino acids residues Gln442 and Glu406 different interactions; H-acceptor with Gln442(O=C...N-C) with a length 3 Å , H-donor with Glu406 (O-H...O=C) with a length 2.9 Å, as well as two H-donor interactions (O-H.... O-H) with a length 2.98 Å and (O-H.... O-H) with a length 2.89 Å with two water molecules.
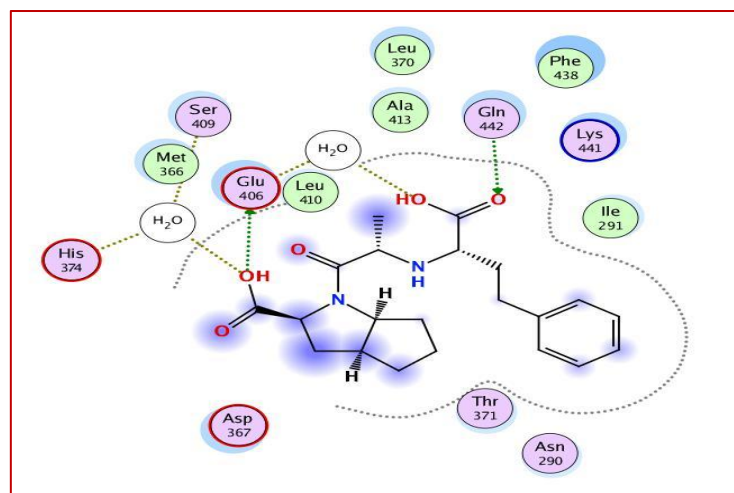
(a)
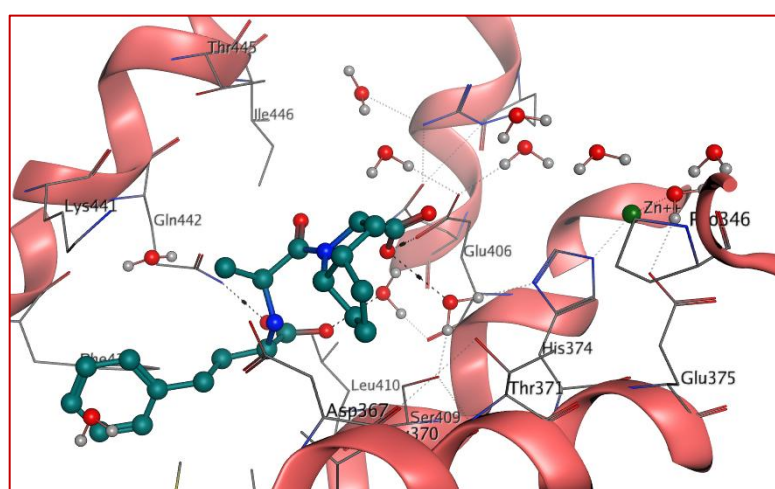
(b)

Figure 4 Interaction between Ramiprilat and 1R42 receptor in site 1(2D (a); 3D (b)).

The results from this Figure 5 showed that **piperaquine** interact with one amino acid Pro346. The interaction was pi-H with Pro346 (benzene cycle…C-H) with a length 4.35 Å.
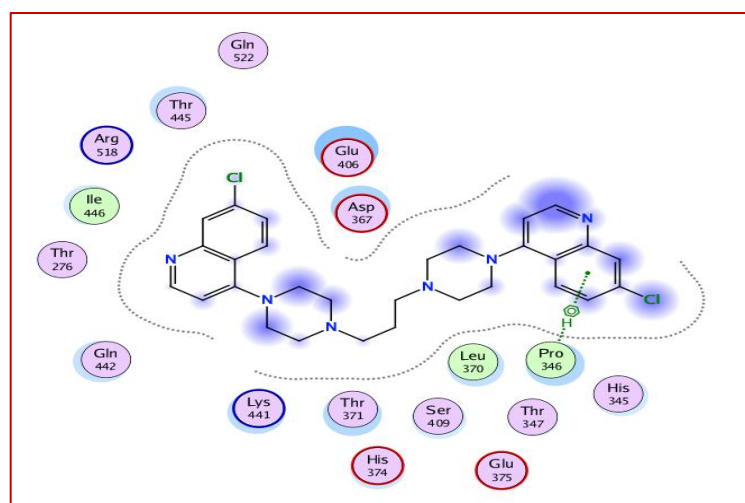
(a)
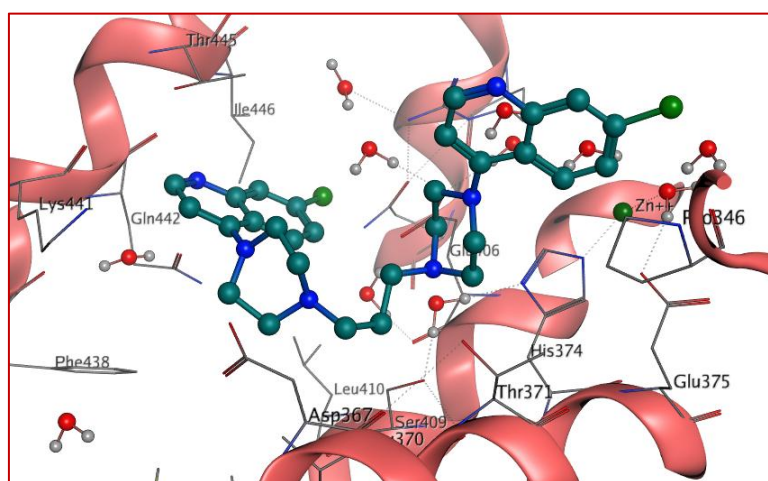
(b)

Figure 5 Interaction between Piperaquine and 1R42 receptor in site 1(2D (a); 3D (b)).

From Table 3, the docking results indicate that twelve ligands have an interaction with the receptor in pocket S2., it can be noticed that **Delapril** had the lowest docking score (-6.5831 kcal/mol) with RMSD (2.0115 Å) followed by **Perindopril**, **Ramipril** and **Chloroquine** with docking score and RMSD values of (-6.2821 Kcal/mol, 1.1895 Å), (-6.1181 Kcal/mol, 1.5054 Å) and (-5.5271 Kcal/mol, 1.3462 Å) respectively.

Table 3 The results obtained from docking of Drugs with 1R42 in site 2.

Drugs	S score (kcal/mol)	RMSD (Å)	Bonds between atoms of compounds and residues of active site 2 of 1R42					
			Atom of compound	Atom of receptor	Involved receptor residues	Type of interaction bond	Distance (Å)	E (kcal/mol)
Chloroquine	-5.5271	1.3462	N-17	O	Ala 348	H-donor	3.05	-2
			6-ring	6-ring	Trp 349	pi-pi	3.96	0
Delapril	-6.5831	2.0115	O-25	O	H_2O 894	H-acceptor	2.9	-0.8
Enalalapril	-6.1282	2.6836	C-28	5-ring	Trp 349	H-pi	3.86	-0.7
Enalaprilat	-5.9910	1.2547	O-40	N	Asp 350	H-acceptor	3.34	-1.3
			C-45	5-ring	Trp 349	H-pi	3.46	-2.6
Hydroxy-chloroquine	-5.6369	1.8041	O-2	O	Arg 393	H-donor	2.99	-0.8
			N-7	N	Asp 350	H-acceptor	3.13	-1.3
Lisinopril	-5.6358	1.7176	O-5	O	Arg 393	H-donor	3.19	-2.4
Perindopril	-6.2821	1.1895	O-23	5-ring	His 401	H-pi	3.51	-0.7
Piperazine	-3.4925	2.5032	C-5	5-ring	Trp 349	H-pi	3.86	-0.9
Quinacrine	-5.9184	1.1669	C-37	6-ring	Trp 349	H-pi	4.42	-0.6
			C-37	5-ring	Trp 349		3.8	-1.4
Ramipril	-6.1181	1.5054	O-46	N	Asp 350	H-acceptor	3	-3.2
			O-58	O	H_2O 892		3.07	-1
Ramiprilat	-5.8613	1.8268	O-51	O	Leu 391	H-donor	2.92	-1.4
			O-46	ND2	Asn 394	H-acceptor	3.02	-0.8
			O-49	NZ	Lys 562		3.01	-5.7
			O-54	ND2	Asn 394		2.85	-0.9
Trandolaprilat	-5.7171	2.8424	O-53	O	H_2O 952	H-donor	2.97	-2.2

The interactions of drugs with site 2 were also examined for bond lengths and hydrogen bonds and depicted in Figures 6-9. Figure 6 showed that **Delapril** had only one interaction, H-acceptor interaction with water (O=C… O-H) with a length 2.9 Å.
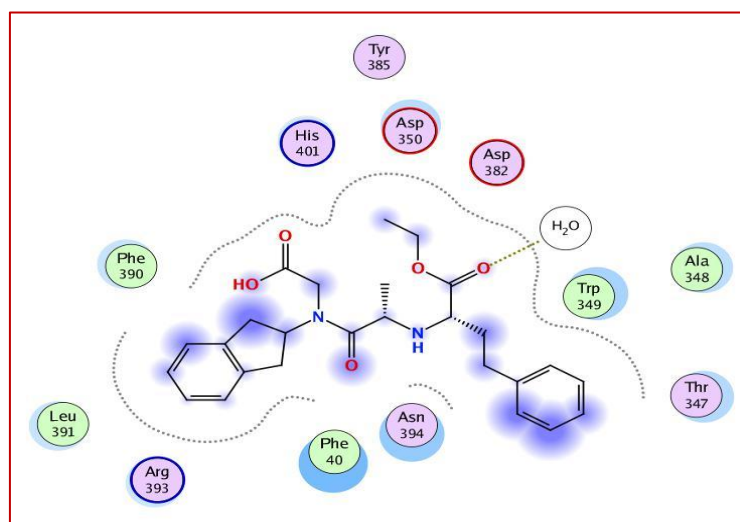
(a)
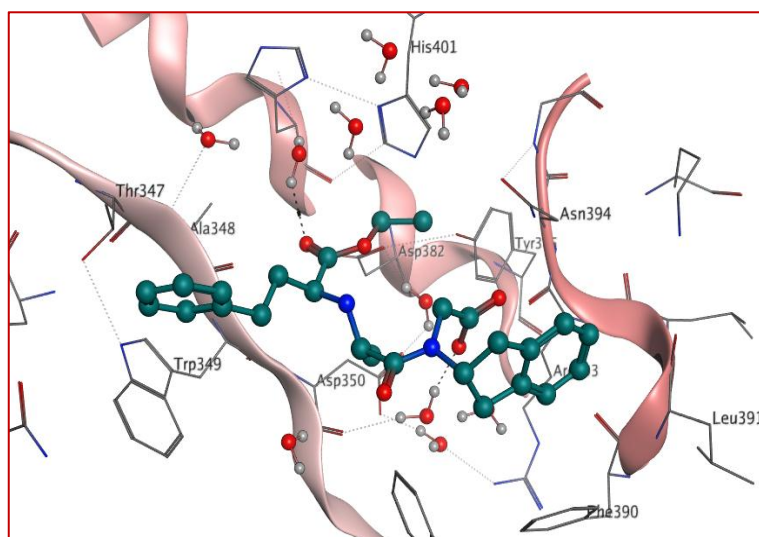
(b)

Figure 6 Interactions between Delapril and 1R42 receptor in site 2(2D (a); 3D (b)).

Figure 7 showed that **Perindopril** forming only one interaction with amino acid His401. The interaction was H-pi with His401 (O-H… imidazol) with a length 3.51 Å.
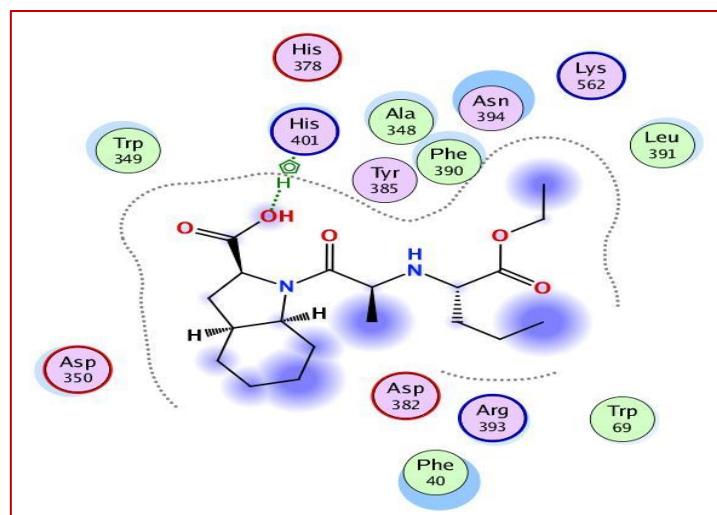
(a)
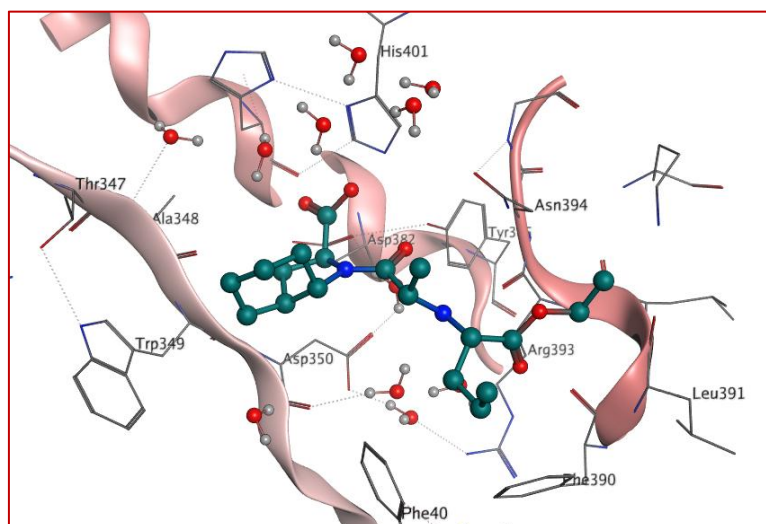
(b)

Figure 7 Interactions between Perindopril and 1R42 receptor in site 2(2D (a); 3D (b)).

Meanwhile, Figure 8 showed that **Ramipril** forming only one interaction with amino acid Asp350 and with water. The interaction was H-acceptor to Asp350 (O=C… N-H) with a length 3 Å and H-acceptor to water (O=C… O-H) with a length 3.07 Å
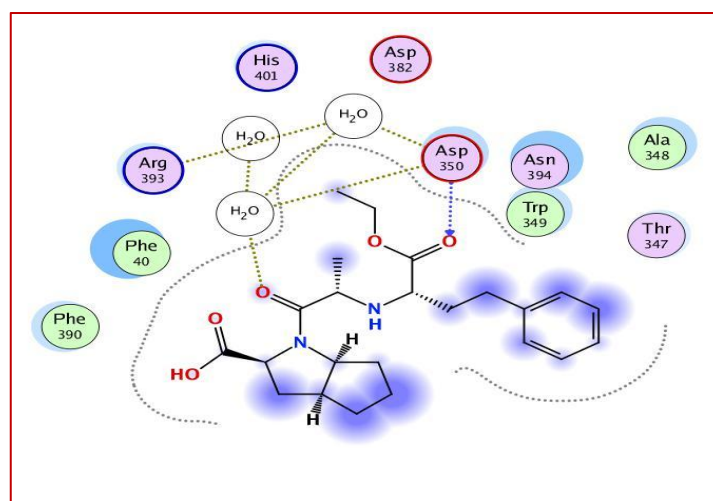
(a)
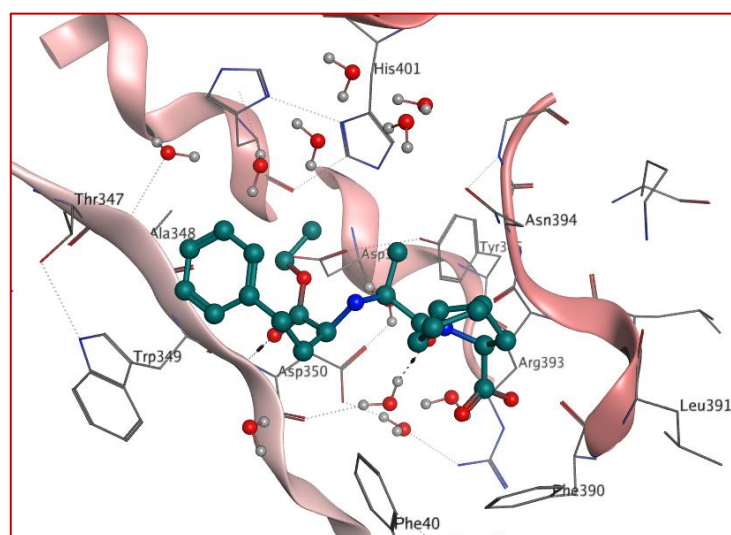
(b)

Figure 8 Interactions between Ramipril and 1R42 receptor in site 2(2D (a); 3D (b)).

Figure 9 showed that **Chloroquine** forming two interactions with two amino acid Ala348 and Trp349. The interaction was H-donor interaction with Ala348(N-H… O=C) with a length 3.05 Å and pi-pi interaction with Trp349 (benzene… benzene) with a length 3.96 Å.
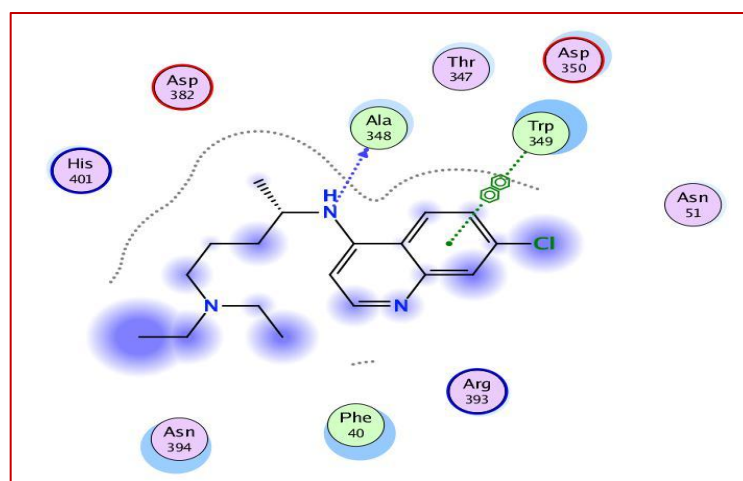
(a)
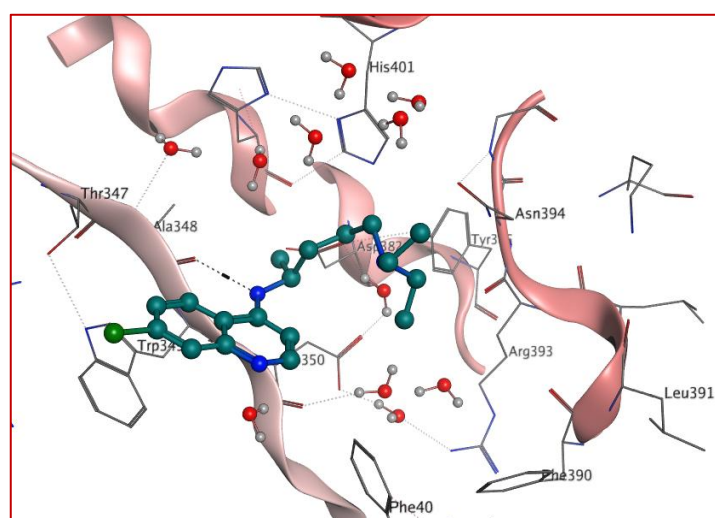
(b)

Figure 9 Interactions between Chloroquine and 1R42 receptor in site 2(2D (a); 3D (b)).

I.2.1.2.   The binding affinities of the drugs into SARS-CoV-2 spike receptor-binding with ACE2 complex active sites

Molecular docking of Chloroquine, Hydroxychloroquine, Quinacrine, Quinacrine mustard, Piperaquine, Ramipril, Trandolapril, Ramiprilat, Enalapril, Trandolaprilat, Lisinopril, Perindopril, Enalaprilat, Delapril, ORE-1001, N-(2-Aminoethyl)-1-aziridineethanamine, Triethylenetetramine, Piperazine into SARS-CoV-2 spike receptor-binding with ACE2 complex active sites (pockets S1 and S2 respectively) **PDB ID: 6M0J** [9] was performed.

Tables 4 show the binding score and RMSD value of docking results of the drugs in 6M0J pockets S1. Their score binding   order was: Piperaquine < Quinacrine < Enalapril <

Quinacrine Mustard < Ramipril< Lisinopril < Delapril < ORE-1001< Hydroxychloroquine < Ramiprilat < Enalaprilat < Chloroquine < Perindopril.

Table 4 The results obtained from docking of Drugs with 6M0J in site 1.

Drugs	S score (kcal/mol)	RMSD (Å)	Bonds between atoms of compounds and residues of active site 1 of 6M0J					
			Atom of compound	Atom of receptor	Involved receptor residues	Type of interaction bond	Distance (Å)	E (kcal/mol)
Chloroquine	-6.8442	1.9853	6-ring	6-ring	Phe 438	pi-pi	3.37	0
Delapril	-7.5271	2.1735	O-31	OE2	Glu 375	H-donor	3.01	-4.5
			O-25	NH2	Arg 514	H-acceptor	3.04	-1.4
			O-26	ZN	Zn 901		1.96	-2.1
				NE2	His 374	metallic	2.4	-3.2
				NE2	His 378		2.27	-5.7
			Zn-901	OE1	Glu 402		2.1	-5.6
				NE2	His 378	ionic	2.27	-11.7
				OE1	Glu 402		2.1	-14.4
				OE2	Glu 402		3.13	-3.7
			6-ring	OH	Tyr 515	Pi-H	3.38	-0.9
				6-ring	Tyr 510	pi-pi	3.93	0
Enalapril	-7.8671	1.9897	O-22	O	Pro 289	H-donor	3.39	-0.8
Enalaprilat	-6.9279	1.8459	O-44	NZ	Lys 441	H-acceptor	3.16	-8.4
			6-ring	6-ring	Phe 438	pi-pi	3.73	0
Hydroxy-chloroquine	-7.2272	2.1035	6-ring	CB	Phe 438	pi-H	3.82	-0.8
			6-ring	6-ring	Phe 438	pi-pi	3.81	0
Lisinopril	-7.5918	1.3368	N-11	NE2	Gln 442	H-acceptor	3.18	-2.8
			6-ring	CA	Asn 290	Pi-H	4.07	-0.8
			6-ring	N	Ile 291		4.22	-0.9
ORE-1001	-7.3872	1.5557	Cl	O	Leu 410	H-donor	3.49	-0.8

			5-ring	CB	Phe 438	pi-H	4.43	-0.7
			6-ring	6-ring	Phe 438	pi-pi	3.37	0
Perindopril	-6.4327	2.4655	N-26	O	Ile 291	H-donor	3.21	-0.8
Piperaquine	-8.6132	2.3325	6-ring	6-ring	Phe 438	pi-pi	3.35	0
Quinacrine	-8.2350	1.6346	6-ring	N	Ile 291	pi-H	4.81	-0.6
			6-ring	N	Ile 291		3.98	-1.1
Quinacrine Mustard	-7.8570	1.4398	Cl-58	SD	Met 366	H-donor	3.74	-0.4
			6-ring	N	Ile 291	pi-H	3.98	-1.4
			6-ring	6-ring	Phe 438	pi-pi	3.58	0
Ramipril	-7.7464	1.6166	O-58	N	Ile 291	H-acceptor	3.47	-0.8
Ramiprilat	-6.9943	2.4607	O-49	Zn	Zn 901		2.01	-3.9
				NE2	His 374	metallic	2.4	-3.2
				NE2	His 378		2.27	-5.7
			Zn-901	OE1	Glu 402		2.1	-5.6
				NE2	His 378	ionic	2.27	-11.7
				OE1	Glu 402		2.1	-14.4
				OE2	Glu 402		3.13	-3.7

The results of the binding of drugs with **6M0J** in site **1** were further examined for bond lengths and hydrogen bonds and are shown in figures 10-13. From the Figure 10, it is apparent that **Piperaquine** interact with one amino acid Phe438. The interaction was pi-pi interaction with Phe438 (pyridine…benzene) with a length 3.35 Å.
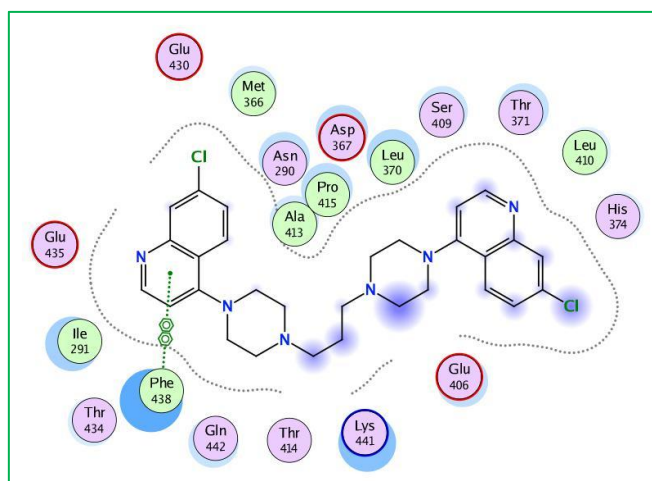
(a)
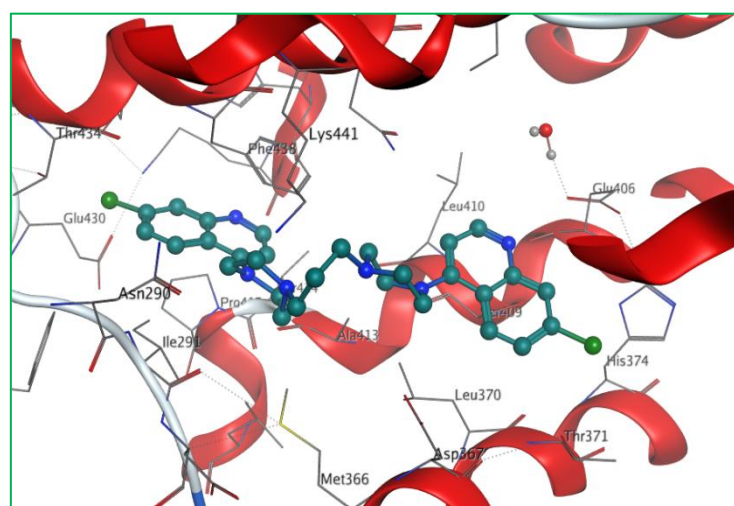
(b)

Figure 10 Interaction between Piperaquine and 6M0J receptor in site 1(2D (a); 3D (b)).

Whereas, Figure 11, indicate that **Hydroxychloroquine** forming two interactions with amino acid Phe438. The interactions were pi-H (benzene…C-C) with a length 3.82 Å and pi-pi interaction (benzene…benzene) with a length 3.81 Å.
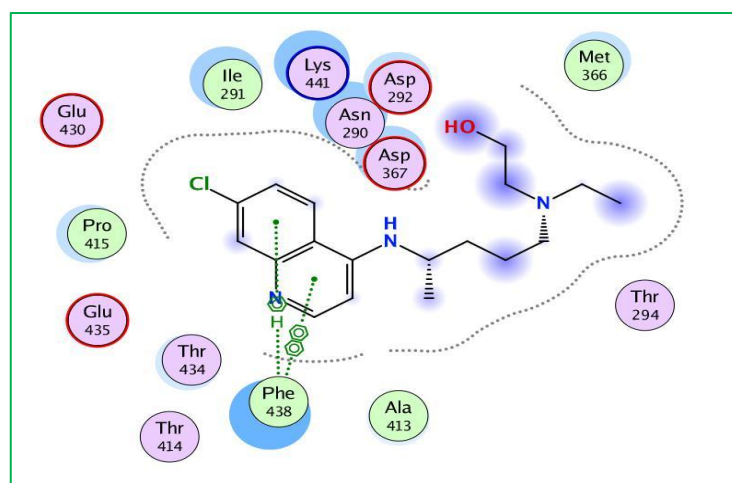
(a)
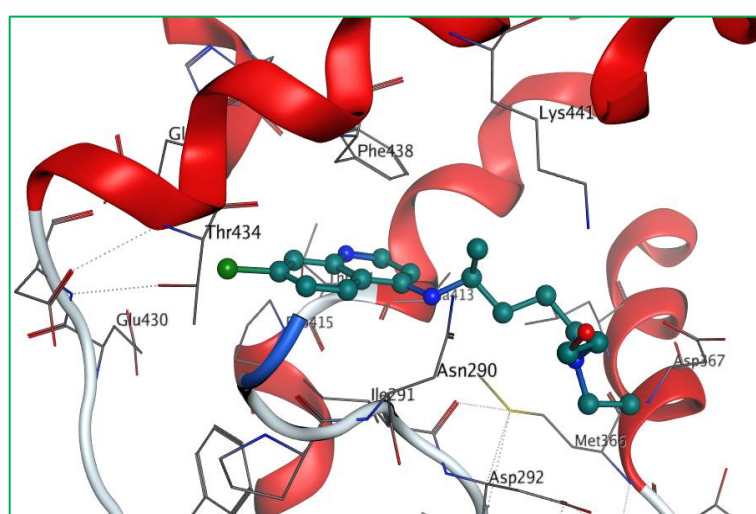
(b)

Figure 11 Interaction between Hydroxychloroquine and 6M0J receptor in site 1(2D (a); 3D (b)).

From Figure 12, **Delapril** forming four interactions with amino acids Glu375, Arg514, Tyr515, Tyr510, and one interaction with zinc. The interaction was; H-donor interaction with Glu375 (O-H…O-H) with a length 3.01 Å, H-acceptor with Arg514 (O=C…N-H) with a length 3.04 Å, pi-H interaction with Tyr515 (benzene…O-H) with a length 3.38 Å, pi-pi interaction with Tyr510 (benzene … benzene) with a length 3.93 Å and metallic interaction with zinc(O=C...Zn) with a length 1.96 Å. Meanwhile Zn interacts with three amino acids by two types of interactions ionic and one metallic. The interactions were metallic with His374, His378, Glu402 with length 2.4, 2.27 and 2.1 Å respectively, ionic interactions one with His378 and two with Glu402 with length 2.27, 2.1 and 3.13 Å respectively.
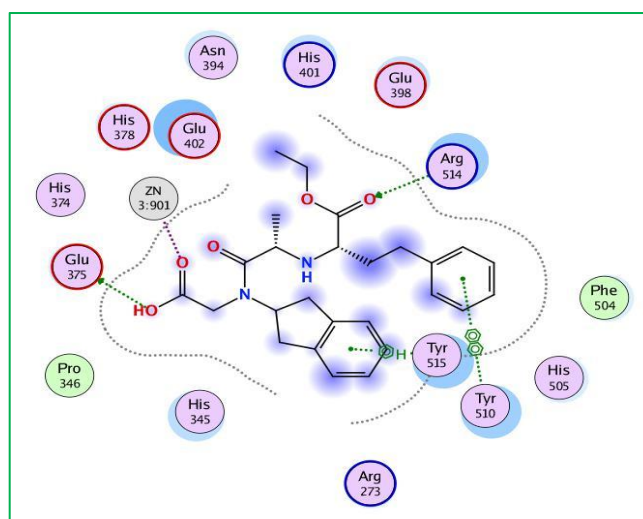
(a)
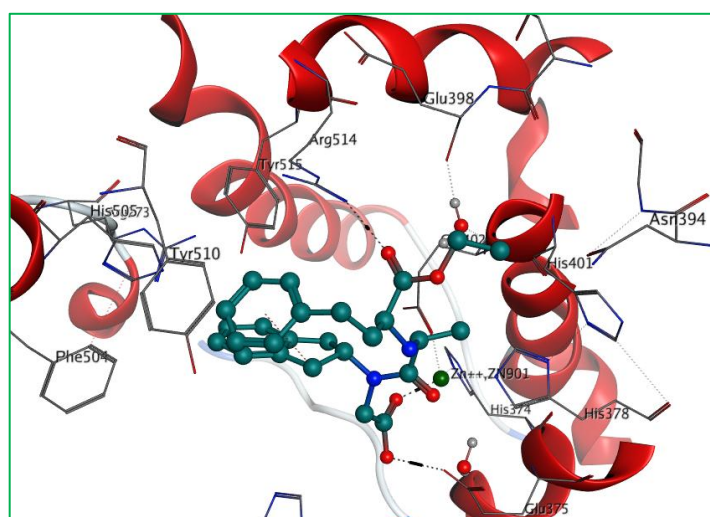
(b)

Figure 12 Interaction between Delapril and 6M0J receptor in site 1(2D (a); 3D (b)).

Figure 13 showed that **Lisinopril** forming three interactions with amino acids Gln442, Asn290 and Ile291. The interactions were; H-acceptor with Gln442 (N-H…N-H) with a length 3.18 Å, and two pi-H interactions with Asn290 and Ile291(benzene…C=O) with a length 4.07 Å and (benzene…N-H) with a length 4.22 Å respectively.
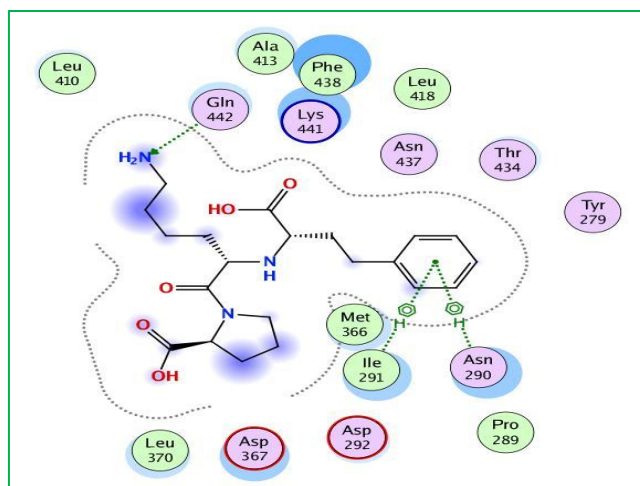
(a)
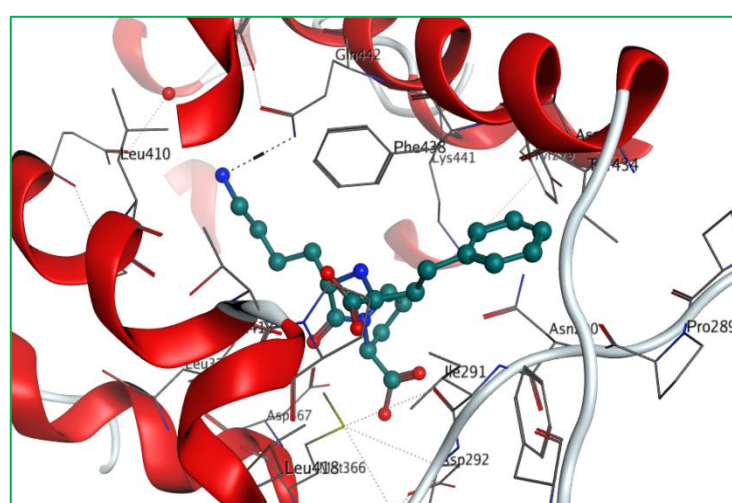
(b)

Figure 13 Interaction between Lisinopril and 6M0J receptor in site 1(2D (a); 3D (b)).

The results of docking of drugs with **6M0J** in site **2** are shown in Table 5. According to the results in this site 2, almost all drugs make interacted in pocket S2 via zinc. **Delapril** showed excellent docking score -8.1604 Kcal/mol and RMSD 1.5603 Å compared with **Perindopril**, **Lisinopril**, **Hydroxychloroquine** and **Ramipril** with energy scores and RMSD values of (-6.7968 kcal/mol, 2.2965 Å), (-6.6966 Kcal/mol, 1.9981 Å), (-6.3125 Kcal/mol, 1.8513 Å) and (-7.6305 kcal/mol, 2.4853 Å) respectively.

Table 5 The results obtained from docking of Drugs with 6M0J in site 2.

| Drugs | S score (kcal/mol) | RMSD (Å) | Bonds between atoms of compounds and residues of active site 2 of 6M0J | | | | | |
			Atom of compound	Atom of receptor	Involved receptor residues	Type of interaction bond	Distance (Å)	E (kcal/mol)
Chloroquine	-5.4920	2.3627	C-45	5-ring	His 401	H-pi	4.25	-0.9
Delapril	-8.1604	1.5603	O-26	ZN	Zn 901	metallic	2.13	-3.6
				NE2	His 374		2.4	-3.2
					His 378		2.27	-5.7
			Zn-901	OE1	Glu 402		2.1	-5.6
				NE2	His 378	ionic	2.27	-11.7
				OE1	Glu 402		2.1	-14.4
				OE2	Glu 402		3.13	-3.7
Enalalapril	-6.7570	2.6763	O-14	ZN	Zn 901	metallic	2	-2.5
				NE2	His 374		2.4	-3.2
				NE2	His 378		2.27	-5.7
			Zn-901	OE1	Glu 402		2.1	-5.6
				NE2	His 378		2.27	-11.7
				OE1	Glu 402	ionic	2.1	-14.4
				OE2	Glu 402		3.13	-3.7
			C-52	5-ring	His 378	H-pi	3.88	-1
Hydroxy-chloroquine	-6.3125	1.8513	O-2	OE2	Glu 375	H-donor	2.86	-1.9
			O-2	ZN	Zn 901		2	-2.6
			Zn-901	NE2	His 374	Metallic	2.4	-3.2
				NE2	His 378		2.27	-5.7
				OE1	Glu 402		2.1	-5.6

			NE2	His 378	ionic	2.27	-11.7
			OE1	Glu 402		2.1	-14.4
			OE2	Glu 402		3.13	-3.7
			C-47	5-ring	His 378	H-pi	4.12	-0.6
Lisinopril	-6.6966	1.9981	O-5	O	H$_2$O 1004	H-donor	2.97	-2
			O-1	ZN	Zn 901		2.06	-2.3
				NE2	His 374	metallic	2.4	-3.2
				NE2	His 378		2.27	-5.7
			Zn-901	OE1	Glu 402		2.1	-5.6
				NE2	His 378	ionic	2.27	-11.7
				OE1	Glu 402		2.1	-14.4
				OE2	Glu 402		3.13	-3.7
ORE-1001	-6.2755	2.5319	N-6	OH	Tyr 515	H-acceptor	3.09	-2.1
			O-25	ZN	Zn 901		2.09	-2.3
			O-31	ZN	Zn 901	metallic	2.31	-0.9
				NE2	His 374		2.4	-3.2
				NE2	His 378		2.27	-5.7
			Zn-901	OE1	Glu 402		2.1	-5.6
				NE2	His 378	ionic	2.27	-11.7
				OE1	Glu 402		2.1	-14.4
				OE2	Glu 402		3.13	-3.7
Perindopril	-6.7968	2.2965	O-23	O	Glu 398	H-donor	2.84	-3.1
			N-26	OE1	Glu 402		3.11	-1.4
			C-46	OE2	Glu 375		3.49	-0.6
			O-16	O	H$_2$O 1033	H-acceptor	2.86	-1.9
			O-25	NH2	Arg 514		2.91	-1.9

		O-42	ZN	Zn 901		1.97	-2.9
			NE2	His 374	Metallic	2.4	-3.2
			NE2	His 378		2.27	-5.7
		Zn-901	OE1	Glu 402		2.1	-5.6
			NE2	His 378	ionic	2.27	-11.7
			OE1	Glu 402		2.1	-14.4
			OE2	Glu 402		3.13	-3.7
		O-53	ZN	Zn 901		2.13	-1.7
		O-58	ZN	Zn 901	metallic	2.44	-1.4
			NE2	His 374		2.4	-3.2
			NE2	His 378		2.27	-5.7
Ramipril	-7.6305	2.4853	Zn-901	OE1	Glu 402		2.1	-5.6
			NE2	His 378	ionic	2.27	-11.7
			OE1	Glu 402		2.1	-14.4
			OE2	Glu 402		3.13	-3.7
		O-45	Zn	Zn 901		1.94	-2.9
			NE2	His 374	metallic	2.4	-3.2
			NE2	His 378		2.27	-5.7
Ramiprilat	-7.1864	1.7252	Zn-901	OE1	Glu 402		2.1	-5.6
			NE2	His 378	ionic	2.27	-11.7
			OE1	Glu 402		2.1	-14.4
			OE2	Glu 402		3.13	-3.7
		O-1	O	H$_2$O 1030	H-acceptor	3.04	-1
Trandolapril	-7.1160	1.9818	O-4	ZN	Zn 901	metallic	2.07	-3.8
		Zn-901	NE2	His 374		2.4	-3.2
			NE2	His 378		2.27	-5.7

	OE1	Glu 402		2.1	-5.6
	NE2	His 378	Ionic	2.27	-11.7
	OE1	Glu 402		2.1	-14.4
	OE2	Glu 402		3.13	-3.7
6-ring	CA	Glu 398	pi-H	3.63	-0.6

Figures 14-18 present the interactions of drugs with **6M0J** in site **2**. From Figure 14, it can be seen that **Delapril** had a metallic interaction with Zn (O=C…Zn) with length 2.13 Å. Meanwhile Zn interacts with three amino acids by two types of interactions ionic and one metallic. The interactions were metallic with His374, His378, Glu402 with length 2.4, 2.27 and 2.1 Å respectively, ionic interactions one with His378 and two with Glu402 with length 2.27, 2.1 and 3.13 Å respectively.

(a)

(b)

Figure 14 Interaction between Delapril and 6M0J receptor in site 2 (2D (a); 3D (b)).

Figure 15 showed that **Perindopril** forming interactions with amino acids Glu398, Glu402, Glu375, Arg514, water and zinc. The interactions were; H-donor with Glu398 (O-H…O=C) with length 2.84 Å, H-donor with Glu402 (N-H…O=C) with length 3.11 Å, H-donor with Glu375 (C-H…O-H) with length 3.49 Å, H-acceptor with water (O=C…O-H) with length

2.86 Å and H-acceptor with Arg514 (O=C…N-H) with length 2.91 Å as well as metallic interaction with Zn (O=C…Zn) with length 2.91 Å. Meanwhile Zn interacts with three amino acids by two types of interactions ionic and one metallic. The interactions were metallic with His374, His378, Glu402 with length 2.4, 2.27 and 2.1 Å respectively, ionic interactions one with His378 and two with Glu402 with length 2.27, 2.1 and 3.13 Å respectively.
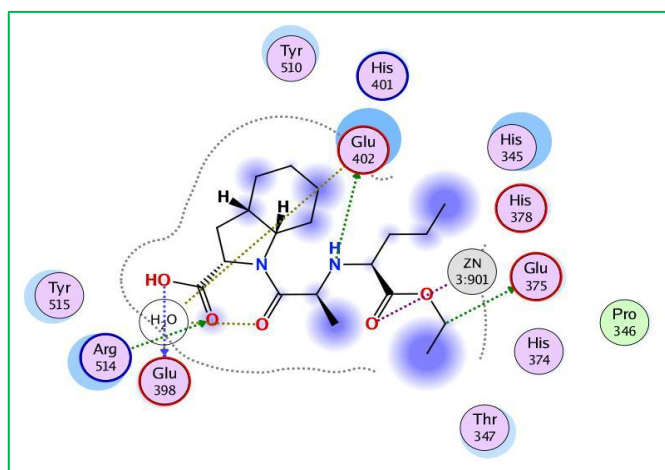
(a)
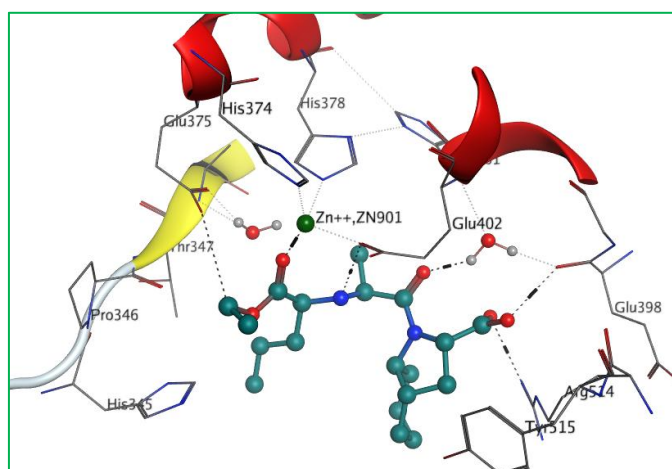
(b)

Figure 15 Interactions between Perindopril and 6M0J receptor in site 2(2D (a); 3D (b)).

In Figure 16, **Hydroxychloroquine** forming interactions with two amino acids Glu375, His378 and zinc. The interactions were, H-donor interaction with Glu375 (O-H…O-H) with length 2.86 A°, metallic interaction with Zn (O-H…Zn) with length 2 Å, H-pi interaction with His378 (C-H…imidazol) with length 4.12 Å. Meanwhile Zn interacts with

three amino acids by two types of interactions ionic and one metallic. The interactions were metallic with His374, His378, Glu402 with length 2.4, 2.27 and 2.1 Å respectively, ionic interactions one with His378 and two with Glu402 with length 2.27, 2.1 and 3.13 Å respectively.
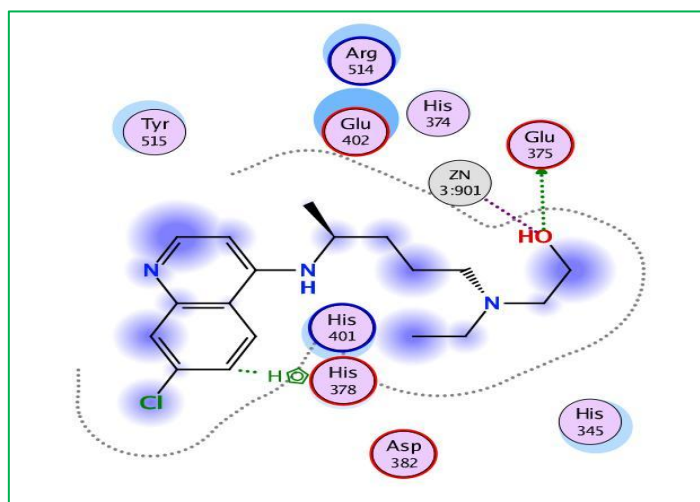
(a)
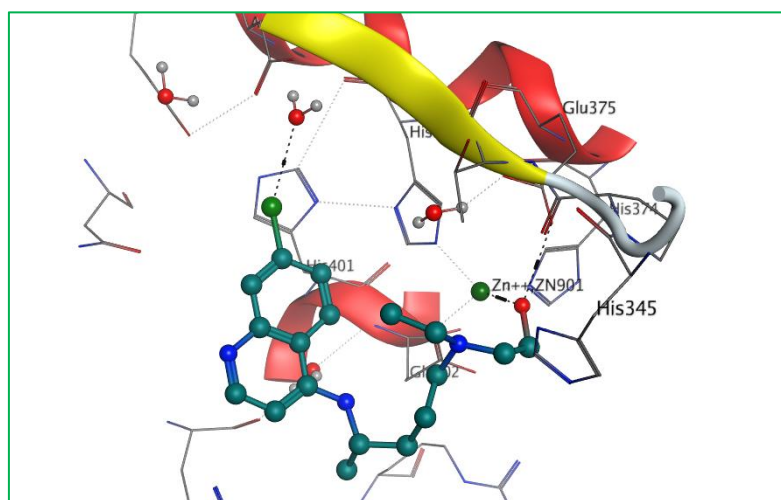
(b)

Figure 16 Interactions between Hydroxychloroquine and 6M0J receptor in site 2(2D (a); 3D (b)).

From Figure 17, **Lisinopril** forming interactions with water and zinc. The interactions were; H-donor with water (O-H…O-H) with length 2.97 Å, metallic with Zn (O-C…Zn) with length 2.06 Å. Meanwhile Zn interacts with three amino acids by two types of interactions ionic and one metallic. The interactions were metallic with His374, His378,

Glu402 with length 2.4, 2.27 and 2.1 Å respectively, ionic interactions one with His378 and two with Glu402 with length 2.27, 2.1 and 3.13 Å respectively.
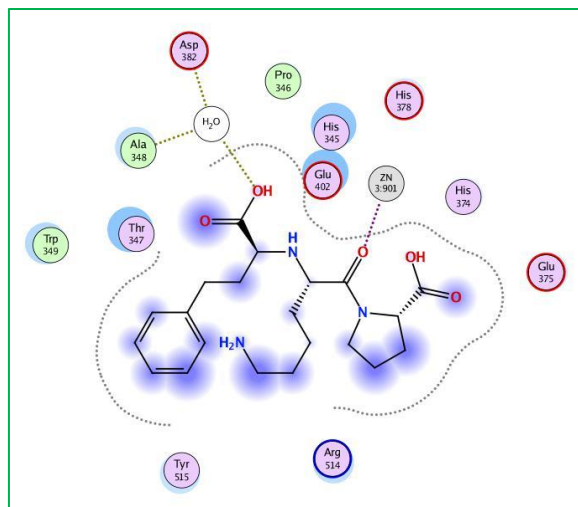
(a)
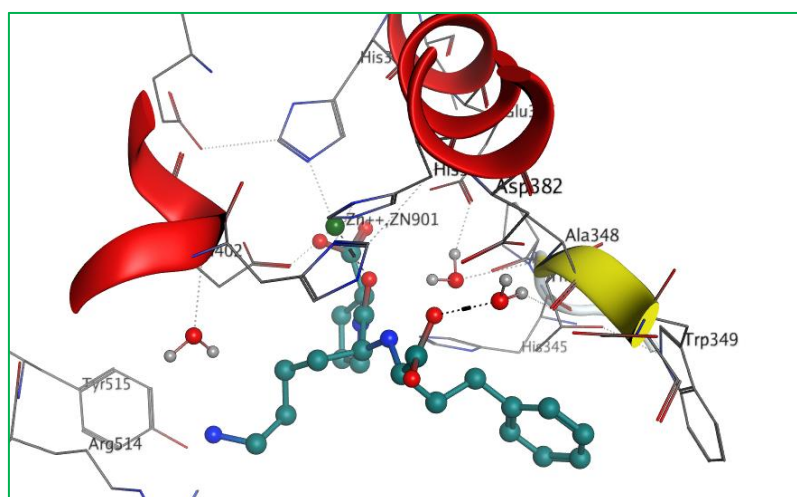
(b)

Figure 17 Interactions between Hydroxychloroquine and 6M0J receptor in site 2(2D (a); 3D (b)).

In Figure 18, **Ramipril** had two metallic interactions with Zn (O=C…Zn) with length 2.13 Å and O=C…Zn) with length 2.44 Å. Meanwhile Zn interacts with three amino acids by two types of interactions ionic and one metallic. The interactions were metallic with His374, His378, Glu402 with length 2.4, 2.27 and 2.1 Å respectively, ionic interactions one with His378 and two with Glu402 with length 2.27, 2.1 and 3.13 Å respectively.
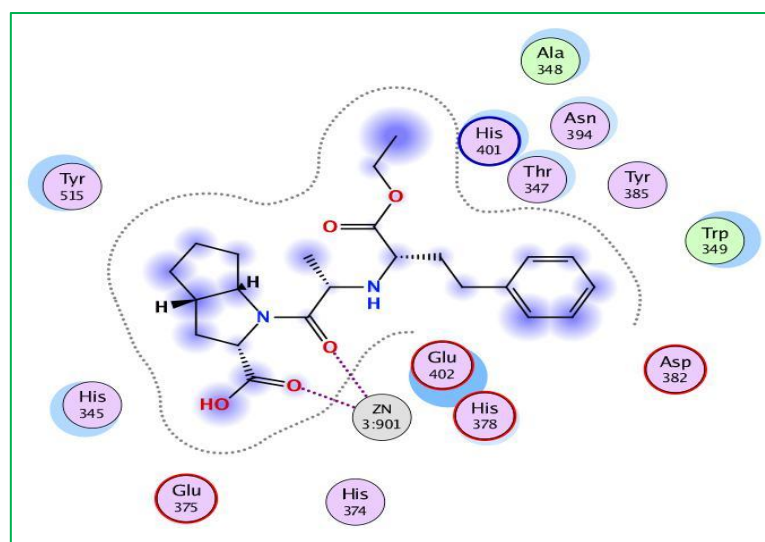
(a)
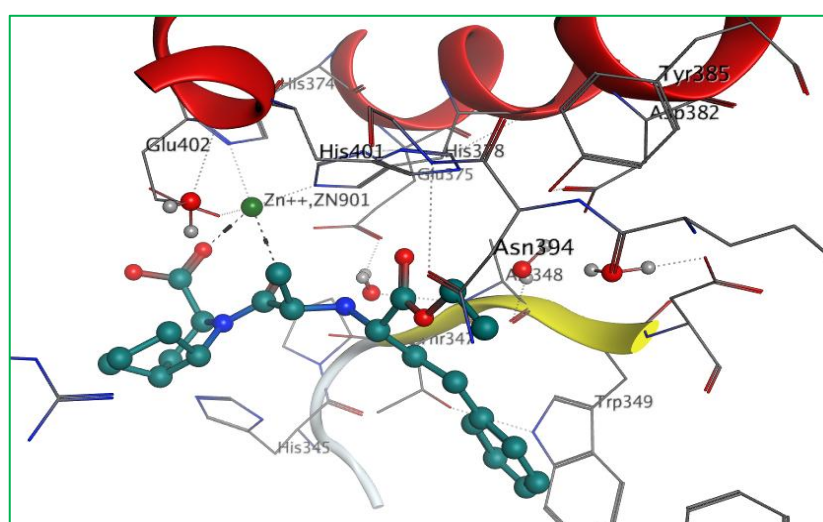
(b)

Figure 18 Interactions between Ramipril and 6M0J receptor in site 2(2D (a); 3D (b)).

I.2.2.   Discussion

The present study emphasizes on the molecular docking of two receptors; human Angiotensin Converting Enzyme-Related Carboxypeptidase (ACE2) [8] and SARS-CoV-2 spike receptor-binding domain bound with ACE2 [9]. The drugs were chosen due to their similarities in structure with chloroquine and hydroxychloroquine from DrugBank database [10]. Chloroquine was chosen as inhibitor of SARS coronavirus infection [11,12]. A molecular docking for 18 drugs were done, It is known that the best score of RMSD values should be near to 2 Å with an energy score less or equal to -7 Kcal/mol [13,14].

These two values are often used as criterion to validate the result of the molecular docking. Also the bond length must be not exceeding than 3.5 Å to be effective [15].

According to docking results of drugs with ACE2 receptor 1R42 in the first site, **Delapril** and **Lisinopril** gives a good RMSD value and an energy score near to -7 kcal/mol, the lengths were under 3.5 Å. On the other hand, **Ramiprilat** and **Piperaquine** had RMSDs more than 3 Å and **Trandolaprilat**, **Chloroquine** and **Perindopril** had RMSDs less than 1.5 Å, which this is inadequate. In this pocket **Delapril** interact with various residues (Ser409, Gln442 and His374) in comparing to Chloroquine which interact with solvent.

While in the second pocket S2, also **Delapril** had the best score followed by **Perindopril**, **Ramipril** and **Chloroquine.** Even in this site S2, **Chloroquine** had a good score but actually it had an inadequate RMSD value (1.3462 Å), which is less than the accepted limit 1.5 Å. The same things can be said for **Enalaprilat**, **Perindopril, Quinacrine** and **Trandolaprilat.**

The results from Table 3 and figures 6-9, showed that **Delapril** interact to water, **Perindopril** to His401with an accepted length, **Ramipril** to Asp350 and molecule water with an accepted length too and chloroquine interact to Ala348 with good length and to Trp349 with length upper the value 3.5 Å.

The results from Table 4 and figures 10-13 in pocket S1 SARS-CoV-2 spike receptor-binding domain bound with ACE2 6m0j revealed that **Piperaquine** had the lowest docking score (-8.6132 Kcal/mol) and RMSD (2.3325 Å) compared with **Delapril** and **Hydroxychloroquine**, which they had energy scores and RMSD values of (-7.5271 Kcal/mol, 2.1735 Å) and (-7.2272 Kcal/mol, 2.1035 Å) respectively. In spite of **Delapril** and **Hydroxychloroquine** did not have the lowest score, they have the best RMSD values. **Lisinopril** and **Quinacrine Mustard** had RMSD value less than 1.5 Å.

In this pocket **Delapril** interact with various residues (Glu375, Arg514, Zn and Tyr515) with length value except the distance with Tyr510 which is 3.93 Å >3.5 Å. The interaction of carboxylic functional group in **Delapril** with zinc motivates the zinc to interact with His374 by metallic interaction and with His378 and Glu402 by ionic and metallic interactions respectively. As mentioned above, zinc had an antiviral activity and this type of interaction may augments the inhibition of the coronavirus receptor [16]. **Hydroxychloroquine** interacts with Phe438, although this drug have good energy score

and RMSD value but the length binding is upper to 3.5 Å. **Piperaquine** interact with Phe438 with length 3.35 Å. Lisinopril had an acceptable RMSD value and also the length to Asn290 and Ile291 4.07 Å ,4.22 Å respectively are > 3.5 Å.

According to the results in the second pocket of 6M0J S2, **Delapril** showed the best docking score followed by **Ramipril** in compared with **Perindopril**, **Lisinopril** and **Hydroxy-chloroquine. Delapril, Ramipril** and **Lisinopril** interact with Zn and with good length binding. **Perindopril** interacted also with Glu398, Glu402 and Glu375 while **Hydroxychloroquine** with Glu375 with length < 3.5 Å.

Although in site 2, **Enalaprilat**, *N*-**(2-aminoethyl)-1-aziridineethamine**, **Piperaquine**, **Piperazine**, **Quinacrine Mustard**, **Trandolaprilat** and **Quinacrine** have interactions with the active site but they have unacceptable RMSD values.

In all pockets, *N*-**(2-aminoethyl)-1-aziridineethamine**, **Triethylenetetramine** and **Piperazine** had energy docking scores higher than -4 Kcal/mol, they had energy scores out of the accepted limit, therefore these compounds could not be considered. Also, in all results, **Chloroquine** had energy scores higher than **Hydroxychloroquine** and **Delapril**.

I.3.   Molecular Dynamics simulations

I.3.1.   Results

To execute Molecular Dynamics process, the top three complexes were selected for each receptor. This selection was based up on the results of reactivity obtained through global reactivity descriptors results: energy gap, hardness and softness, chemical potential. Also, the selection was according to the molecular docking results. However, in this study, it was observed that the results of DFT and molecular docking studies were correlated and represented the same trend.

The Molecular Dynamics analysis was run for 600 ps on the most promising drugs **Delapril**, **Lisinopril** and **Ramipril** to check for the stability in target SARS-CoV-2 spike receptor-binding with ACE2 complex (**6M0J**). The evaluated average MM-GBSA binding energies are given in Table 6.

Table 6 Calculated MM-GBSA binding energies (in kcal/mol) for the Delapril, Lisinopril and Ramipril drugs against 6M0J over MD simulations.

Drugs	Site 1	Site 2
Delapril	-54	-45
Lisinopril	-33	-38
Ramipril	-46	-42

In general, it is apparent from this table that the selected three drugs exhibited considerable binding energies. In site 1, **Delapril** and **Ramipril** showed promising binding energies -54 and -46 kcal/mol respectively. On the other hand, **Lisinopril** showed relatively weak binding energy -33 kcal/mol. Whereas, in site 2, all three drugs **Delapril**, **Lisinopril** and **Ramipril** showed promising binding affinities with binding energies.

To explore the dynamic stability of the 6M0J/inhibitor drugs complexes, the time-dependent potential energy of the complex were calculated during MD trajectories.

Figures 19 showed the results of the atomic potential energy function during dynamic study calculation for **Delapril** in the **6M0J** at site 1.

It is apparent in this figure, that complex **(6M0J/Delapril)** achieved equilibrium around 300 ps. Also, Figure 19 show the interaction energy between a residue and a ligand **(6M0J/Delapril).** The major favourable energy contributions (-2.2 to -1.4 kcal/mol) originate predominately from Glu375 (2.39 Å, -1.4 kcal/mol), H_2O1030 (2.94 Å, -1.5 kcal/mol) and Trp203 (3.79 Å, -2.2 kcal/mol). Meanwhile Zn interacts with three amino acids by two types of interactions ionic and one metallic. The interactions were metallic with His374, Glu375, Glu402 with length (2.45, 1.96 and 2 Å) and energy binding (-2.8, -5.8 and -5.6 kcal/mol) respectively, ionic interactions one with Glu375, His378 and Glu402 with length (1.96, 2.12 and 2 Å) and energy binding (-16.9, -14.1, -16.3 kcal/mol) respectively.
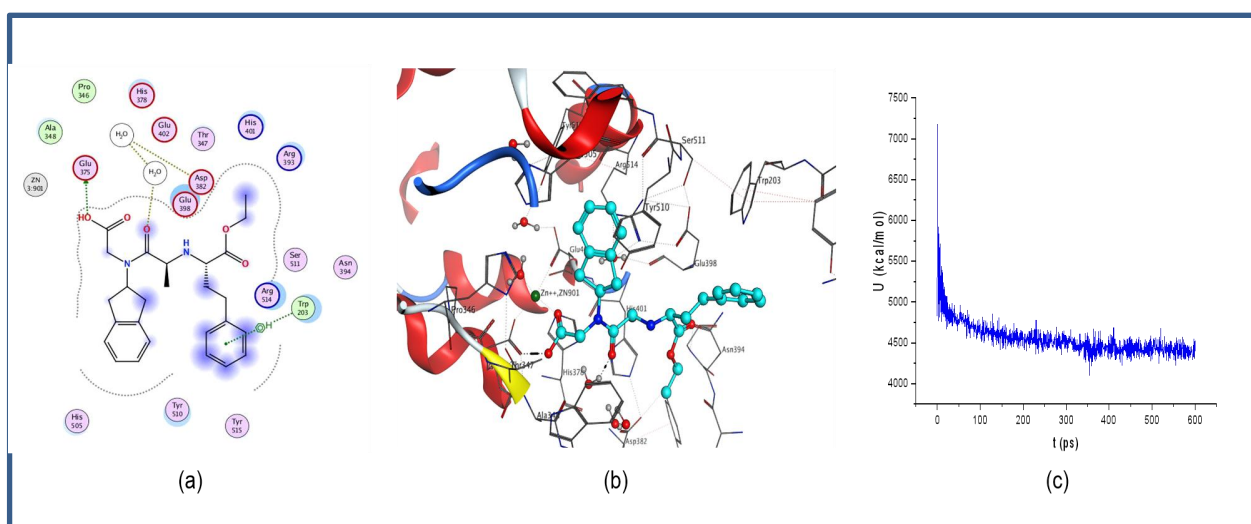
Figure 19 Molecular dynamics result of Delapril complexed with 6M0J receptor site 1. (a) 2D interaction diagrams, (b)3D interaction diagrams and (c) The evaluation of potential energy as function of time.

Figures 20, showed the results of the atomic potential energy function during dynamic study calculation for **Lisinopril** in the **6M0J** at site 1. Figure 20, indicate that complex **(6M0J/Lisinopril)** achieved the equilibrium around 350 ps.

Also, figure 20 showed the interaction energy between a residue and a ligand **(6M0J/Lisinopril).** This complex had energy binding with Asp292 (2.59 Å, -7.8 kcal/mol) and Ala413 (2.89 Å, -4.7 kcal/mol).
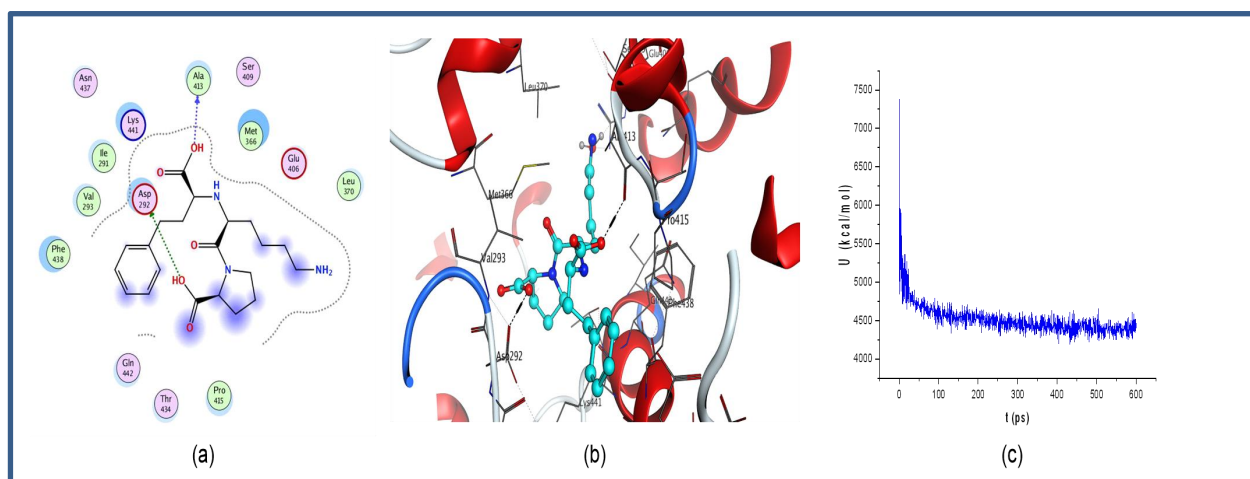
Figure 20 Molecular dynamics result of Lisinopril complexed with 6M0J receptor site 1. (a) 2D interaction diagrams, (b) 3D interaction diagrams and (c) The evaluation of potential energy as function of time.

Figure 21 shows the results of the atomic potential energy function during molecular dynamic simulation for **Ramipril** in the **6M0J** at site 1. Figure 21 indicates that complex **(6M0J/Ramipril)** achieved the equilibrium stability around 350 ps. Also, it shows that **(6M0J/Ramipril)** didn't interact in this site.
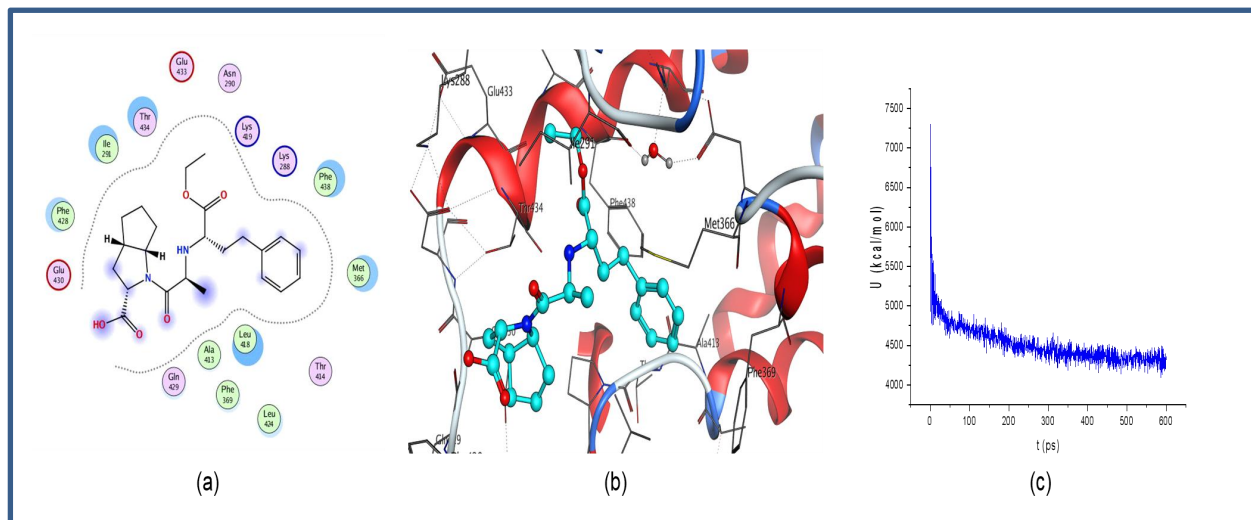
Figure 21 Molecular dynamics result of Ramipril complexed with 6M0J receptor site 1. (a) 2D interaction diagrams, (b) 3D interaction diagrams and (c) The evaluation of potential energy as function of time.

It can be seen from Figure 22, **site 2,** that the complex **(6M0J/Delapril)** achieved the equilibrium stability around 400 ps. While, this complex had interactions with Glu375 (2.69Å, -8.7 kcal/mol) and Zn901 (2.25 Å, -3.4 kcal/mol). Meanwhile Zn interacts with three amino acids by two types of interactions ionic and one metallic. The interactions were metallic with His374, Glu375, His378 and Glu402 with length (2.27, 2.17, 2.08 and 2.04 Å) and energy binding (-1.4, -5, -3.4 and -5.4 kcal/mol) respectively, ionic interactions one with Glu375, His378 and Glu402 with length (2.17, 2.08 and 2.04 Å) and energy binding (-13.3, -14.7, -15.4 kcal/mol) respectively.

(a)   (b)   (c)
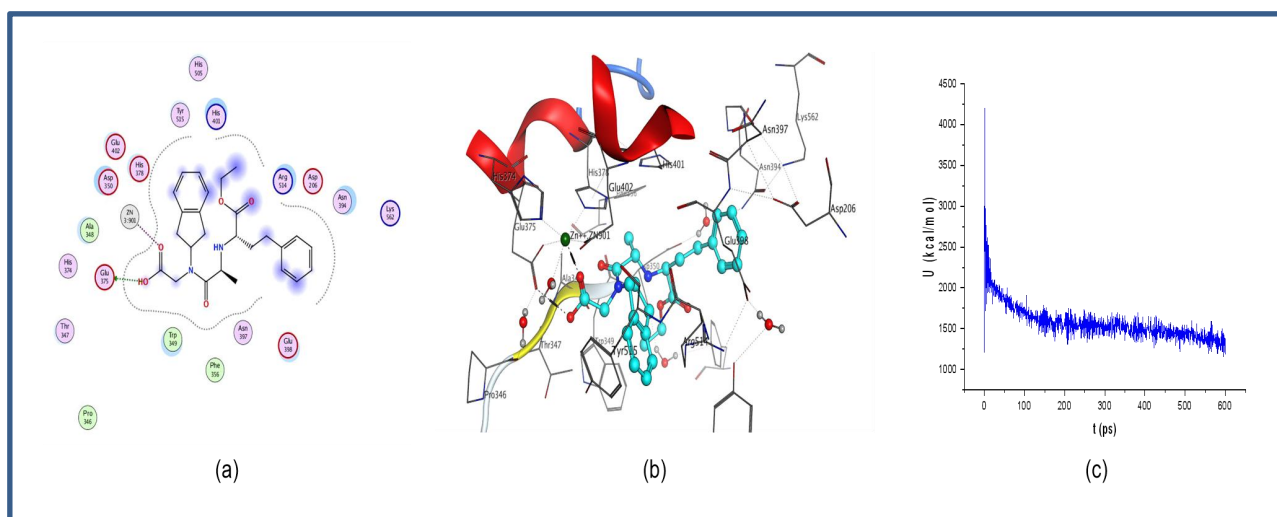
Figure 22 Molecular dynamics result of Delapril complexed with 6M0J receptor site 2. (a) 2D interaction diagrams, (b) 3D interaction diagrams and (c) The evaluation of potential energy as function of time.

Figure 23, showed that complex **(6M0J/Lisinopril)** achieved the equilibrium stability around 400 ps. while in figure 23 the complex had the major favourable energy contributions (-0.6 to -6.2 kcal/mol) which originate predominately from Glu402 (2.51 A°, -2.3 kcal/mol), Asp382 (2.55 Å, -6.2 kcal/mol), H_2O1033 (2.86 Å, -1.3 kcal/mol), Tyr510 (2.66 Å, -2.8 kcal/mol), H_2O1004 (2.81 Å, -1.5 kcal/mol), His401 (4.60 Å, -0.6 kcal/mol) and Trp349 (4.61 Å, -1 kcal/mol).
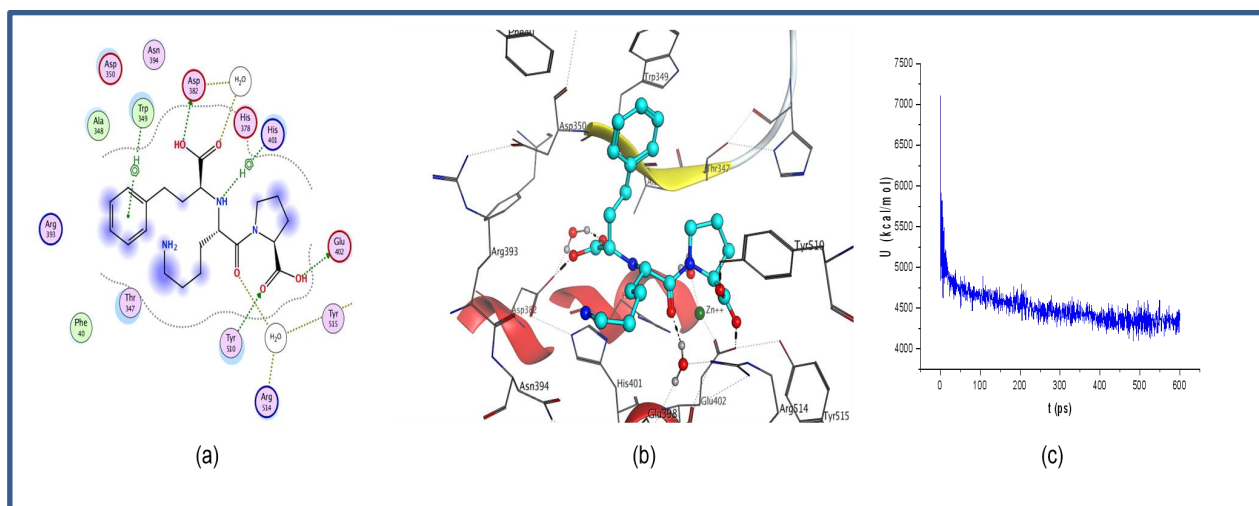
Figure 23 Molecular dynamics result of Lisinopril complexed with 6M0J receptor site 2. (a) 2D interaction diagrams, (b) 3D interaction diagrams and (c) The evaluation of potential energy as function of time.

Figure 24, showed that complex **(6M0J/Ramipril)** achieved the equilibrium stability around 350 ps. While, from figure 24, the Complex showed more favourable interactions with residues Glu402 (2.52 Å, -3.8 kcal/mol), H_2O1030 (2.77 Å, -1.3 kcal/mol), H_2O1002 (3.03 Å, -0.9 kcal/mol), Zn901 (2.21 Å, -4.1 kcal/mol) and Asp350 (4.39 Å, -2 kcal/mol). Meanwhile Zn interacts with three amino acids by two types of interactions ionic and one metallic. The interactions were metallic with His374, Glu375, His378 and Glu402 with length (2.41, 1.92, 1.94 and 1.96 Å) and energy binding (-1.6, -6.2, -3.9 and -7.2 kcal/mol) respectively, ionic interactions one with Glu375, His378 and Glu402 with length (1.92, 1.94 and 1.96 Å) and energy binding (-17.7, -17.5, -16.9 kcal/mol) respectively.
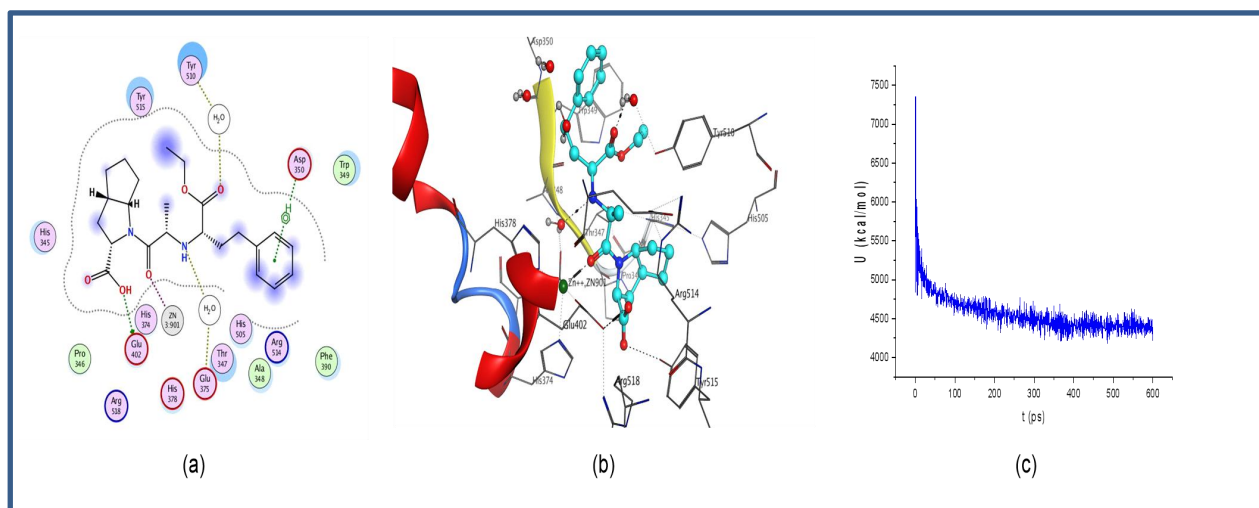
Figure 24 Molecular dynamics result of Ramipril complexed with 6M0J receptor site 2. (a) 2D interaction diagrams, (b) 3D interaction diagrams and (c) The evaluation of potential energy as function of time.

I.3.2.   Discussion

In order to examine the conformational flexibilities of docked drug-receptor complexes and to attain dependable drug-receptor–binding affinities, the MD process combined with binding energy (MM-GBSA) [17,18] calculations was run for 600 ps on the most promising drugs **Delapril**, **Lisinopril** and **Ramipril** to target SARS-CoV-2 spike receptor-binding with ACE2complex (**6M0J**). According to results from Table 6 only Lisinopril have the weak binding energy -33 kcal/mol >-35 kcal/mol. While in S2 all drugs have good energy < -35kcal/mol.

In general, if the interaction energy between a residue and ligand is lower than -0.8 kcal/mol, the residue is regarded as an important residue in the molecular recognition of the ligand. From figure 19, first complex all binding energy and length between the residue and ligand considered as good value, it is the same for the second complex figure 20. In the first site S1 the interaction binding and the value of   MM-GBSA indicate that Delapril is good than Lisinopril. Meanwhile in site 2 S2, figure 22 indicate that the complex **(6M0J/Delapril)** had good binding energy and length between the residue and ligand and Zn plays an important role.

The results from Figure 23, indicate that the complex **(6M0J/Lisinopril)** had good binding energy and length between the residue and ligand. Nevertheless, His401 cannot be considered as an important residue because of the energy -0.6 kcal/mol > -0.8 kcal/mol and

127

the length between Lisinopril and Trp349 is 4.61 Å >3.5 Å. Figure 24 indicate that the complex (**6M0J/Ramipril**) had good binding energy and length between the residue and ligand, also the Zn interact with different residue with good binding energy and length.

In this site, **Delapril** and **Ramipril** have interacted with Zn. While, the energy binding and the length in complex 3 is better than complex 1.

II. Result and discussion of Various Quinazolines and Pyridopyrimidines as Inhibitors of the Epidermal Growth Factor Receptor

II.1. Reactivity

II.1.1. Results

Table 7 summarises the chemical reactivity descriptor calculated to 7 drugs and 27 compounds. According to Table 7, compound **25** has the lowest energy gap ($\Delta E = 3.3402$ eV) followed by compounds **23, 26, 27, 9** and **24** respectively. Also, compound **25** was the hardest and softest compound with $\eta = 1.6701$ eV and $S = 0.2994$ followed by compound **23**, **26**, **27**, **9**, **24** respectively.

The electronic chemical potential (μ) for compound **7** ($\mu = -3.0742$ eV) was higher than other compounds followed by compounds **10** and **9**.

According to the results in Table 7, compound **7** had the highest nucleophilicity value ($N = 3.6964$ eV) followed by **10** and **9** ($N = 3.2659$ eV), ($N = 3.2199$ eV) respectively.

From Table 7, compounds **23, 25, 26, 27, 24** and **17** have the highest value of ω (5.3337 eV, 5.2391 eV, 4.9509 eV, 4.8041 eV and 4.1171 eV) respectively. Compound **24** and **lapatinib** have similar values of ΔE, η and S. Also compounds **9, 23, 24, 25** and **26** have good values of ΔE, η and **S** in comparing with **gefitinib**, **erlotinib**, **lapatinib**, **canartinib**, **pelitinib**, **neratinib** and **afatinib**.

Table 7 HOMO and LUMO energy, energy gap ΔE and global reactivity indices μ, ω, η and N for 27 compounds with 7 referenced drugs.

Compounds	HOMO (eV)	LUMO (eV)	ΔE (eV)	η (eV)	S (eV)	μ (eV)	ω (eV)	N (eV)
Gefitinib	-5.8777	-1.6599	4.2178	2.1089	0.2371	-3.7688	3.3676	2.7783
Erlotinib	-5.8042	-1.5538	4.2504	2.1252	0.2353	-3.679	3.1844	2.8518
Lapatinib	-5.7441	-2.0278	3.7163	1.8581	0.2691	-3.8859	4.0633	2.9119
Canartinib	-6.1084	-2.0885	4.0199	2.0100	0.2488	-4.0984	4.1785	2.5475
Pelitinib	-6.1305	-2.116	4.0145	2.0072	0.2491	-4.1232	4.2349	2.5255
Neratinib	-5.8456	-1.9228	3.9228	1.9614	0.2549	-3.8842	3.8459	2.8104
Afatinib	-5.9155	-2.0107	3.9048	1.9524	0.2561	-3.9631	4.0222	2.7405
L1	-5.6983	-1.71	3.9884	1.9942	0.2507	-3.7042	3.4402	2.9576
L2	-5.6194	-1.7339	3.8855	1.9428	0.2574	-3.6767	3.4791	3.0365
L3	-5.6257	-1.7013	3.9244	1.9622	0.2548	-3.6635	3.4199	3.0303
L4	-5.6774	-1.5494	4.128	2.0640	0.2422	-3.6134	3.1630	2.9786
L5	-6.0028	-1.907	4.0959	2.0479	0.2442	-3.9549	3.8188	2.6531
L6	-5.2703	-1.4112	3.8591	1.9296	0.2591	-3.3407	2.8920	3.3856
L7	-4.9595	-1.1821	3.7775	1.8887	0.2647	-3.0742	2.4963	3.6964
L8	-5.6695	-1.7862	3.8833	1.9417	0.2575	-3.7278	3.5785	2.9865
L9	-5.39	-1.7138	3.6763	1.8381	0.2720	-3.5519	3.4318	3.2659
L10	-5.436	-1.6656	3.7704	1.8852	0.2652	-3.5508	3.3440	3.2199
L11	-5.5645	-1.6942	3.8703	1.9351	0.2584	-3.6293	3.4034	3.0915
L12	-5.6232	-1.8376	3.7856	1.8928	0.2642	-3.7304	3.6760	3.0327
L13	-5.7683	-1.7285	4.0398	2.0199	0.2475	-3.7484	3.4780	2.8877
L14	-5.5835	-1.7217	3.8618	1.9309	0.2589	-3.6526	3.4547	3.0724
L15	-5.6287	-1.858	3.7707	1.8853	0.2652	-3.7433	3.7162	3.0273
L16	-5.9114	-1.9843	3.9271	1.9636	0.2546	-3.9478	3.9686	2.7445
L17	-6.0782	-2.0583	4.0199	2.0100	0.2488	-4.0682	4.1171	2.5777

L18	-5.5242	-1.7345	3.7897	1.8949	0.2639	-3.6293	3.4757	3.1318
L19	-5.5938	-1.7173	3.8765	1.9383	0.2580	-3.6556	3.4472	3.0621
L20	-5.6026	-1.7418	3.8608	1.9304	0.2590	-3.6722	3.4928	3.0534
L21	-5.6967	-1.7804	3.9163	1.9581	0.2553	-3.7386	3.5690	2.9592
L22	-5.7528	-1.7989	3.9538	1.9769	0.2529	-3.7759	3.6059	2.9032
L23	-6.0605	-2.5696	3.4909	1.7455	0.2865	-4.3150	5.3337	2.5954
L24	-6.0779	-2.3668	3.7111	1.8555	0.2695	-4.2224	4.8041	2.5780
L25	-5.8807	-2.5405	3.3402	1.6701	0.2994	-4.2106	5.3077	2.7753
L26	-6.0858	-2.5375	3.5484	1.7742	0.2818	-4.3116	5.2391	2.5701
L27	-5.9919	-2.4194	3.5726	1.7863	0.2799	-4.2057	4.9509	2.6640

Notes: the HOMO energy -8.6559 eV. of the reference system (TCE) had been calculated at DFT/B3LYP 6-31G

II.1.2. Discussion

Analysis of density functional theory descriptors allows knowing more about the characteristics stability, electrophilic and nucleophilic compound. Negative values for E_{HOMO} and E_{LUMO} [2], refer to the stability of the examined compounds.

According to electronic chemical potential (μ) results , compounds 7, 9 and 10 can exchange electron density with the environment efficiently more than the others [4].

A further classification of organic molecules as strong (N > 3 eV), moderate ($2.0 \text{ eV} \leq N \leq 3.0 \text{ eV}$) and marginal nucleophile (N < 2.0 eV) were obtained by analysis of a series of common nucleophilic species participating in polar organic reaction [5]. All compounds under investigation were classified as moderate nucleophile except **2**, **3, 6, 7, 9-12**, **14**, **15**, **18-20** which were classified as strong nucleophile.

Also, compound **25** was the hardest and softest compound with $\eta = 1.6701$ eV and S = 0.2994 followed by compound **23**, **26**, **27**, **9**, **24** respectively, which means that those compounds are more stable and more reactive than others.

The electrophilicity ω had become a potent tool for the study of the reactivity of organic compounds that can participate easily in polar reaction with value more than **2.0 eV** [6,7]. All compounds have value more than 2.0 eV.

II.2. Molecular Docking

II.2.1. Results

II.2.1.1. *The binding affinities of the ligands into wild-type*

Table 8 present the results of docking of the drugs and ligands in **1XKK** active site. The results, as shown in Table 8, indicate that all drugs and ligands under investigation have interactions with the site. Closer inspection of the table shows ligands **27, 9, 14, 25, 12, 11, 7, 22, 20, 18** and **24** have the best RMSDs value ranging from 2.16 to 1.88 Å, while the energy score range was from -11.6977 to -7.0035 kcal/mol. However, the ligands **2**, **3**, **4**, **5**, **6** and **23** were excluded because they have invalid RMSDs values, which were either less or more than the validation range.

Table 8 The results obtained from docking of ligands with wild-type receptor

Ligands	S score (kcal/mol)	RMSD (Å)	Bonds between atoms of compounds and residues of active site of 1XKK					
			Atom of compound	Atom of receptor	Involved receptor residues	Type of interaction bond	Distance (Å)	E (kcal/mol)
Gefitinib	-8.6810	1.8022	O-22	N	Met 793	H-acceptor	3.07	-1.5
			6-ring	CB	Leu 718	Pi-H	4.10	-1.1
			6-ring	CD2	Leu 718		4.03	-0.6
Erlotinib	-7.0035	1.8545	6-ring	CD1	Leu 718	Pi-H	4.19	-0.6
Lapatinib	-10.1987	1.1771	C-21	O	Cys 775	H-donor	3.30	-1.0
			N-5	N	Met 793	H-acceptor	3.34	-1.2
			6-ring	CD1	Leu 718	Pi-H	3.91	-0.6
Canartinib	-7.6343	1.7095	N-26	O	H_2O 22	H-donor	3.06	-2.1
			N-14	N	Met 793	H-acceptor	3.37	-2.6
			O-23	O	H_2O 2		2.74	-0.8
			6-ring	CD1	Leu 718	Pi-H	4.07	-0.6
Pelitinib	-7.6343	1.5881	N-25	SG	Cys 797	H-donor	3.64	-1.0
Neratinib	-9.5907	1.7014	6-ring	CB	Leu 718	Pi-H	4.12	-0.6
Afatinib	-8.1328	1.5950	N-26	O	H_2O 22	H-donor	2.96	-2.4
			N-14	N	Met 793	H-acceptor	3.40	-2.1
			6-ring	CD1	Leu 718	Pi-H	3.78	-1.1
L1	-8.1825	1.8759	N-27	O	H_2O 22	H-donor	2.96	-2.4
			N-11	N	Met 793	H-acceptor	3.30	-3.2
L2	-8.22279	3.3036	N-27	O	H_2O 22	H-donor	2.78	-1.9
			CL-35	O	Leu 788		3.38	-0.4
			N-11	N	Met 793	H-acceptor	3.40	-0.7

			6-ring	CD1	Leu 718	Pi-H	4.36	-0.6
			N-29	O	H$_2$O 22	H-donor	2.76	-1.7
	-8.2935	1.4997	CL-37	O	Leu 788		3.44	-0.4
			N-13	N	Met 793	H-acceptor	3.39	-0.7
L3			6-ring	CD1	Leu 718	Pi-H	4.30	-0.6
			O-22	O	H$_2$O 71	H-acceptor	3.08	-1.0
	-7.3908	1.1254	F-33	N	Met 793		2.99	-0.9
			6-ring	CB	Leu 718	Pi-H	4.17	-0.7
L4			6-ring	CD1	Leu 718		4.07	-0.6
			N-18	O	H$_2$O 22	H-donor	3.08	-1.9
	-7.6936	1.3033	N-10	N	Met 793	H-acceptor	3.31	-3.2
L5			6-ring	CD1	Leu 718	Pi-H	3.95	-0.7
			N-27	O	Ser 720	H-donor	3.08	-1.4
	-7.2685	1.2154	O-16	N	Met 793	H-acceptor	3.13	-0.8
			6-ring	CB	Leu 718	Pi-H	4.12	-0.8
L6			6-ring	CD2	Leu 718		4.08	-0.7
			N-18	O	H$_2$O 22	H-donor	2.81	-2.3
	-10.4063	1.9525	N-10	N	Met 793	H-acceptor	3.30	-1.3
			C-31	6-ring	Phe 856	H-pi	3.51	-0.6
L7			6-ring	CD1	Leu 718	Pi-H	3.68	-1.0
			N-18	O	H$_2$O 22	H-donor	2.82	-2.5
	-10.3245	1.7545	N-10	N	Met 793	H-acceptor	3.32	-1.5
L8			6-ring	CD1	Leu 718	Pi-H	3.67	-0.8
			N-23	O	H$_2$O 22	H-donor	2.84	-2.5
	-11.0950	2.1277	N-14	N	Met 793	H-acceptor	3.11	-4.0
L9			6-ring	CD1	Leu 718	Pi-H	3.69	-0.7

			N-27	O	H_2O 22	H-donor	2.72	-0.6
			N-18	N	Met 793	H-acceptor	3.14	-1.3
	-8.4395	1.8280	6-ring	CD1	Leu 718	Pi-H	3.95	-0.8
L10			6-ring	N	Asp 855		4.66	-0.7
			C-2	SG	Cys 797	H-donor	3.76	-0.7
			N-25	O	H_2O 22		2.73	-1.4
	-10.6909	1.9653	O-5	O	H_2O 22	H-acceptor	2.96	-0.8
L11			6-ring	CD1	Leu 718	Pi-H	4.28	-0.6
	-9.9975	2.0094	N-6	SG	Cys 797	H-donor	3.55	-0.9
L12			N-26	O	H_2O 22		2.70	-0.6
			N-26	O	H_2O 22	H-donor	2.78	-2.4
	-11.1402	1.7227	O-5	O	H_2O 22	H-acceptor	2.93	-2.0
			N-17	N	Met 793		3.43	-0.7
L13			6-ring	CD1	Leu 718	Pi-H	3.61	-0.7
			C-2	OD2	Asp 800		3.49	-0.7
	-10.8744	2.0370	N-6	SG	Cys 797	H-donor	3.65	-0.8
			N-27	O	H_2O 22		2.68	-1.0
L14			6-ring	CD1	Leu 718	Pi-H	4.27	-0.6
			N-28	O	H_2O 22	H-donor	2.78	-2.3
	-10.8490	1.6001	O-5	O	H_2O 22	H-acceptor	2.86	-1.5
			C-42	6-ring	H_2O 4	H-pi	3.57	-0.6
L15			6-ring	CD1	Leu 718	Pi-H	3.60	-0.6
			N-26	O	H_2O 22	H-donor	2.92	-2.4
	-9.1520	1.8735	N-18	N	Met 793	H-acceptor	3.33	-3.0
L16			6-ring	CD1	Leu 718	Pi-H	3.89	-0.7
L17	-8.3338	1.7795	N-25	O	H_2O 22	H-donor	3.07	-2.0

			N-17	N	Met 793	H-acceptor	3.34	-2.9
			6-ring	CD1	Leu 718	Pi-H	3.94	-0.7
L18	-9.8021	1.8932	N-25	O	H$_2$O 22	H-donor	2.90	-0.7
			6-ring	CB	Leu 718	Pi-H	4.20	-0.6
			N-27	O	H$_2$O 22	H-donor	2.80	-2.3
L19	-10.7588	1.8332	C-41	6-ring	Phe 856	H-pi	3.55	-0.6
			6-ring	CD1	Leu 718	Pi-H	3.61	-0.6
L20	-11.6977	1.8986	N-29	O	H$_2$O 22	H-donor	2.70	-1.3
			6-ring	CD1	Leu 718	Pi-H	4.14	-0.7
L21	-7.7595	1.8226	CL-43	O	Met 793	H-donor	3.09	-1.5
			6-ring	CD1	Leu 718	Pi-H	3.82	-1
L22	-9.1728	1.9259	6-ring	CB	Leu 718	Pi-H	4.43	-0.8
			N-20	O	H$_2$O 22	H-donor	2.95	-2.4
	-8.4096	1.4905	N-10	N	Met 793	H-acceptor	3.05	-5.0
			N-12	O	H$_2$O 4		2.90	-1.0
L23			6-ring	CD1	Leu 718	Pi-H	3.86	-0.7
			N-12	O	H$_2$O 22	H-donor	2.91	-2.3
	-9.2230	1.8886	N-19	N	Met 793	H-acceptor	3.27	-2.0
			N-22	O	H$_2$O 22		3.26	-0.8
L24			6-ring	CD1	Leu 718	Pi-H	4.14	-0.9
			N-23	O	H$_2$O 22	H-donor	3.09	-2.0
	-8.7555	2.0260	N-13	N	Met 793	H-acceptor	3.15	-4.4
L25			6-ring	CD1	Leu 718	Pi-H	3.87	-0.8
			N-24	O	H$_2$O 22	H-donor	3.14	-0.7
	-9.4776	1.8443	N-14	N	Met 793	H-acceptor	3.16	-3.2
L26			6-ring	CD1	Leu 718	Pi-H	4.19	-0.8

			N-20	O	H$_2$O 22	H-donor	2.91	-2.5
			N-10	N	Met 793	H-acceptor	3.00	-5.1
	-10.8533	2.1690	N-12	O	H$_2$O 4		3.15	-0.8
			C-33	6-ring	Phe 856	H-pi	3.62	-0.7
L27			6-ring	CD1	Leu 718	Pi-H	3.81	-0.8
			N22-37	O	H$_2$O 22	H-donor	2.88	-2.5
			O4-7	N	Ser 720		2.92	-2.5
			N18-32	N	Met 793	H-acceptor	2.96	-5.5
	-11.8277	2.6476	N20-35	O	H$_2$O 4		3.05	-1.1
			C31-52	6-ring	Phe 856	H-pi	3.62	-0.7
			5-ring	CB	Leu 718	Pi-H	4.38	-0.8
Ref			6-ring	CD1	Leu 718		3.80	-0.6

Figure 25 shows the interactions of the most active ligands which gave the best docking results. From the data in Figure 25, it is apparent that **L11, L12** and **L14** had H-donor interaction with Cys797 amino acid which considered as important residue [19,20]. Several tyrosine kinase inhibitors combined with Methionine [21]. Meanwhile, **L27** had interactions almost as same as the reference ligand which were with H_2O 22, H_2O 4, Met793 and Leu718, except Ser720 which had no interaction with this ligand. In addition, almost all ligands interacted with Met793 and Leu718 amino acids.

L7   L9   L11

L12   L14   L18

L20   L22   L24
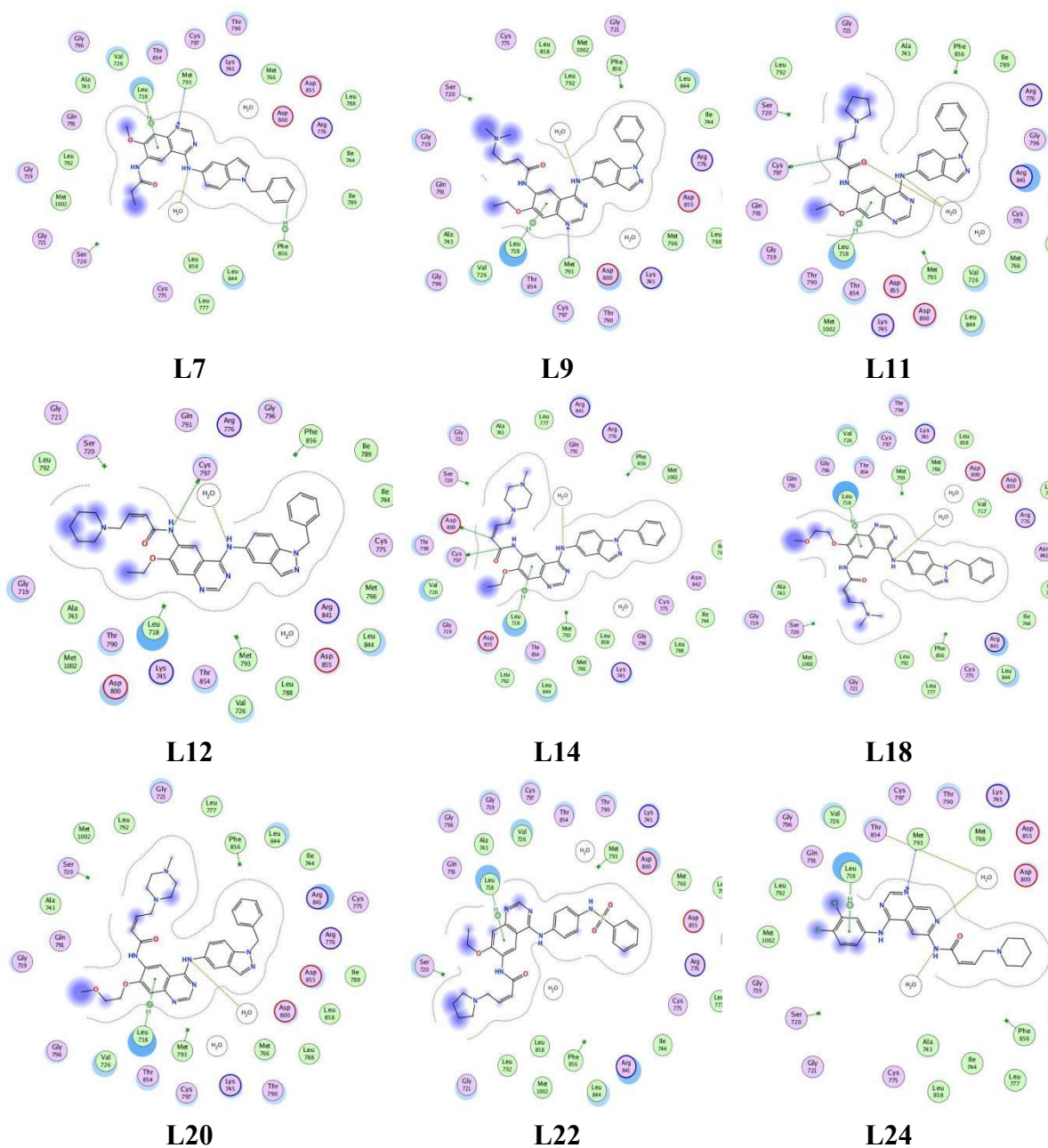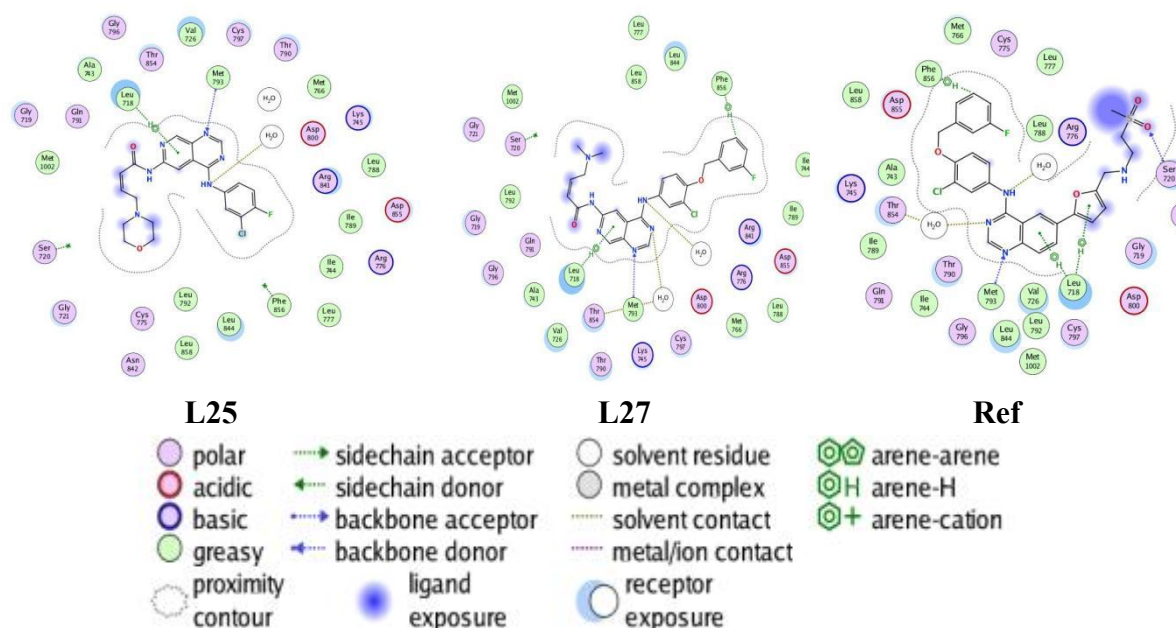
Figure 25 Compounds binding with wild-type PDB ID: 1XKK

II.2.1.2. *The binding affinities of the ligands into L858R mutation*

Table 9 present the results of docking the drugs and ligands in active site of L858R mutation **PDB ID: 2ITV**. The results, as shown in Table 9, indicate that the drugs have interactions with the active site except **lapatinib**, **L5** and **L16**. According to Table 9, all compounds have valid RMSD values. However, compounds **canartinib**, **L3**, **L9**, and **L22** have invalid RMSDs values which they were more than 2.5 Å, while Ligands **L2**, **L8** and **L25** have RMSD value less than 1.5 Å. The derivatives of pyrido[3,4-d]pyrimidine namely ligands **L23**, **L24** and **L26** have bonded to receptor with more than three residues, also they have an acceptable RMSD values. These results of docking are close to reference compound.

Table 9 The results obtained from docking of ligands L858R mutation receptor

Ligands	S score (kcal/mol)	RMSD (Å)	Bonds between atoms of compounds and residues of active site of 2ITV					
			Atom of compound	Atom of receptor	Involved receptor residues	Type of interaction bond	Distance (Å)	E (kcal/mol)
Gefitinb	-6.5191	2.1360	N-7	NZ	Lys 745	H-acceptor	3.18	-6.6
Erlotinib	-6.7655	1.8561	C-6	OE2	Glu 762	H-donor	3.45	-0.8
			6-ring	NZ	Lys 745	Pi-cation	3.74	-1.9
Pelitinib	-6.8940	1.6231	N-7	NZ	Lys 745	H-acceptor	3.30	-4.2
			N-24	N	Met 793		3.73	-0.7
			N-24	O	H_2O 3148		3.31	-1
Canartinib	-7.0974	2.7081	CL-33	O	Met 793	H-donor	3.46	-0.4
Neratinib	-7.8134	1.6294	N-24	NZ	Lys 745	H-acceptor	3.02	-1
			N-24	CA	Asp 855		3.45	-0.7
			6-ring	6-ring	Phe 723	Pi-pi	3.53	-0
Afatinib	-6.7917	2.4191	C-15	OE2	Glu 762	H-donor	3.45	-0.7
			O-21	N	Met 793	H-acceptor	3.09	-1.4
			6-ring	NZ	Lys 745	Pi-cation	3.64	-1.5
L1	-7.2740	1.9105	O-4	NZ	Lys 745	H-acceptor	2.88	-4.5
L2	-7.3767	1.2397	C-2	OE2	Glu 762	H-donor	3.47	-0.7
			O-5	NZ	Lys 745	H-acceptor	2.90	-1.3
			O-23	N	Met 793		3.11	-2.4
L3	-7.5851	3.3690	CL-37	O	Gln 791	H-donor	3.14	-2.2
			6-ring	CG1	Val 726	Pi-H	4.12	-0.6
			6-ring	NZ	Lys 745	Pi-cation	4.76	-1
L4	-7.0028	2.2778	O-4	NZ	Lys 745	H-acceptor	3.03	-1.5
L6	-6.2313	1.7183	5-ring	O	H_2O 3148	Pi-H	4.29	-1.6
L7	-7.4339	2.1022	N-12	NZ	Lys 745	H-acceptor	3.65	-1.9
L8	-7.0160	1.2040	N-12	NZ	Lys 745	Pi-cation	3.40	-4.2

			6-ring	CG1	Val 726	Pi-H	4.10	-0.9
L9	-8.1857	3.1897	N-7	O	H$_2$O 3148	H-acceptor	3.03	-1.6
			5-ring	O	H$_2$O 3146	Pi-H	4.29	-0.8
L10	-7.7021	1.6733	C-19	OE2	Glu 762	H-donor	3.32	-0.7
			6-ring	NZ	Lys 745	Pi-cation	3.43	-1
L11	-8.0442	2.2960	N-18	NZ	Lys 745	H-acceptor	3.06	-6.4
L12	-8.2363	1.7831	N-19	NZ	Lys 745	H-acceptor	3.05	-8.7
L13	-7.7816	1.8147	N-12	O	H$_2$O 3148	H-acceptor	2.93	-1
			6-ring	CG2	Val 726	Pi-H	4.07	-0.8
L14	-8.1053	2.1375	6-ring	CG1	Val 726	Pi-H	4.51	-0.7
L15	-8.1043	2.2123	N-21	NZ	Lys 745	H-acceptor	3.03	-1.7
L17	-7.0768	1.6813	6-ring	CD	Lys 745	Pi-H	3.58	-0.6
L18	-7.7213	1.7411	6-ring	SG	Cys 797	Pi-H	4.02	-0.9
L19	-8.3914	2.0323	N-18	NZ	Lys 745	H-acceptor	3.28	-4.2
L20	-7.9863	2.3374	N-9	NZ	Lys 745	H-acceptor	3.62	-1.6
			5-ring			Pi-cation	3.84	-1.8
L21	-7.8857	2.4172	6-ring	CG2	Val 726	Pi-H	4.45	-0.8
			N-20	NZ	Lys 745	H-acceptor	3.30	-4.4
			O-5	CA	Gly 719		3.33	-0.8
L22	-7.7949	2.6000	C-38	OE1	Glu 762	H-donor	3.55	-0.7
L23	-6.4924	2.4441	N-6	OD2	Asp 855	H-donor	3.42	-0.6
			C-15	OE2	Glu 762		3.30	-1
			CL-28	O	Gln 791		3.33	-1.4
			6-ring	CG1	Val 726	Pi-H	4.55	-0.7
			6-ring	CD	Lys 745		3.90	-1.1
L24	-7.1974	2.1932	C-21	OE2	Glu 762	H-donor	3.26	-0.7
			CL-31	O	Gln 791		3.62	-0.6
			O-11	NZ	Lys 745	H-acceptor	3.07	-2.5
			6-ring	CG1	Val 726	Pi-H	4.67	-0.6

L25	-6.7419	1.3269	O-5	NZ	Lys 745	H-acceptor	2.98	-6.2
L26	-6.6911	1.8510	CL-32	OD1	Asp 855	H-donor	3.54	-0.6
			N-12	NZ	Lys 745	H-acceptor	3.15	-4.8
			N-18	CA	Gly 719		3.60	-0.7
			6-ring	CG2	Val 726	Pi-H	3.71	-0.6
L27	-6.7599	1.8714	6-ring	CG1	Val 726	Pi-H	3.74	-0.7
Ref	-6.8909	2.2435	O3G-2	OG1	Thr 854	H-donor	3.11	-0.7
			O1B-8	OD2	Asp 855		2.91	-3
			N6-41	O	Gln 791		2.97	-3
			O2G-4	NZ	Lys 745	H-acceptor	3.17	-1.8
			N1-42	N	Met 793		3.12	-4.5
			N3-46	O	H$_2$O 3148		2.97	-2.1
			5-ring	CG1	Val 726	Pi-H	4.02	-1.3

The results from Figure 26 showed that **L19** had H-acceptor interaction with Lys745, while, **L21** had Pi-H interaction with Val726 amino acid and H-acceptor interaction with amino acids Lys745 and Gly719. Meanwhile, **L23** had H-donor interactions with amino acids Asp855, Glu762 and Gln791 as well as pi-H interactions with Val726 and Lys745. **L24** had H-donor interactions with amino acids Glu762 and Gln791, H-acceptor interaction with amino acid Lys745 and Pi-H interaction with amino acid Val726. **L26** had H-donor interaction with amino acid Asp855, H-acceptor interactions with amino acids Lys745 and Gly719 and Pi-H interaction with amino acid Val726.
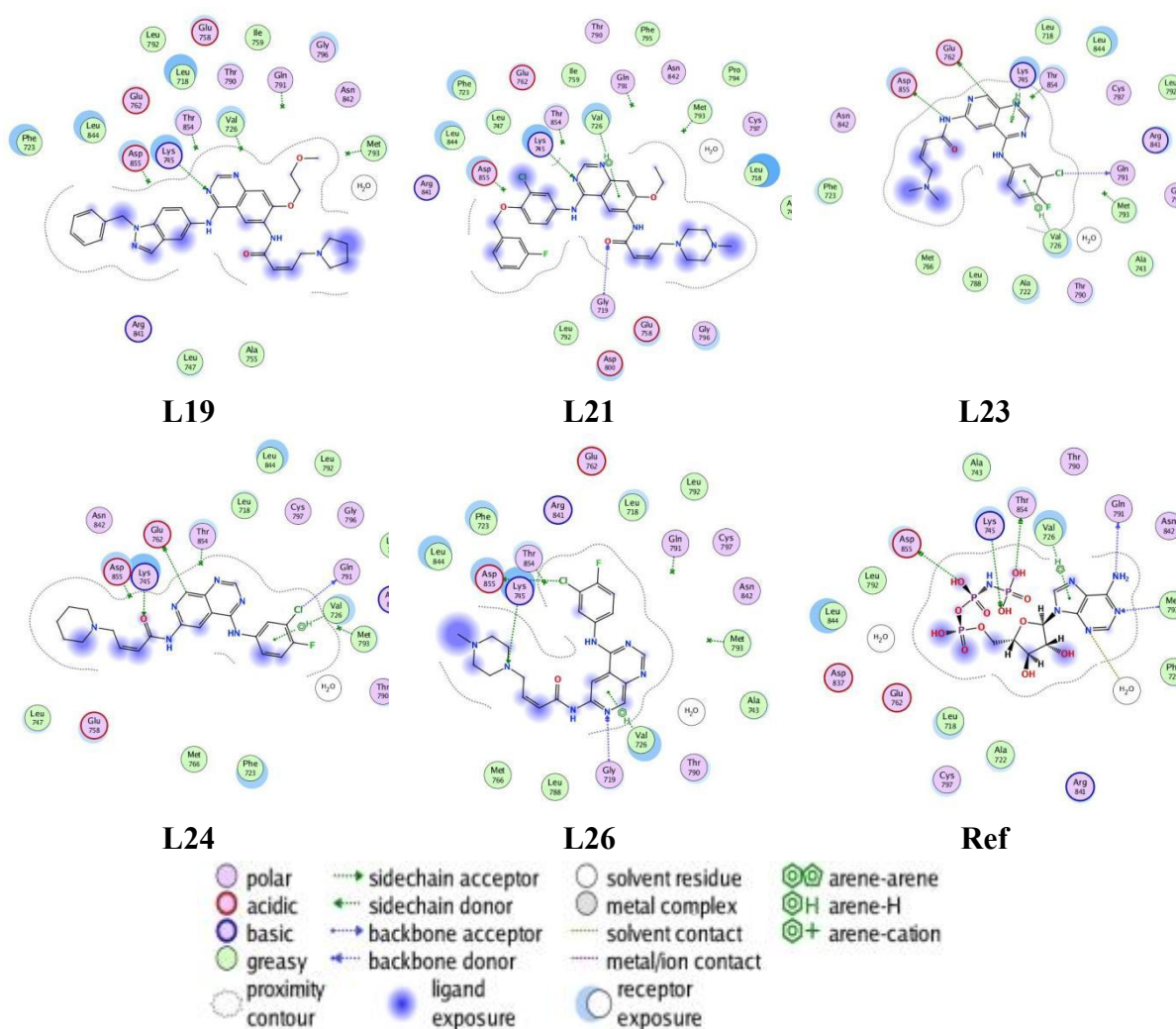
Figure 26 Compounds binding with L858R mutation PDB ID: 2ITV.

II.2.1.3. The binding affinities of the ligands into T790M mutation.

Table 10 present the results of docking of the drugs and ligands in active site of T790M mutation **PDB ID: 5HG5**. It can be seen from Table 10 that some compounds have invalid RMSDs values in instance **lapatinib**, **canartinib** and ligands **2**, **3**, **10**, **18**, **23** have RMSDs values less than1.50 Å while ligands **7**, **25**, **26**, **27** have RMSDs value more than 2.50 Å. Therefore, these compounds were excluded. **Gefitinib** and ligands **1**, **4**, **8**, **9**, **16**, **22**, **24** have good energy scores ranging from -8.4627 to -7.0602 kcal/mol. Ligand **22** has the best energy score -8.4627 kcal/mol and RMSD value 2.0220 Å in comparing with the other ligands.

Table 10 The results obtained from docking of ligands with T790M mutation receptor

Ligands	S score (kcal/mol)	RMSD (Å)	Bonds between atoms of compounds and residues of active site of 5HG5					
			Atom of compound	Atom of receptor	Involved receptor residues	Type of interaction bond	Distance (Å)	E (kcal/mol)
Gefitinib	-7.4327	2.4819	6-ring 6-ring	CD2 CD2	Leu 718 Leu 718	Pi-H	4.15 4.32	-0.8 -0.8
Lapatinib	-7.8348	0.9699	N-7	N	Met 793	H-acceptor	3.25	-3.2
Canartinib	-7.8348	1.3039	6-ring	CA	Gly 719	Pi-H	4.42	-1
L1	-7.7387	1.9402	C-21 6-ring 6-ring	6-ring CB CB	Phe 856 Leu 718 Leu 718	H-pi Pi-H	3.57 4.12 4.39	-0.6 -0.9 -0.9
L2	-6.5994	1.1735	N-27 6-ring	O CA	H_2O 9307 Gly 796	H-donor Pi-H	3.06 3.60	-0.6 -0.6
L3	-8.0512	1.3172	6-ring	CA	Gly 719	Pi-H	3.87	-1.2
L4	-7.9987	2.1416	O-22 C-32	O 6-ring	H_2O 9245 Phe 856	H-acceptor H-pi	2.95 3.58	-0.9 -0.9
L5	-6.7228	1.2709	6-ring 6-ring	CB CA	Leu 718 Gly 719	Pi-H	4.46 4.42	-0.7 -0.8
L6	-6.9434	1.2182	6-ring 6-ring	CD2 CD2	Leu 718 Leu 718	Pi-H	4.12 4.33	-0.7 -0.6
L7	-7.0482	2.9125	6-ring	CB	Leu 718	Pi-H	4.16	-0.8
L8	-7.0602	2.1801	6-ring	CD1	Leu 718	Pi-H	3.79	-0.8
L9	-7.8399	2.4433	6-ring	CD2	Leu 718	Pi-H	4.42	-0.7
L10	-7.7384	1.2475	5-ring	CD1	Leu 718	Pi-H	3.66	-0.6
L16	-7.8021	1.6821	6-ring 6-ring	CD2 CA	Leu 718 Gly 796	Pi-H	4.06 3.72	-0.8 -0.6

L18	-8.0907	1.2399	6-ring	CD2	Leu 718	Pi-H	4.16	-0.7
L22	-8.4627	2.0220	O-31	O	H$_2$O 9153	H-acceptor	3.32	-0.6
			6-ring	CD	Arg 841	Pi-H	3.82	-0.6
L23	-6.9528	0.6334	CL-28	OE2	Glu 804	H-donor	4.01	-0.6
			O-5	N	Met 793	H-acceptor	3.09	-2.5
			6-ring	CB	Leu 718	Pi-H	3.98	-1.1
			6-ring	CD1	Leu 718		4.13	-0.6
L24	-7.7626	1.5681	6-ring	CB	Leu 718	Pi-H	4.12	-0.9
			6-ring	CD1	Leu 718		4.02	-0.9
			6-ring	CD2	Leu 718		4.19	-1
			6-ring	CA	Gly 796		3.71	-0.9
L25	-7.5090	3.2579	6-ring	CB	Leu 718	Pi-H	4.33	-0.6
			6-ring	CD1	Leu 718		4.05	-0.7
			6-ring	CD2	Leu 718		4.13	-0.7
			6-ring	CA	Gly 796		3.66	-0.6
L26	7.4905	2.5226	6-ring	CB	Leu 718	Pi-H	4.46	-0.8
			6-ring	CA	Gly 719		3.92	-1
L27	-7.3109	3.2637	N-10	N	Met 793	H-aaceptor	3.63	-0.7
Ref	-8.2767	1.8158	N7-21	O	Gln 791	H-donor	2.96	-4.5
			N17-33	O	H$_2$O 9159		3.04	-2
			C31-51	O	H$_2$O 9146		3.14	-0.5
			N6-20	N	Met 793	H-acceptor	3.26	-2.4
			N32-54	OE2	Glu 804	Ionic	3.92	-0.7

The results from Figure 27 showed that **L22** had Pi-H interaction with Arg841 amino acid and H-acceptor interaction with water, while **L4** had H-acceptor interaction with water and H-pi interaction amino acid Phe856. **L1** had H-pi interaction with amino acid Phe856 and two Pi-H interactions with amino acid Leu718. **L8** and **L9** had Pi-H interaction with Leu718, whereas **L16** had two Pi-H interactions with amino acids Leu718 and Gly796. **L24** had three Pi-H interactions with amino acid Leu718 and one with Gly796.

L1   **L4**   **L8**

L9   **L16**   **L22**

L24   **Ref**
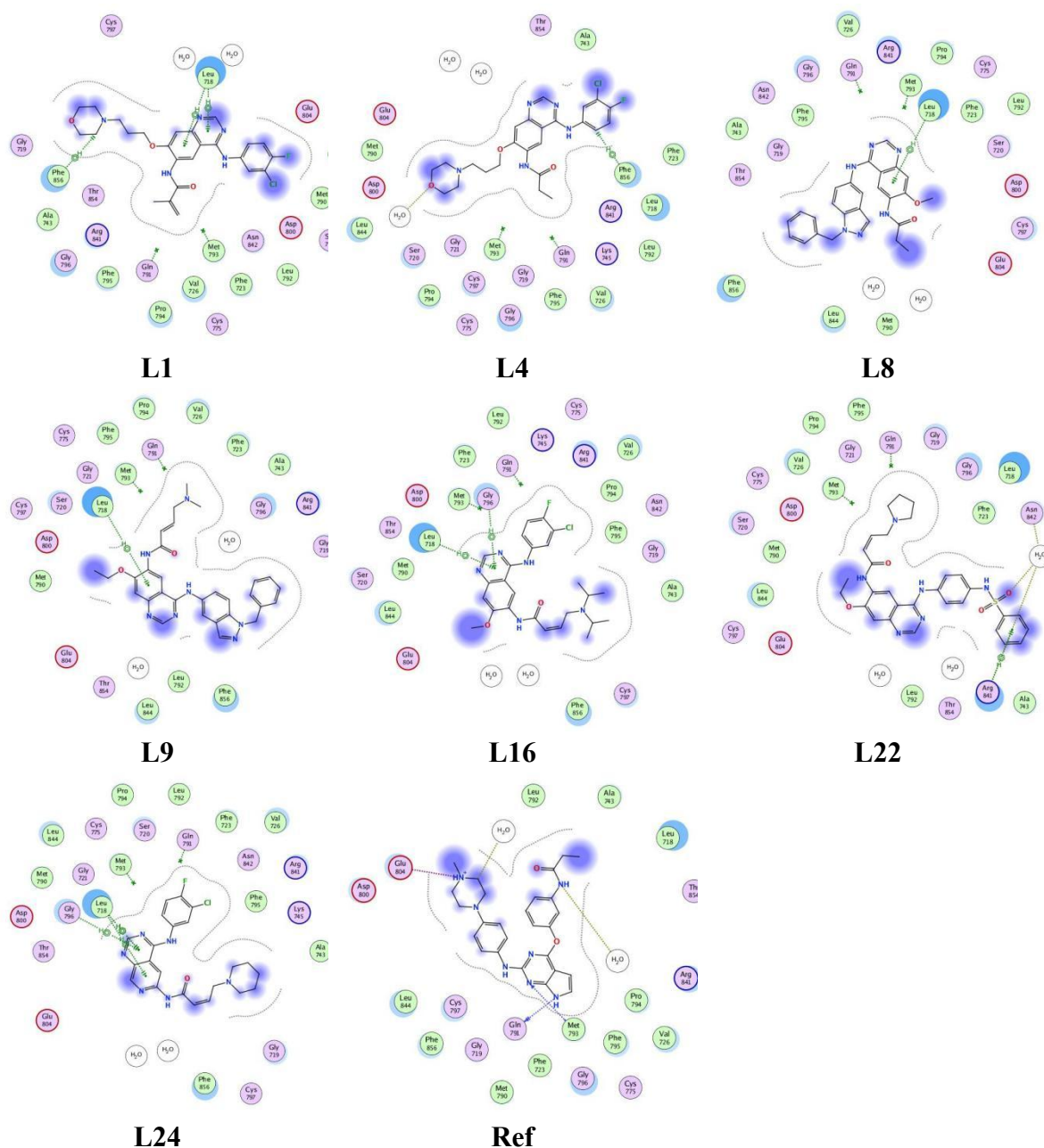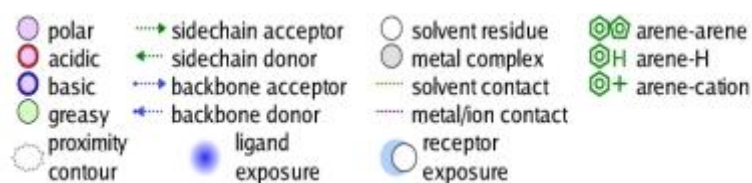
Figure 27 Compounds binding with T790M mutation PDB ID: 5HG5.

II.2.2. Discussion

In this section, molecular docking of three receptors were done; The crystal structures of EGFR wild-type (PDB entry: **1XKK)**[22], the crystal structure of EGFR L858R mutation (PDB entry: **2ITV**) [20] and the crystal structure of EGFR T790M mutation (PDB entry: **5HG5**) [23]. A dataset of substituted quinazoline and pyrido[3,4-d]pyrimidine derivatives as irreversible tyrosine kinase inhibitors of the epidermal growth factor receptor family were extracted from the literature [24]. A molecular docking for 27compounds and 7 referenced drugs were done, It is known as mention above that the best score of RMSD values should be near to 2 Å with an energy score less or equal to -7 Kcal/mol [13,14]. These two values are often used as criterion to validate the result of the molecular docking. Also the bond length must be not exceeding than 3.5 Å to be effective [15].

According to docking results of compounds with the first receptor 1XKK, **ligands 27, 9, 14, 25, 12, 11, 7, 22, 20, 18 and 24** gives a good RMSD value and energy score less than -7 kcal/mol. On the other hand, **L2** had RMSD more than 3 Å meanwhile, ligands **3**, **4**, **5**, **6**, and **23** had RMSDs less than 1.5 Å, which this is inadequate. From the data in this site, it is apparent that **L11, L12** and **L14** had H-donor interaction with Cys797 amino acid which considered as important residue [19,20]. Several tyrosine kinase inhibitors combined with Methionine [21].

While in the second receptor 2ITV, **L19** had the best score followed by **L12**, **L14** and **L15.** Even in this site, **L9** had a good score but actually it had an inadequate RMSD value (3.1897 Å), which is more than the accepted limit 2.5 Å. **L21**, **L23**, **L24**, and **L26** interacted with more than two residues and with almost the same lengths as reference compound residue's.

Meanwhile in the third receptor **5HG5**, only three drugs and 18 ligands gave interaction with the receptor. The results from Table 10 showed that **L1**, **L4**, **L8**, **L9**, **L16** and **L24** interacted to the same residues as referenced drugs.

II.3.   Molecular Dynamics simulation

II.3.1. Results

It is apparent from Table 11 that the selected ligands exhibited considerable binding energies in wild-type receptor **1XKK** ($<$ −35 kcal/mol) and L858R mutation receptor **2ITV** ($<$ -32kcal/mol). Meanwhile, the binding energy was $>$-38 kcal/mol for T790M mutation receptor **5HG5**. Wild-type receptor complexed with **L9, L11, L20, L22, L24** and **L27** showed promising binding energies -50, -54, -72, -51, -64, -51 kcal/mol respectively. In addition, in L858R mutation, compound **L19** showed promising binding energies -48 kcal/mol. Whereas, in T790M Mutation, only **L1** and **L22** showed promising binding energy -37 kcal/mol, however, all the other ligands showed relatively weak binding energy $>$ -33 kcal/mol.

Table 11 Calculated MM-GBSA binding energies (in kcal/mol) for the most active molecules against 1XKK, 2ITV and 5HG5 over MD simulations.

Molecules	1XKK	2ITV	5HG5
L1	-	-	-37.98
L4	-	-	-29.74
L7	-43.72	-	-
L 8	-	-	-33.29
L 9	-50.15	-	-33.84
L 11	-54.74	-	-
L 12	-43.69	-	-
L 14	-41.36	-	-
L 16	-	-	-21.28
L 18	-41.41	-	-
L 19	-	-48.05	-
L 20	-72.14	-	-
L 21	-	-42.29	-
L 22	-51.70	-	-37.07
L 23	-	-32.06	-
L 24	-64.32	-35.50	-33.57
L 25	-35.31	-	-
L 26	-	-38.04	-
L 27	-51.30	-	-

It is apparent from result, that all complexed ligands with wild-type receptor (**1XKK**) achieved equilibrium around 50 ps except complex of L**24** with **1XKK** which achieved equilibrium around 1000 ps Figure 28 Meanwhile the complexed ligands with L858R receptor **(2ITV)**, achieved the equilibrium also around 50 ps. Whereas the complexed

ligands with T790M mutation **(5HG5)**, achieved equilibrium around 50 ps except complex of L**24** which achieved the equilibrium around 1300 ps in Figure 28.

From Figure 28, it can be noticed that the complex of **L24/1XKK**: N12, N23, O11 and O11 bonded to several deferent water molecules with interaction energy -3, -2.2, -1 and -1.1 kcal/mol in distance of 2.68, 2.99, 2.81 and 2.66 Å. Also, N6 bonded to NH of Asp855 with energy -1.3 kcal/mol and distance of 3.49 Å. Whereas N19 bonded to N of Met793 with energy -0.6 kcal/mol and distance of 3.76 Å. Whereas, 6-ring bonded to CD1and 6-ring bonded to CD1 of Leu718 and Leu844 with energy -0.7 kcal/mol in distance 4 and 3.74 Å respectively.

Although the complex **L25/1XKK** interacted with different amino acids, he showed the highest MM/GBSA energy -35 kcal/mol in comparing with other complexes.

With respect to the complex of **L24/2ITV**, N12, N23, O11, N17 and N22 bonded to several deferent water molecules with interaction energies 0.3, -2.4, -2.2, -1 and -2.2 kcal/mol in distances of 3.17, 2.87, 2.80, 3.16 and 3.02 Å respectively. In addition, N6 bonded to NZ and 6-ring bonded to CE of Lys745 with interaction energies -8.5 and -0.8 kcal/mol and in distances of 3.20 and 4.27 Å respectively.

Only the complex of **L21/2ITV** and **L23/2ITV** bonded to more than one amino acid and had MM/GBSA energies -42 and -32 kcal/mol respectively as show in Table 8, which indicates that L21 and L23 can be considered as inhibitors for L858R Mutation. Meanwhile, the complexes **L19/2ITV**, **L24/2ITV** and **L26/2ITV** bonded to one amino acid and water molecules in MD pose and showed good MM/GBSA energies -48, -32 and -38 kcal/mol respectively.

In complex of **L24/5HG5**, N12, N23, N19 and N22 bonded to several deferent water molecules with energies -3.1, -1.7, -1.5 and -2.1 kcal/mol in distances of 2.90, 3.16, 3.30 and 2.85 Å respectively. Moreover 6-ring bonded to CB of Leu718 with -0.6 kcal/mol and 4.51Å. Whereas 6-ring bonded with CA of Gly796 with -1.2 kacl/mol and 4.18 Å.

The complexes of **L4/5HG5, L9/5HG5** and **L22/5HG5** interacted only with water and also had highest MM/GBSA energies -29, -33 and -37 kcal/mol respectively. The other complexes, **L1/5HG5, L8/5HG5** and **L24/5HG5**, showed good interaction and acceptable

MM/GBSA energies -37, -33 and -33 kcal/mol respectively. Meanwhile **L16/5HG5** had low value of MMGBSA -22 kcal/mol.
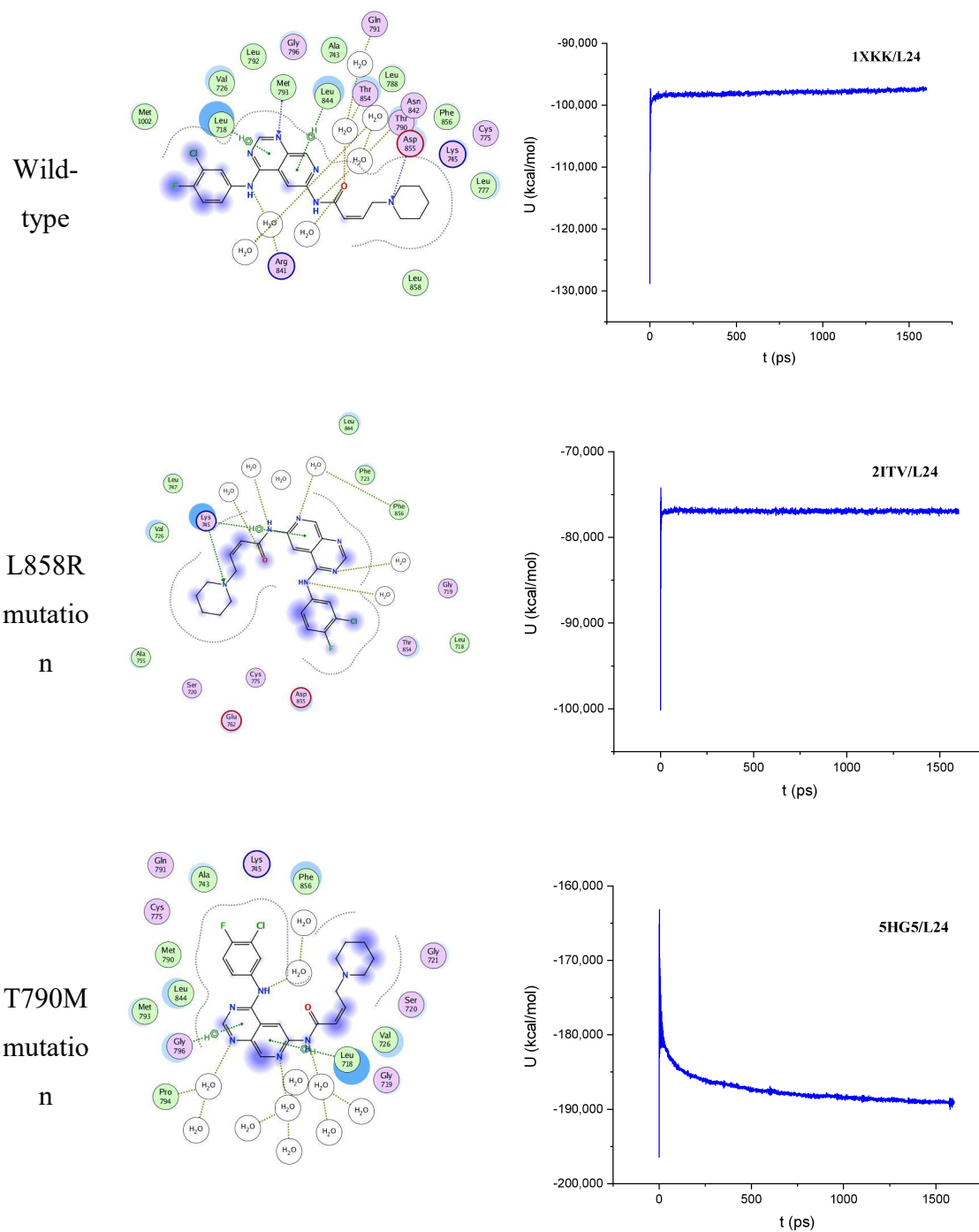
Figure 28 MD pose and the evolution of potential energy of L24 complexed with WT, L858R and T790M receptors as function of time.

II.3.2. Discussion

The molecular dynamics (MD) approach was integrated with binding energy (MM-GBSA) to assess the conformational flexibility of docked drug-receptor complexes and to achieve reliable drug-receptor-binding affinities [17,18] was performed. The calculations process was run for 1600 ps on the most promising ligands to target of three selected receptors (**1XKK, 2ITV** and **5HG5**). According to results from Table 11 only ligands in **5HG5** receptor have the weak binding energy >-35 kcal/mol

In general, a residue is considered a significant residue in the molecular recognition of a ligand if the interaction energy between it and the ligand is less than -0.8 Kcal/mol.

The results from figure 28 indicate that the complex **L24/1XKK** had good binding energy and length between solvent and ligand. Nevertheless, Asp855 considered as an important residue because of the energy -1.3 kcal/mol <-0.8 kcal/mol, Whereas N19 bonded to N of Met793 with energy -0.6 kcal/mol and distance of 3.76 Å. Whereas, Leu718 and Leu844 cannot considered as important residue because energy -0.7 kcal/mol and length 4 and 3.74 Å> 3.5 Å respectively.

Figure 28 indicate that the complex **L24/2ITV** had good binding energy and length between solvent and ligand. Also, the complex had good binding energy and length between the Lys745 and ligand with -8.5 and -0.8 kcal/mol <-0.8 kcal/mol.

Complex **L24/5HG5** had good binding energy and length between solvent and ligand. **L24** bonded Leu718 with -0.6 kcal/mol > -0.8kcal/mol. And to Gly796 with -1.2 kacl/mol < -0.8kcal/mol.

II.4.   Pharmacokinetics properties

II.4.1. Results and discussion

ADMET properties for quinazoline and pyrido[3,4-d]pyrimidine derivatives were cited in Table 12. **L5** and **L23** have value of caco-2 >-5.15, all ligands are listed as P-gp inhibitor, passed human intestinal absorption HIA and none of the ligands were substrate P-gp, only **L22** didn't pass F 20% bioavailability, **L1-L8**, **L16, L17** and **L23-L26** passed F 30% bioavailability.

L6, L14, L15 and **L20** have PPB value less than 90% (low PPB-bound), others are high PPB-bound, **L10** and **L15** didn't passed BBB criteria and for VD distribution value:

<0.07L/kg highly hydrophilic, 0.07-0.7 evenly distributed and >0.7 highly lipophilic, **L14** is highly lipophilic, **L1-L5, L8, L16, L21-L23, L25** and **L27** are highly hydrophilic, other ligands are evenly distributed.

L5-L8 were considered as inhibitors of CYP450-1A2, whereas the other were not; only **L7, L8**, **L15** were not substrate of CYP450-1A2; all ligands were inhibitors and substrate of CYP450-3A4. All ligands were inhibitors of CYP450-2C9 except **L23-L26,** only **L21** and **L23-L27** were substrate of CYP-2C9. All ligands were inhibitors of CYP-2C19 except **L20, L22** and **L26**, also all ligands were substrate of CYP450-2C19 except **L6, L8, L10-L13, L15, L18** and **L19.** Only **L6** and **L8** were not inhibitors of CYP450-2D6, whereas only **L9, L10, L15, L18, L22** and **L23** were not substrate of CYP450-2D9.

All ligands have T1/2 value >0.5h and CL<5 ml/min/kg as **canartinib** value, for toxicity **L20** is H-HT human hepatotoxic compound, all ligands are hERG blockers, **L1-L6, L9, L10, L16-L18** and **L22-L27** have not Ames mutagenicity. The LD50 acute of toxicity value should be > 500 mg/kg to considered as low toxic, 50-500 mg/kg toxic and <50 high toxic. All ligand have low toxicity value except **L10** and **L15** are toxic compounds.

Table 12 The ADMET properties of 27 compounds and canartinib

Compounds	Absorption						Distribution			Metabolism CYP450										Excretion		Toxicity			
	Caco-2 permeability	P-gp inhibitor	P-gp substrate	HIA	f-20%	f-30%	PPB %	BBB	VD (L/kg)	1A2-inhibitor	1A2-substrat	3A4-inhibitor	3A4-substrat	2C9-inhibitor	2C9-substrat	2C19-inhibitor	2C19-substrat	2D6-inhibitor	2D6-substrat	T1/2 (h)	CL (ml/min/kg)	hERG	HHT	AMES	LD50 (>500mg/kg)
Canartinib	-5.16	1	0	1	1	1	93.87	1	-0.12	0	1	1	1	1	0	1	1	1	1	2.12	1.03	1	1	0	1417.72
L1	-5.16	1	0	1	1	1	94.59	1	-0.11	0	1	1	1	1	0	1	1	1	1	2.06	1.01	1	1	0	1276.28
L2	-5.21	1	0	1	1	1	94.72	1	-0.03	0	1	1	1	1	0	1	1	1	1	2.05	0.94	1	1	0	1276.28
L 3	-5.19	1	0	1	1	1	94.74	1	-0.01	0	1	1	1	1	0	1	1	1	1	1.97	0.98	1	1	0	1078.94
L 4	-5.16	1	0	1	1	1	91.18	1	-0.05	0	1	1	1	1	0	1	1	1	1	2.24	1.06	1	1	0	1423.57
L 5	-4.90	1	0	1	1	1	91.75	1	-0.19	1	1	1	1	1	0	1	1	1	1	1.91	1.36	1	1	0	1499.01
L 6	-5.34	1	0	1	1	1	87.55	1	0.21	1	1	1	1	1	0	1	0	0	1	1.77	2.02	1	1	0	950.59
L 7	-5.36	1	0	1	1	1	96.32	1	0.20	1	0	1	1	1	0	1	1	1	1	1.89	1.63	1	1	1	1176.76
L 8	-5.40	1	0	1	1	1	96.75	1	-0.03	1	0	1	1	1	0	1	0	0	1	1.93	1.55	1	1	1	1326.28
L 9	-5.29	1	0	1	1	0	96.34	1	0.14	0	1	1	1	1	0	1	1	1	0	1.97	1.35	1	1	0	1107.54
L 10	-5.18	1	0	1	1	0	94.65	0	0.58	1	1	1	1	1	0	1	0	1	0	2.13	1.35	1	1	0	420.46
L 11	-5.36	1	0	1	1	0	92.51	1	0.49	0	1	1	1	1	0	1	0	1	1	2.09	1.25	1	1	1	712.06
L 12	-5.31	1	0	1	1	0	92.63	1	0.43	0	1	1	1	1	0	1	0	1	1	2.08	1.26	1	1	1	613.05
L 13	-5.33	1	0	1	1	0	93.14	1	0.24	0	1	1	1	1	0	1	0	1	1	2.00	1.32	1	1	1	703.10
L 14	-5.25	1	0	1	1	0	89.00	1	0.75	0	1	1	1	1	0	1	1	1	1	2.07	1.30	1	1	1	505.77
L 15	-5.33	1	0	1	1	0	89.97	0	0.64	0	0	1	1	1	0	1	0	1	0	2.13	1.35	1	1	1	459.61
L 16	-5.17	1	0	1	1	1	93.36	1	-0.04	0	1	1	1	1	0	1	1	1	1	1.98	1.08	1	1	0	1147.17
L 17	-5.22	1	0	1	1	1	96.38	1	0.08	0	1	1	1	1	0	1	1	1	1	1.93	0.96	1	1	0	1339.83
L 18	-5.27	1	0	1	1	0	93.65	1	0.04	0	1	1	1	1	0	1	0	1	0	1.87	1.34	1	1	0	884.43
L 19	-5.32	1	0	1	1	0	93.40	1	0.29	0	1	1	1	1	0	1	0	1	1	1.99	1.28	1	1	1	728.95

L 20	-5.25	1	0	1	1	0	85.01	1	0.47	0	1	1	1	1	0	0	1	1	1	1.99	1.27	1	0	1	663.74
L 21	-5.21	1	0	1	1	0	90.06	1	-0.07	0	1	1	1	1	1	1	1	1	1	1.87	0.94	1	1	1	727.51
L 22	-5.49	1	0	1	0	0	92.93	1	-0.16	0	1	1	1	1	0	0	1	1	0	1.70	1.04	1	1	0	592.82
L 23	-4.94	1	0	1	1	1	92.68	1	-0.15	0	1	1	1	0	1	1	1	1	0	1.93	1.01	1	1	0	1409.21
L 24	-5.26	1	0	1	1	1	94.98	1	0.19	0	1	1	1	0	1	1	1	1	1	2.01	0.67	1	1	0	1449.94
L 25	-5.16	1	0	1	1	1	92.51	1	0.01	0	1	1	1	0	1	1	1	1	1	1.90	0.79	1	1	0	1473.29
L 26	-5.23	1	0	1	1	1	92.63	1	0.13	0	1	1	1	0	1	0	1	1	1	1.93	0.72	1	1	0	1364.25
L 27	-5.29	1	0	1	1	0	95.79	1	-0.49	0	1	1	1	1	1	1	1	1	1	1.67	0.80	1	1	0	1291.16

III.   References

1.   Dennington R, Keith TA, Millam JM. GaussView, version 6.0. 16. Semichem Inc. Shawnee Mission KS. 2016.

2.   Zhu W, Wu P. Surface energetics of hydroxyapatite: A DFT study. Chem Phys Lett. 2004;396(1–3):38–42.

3.   Aihara JI. Reduced HOMO-LUMO Gap as an Index of Kinetic Stability for Polycyclic Aromatic Hydrocarbons. J Phys Chem A. 1999;103(37):7487–95.

4.   Azarhazin E, Izadyar M, Housaindokht MR. Drug-DNA interaction, a joint DFT-D3/MD study on safranal as an anticancer and DNA nanostructure model. Can J Chem. 2019;97(2):120–30.

5.   Jaramillo P, Domingo LR, Chamorro E, Pérez P. A further exploration of a nucleophilicity index based on the gas-phase ionization potentials. J Mol Struct THEOCHEM. 2008;865(1–3):68–72.

6.   Srivastava R. Chemical reactivity theory (CRT) study of small drug-like biologically active molecules. J Biomol Struct Dyn. 2020;1–10.

7.   Domingo LR, Ríos-Gutiérrez M, Pérez P. Applications of the conceptual density functional theory indices to organic chemistry reactivity. Molecules. 2016;21(6).

8.   Towler P, Staker B, Prasad SG, Menon S, Tang J, Parsons T, et al. ACE2 X-Ray Structures Reveal a Large Hinge-bending Motion Important for Inhibitor Binding and Catalysis. J Biol Chem. 2004;279(17):17996–8007.

9.   Lan J, Ge J, Yu J, Shan S, Zhou H, Fan S, et al. Structure of the SARS-CoV-2 spike receptor-binding domain bound to the ACE2 receptor. Nature. 2020;581(7807):215–20.

10.   DS W, YD F, AC G, EJ L, A M, JR G, et al. DrugBank [Internet]. 2020. Available from: https://www.drugbank.ca/.

11.   Vincent MJ, Bergeron E, Benjannet S, Erickson BR, Rollin PE, Ksiazek TG, et al. Chloroquine is a potent inhibitor of SARS coronavirus infection and spread. Virol J. 2005;2(1):1–10.

12.   Devaux CA, Rolain JM, Colson P, Raoult D. New insights on the antiviral effects of chloroquine against coronavirus: what to expect for COVID-19? Int J Antimicrob Agents [Internet]. 2020;55(5):105938. Available from: https://doi.org/10.1016/j.ijantimicag.2020.105938

13.   Ramalho TC, Caetano MS, da Cunha EFF, Souza TCS, Rocha MVJ. Construction and assessment of reaction models of class i epsp synthase: Molecular docking and density functional theoretical calculations. J Biomol Struct Dyn. 2009;27(2):195–207.

14.   Kellenberger E, Rodrigo J, Muller P, Rognan D. Comparative evaluation of eight docking tools for docking and virtual screening accuracy. Proteins Struct Funct Genet. 2004;57(2):225–42.

15.   Althagafi I, El-Metwaly N, Farghaly TA. New series of thiazole derivatives: Synthesis, structural elucidation, antimicrobial activity, molecular modeling and MOE docking. Molecules. 2019;24(9).

16.   te Velthuis AJW, van den Worml SHE, Sims AC, Baric RS, Snijder EJ, van Hemert MJ. Zn2+ inhibits coronavirus and arterivirus RNA polymerase activity in vitro and zinc ionophores block the replication of these viruses in cell culture. PLoS Pathog. 2010;6(11):e1001176.

17.   Kerrigan JE. Molecular dynamics simulations in drug design. Methods Mol Biol. 2013;993:95–113.

18. De Vivo M, Masetti M, Bottegoni G, Cavalli A. Role of Molecular Dynamics and Related Methods in Drug Discovery. J Med Chem. 2016;59(9):4035–61.

19. Mannhold R, Kubinyi H, Folkers G. Protein crystallography in drug discovery [Internet]. Vol. 20, Wiley Interdisciplinary Reviews: Computational Molecular Science. Wiley-VCH; 2004. 875–900 p. Available from: http://www.eurekaselect.com/openurl/content.php?genre=article&issn=1389-4501&volume=9&issue=12&spage=1048

20. Yun CH, Boggon TJ, Li Y, Woo MS, Greulich H, Meyerson M, et al. Structures of Lung Cancer-Derived EGFR Mutants and Inhibitor Complexes: Mechanism of Activation and Insights into Differential Inhibitor Sensitivity. Cancer Cell. 2007;11(3):217–27.

21. Giubellino A, Linehan WM, Bottaro DP. Targeting the Met signaling pathway in renal cancer. Expert Rev Anticancer Ther. 2009;9(6):785–93.

22. Wood ER, Truesdale AT, McDonald OB, Yuan D, Hassell A, Dickerson SH, et al. A unique structure for epidermal growth factor receptor bound to GW572016 (Lapatinib): Relationships among protein conformation, inhibitor off-rate, and receptor activity in tumor cells. Cancer Res. 2004;64(18):6652–9.

23. Cheng H, Nair SK, Murray BW, Almaden C, Bailey S, Baxi S, et al. Discovery of 1-{(3R,4R)-3-[({5-Chloro-2-[(1-methyl-1H-pyrazol-4-yl)amino]-7H-pyrrolo[2,3-d]pyrimidin-4-yl}oxy)methyl]-4-methoxypyrrolidin-1-yl}prop-2-en-1-one (PF-06459988), a Potent, WT Sparing, Irreversible Inhibitor of T790M-Containing EGFR Mutants. J Med Chem. 2016;59(5):2005–24.

24. Smaill JB, Gonzales AJ, Spicer JA, Lee H, Reed JE, Sexton K, et al. Tyrosine Kinase Inhibitors . 20 . Optimization of substituted quinazoline and pyrido [3 , 4-d] pyrimidine derivatives as orally active , irreversible inhibitors of the epidermal growth factor receptor family . J Med Chem. 2016;

Conclusion

Conclusion

In the field of drug discovery and development, the computational method has proven to be a beneficial and successful approach. According to this, the aim of the thesis is to apply a computational approach to develop therapeutic agents.

In this thesis we studied two disease, severe acute respiratory syndrome coronavirus-2 and epidermal growth factor receptor tyrosine kinase mutation.

In the first study, we have examined the binding of eighteen candidate drugs with ACE2 enzyme and severe acute respiratory syndrome coronavirus-2 receptor correlated with ACE2 complex using docking analysis. The docking ranking results in this study showed that some of these ligands might have the ability to inhibit SARS-CoV-2. The results of docking these ligands with ACE2 enzyme (1R42) in two pockets indicated that Delapril have the lowest energy score and good RMSD value followed by Lisinopril (site1) and Ramipril (site 2). In addition, the docking results with 6M0J showed that only Delapril and Ramiprilat interacted with Zn in site 1, while in site 2 Delapril gave the best energy score followed by Ramipril. The drugs mentioned above presented good results with the two chosen enzymes compared with Chloroquine and Hydroxychloroquine.

Moreover, the results obtained from global reactivity indexes indicated that Ramipril is the most reactive drug, it had the highest electrophilicity value followed by ORE-1001, Chloroquine and Lisinopril. The most obvious finding to emerge from this study is that Ramipril, Delapril and Lisinopril gave good docking results compared with Chloroquine and Hydroxychloroquine. Also, Delapril, Lisinopril and Ramipril showed encouraging binding affinity, MM/GBSA energies, to [SARS-CoV-2/ACE2] complex. Further investigation and experimentation into Delapril, Lisinopril and Ramipril, which they are promising candidate drugs for COVID-19 patients, is strongly recommended.
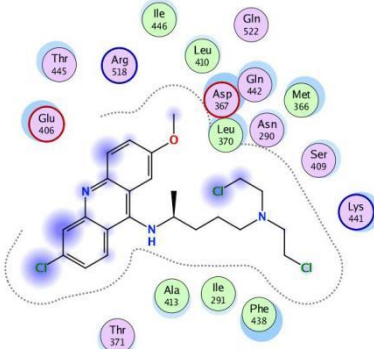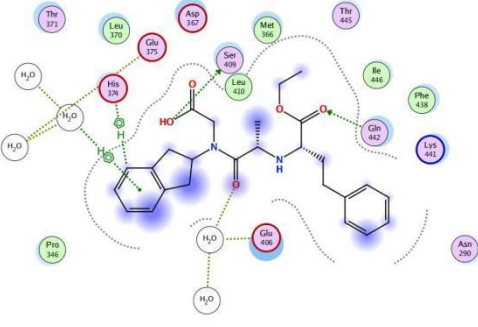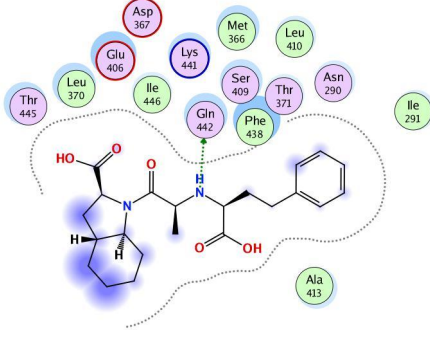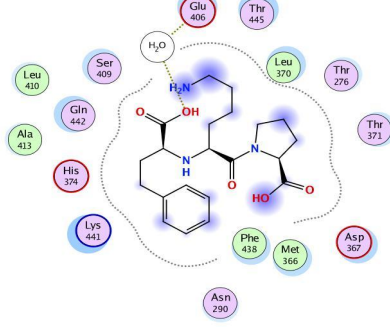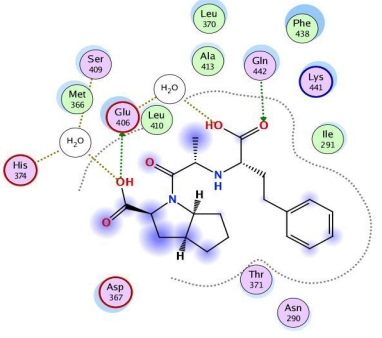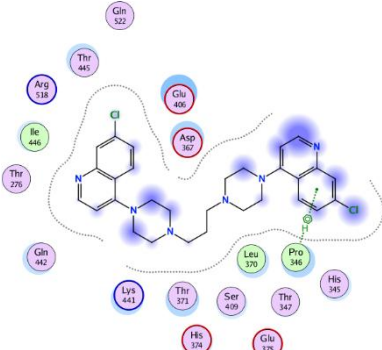
In the second study, twenty seven of quinazoline and pyrido[3,4-d]pyrimidine derivatives were evaluated for their inhibitory activities towered three different EGFR mutations Wild-Type, L858R and T790M. The docking result of these compounds with 1XKK, 2ITV and 5HG5 indicated that most studied compounds interacted with WT. While the compounds L19, L21, L23, L24 and L26 interacted with L858R mutation. With respect to T790M mutation, only compounds L1, L8 and L24 interacted with this mutation. These
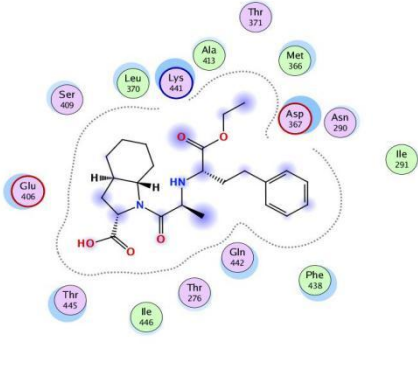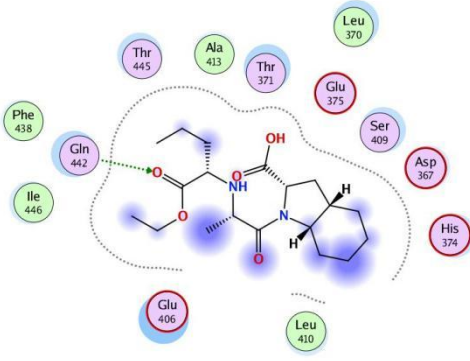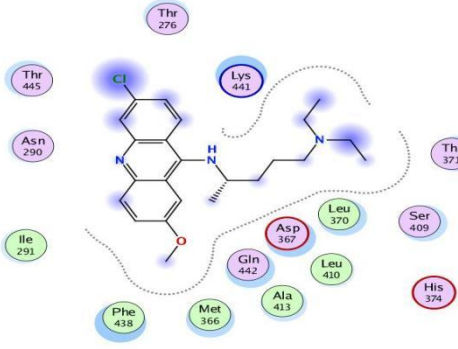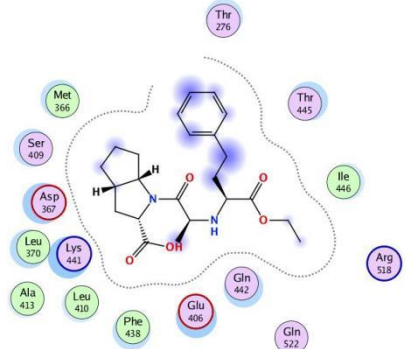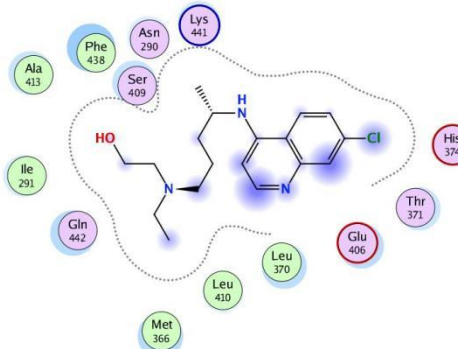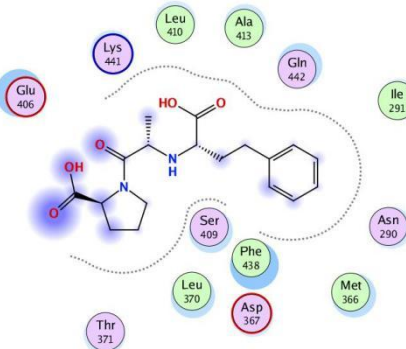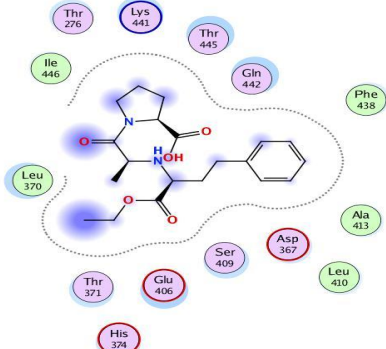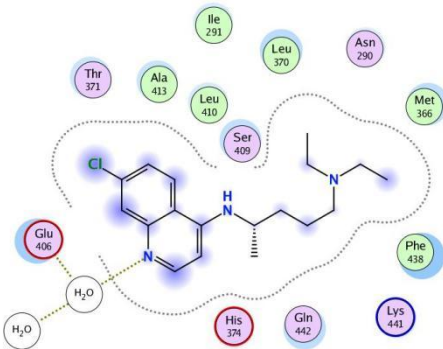
interactions were further confirmed by MD simulation. The study considered L24 as a good inhibitor for WT, L858R and T790M mutations. The ligands L23, L24, L25, L26 and L27 have good values of global reactivity descriptors. All compounds under investigation have passed ADME property and have no toxicity.

In summary, all the results indicated that a combined computational approach, including global reactivity descriptors, molecular docking and molecular dynamic simulation could provide an alternative way to features of binding mechanism for quinazoline and pyrido[3,4-d]pyrimidine derivatives as good inhibitors of EGFR mutation.

APPENDIX

Table 1 score of docking and RMSD values of Drugs and their interaction in site 1 with 1R42

Quinacrine mustard	S= -7.0419 kcal/mol	Delapril	S= -6.9809 kcal/mol
	RMSD = 1.1582 Å		RMSD = 2.2570 Å
Trandoprilat	S= -6.7507 kcal/mol	Lisinopril	S= -6.6886 kcal/mol
	RMSD = 1.4433Å		RMSD = 1.5417Å
Ramiprilat	S= -6.6703 kcal/mol	Piperaquine	S= -6.6531 kcal/mol
	RMSD = 4.3112 Å		RMSD = 3.2826 Å
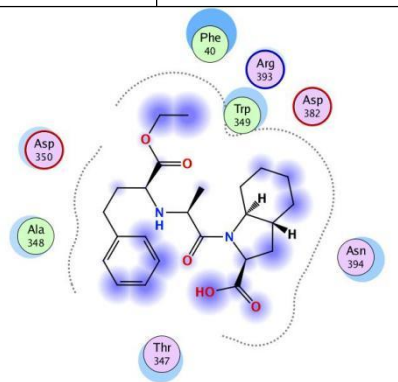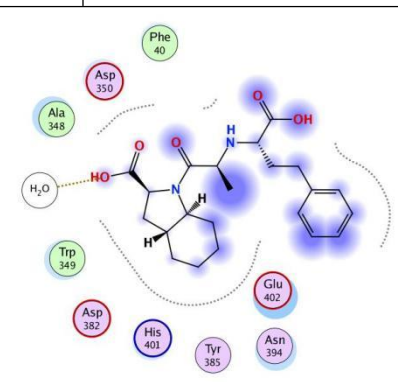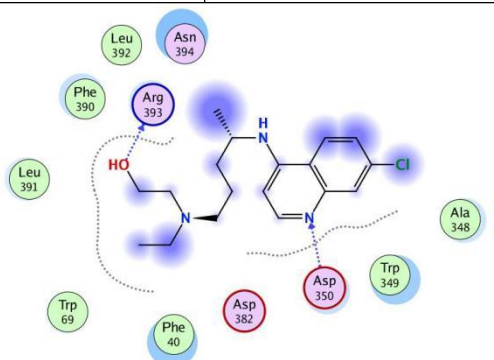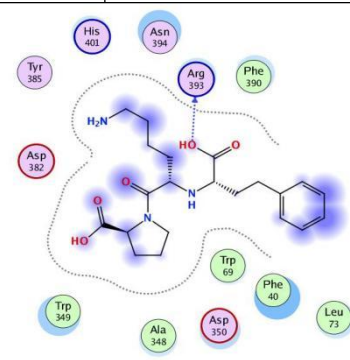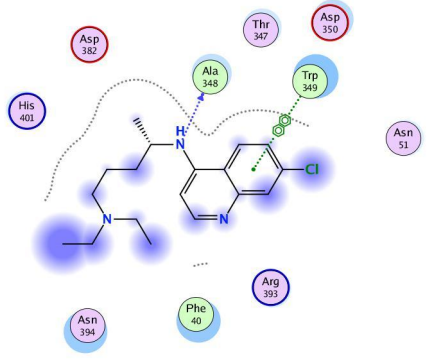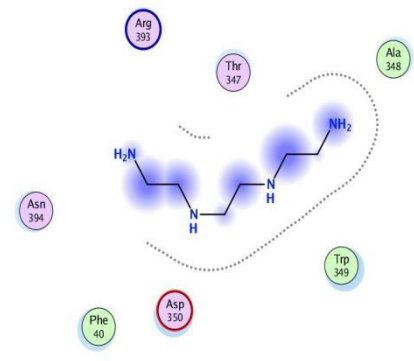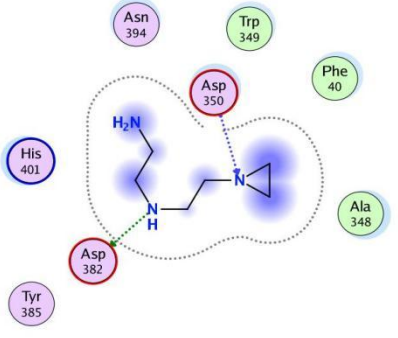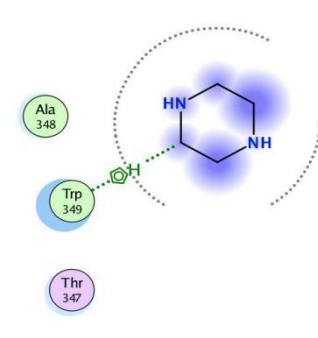
Trandolapril	S= -6.6486 kcal/mol	Perindopril	S= -6.5856 kcal/mol
	RMSD = 1.4374 Å		RMSD = 1.1260 Å
Quinacrine	S= -6.5293 kcal/mol	Ramipril	S= -6.4267 kcal/mol
	RMSD = 2.0118 Å		RMSD = 3.3943 Å
Hydroxy-chloroquine	S= -6.3423 kcal/mol	Enalaprilat	S= -6.2633 kcal/mol
	RMSD = 1.0450 Å		RMSD = 2.5392 Å
Enalapril	S= -6.2340 kcal/mol	Chloroquine	S= -6.1074 kcal/mol

	RMSD = 1.5934 Å		RMSD = 1.1063 Å
ORE-1001	S= -6.0954 kcal/mol	Triethylene-tetramine	S= -4.5443 kcal/mol
	RMSD = 3.0354 Å		RMSD = 1.5013 Å
N-(2-aminoethyl)-1-aziridineethamine	S= -4.2518 kcal/mol	Piperazine	S= -3.6988 kcal/mol
	RMSD = 1.8889 Å		RMSD = 0.8732Å

Table 2 score of docking and RMSD values of Drugs and their interaction in site 2 with 1R42
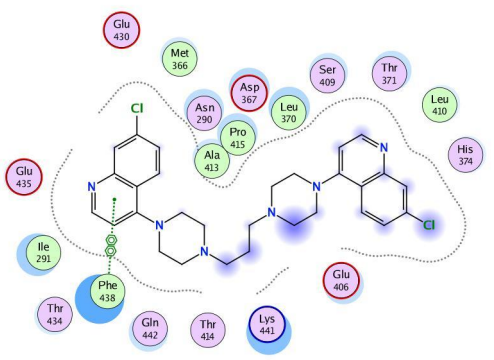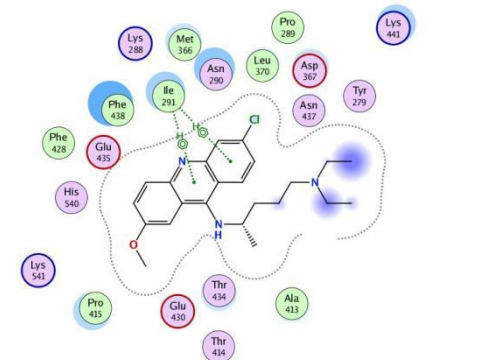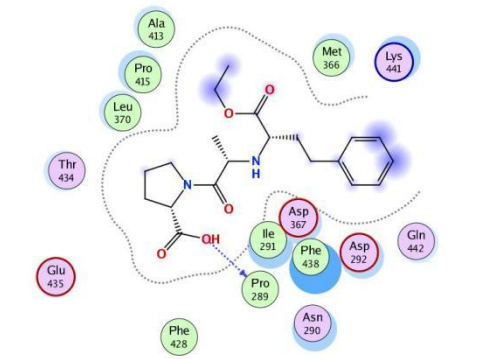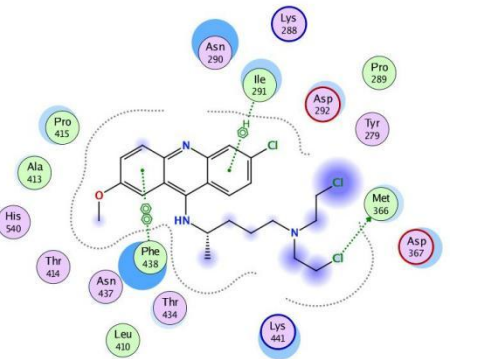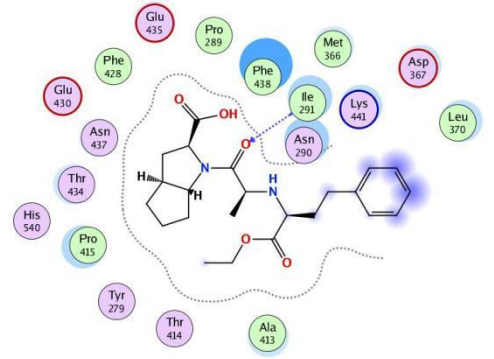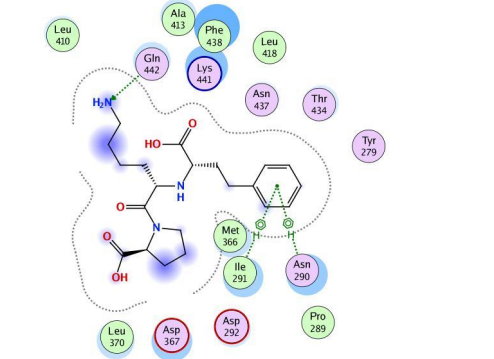
Piperaquine	S= -6.5176 kcal/mol	Delapril	S= -6.5831 kcal/mol
	RMSD = 2.4998 Å		RMSD = 2.0115Å
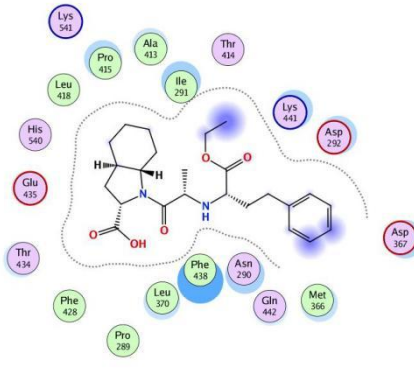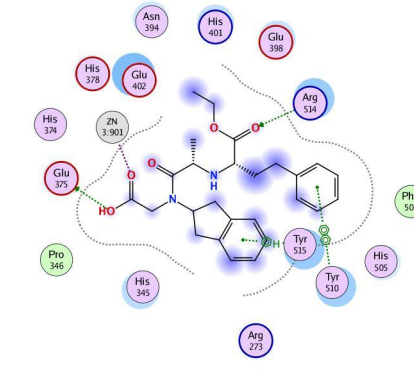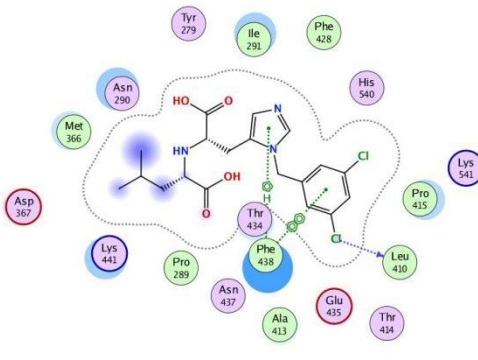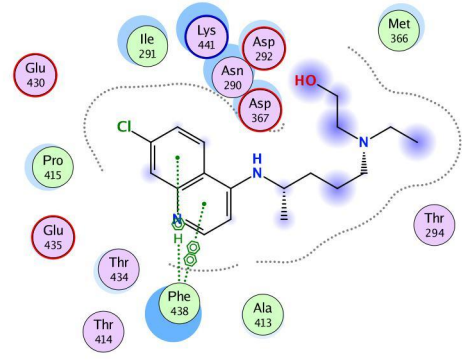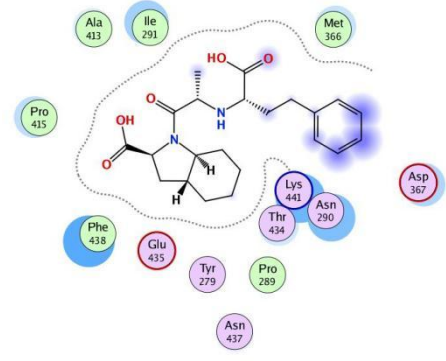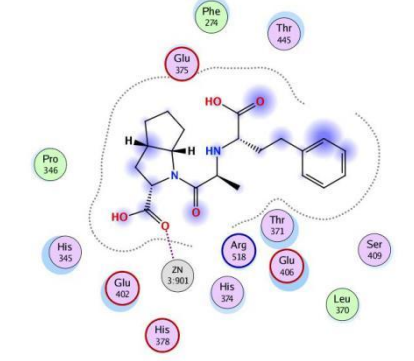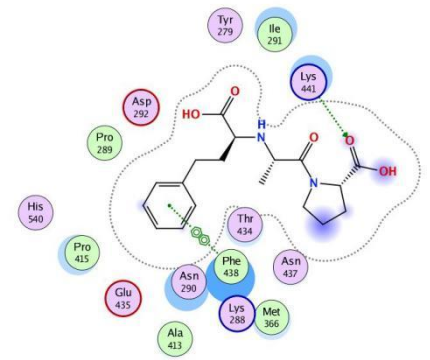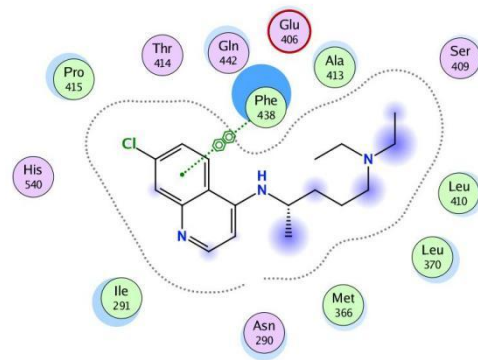
Perindopril	S= -6.2821kcal/mol	Enalapril	S= -6.1282 kcal/mol
	RMSD = 1.4433 Å		RMSD = 2.6836 Å
Ramipril	S= -6.1181 kcal/mol	Enalaprilat	S= -5.9910kcal/mol
	RMSD = 1.5054 Å		RMSD = 1.2547Å
Quinacrine mustard	S= -5.9526 kcal/mol	Quinacrine	S= -5.9184 kcal/mol
	RMSD = 1.8415Å		RMSD = 1.1669 Å
Ramiprilat	S= -5.8613 kcal/mol	ORE-1001	S= -5.7682 kcal/mol

	RMSD = 1.8268 Å		RMSD = 0.9417 Å
Trandolapril	S= -5.7637 kcal/mol	Trandolaprilat	S= -5.7171kcal/mol
	RMSD = 1.6382 Å		RMSD = 2.8424Å
Hydroxy-chloroquine	S= -5.6369 kcal/mol	Lisinopril	S= -5.6358 kcal/mol
	RMSD = 1.8041Å		RMSD = 1.7176Å
Chloroquine	S= -5.5271 kcal/mol	Triethylene-tetramine	S= -4.1376 kcal/mol
	RMSD = 1.3462 Å		RMSD = 2.5349 Å
N-(2-aminoethyl)	S= -4.2127 kcal/mol	Piperazine	S= -3.4925 kcal/mol

-1-aziridineethamine	RMSD = 0.8803 Å		RMSD = 2.5032 Å

Table 3 score of docking and RMSD values of Drugs and their interaction in site 1 with 6M0J
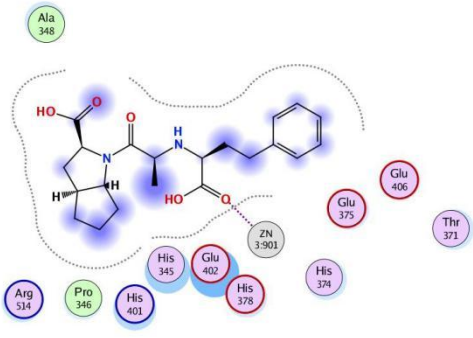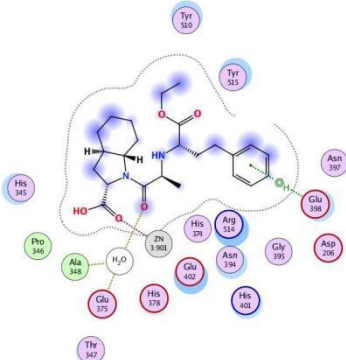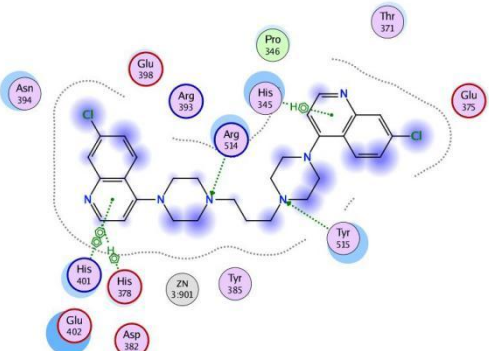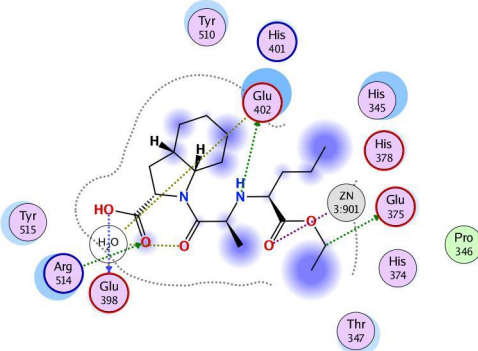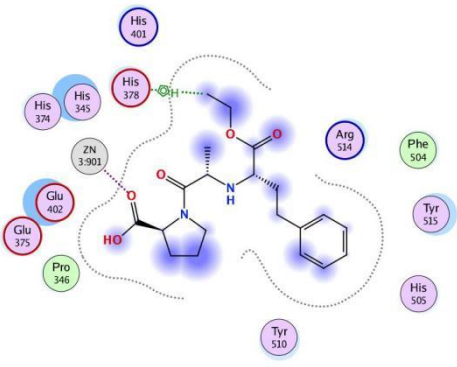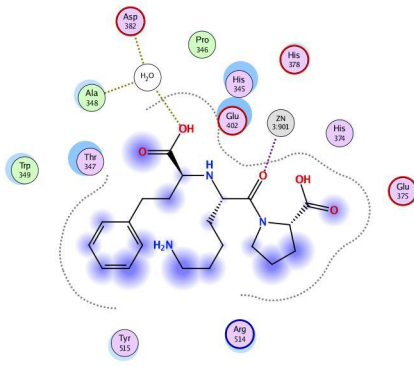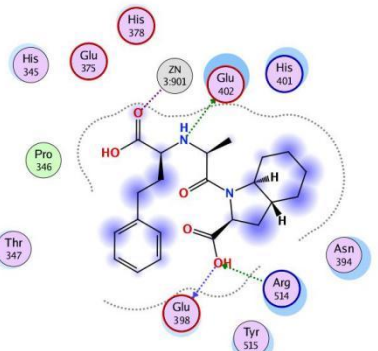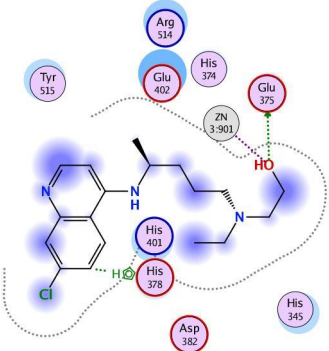
Piperaquine	S= -8.6132 kcal/mol	Quinacrine	S= -8.2350 kcal/mol
	RMSD = 2.3325 Å		RMSD = 1.6346 Å
Enalapril	S= -7.8671 kcal/mol	Quinacrine mustard	S= -7.8570 kcal/mol
	RMSD = 1.9897 Å		RMSD = 1.4398 Å
Ramipril	S= -7.7464 kcal/mol	Lisinopril	S= -7.5918 kcal/mol
	RMSD = 1.6166 Å		RMSD = 1.3368 Å
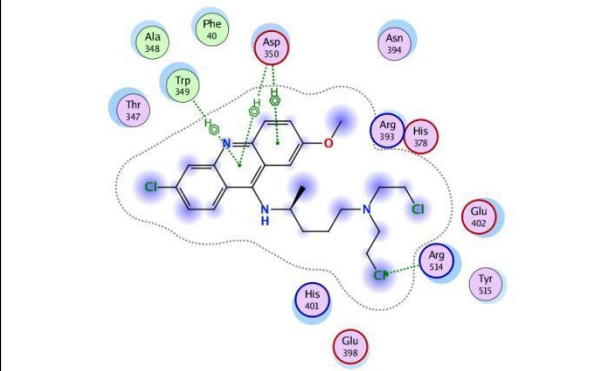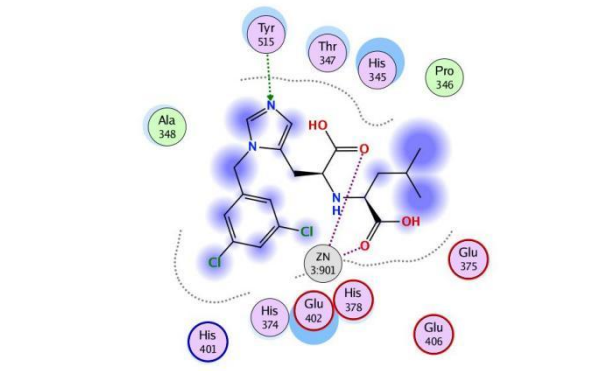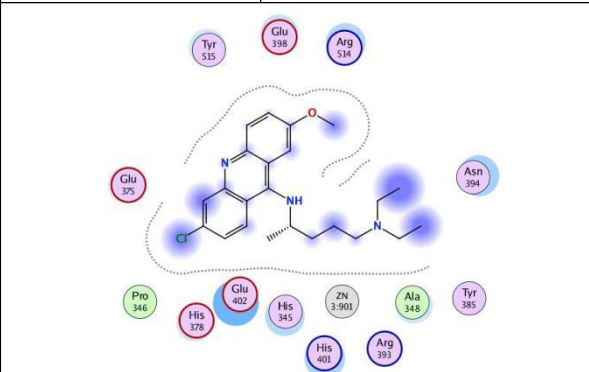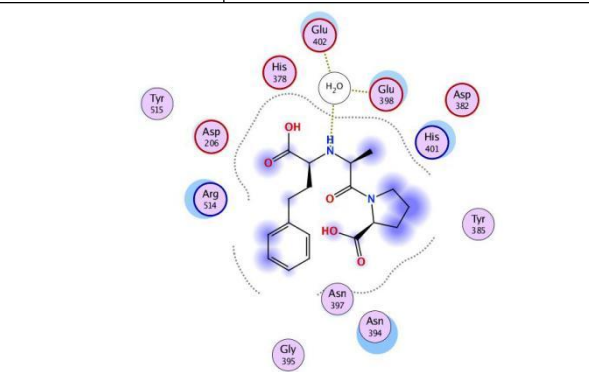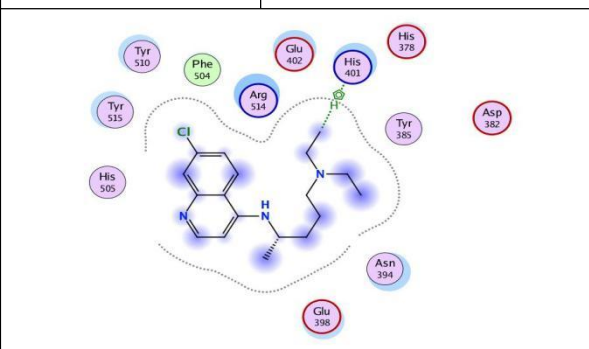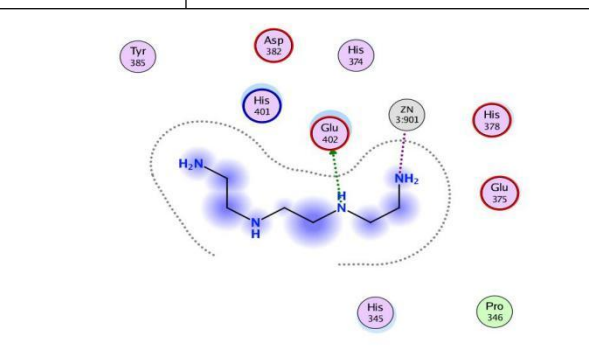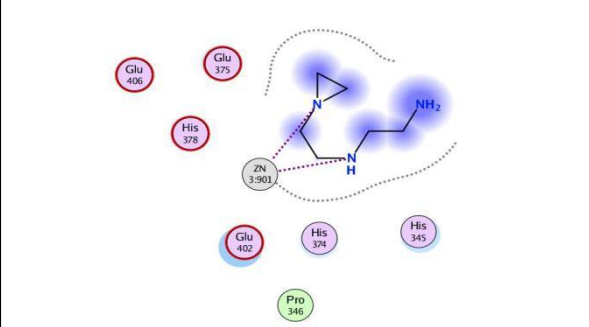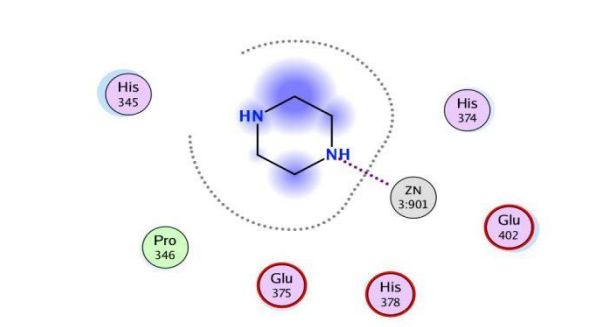
Trandolapril	S= 7.5529 kcal/mol	Delapril	S= -7.5271 kcal/mol
	RMSD = 1.3852 Å		RMSD = 2.1735 Å
ORE-1001	S= -7.3872 kcal/mol	Hydroxy-chloroquine	S= -7.2272 kcal/mol
	RMSD = 1.5557 Å		RMSD = 2.1035 Å
Trandoprilat	S= -7.1674 kcal/mol	Ramiprilat	S= -6.9943 kcal/mol
	RMSD = 2.5128 Å		RMSD = 2.4607 Å
Enalaprilat	S= -6.9279 kcal/mol	Chloroquine	S= -6.8442 kcal/mol

	RMSD = 1.8459 Å		RMSD = 1.9853 Å
Perindopril	S= -6.4327 kcal/mol	Triethylene-tetramine	S= --5.3677 kcal/mol
	RMSD = 2.4655 Å		RMSD = 2.9138 Å
N-(2-aminoethyl)-1-aziridineethamine	S= -5.1378 kcal/mol	Piperazine	S= -4.1089 kcal/mol
	RMSD = 2.8505 Å		RMSD = 0.6037 Å

Table 4 score of docking and RMSD values of Drugs and their interaction in site 2 with 6M0J

Delapril	S= -8.1604 kcal/mol	Ramipril	S= -7.6305 kcal/mol
	RMSD = 1.5603 Å		RMSD = 2.4853 Å

168

Ramiprilat	S= -7.1864 kcal/mol	Trandolapril	S= -7.1160 kcal/mol
	RMSD = 1.7252 Å		RMSD = 1.9818 Å
Piperaquine	S= -6.9190 kcal/mol	Perindopril	S= -6.7968 kcal/mol
	RMSD = 1.3824 Å		RMSD = 2.2965 Å
Enalapril	S= -6.7570 kcal/mol	Lisinopril	S= -6.6966 kcal/mol
	RMSD = 2.6763 Å		RMSD = 1.9981 Å
Trandoprilat	S= -6.3980 kcal/mol	Hydroxy-	S= -6.3125 kcal/mol

	RMSD = 1.3776 Å	chloroquine	RMSD = 1.8513 Å

Quinacrine mustard	S= -6.2815 kcal/mol	ORE-1001	S= -6.2755 kcal/mol
	RMSD = 1.2213 Å		RMSD = 2.5319 Å

Quinacrine	S= -6.0647 kcal/mol	Enalaprilat	S= -6.0045 kcal/mol
	RMSD = 3.9864 Å		RMSD = 1.1323 Å

Chloroquine	S= -5.4920 kcal/mol	Triethylene-tetramine	S= -4.2183 kcal/mol
	RMSD = 2.3627 Å		RMSD = 1.92260 Å

N-(2-aminoethyl)-1-aziridineethamine	S= -4.5602 kcal/mol	Piperazine	S= --3.4842 kcal/mol
	RMSD = 0.9986 Å		RMSD = 1.2687 Å
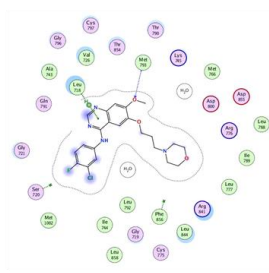
gefitinib
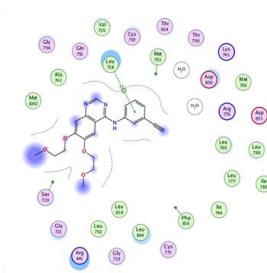
erlotinib
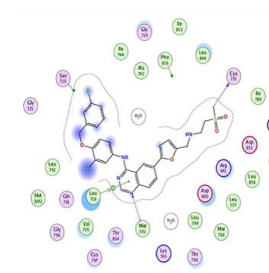
lapatinib
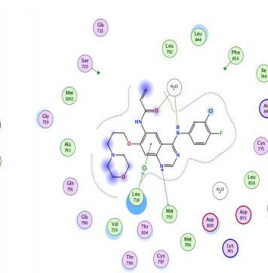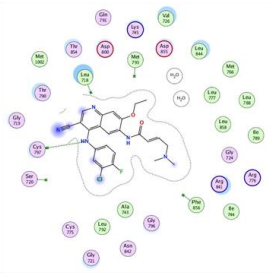
canartinib
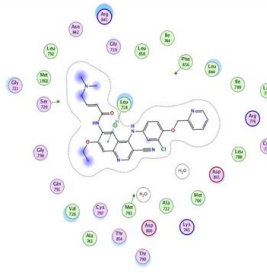
pelitinib
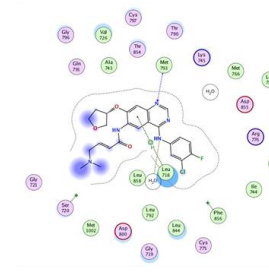
neratinib

afatinib

L1

L2

L3

L4
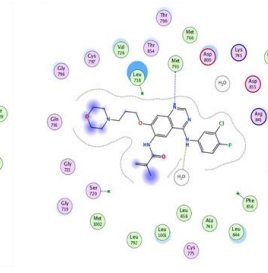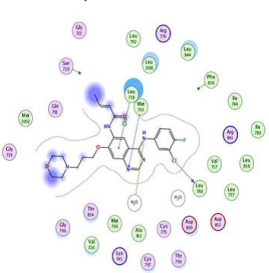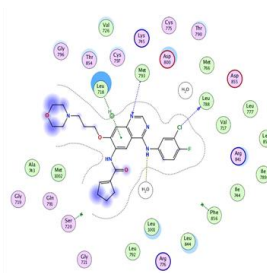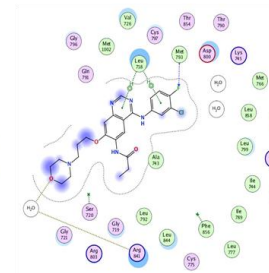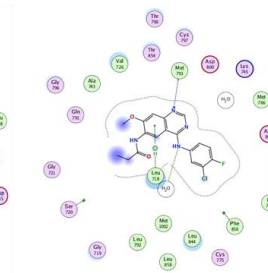
L5

L6

L7
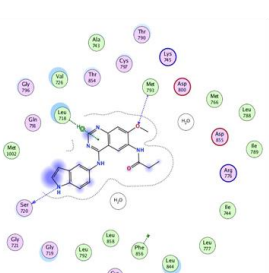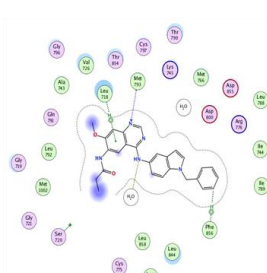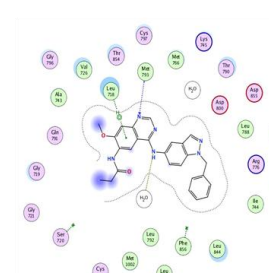
L8
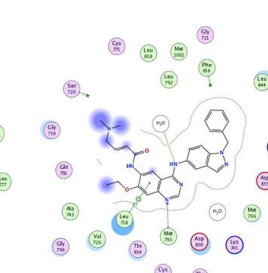
L9
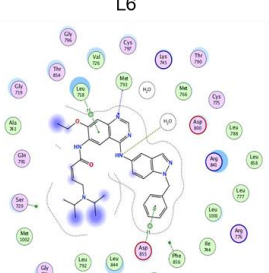
L10
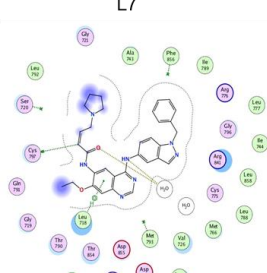
L11
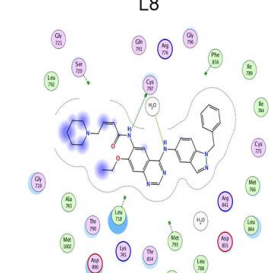
L12
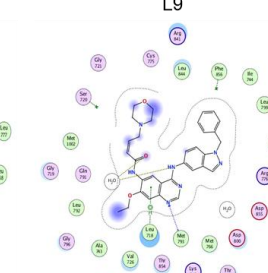
L13
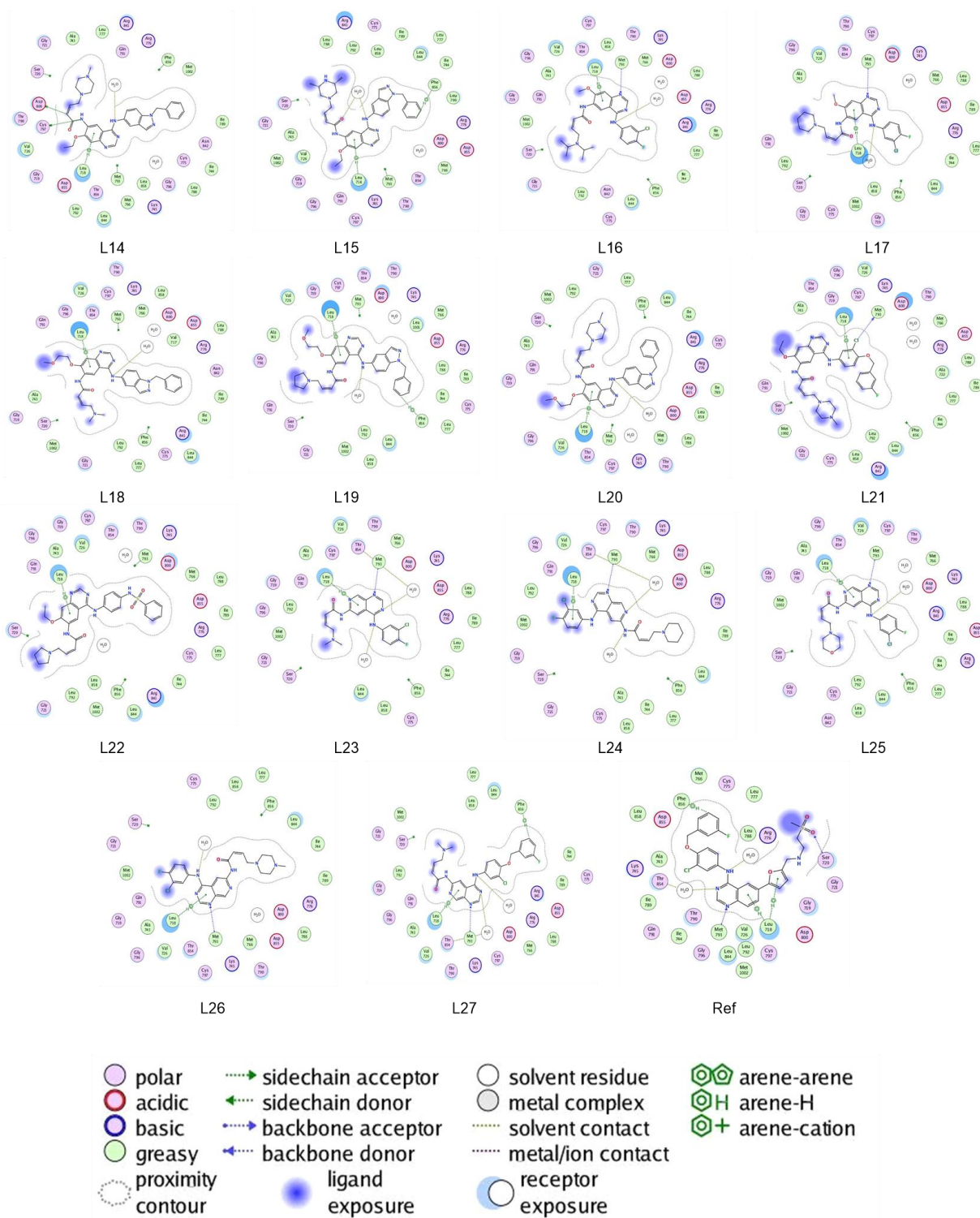
Figure 1 Compounds binding with wild-type PDB ID 1XKK.
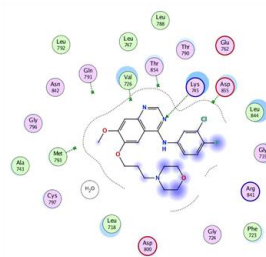
gefitinib
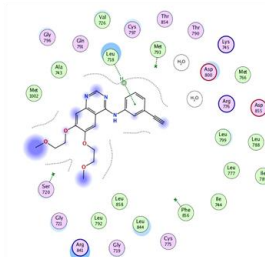
erlotinib
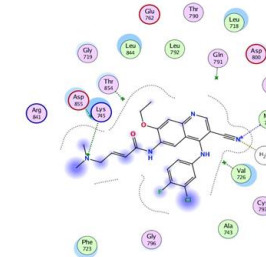
pelitinib
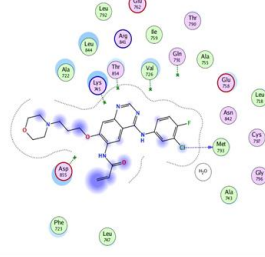
canartinib
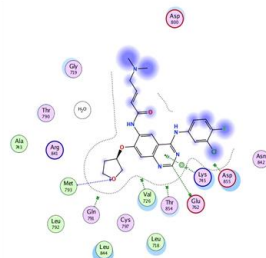
afatinib
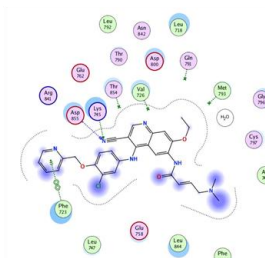
neratinib
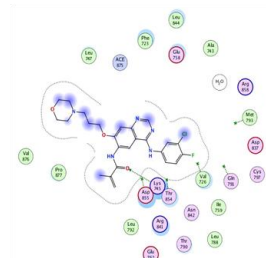
L1
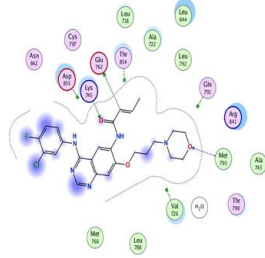
L2
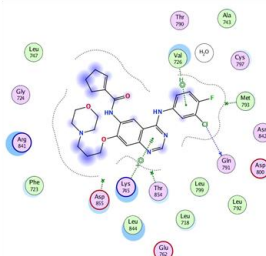
L3
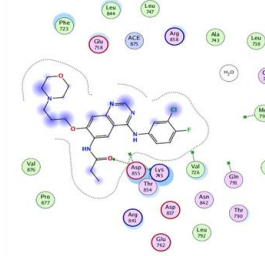
L4

L6

L7
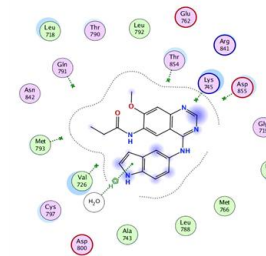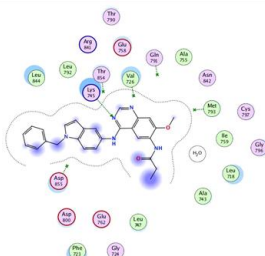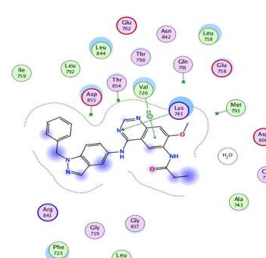
L8
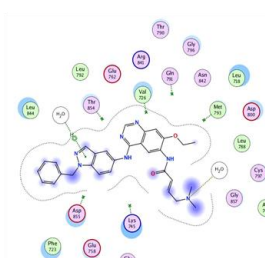
L9
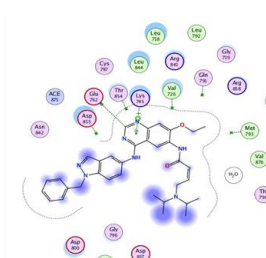
L10
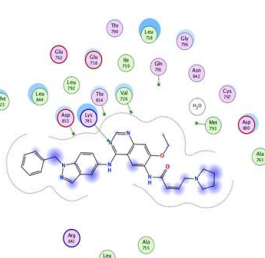
L11
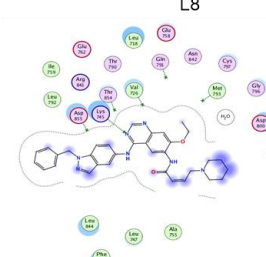
L12
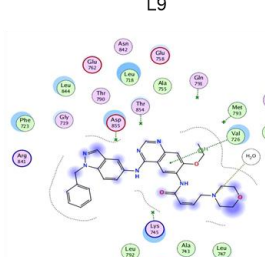
L13
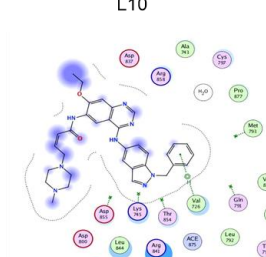
L14
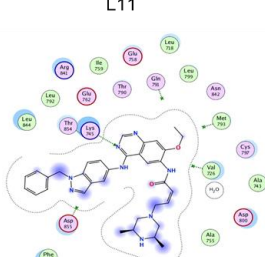
L15
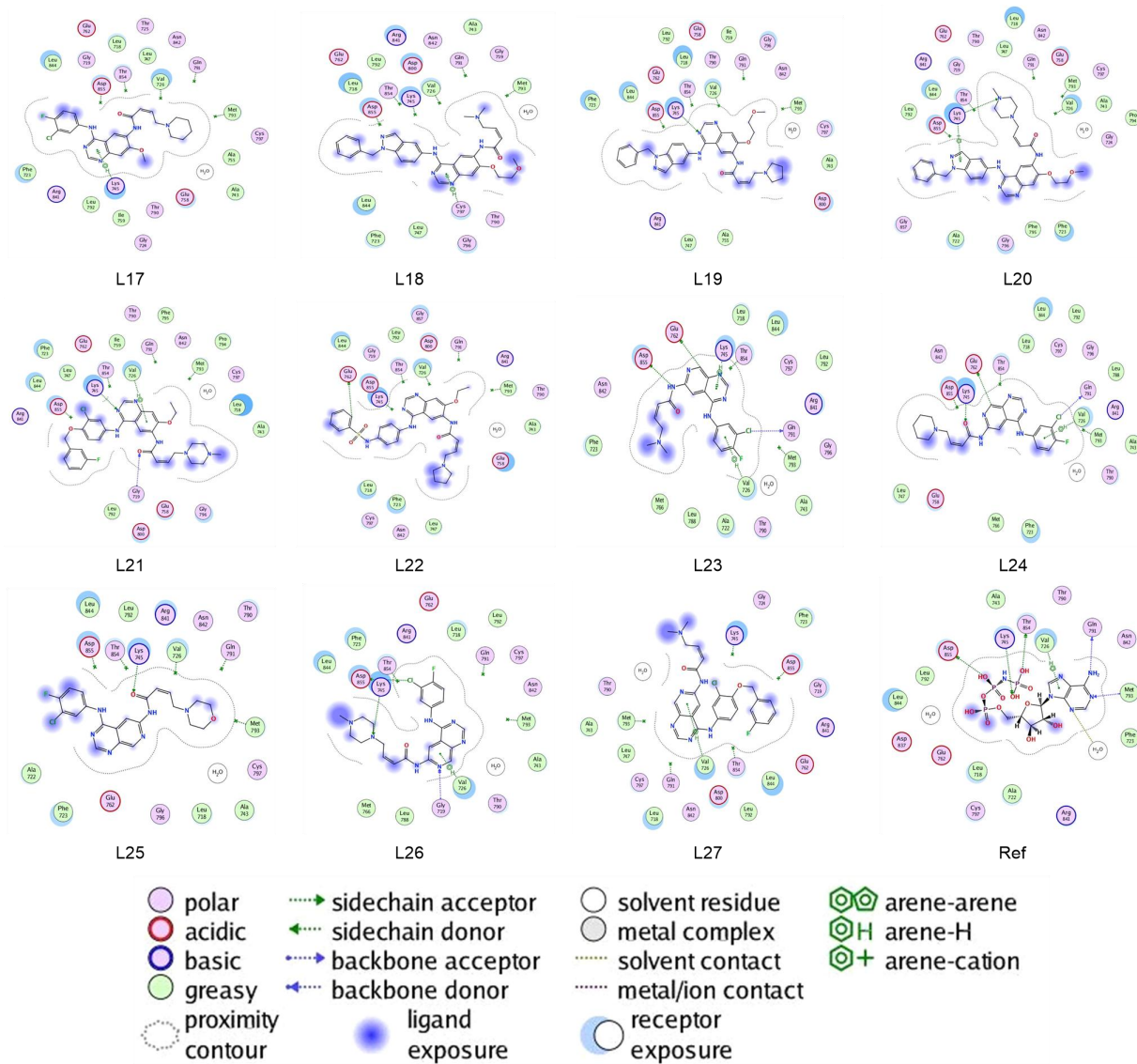
Figure 2 Compounds binding with L858R PDB ID: 2ITV.
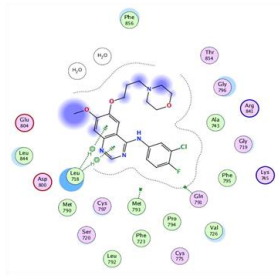
gefitinib
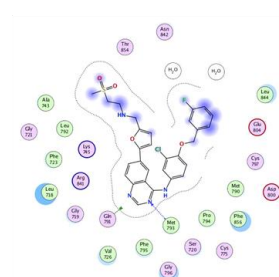
lapatinib
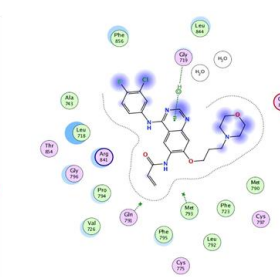
canartinib

L1

L2

L3

L4
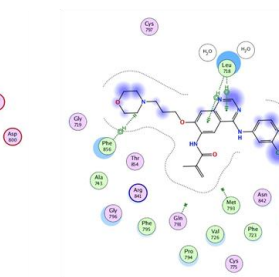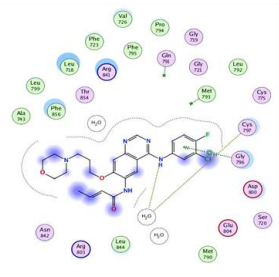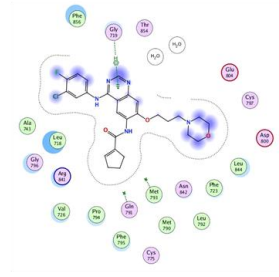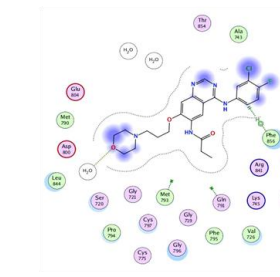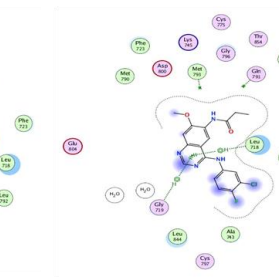
L5
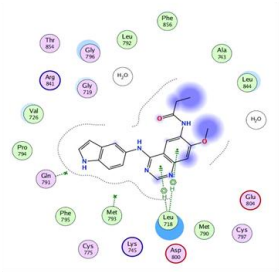
L6
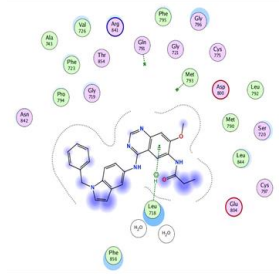
L7
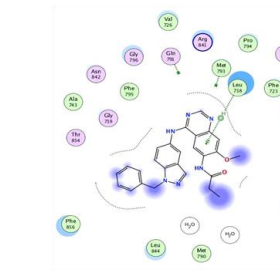
L8
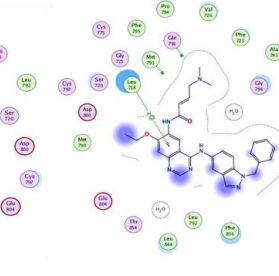
L9

L10

L16

L18

L22

L23

L24

L25

L26
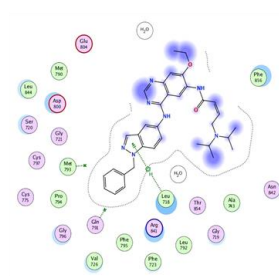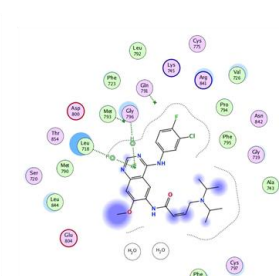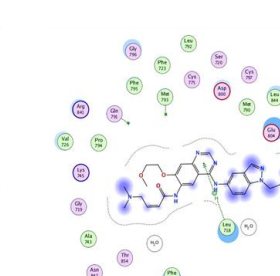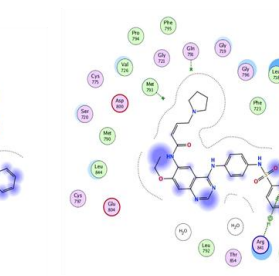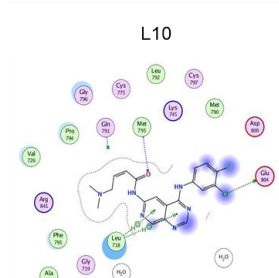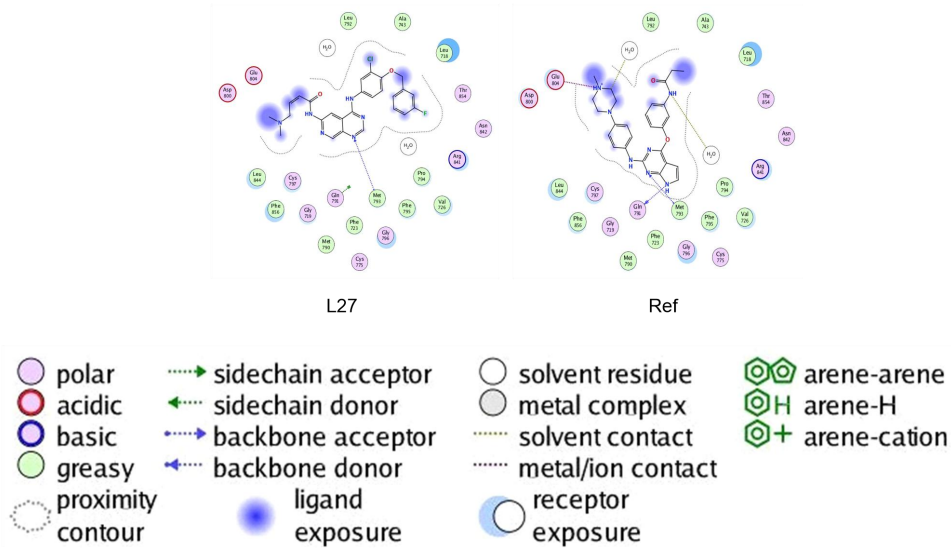
Figure 3 Compounds binding with T790M PDB ID: 5HG5.

L7

L9

L11

L12

L14

L18

L20

L22

L24

L25

L27

Figure 4 The evaluation of potential energy and binding interaction of complex of 7, 9, 11, 12, 14, 18, 20, 22, 24, 25 and 27 with 1XKK wild-type receptor as function of time.
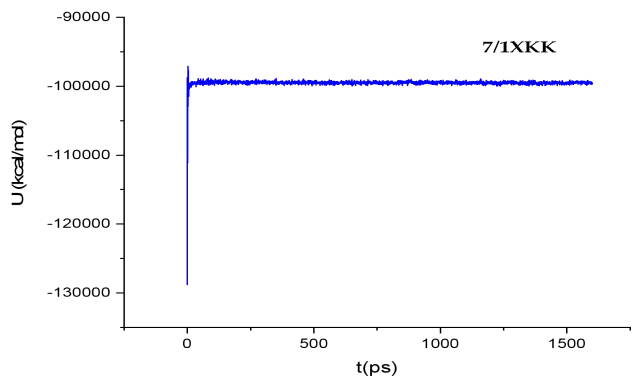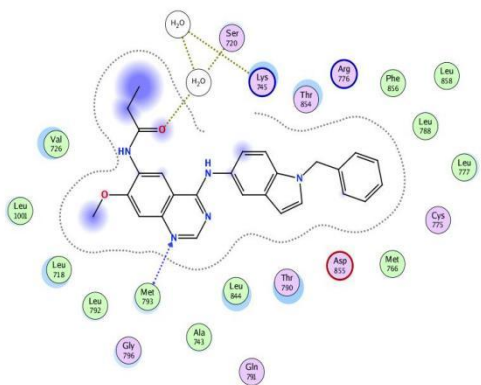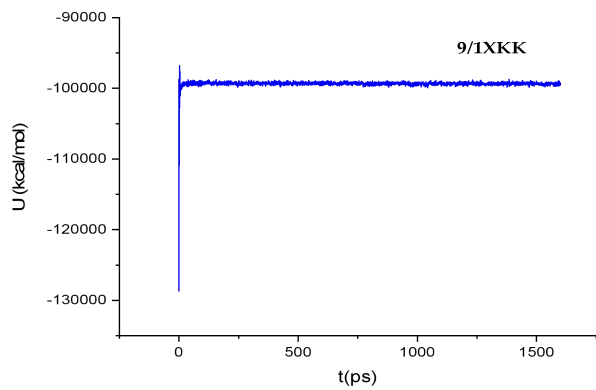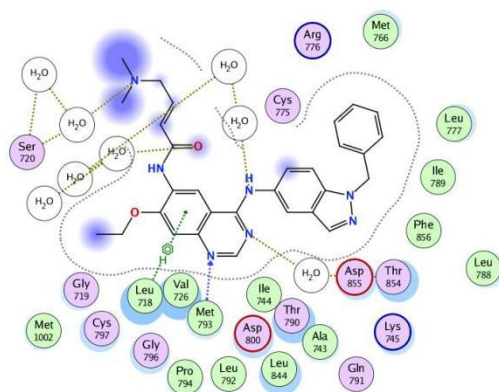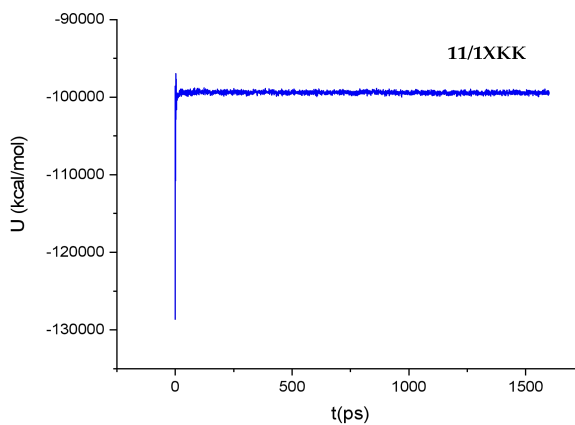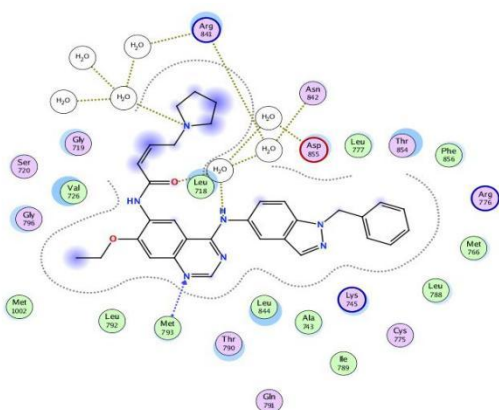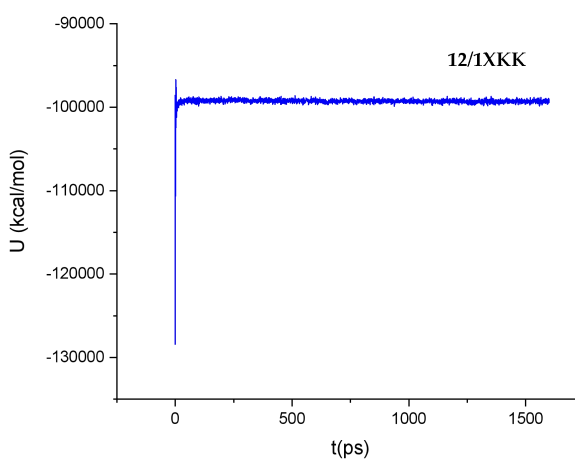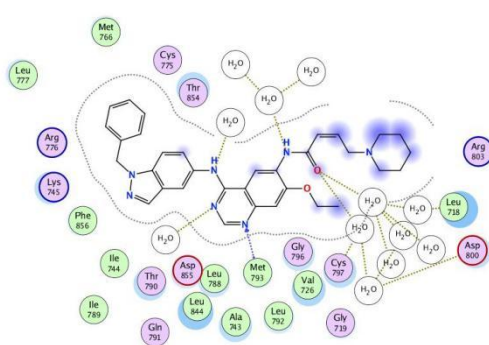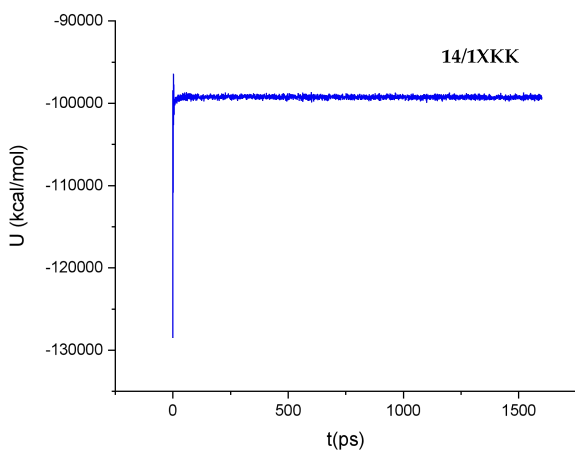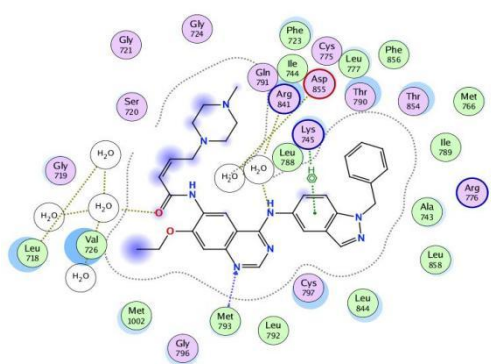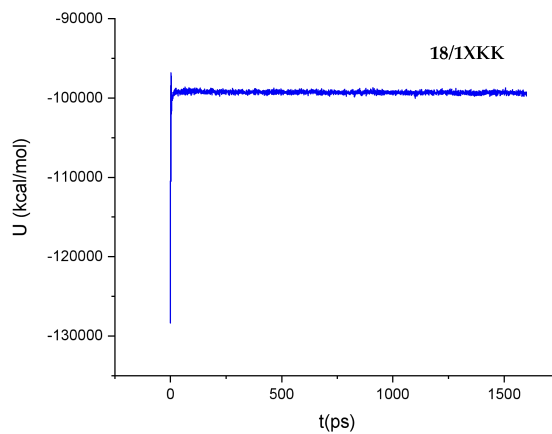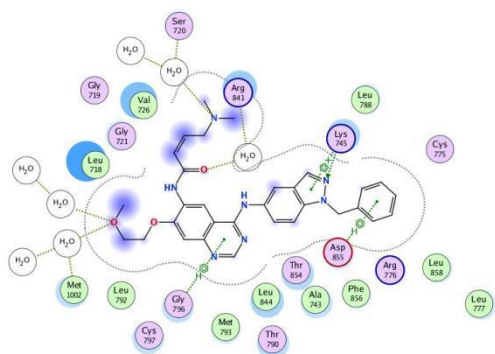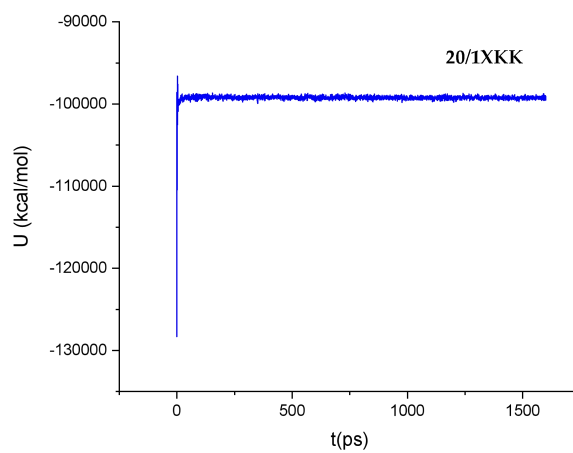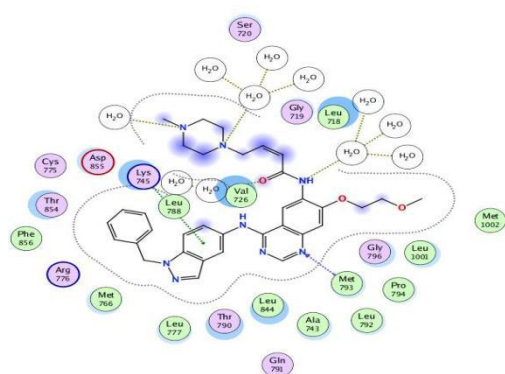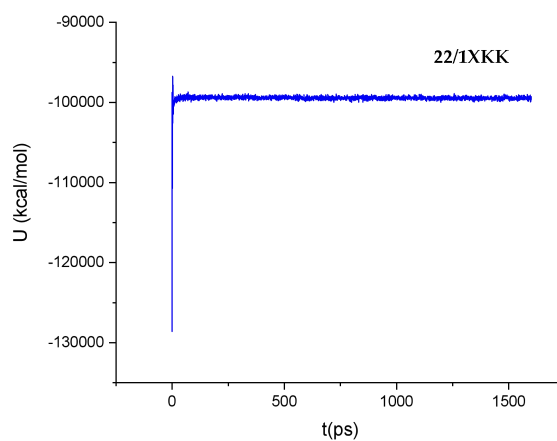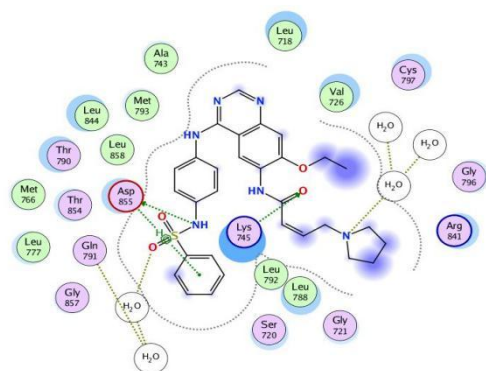
L19
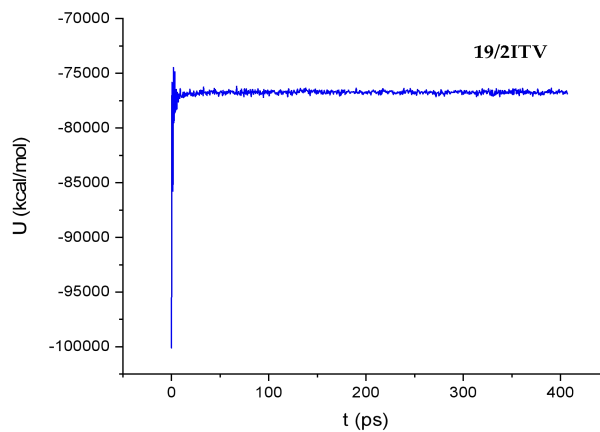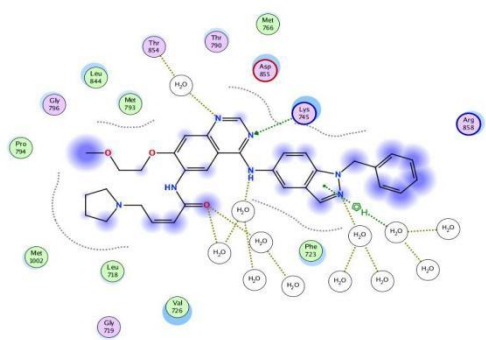
L21
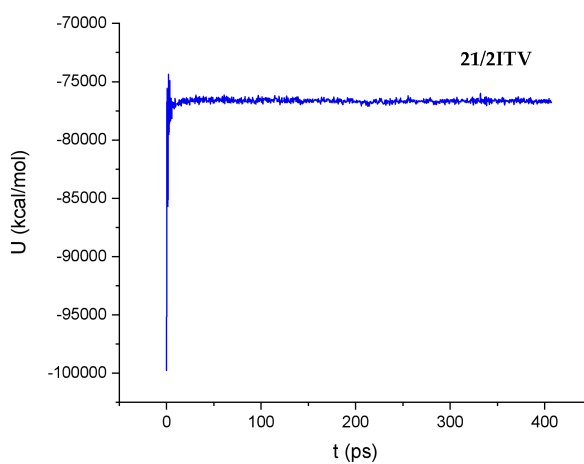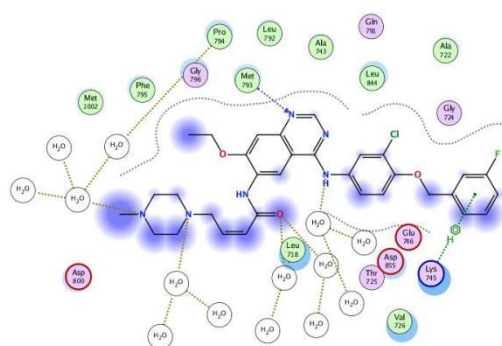
L23
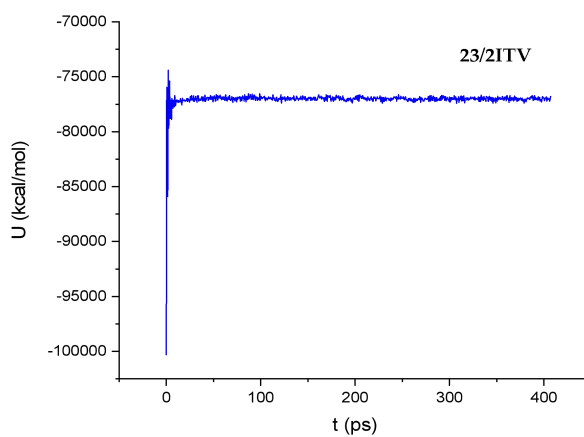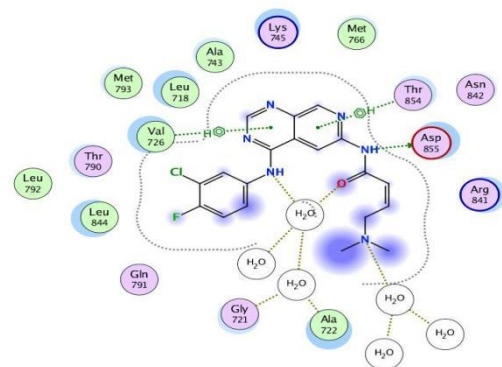
L24
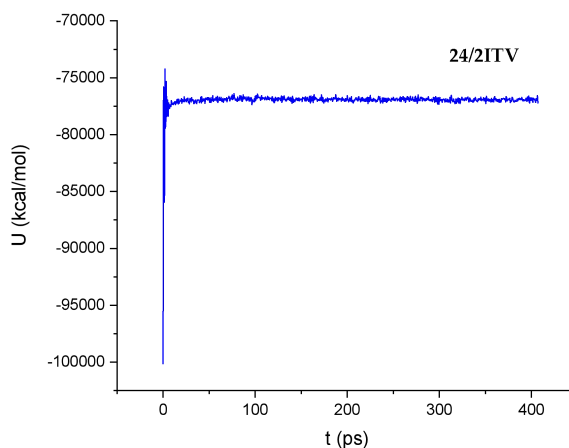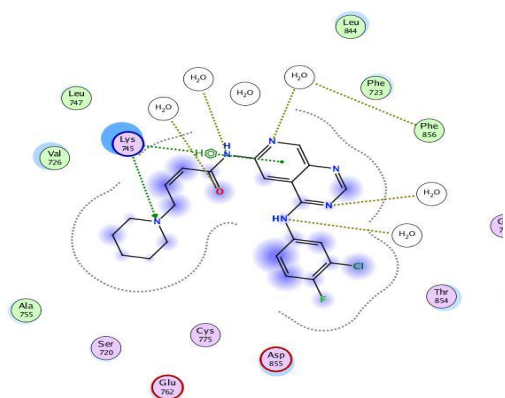
L26
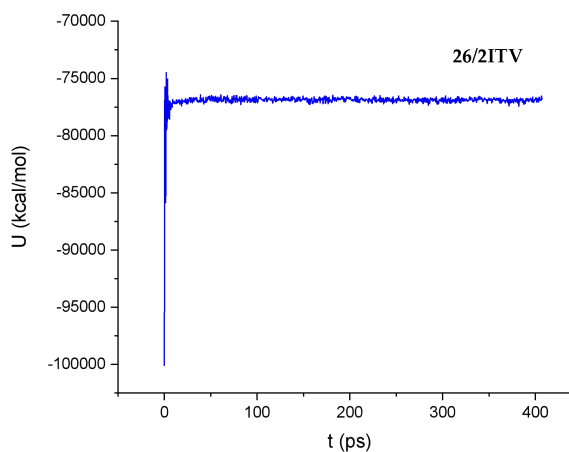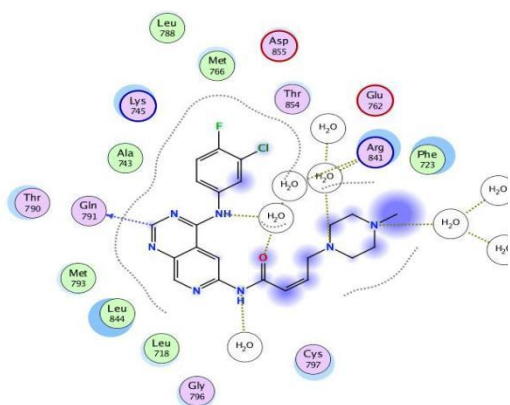
Figure 5 The evaluation of potential energy and binding interaction of complex of 19, 21, 23, 24 and 26 with 2ITV L858R mutation receptor as function of time.
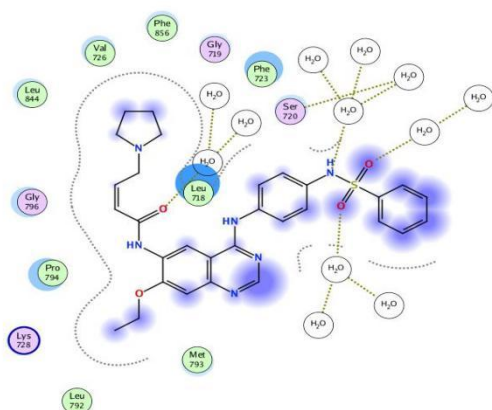
L1
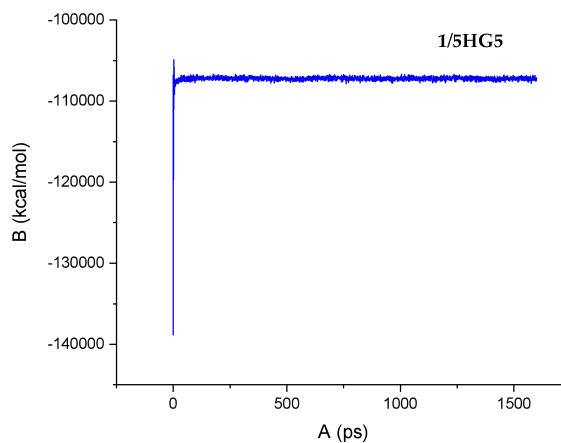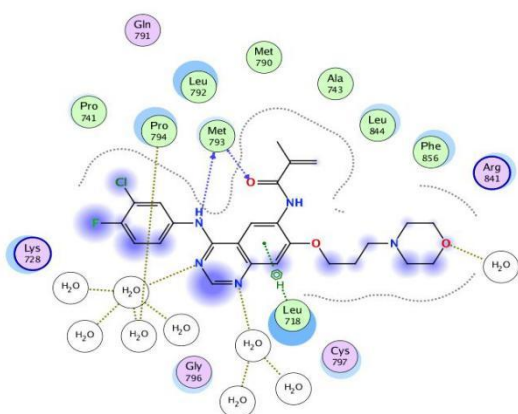
L4
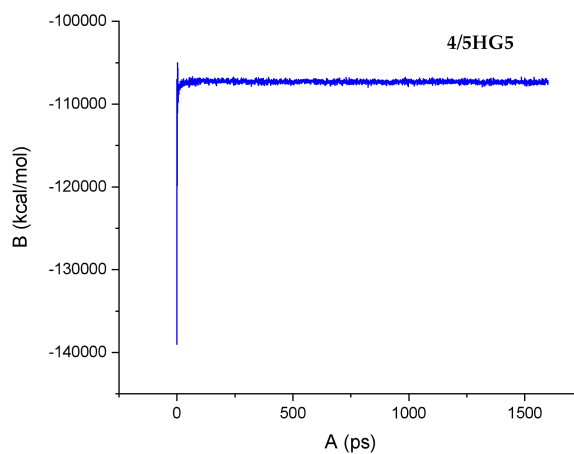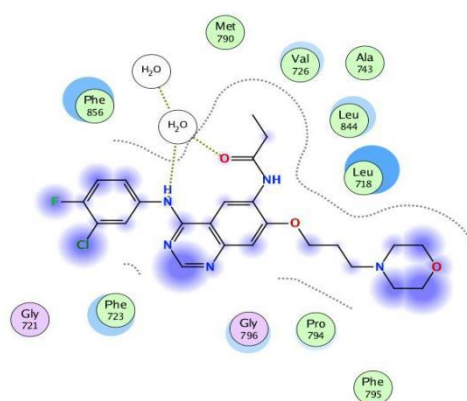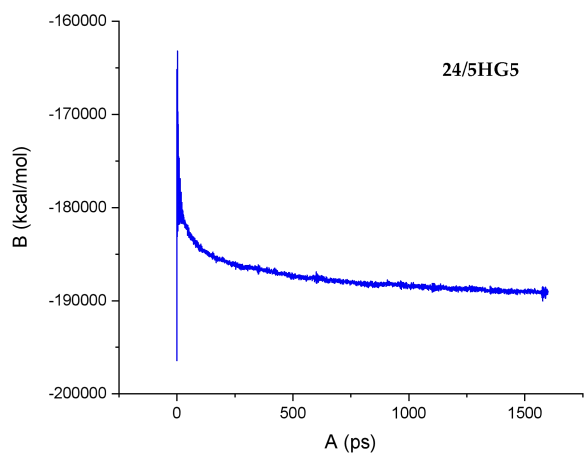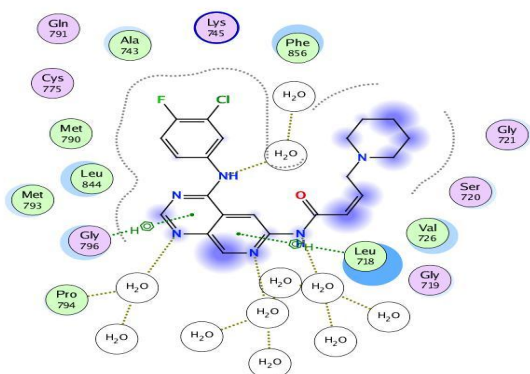

L8
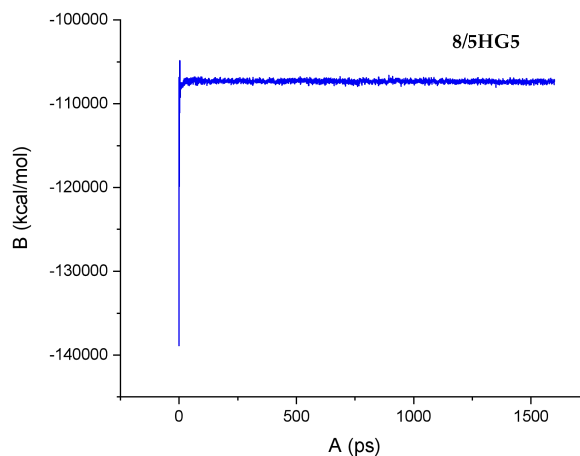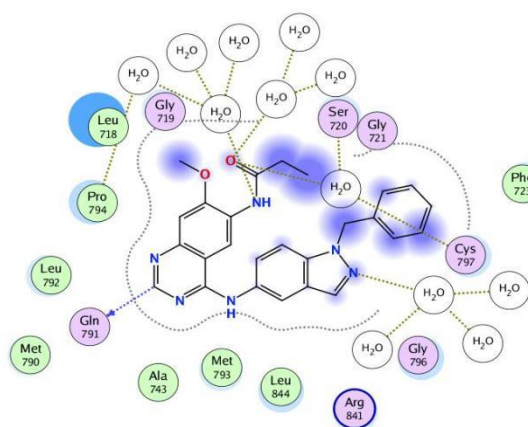
L9
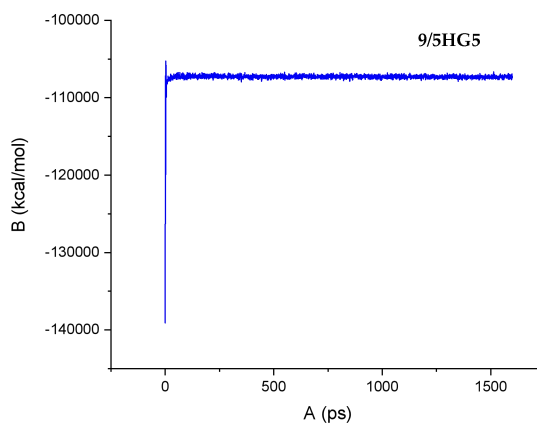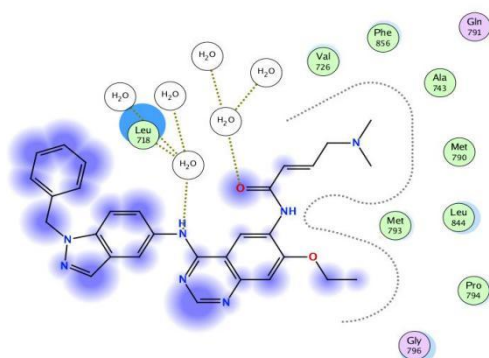
L16
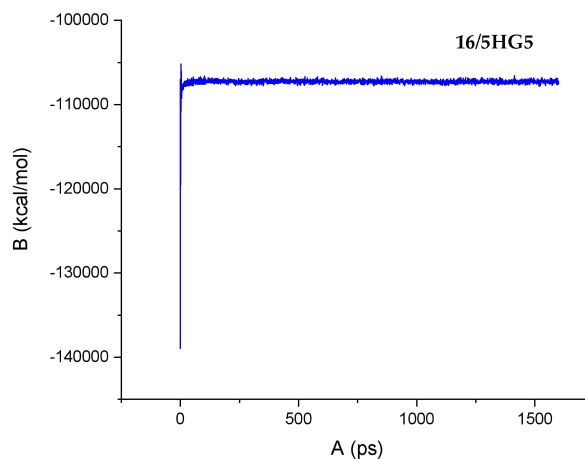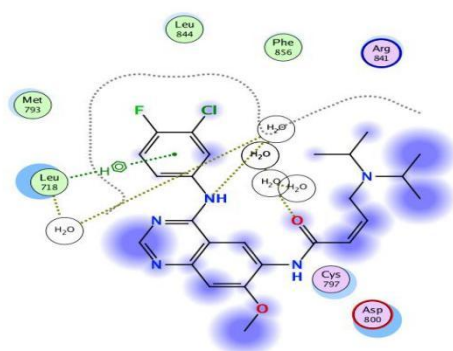
L22
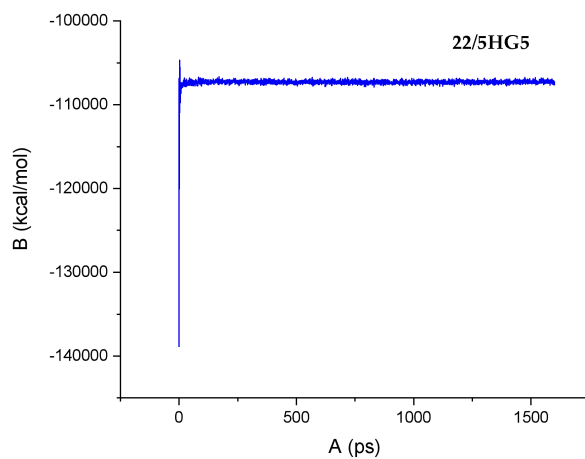
L24

Figure 6 The evaluation of potential energy and binding interaction of complex of 1, 4, 8, 9, 16, 22 and 24 with 5HG5 T790M receptor as function of time